
THE UNIVERSITY OF QUEENSLAND

AUSTRALIA

# Photosynthesis of microalgae in outdoor mass cultures and modelling its effects on biomass productivity for fuels, feeds and chemicals

Jennifer Elizabeth Yarnold

B.Sc. (Hons)

*A thesis submitted for the degree of Doctor of Philosophy at*

*The University of Queensland in 2016*

The Institute for Molecular Biosciences

**Abstract**

Practical applications of microalgae include uses as feedstocks for sustainable fuels, feeds, nutraceuticals, and chemicals; for the treatment of wastewater and industrial flue gas; and for use as recombinant protein expression systems. Improvements in biomass yields are required for commercially viable and sustainable algal technologies, particularly for low value commodities such as biofuels.

Although several algae exhibit higher growth rates than terrestrial crops, with theoretical upper limits of 8-10% photon conversion efficiency (PCE), solar-illuminated outdoor microalgal production systems typically have a PCE far below this and even below those achieved under laboratory conditions. The most intractable limiting factor is poor light distribution through the mass culture, where photoinhibitory light at the surface and dark zones deeper in the culture reduce photosynthetic productivity. Moreover, microalgae have evolved a suite of photoacclimation and photoregulation mechanisms to cope with rapid (seconds to minutes) light fluxes in natural environments, yet these processes remain poorly understood in well-mixed photobioreactors.

The aim of this thesis study was to combine an experimental and theoretical approach to: 1) investigate and understand the photosynthetic response of algae under mass culture conditions; 2) develop a mathematical model which could accurately predict light-to-biomass productivities under a broad range of design scenarios for outdoor production systems; and 3) identify key biological and design parameters to maximise biomass yields.

In the first part of the study, a light-to-biomass model was developed that could be easily applied to rapidly assess biomass yields of different algal strains under a range of design scenarios. This model predicts temporal and spatial irradiance at the reactor surface and through the mass culture with inputs of local solar radiation data, local coordinates, system properties and the optical properties of the culture. Local growth rates are then coupled to local light intensities within the reactor based on a static Haldane growth model derived from empirical growth-irradiance curves. Growth rates are integrated over space and time to compute areal and volumetric productivities.

Validation of the model was attempted by conducting batch harvest experiments in a laboratory scale photobioreactor matrix which simulated diurnal light cycles representative of three ‘typical’ days of solar radiation in Brisbane. The strains used were

*Chlamydomonas reinhardtii* and its truncated light-harvesting antenna mutant, *tla1*, reported to possess improved optical properties. Initially, the model did not satisfactorily predict growth under batch cultivation for the three different incident light conditions, overestimating productivity under low light days and overestimating on high light days. Subsequent adjustment of the model to include photoacclimative changes in the optical properties of the cell and a re-fit of the growth parameter values provided a more accurate match to the experimental data.

Model simulations were performed to compare productivities of *C. reinhardtii*, *tla1* and a fast-growing strain (*Chlorella* sp. 11_H5) in open pond and flat panel reactors (FPRs) under various optimal operating concentrations and, for FPRs, various spacing distances between adjacent panels and orientation.

One limitation of the simple model is that it does not incorporate physiological adaptation of algae to the variable light conditions experienced in bioreactors during mixing cycles. The second part of the study investigated the effects of photoacclimation on the productivity of *C. reinhardtii* under fluctuating light cycles which simulated cells mixing in dilute (low-density; $LD_{Fluc}$) and dense (high-density; $HD_{Fluc}$) outdoor mass cultures. Fluctuating light cycles were compared to non-fluctuating light regimes of the same average irradiance ($LD_{Avg}$ and $HD_{Avg}$) to discriminate between total light dosage and light regime. It was shown that $HD_{Fluc}$ cells that spent a large portion of time in the dark (0.5 of the duty cycle) became low-light acclimated, even though cells under non-fluctuating light of the same irradiance ($HD_{Avg}$) become high light acclimated. The main phenotypes of low light acclimation were a two-fold increase in pigment concentration; reduced maximum energy-dependent NPQ (qE) attributed to low expression of the light harvesting complex stress protein LHCSR3; and higher NPQ under low light, possibly due to enhanced cyclic electron flows. It was found that these responses were maladapted to mass culture conditions, resulting in a three-fold lower biomass accumulation efficiency in comparison to cells under non-fluctuating light of the same average irradiance. This suggests that excess photon absorption during high light periods of the cycle, and an inability to safely dissipate them via NPQ may have contributed to photodamage, subsequently increasing metabolic costs for repair. In contrast, the small dark fraction (0.1 of the duty cycle) of $LD_{Fluc}$ led to high light acclimated cells and a slightly higher biomass accumulation efficiency than $LD_{Avg}$.

Based on these findings, a more mechanistic model was proposed in an attempt to describe the underlying dynamic photoacclimation and regulation processes that occur in diel light cycles and under an evolving batch culture.

Finally, the suitability of the two different modelling approaches presented as well as possibilities for improvement of productivity in mass culture conditions are discussed.

**Declaration by author**

This thesis is composed of my original work, and contains no material previously published or written by another person except where due reference has been made in the text. I have clearly stated the contribution by others to jointly-authored works that I have included in my thesis.

I have clearly stated the contribution of others to my thesis as a whole, including statistical assistance, survey design, data analysis, significant technical procedures, professional editorial advice, and any other original research work used or reported in my thesis. The content of my thesis is the result of work I have carried out since the commencement of my research higher degree candidature and does not include a substantial part of work that has been submitted to qualify for the award of any other degree or diploma in any university or other tertiary institution. I have clearly stated which parts of my thesis, if any, have been submitted to qualify for another award.

I acknowledge that an electronic copy of my thesis must be lodged with the University Library and, subject to the policy and procedures of The University of Queensland, the thesis be made available for research and study in accordance with the Copyright Act 1968 unless a period of embargo has been approved by the Dean of the Graduate School.

I acknowledge that copyright of all material contained in my thesis resides with the copyright holder(s) of that material. Where appropriate I have obtained copyright permission from the copyright holder to reproduce material in this thesis.

## Publications during candidature

### Peer-reviewed papers

**Yarnold, J.E**., Ross, I.R., & Hankamer, B. (2016). Photoacclimation and productivity of *Chlamydomonas reinhardtii* grown in fluctuating light regimes which simulate outdoor algal culture conditions. *Algal Research,* January 2016.

Wolf, J., Stephens, E., Steinbusch, S., **Yarnold J.,** Ross, I.L., Steinweg, C., Doebbe, A., Krolovitsch, C., Müller, S., Jakob, G., Kruse, O, Posten, C., Hankamer, B. (2016). Multifactorial comparison of photobioreactor geometries in parallel microalgae cultivations. *Algal Research (In press)*.

### Conference abstracts

Work described in this thesis has been presented in the following poster presentations:

**Yarnold, J.E.**, Ross, I.R., & Hankamer, B. (2015) Effect of light regimes simulating outdoor algal cultures on acclimation and productivity of *Chlamydomonas reinhardtii***.** *Gordon Research Conference on Photosynthesis*, 28 June – 2 July 2015, Boston, US.

**Yarnold, J.E.**, Ross, I.R., & Hankamer, B. (2014) A numerical study comparing *Chlamydomonas reinhardtii* CC125 and its antenna mutant *tla1* under solar microalgae production systems. *Conference for the International Symposium of Applied Phycology*, June 2014, Sydney Australia.

**Yarnold, J.E.**, Ross, I.R., & Hankamer, B. (2012) Solar powering biofuel production: integrating optimisation of light regime and transfer from the sun to the cell. *"Algae for the future." 8th Asia-Pacific Conference on Algal Biotechnology*, June 2012, Adelaide, Australia.

Work described in this thesis has been presented in the following oral presentations:

**Yarnold, J.E**. (2015) The Effects of Photoacclimation and Light Regulation on Productivity of *Chlamydomonas reinhardtii* under Fluctuating Light. *Gordon Research Seminar on Photosynthesis*, 27-28 June 2015, Boston, US.

## Publications included in this thesis

**Yarnold, J.E**., Ross, I.R., & Hankamer, B. (2016). Photoacclimation and productivity of *Chlamydomonas reinhardtii* grown in fluctuating light regimes which simulate outdoor algal culture conditions. *Algal Research,* January 2016.
– Incorporated as **Chapter 4**.

| Contributor | Statement of contribution |
|---|---|
| **J. Yarnold** (Candidate) | Designed experiments (70%)<br>Performed the experiments (80%)<br>Wrote the paper (65%) |
| I.L. Ross | Designed experiments (30%)<br>Performed the experiments (20%)<br>Wrote and edited paper (15%) |
| B. Hankamer | Wrote and edited paper (20%) |

## Contributions by others to the thesis

I would like to acknowledge Mr. Simon Biggs for tutoring of MATLAB® programming software, mathematics and modelling techniques; Ms. Melinda White for input with an initial draft of the model proposed in Chapter 2; Mr. Marcello Pietro Vendruscolo and Ms. Franziska Messinger for assistance with conducting laboratory experiments; Prof. Peter Ralph, Mr. Dale Radford and Dr. Bojan Tamburic at University of Technology Sydney, for use of their photobioreactor matrix and facilities, assistance with conducting model validation experiments and intellectual input into the model validation part of the project; Ms. Janina Steinbeck and Ms. Sarah Piper for assistance with Western blot analysis; Ms. Juliane Wolf for technical assistance using the TECAN robotic system; Mr. John Srnka for collaborating on the design of the TECAN's LED lighting system and conducting all related electrical work; and my supervisors Prof. Ben Hankamer and Dr Ian Ross for their guidance, input into the project and for their critical reviews of this thesis.

## Statement of parts of the thesis submitted to qualify for the award of another degree

None.

**Acknowledgements**

The research presented here was performed at the Institute for Molecular Bioscience at The University of Queensland, Brisbane, Australia and was financially supported by an Australian Postgraduate Award and a Smart Futures PhD Scholarship.

I would like to give my sincerest thanks to the following people. To my principal supervisor Prof. Ben Hankamer for providing me with this tremendous opportunity to study in his laboratory and for his guidance of the project. To my associate supervisor, Dr Ian Ross, for his in-depth knowledge across the spectrum of all things algae and science-related and generous donation of his time and patience to assist with matters relating to this study. To Simon Biggs for tutorial support of the MATLAB® programming language and model development, who brought the skills of a biology graduate up to speed for the complex world of mathematical modelling, as good as could be expected. To John Srnka, for all his efforts with the creation of the excellent TECAN lighting system. To my examination committee Dr Timothy Nicholson and Dr James LeFevre for their valuable feedback throughout the project. To the other PhD students in the lab for their guidance, friendship and sharing of knowledge, among them are: Anne Sawyer, Juliane Wolf, Janina Steinbeck, Eugene Zhang, Sarah Piper, Gisela Jakob, Tony Bui, Gamma Chi, Rubbiya Ali, Alex Foo, John Roles, Rafael Feller, and Winnie Waudo. To the interns Franziska Messinger and Marcello Vendruscolo for their assistance with experimental work. To the Institute of Molecular Biosciences (IMB) and all of its staff – a truly world-class facility that I have felt privileged to be a part of. And to the IMB's wonderful postgraduate coordinator Amanda Carozzi who always has a smile and is ready to help in any way she can.

Finally, I would like to thank my wonderfully supportive fiancé Adam for putting up with me and all my grievances and for his kind words of encouragement despite admitting to knowing little about academia or research. To my beautiful darling daughter Kaitlyn – the best thing that ever happened to me – for teaching me patience, kindness and that the most important things in life are love and laughter – those things which she provides me in abundance. To my wonderful parents who are always there to give their time, unconditional love and childminding facilities. And to my friends and family for their support, encouragement and good humour, in particular my dear friend Paola Spadaro who has shared the journey with me from undergraduate to PhD candidate.

**Keywords**

photosynthesis, microalgae, *Chlamydomonas reinhardtii*, mathematical model, light, biomass, photoacclimation, photoinhibition

**Australian and New Zealand Standard Research Classifications (ANZSRC)**

ANZSRC code: 010202 Biological Mathematics, 50%
ANZSRC code: 060701 Phycology (incl. Marine Grasses), 30%
ANZSRC code: 100305 Industrial Microbiology (incl. Biofeedstocks), 20%

**Fields of Research (FoR) Classification**

FoR code: 0607, Plant Biology, 45%
FoR code: 0102, Applied Mathematics, 45%
FoR code: 1003, Industrial Biotechnology, 10%

# Dedication

For Adam, Kaitlyn, Mum and Dad.

You are my world.

# Table of Contents

# Table of figures

# List of tables

# Abbreviations

## Model Abbreviations

| | |
|---|---|
| $a_{cm}$ | Volumetric absorption coefficient for the cell material [$m^{-1}$] |
| $a_v$ | Parameter for determination of $P/P_{max}$ [dimensionless] |
| $b$ | Backward scattering fraction of the particle [dimensionless] |
| $C_{abs}$ | Absorption cross section of the particle [$m^2$] |
| $C_{sca}$ | Scattering cross section of the particle [$m^2$] |
| $C_{ext}$ | Extinction cross section of the particle [$m^2$] |
| $C_{Chla}$ | Concentration of chlorophyll *a* [kg $m^{-3}$] |
| $C_{Chlb}$ | Concentration of chlorophyll *b* [kg $m^{-3}$] |
| $C_{Car}$ | Concentration of total carotenoids [kg $m^{-3}$] |
| $C_{max.i}$ | Upper concentration limit of pigment *i* [kg $m^{-3}$] |
| $C_{max.i}$ | Lower concentration limit of pigment *i* [kg $m^{-3}$] |
| $C_{pig.i}$ | Concentration of pigment *i* [kg $m^{-3}$] |
| $C_x$ | Dry biomass concentration [kg $m^{-3}$] |
| $E_a$ | Mass absorption coefficient for the particle [$m^2$ $kg^{-1}$] |
| $E_{a,pig.i}$ | Mass absorption coefficient for pigment *i* [$m^2$ $kg^{-1}$] |
| $E_f$ | Photosynthetic efficiency conversion of solar radiation to PAR |
| $E_s$ | Mass scattering coefficient for the particle [$m^2$ $kg^{-1}$] |
| $E_{ext}$ | Mass extinction coefficient for the particle [$m^2$ $kg^{-1}$] |
| $f_{illum}$ | Non-shaded fraction of the illuminated face of the FPR [dimensionless] |
| $f_{ir,HB}$ | Fraction of ground between FPRs receiving direct light [dimensionless] |
| $f_{shaded}$ | Fraction of the illuminated face of the FPR shaded from direct beam radiation [dimensionless] |
| $f_{refl}$ | Fraction of the illuminated face of the FPR shaded from direct beam radiation and receiving specular reflected radiation [dimensionless] |
| $h_{reactor}$ | Height of reactor illuminated area [m] |
| $h_{illum}$ | Height of the non-shaded fraction of the illuminated face of the FPR [m] |
| $H_o$ | Daily extraterrestrial radiation [W $m^{-2}$] |
| $H$ | Total daily radiation on a horizontal surface [W $m^{-2}$] |
| $I$ | Irradiance [µmol $m^{-2}$ $s^{-1}$] |

| | |
|---|---|
| $I_0$ | Hourly incident PAR on a horizontal surface [µmol $m^{-2}$ $s^{-1}$] |
| $I_{avg}$ | Average local irradiance integrated over reactor depth [µmol $m^2$ $s^1$] |
| $I_c$ | Compensation irradiance of growth where $R_s + \mu = 0$ [$s^{-1}$] |
| $I_{dif}$ | Hourly incident diffuse PAR on a horizontal surface [µmol $m^{-2}$ $s^{-1}$] |
| $I_{dif,t}$ | Hourly incident diffuse PAR on a tilted surface [µmol $m^{-2}$ $s^{-1}$] |
| $I_{dir}$ | Hourly incident direct beam PAR on a horizontal surface [µmol $m^{-2}$ $s^{-1}$] |
| $I_{dir,t}$ | Hourly incident direct beam PAR on a tilted surface [µmol $m^{-2}$ $s^{-1}$] |
| $I_{ETC}$ | Irradiance available for photochemistry [µmol $m^2$ $s^1$] |
| $I_k$ | Photosynthetic saturation irradiance [µmol $m^{-2}$ $s^{-1}$] |
| $I_{loc}$ | Local photosynthetic photon fluence rate in the culture broth [µmol $m^{-2}$ $s^{-1}$] |
| $I_{loc,dir}$ | Local direct beam photon fluence rate in the culture broth [µmol $m^{-2}$ $s^{-1}$] |
| $I_{loc,dif}$ | Local diffuse photon fluence rate in the culture broth [µmol $m^{-2}$ $s^{-1}$] |
| $I_{NPQ}$ | Irradiance constant for determination of $K_{NPQ}$ [µmol $m^{-2}$ $s^{-1}$] |
| $I_p$ | ‘Perceived’ irradiance as a function of $I_{avg}$ and ε [µmol $m^{-2}$ $s^{-1}$] |
| $I_{ref}$ | Reflected radiation on a tilted plane [µmol $m^{-2}$ $s^{-1}$] |
| $k_a$ | kinetic rate constant of PSU activation [$m^2$ µmol] |
| $k_{acc}$ | kinetic rate constant of acclimation [$m^2$ µmol] |
| $k_d$ | kinetic rate constant of photochemical quenching [$s^{-1}$] |
| $k_i$ | kinetic rate constant of PSU photoinhibition [m µmol] |
| $k_r$ | kinetic rate of the of PSU recovery [$s^{-1}$] |
| $k_p$ | proportionality constant of photochemical quenching and biomass growth [s/h] |
| $K$ | Extinction coefficient of the surface material [$m^{-1}$] |
| $K_i$ | Photoinhibition constant [µmol $m^{-2}$ $s^{-1}$] |
| $K_{NPQ,max}$ | Half saturation constant for LHCSR3 acclimation to $I_p$ [µmol $m^2$ $s^1$] |
| $K_{pig}$ | Half saturation constant for pigment acclimation to $I_p$ [µmol $m^2$ $s^1$] |
| $K_s$ | Photosaturation constant [µmol $m^{-2}$ $s^{-1}$] |
| $K_t$ | Daily average clarity index [dimensionless] |
| $L$ | Reactor pathlength [m] |
| $L_c$ | Compensation depth of growth where $I_{loc} = I_c$ [$s^{-1}$] |
| $L_{st}$ | Standard meridian [degrees] |
| $L_{loc}$ | Longitude [degrees] |

| | |
|---|---|
| $L_{surface}$ | Surface material thickness [m] |
| $m$ | Complex refractive index of the particle [dimensionless] |
| $n$ | Real part of the refractive index of the particle [dimensionless] |
| $n_1$ | Refractive index of substance outside the reactor (e.g. Air) [dimensionless] |
| $n_2$ | Refractive index of PBR surface material [dimensionless] |
| $n_3$ | Refractive index of substance within the PBR (e.g. Water) [dimensionless] |
| $n_r$ | Number of specular reflections |
| $N$ | Day of the year |
| $NPQ_{max}$ | maximum capacity of NPQ [dimensionless] |
| $P_{areal}$ | Annual Areal productivity [t $h^{-1}$ $yr^{-1}$] |
| $P/P_{max}$ | Proportionality of maximal photosynthesis at acclimated state [dimensionless] |
| $P_{vol}$ | Mean daily volumetric productivity [g $L^{-1}$ $day^{-1}$] |
| $p(\theta,\theta')$ | Scattering phase function for scattering of the particle [dimensionless] |
| $PBR_{vol}$ | Liquid volume of a single photobioreactor [$m^3$] |
| $PBR_{area}$ | Areal footprint of a single photobioreactor (inc. spacing) [$m^2$] |
| $Q^*$ | Efficiency factor for packaging of the particle [dimensionless] |
| $q_{abs}$ | Absorption efficiency of the particle [dimensionless] |
| $q_{NPQ}$ | proportion of absorbed irradiance dissipated by NPQ processes [dimensionless] |
| $q_{sca}$ | Scattering efficiency of the particle [dimensionless] |
| $q_{ext}$ | Extinction efficiency of the particle [dimensionless] |
| $r^{\perp}$ | Fraction of reflected perpendicular component of polarised radiation through a surface [dimensionless] |
| $r\|\|$ | Fraction of reflected parallel component of polarised radiation through a surface [dimensionless] |
| $r$ | Mean radius of the cell [m] |
| $\tau^{\perp}$ | Fraction of transmitted perpendicular component of polarised radiation through a surface [dimensionless] |
| $R_b$ | Geometric factor [dimensionless] |
| $R_s$ | Respiration rate [$h^{-1}$] |
| $SA_{areal}$ | Areal illuminated surface area, ($m^2$ $m^{-2}$ footprint) |
| $t$ | unit of time |
| $t_{solar}$ | solar time [h] |

| | |
|---|---|
| $u$ | sky view angle [degrees] |
| $V_{32}$ | Mean efficient volume of the particle from $d_{32}$ sauter diameter [$m^3$] |
| $w$ | Width of reactor illuminated area [m] |
| $w_{pig.i}$ | Mass fraction of pigment $i$ [dimensionless] |
| $x_1$ | fraction of PSUs in an 'open' state (oxidised $Q_A$) [dimensionless] |
| $x_2$ | fraction of PSUs in an 'active' state (reduced $Q_A$) [dimensionless] |
| $x_3$ | fraction of PSUs in an 'inactivated' state (damaged) [dimensionless] |
| $x_w$ | Volume fraction of water in the cell [dimensionless] |
| $V_0$ | Parameter for determination of $P/P_{max}$ [dimensionless] |
| $V_p$ | mean volume for the particle from the sauter diameter [$m^3$] |
| $Y_{X,E}$ | Biomass yield on light energy received [g biomass µmol photons$^{-1}$] |
| $z$ | z-abscissa length: perpendicular distance from PBR surface to a point within the PBR [m] |

*Greek symbols*

| | |
|---|---|
| $\alpha$ | Photosynthetic rate in the light-limited region, i.e. initial slope [dimensionless] |
| $\alpha_1$ | Linear scattering modulus of the two-flux radiative transfer equation [dimensionless] |
| $\beta$ | Slope of photoinhibition for P-I curve [degrees] |
| $\varphi$ | Latitude [degrees] |
| $\gamma$ | Reactor surface azimuth angle ($-180° \geq \gamma \geq 180°$) [degrees] |
| $\delta$ | declination of the angular position of the Sun at solar noon with respect to the plane of the equator, north positive ($-23.45° \geq \delta \geq 23.45°$) [degrees] |
| $\delta_{dif}$ | Two-flux extinction coefficient for diffuse radiation [$m^{-1}$] |
| $\delta_{dir}$ | Two-flux extinction coefficient for direct beam radiation [$m^{-1}$] |
| $\varepsilon$ | illuminated ($I_{loc} > I_c$) fraction of the culture [dimensionless] |
| $\hbar$ | Solar hour |
| $\zeta$ | Solar constant, 1,353 [W $m^{-2}$] |
| $\rho$ | Ground reflectivity [dimensionless] |
| $\rho_{dm}$ | Density of the dry material in biomass [kg $m^{-3}$] |
| $\theta$ | Angle of incidence for direct beam radiation between the sun and a plane of a given tilt [degrees] |
| $\theta_2$ | Angle $\theta$ modified by refraction between the air and the material of a surface [degrees] |

| | |
|---|---|
| $\theta'$ | Angle $\theta$ modified by refraction through the surface material and the culture medium [degrees] |
| $\theta_z$ | Zenith angle of the sun [degrees] |
| $\tau$ | Fraction of transmitted radiation through a surface [dimensionless] |
| $\tau_a$ | Transmittance through a material, accounting for absorption losses by the material only [dimensionless] |
| $\tau^{\perp}$ | Fraction of transmitted perpendicular component of polarised radiation through a surface [dimensionless] |
| $\tau\|\|$ | Fraction of transmitted parallel component of polarised radiation through a surface [dimensionless] |
| $\varrho$ | Spacing distance between parallel placed FPRs [m] |
| $\kappa$ | Imaginary part of the refractive index of the particle [$m^{-3}$] |
| $\xi$ | Particle absorption optical thickness [dimensionless] |
| $\mu$ | Specific growth rate [$s^{-1}$] |
| $\mu_m$ | Maximum potential growth rate [$s^{-1}$] |
| $\mu_{max}$ | Maximum specific growth rate [$s^{-1}$] |
| $\vartheta$ | Spacing distance between flat panel reactors [m] |
| $\omega$ | angle corresponding to the solar hour [degrees] |
| $\omega_s$ | hour angle at sunrise [radians] |
| $\chi$ | Reactor tilt angle [degrees] |

*Subscripts*

| | |
|---|---|
| *abs* | relative to absolute |
| *avg* | relative to average value |
| *abs* | relative to the absorption phenomenon |
| *back* | relative to the back side of a two-sided photobioreactor |
| *dir* | relative to direct beam radiation |
| *dif* | relative to diffuse radiation |
| *front* | relative to the front side of a two-sided photobioreactor |
| *max* | relative to maximum value |
| *sca* | relative to the scattering phenomenon |
| $\lambda$ | relative to a given wavelength [nm] |

**General Abbreviations**

| | |
|---|---|
| ATP | adenosine triphosphate |
| Car | total photoprotective carotenoids |
| CBB | Calvin-Bensson-Basham |
| CCM | carbon concentrating mechanism |
| CEF | cyclic electron flow |
| $^3Chl^*$ | triplet excited chlorophyll |
| Chl *a* | chlorophyll *a* |
| Chl *b* | chlorophyll *b* |
| $CO_2$ | carbon dioxide |
| Cyt$b_6f$ | cytochrome $b_6f$ |
| ERoEI | energy return on energy invested |
| ETC | electron transport chain |
| ETR | electron transport rate |
| *F* | Chlorophyll fluorescence emission from light adapted cells |
| $F_0$ | Minimum chlorophyll fluorescence from dark-adapted cells |
| Fd | ferrodoxin |
| Flv | flavodiiron |
| FNR | Ferridoxin NADP Reductase |
| $F_m$ | Maximum chlorophyll fluorescence from dark-adapted cells |
| $F_m$' | Maximum chlorophyll fluorescence from light-adapted cells |
| FPR | flat panel reactor |
| FPQ | ferrodoxin quinone reductase |
| $H_2O_2$ | hydrogen peroxide |
| $HD_{Avg}$ | Light treatment simulating average light of $HD_{Fluc}$ (constant) |
| $HD_{Fluc}$ | Light treatment simulating a high density mixed culture |
| LCA | life cycle analysis |
| $LD_{Avg}$ | Light treatment simulating average light of $LD_{Fluc}$ (constant) |
| $LD_{Fluc}$ | Light treatment simulating a low density mixed culture |
| LEF | linear electron flow |
| LHC | light harvesting complex |

| | |
|---|---|
| LHCII | light harvesting complex predominantly associated with PSII |
| LHCB | light harvesting complex proteins associated with PSII |
| LHCBM9 | major light harvesting complex protein 9 |
| $NADP^+$ | oxidised nicotinamide adenine dinucleotide phosphate |
| NADPH | nicotinamide adenine dinucleotide phosphate |
| NDH | NAD(P)H dehydrogenase |
| NPQ | non-photochemical quenching |
| $^1O^*$ | singlet oxygen |
| $O_2^-$ | superoxide radical |
| OD | optical density |
| PBR | photobioreactor |
| PC | plastocyanin |
| PCE | photosynthetic conversion efficiency |
| PGR | proton gradient regulator |
| *P–I* | Photosynthetic-irradiance |
| PPFD | photosynthetic photon flux density [µmol $m^{-2}$ $s^{-1}$] |
| PPFR | photosynthetic photon fluence rate [µmol $m^{-2}$ $s^{-1}$] |
| PQ | plastoquinone |
| PSI | photosystem I |
| PSII | photosystem II |
| PTOX | plastid terminal oxidase |
| qE | energy-dependent quenching |
| qI | slowly-developing component of NPQ |
| qT | state transitions |
| RC | reaction centre |
| Redox | oxidation/reduction |
| RNAi | Ribonucleic acid interference |
| ROI | return on investment |
| ROS | reactive oxygen species |
| RTE | Radiative transfer equation |
| RuBP | ribulose 1,5-bisphosphate |

| | |
|---|---|
| Rubisco | Ribulose-1,5-bisphosphate carboxylase/oxygenase |
| SA:V | Surface area to volume |
| SBRC | *Solar Biofuels Research Centre* |
| TAP | tris acetate phosphate |
| TEA | techno-economic analysis |
| TRX | thioredoxins |
| $\Phi_{PSII}$ | Quantum yield of PSII fluorescence |
| $\mu$–$I$ | growth-irradiance |

# 1 Introduction

## 1.1 The prospect of algae in the context of today's global challenges

All life on earth is facing parallel and unprecedented threats from unsustainable human activities. Among these are dangerous increases in atmospheric and oceanic $CO_2$ from fossil fuel combustion and deforestation (IPCC, 2014); and the depletion of freshwater, arable lands and natural resources to accommodate a burgeoning population set to exceed nine billion people by 2050 (Stephens et al., 2013).

These environmental challenges, once thought to interfere with the 'business as usual' approach, are now realised to threaten economic and political stability. In Egypt, Iraq, Syria and Yemen, civil unrest and war has been intensified by rapid oil revenue depletion, droughts, diminishing crop yields and water shortages (Sowers et al., 2011). In fact, climate models revealed Syria's worst drought from 2007–2010 was 2–3 times more probable from anthropogenic forcing than from natural variability alone (Kelley et al., 2015). This drove scores of farmers into the cities, escalating existing political tensions into a civil war that is estimated to have killed 200,000 people and displaced ~3.88 million refugees into surrounding countries and into Europe (UNHCR, 2015).

Addressing climate change has now gone from an aspiration to a critical urgency. This was highlighted by a joint agreement in 2014 between the world's two most industrialised nations to make 26–28% reduction in $CO_2$ emissions (US), and a cap in $CO_2$ emissions (China) by 2025 and 2030 respectively (Office of the Press Secretary, 2014). More recently, a global pact was made by the 195 participating countries of the 2015 United Nations Climate Change Conference in Paris to reduce carbon emissions enough to keep global warming "to well below 2$^{o}$C" (UNFCOCC, 2015).

These goals will require, for a start, replacing fossil fuels with $CO_2$-neutral alternatives. The renewable electricity sector is making inroads into the global electricity market. In 2014 Germany's solar and Ireland's wind power outputs peaked at up to 50% total demand on given days, and on one windy day in 2015, Denmark produced 140% of its electricity through wind farms. Despite these proof-of-principle cases, total renewable energies accounted for just 13.5% of world total primary energy supply in 2013 (EIA, 2015). Of this, the vast majority were in the form of solid biofuels (~9%, wood and charcoal) or electricity (~3.6%, geothermal, solar, wind, tide, and hydro). In contrast to electricity (20%), fuels supply 80% of the global energy market (Wagner et al., 2016) emphasising the need to develop sustainable liquid fuel alternatives.

Limiting fossil fuel combustion may reduce $CO_2$ emissions, but it will not lower existing atmospheric levels which, even if emissions were halved by 2050, would result in a global mean temperature rise of up to 2°C (Meinshausen et al., 2009). Biological photosynthesis is currently the most promising means of removing sufficient quantities of $CO_2$ from the atmosphere. Ringsmuth et al. (2016) estimated global net photosynthetic primary production for 2010 resulted in ~110Gt of carbon stored annually, eleven times more than that released by total primary energy consumption of humans. Whilst anthropogenic $CO_2$ emissions seem relatively small to photosynthetic carbon storage, over time these inputs disrupt the delicate balance of the earth's carbon cycle. Moreover, the efficiency of oceanic and terrestrial sinks to take up additional $CO_2$ emissions has declined (Canadell et al., 2007). Consequentially, atmospheric levels have seen a compounded accumulation of $CO_2$ from pre-industrial levels of ~280ppm to ~400ppm today – a geological instant of less than 300 years (Pongratz et al., 2012).

Increasing primary production by planting more terrestrial crops is limited by the fact that nearly all arable land has already been appropriated for agriculture or remaining forests. To this end, second generation algal production systems are an attractive solution to expand photosynthetic capacity as they have demonstrated scalability and can be cultivated in deserts, coastal and semi-arid marginal lands (Stephens et al., 2013) and potentially offshore (for example, NASA's OMEGA project). As photosynthetic organisms, they tap into the huge solar energy resource, of which photosynthetically active radiation (PAR, 400–700 nm) constitutes ~2,600 times the global energy demand in 2010 (Ringsmuth, 2016). This energy drives the conversion of $CO_2$ into stored chemical energy which could theoretically replace existing fossil fuels, increase food production, and sequester vast amounts of $CO_2$ to mitigate the effects of climate change (Ringsmuth, 2016).

First generation biofuels from sugarcane, corn, or sorghum have been exploited for 30 years, however their competition with agriculture for food, land, nutrients and freshwater make them unsustainable in the long-term and played a role in the so-called 'world food crisis' of 2007–2008 (McMichael, 2009). Alternatively, algae can be grown in saline or wastewater, the latter of which can be used to recycle nutrients (Vasconcelos Fernandes et al., 2015), and using $CO_2$-rich flue gas (Borkenstein et al., 2011), further reducing their environmental footprint.

### 1.2 Current state of algal technologies, commodities and market values

In order to survive in extreme and competitive environments, algae have evolved an exquisite metabolism capable of producing a diverse array of compounds. Depending on the species and growth conditions, algae can contain up to 60% protein, 60% carbohydrates, or 70% oils (Draaisma et al.,

2012) and also produce valuable enzymes, pigments and secondary metabolites that can be used for fuels, food, chemicals, antioxidants, natural dyes and pharmaceuticals (Draaisma et al., 2012, Cardozo et al., 2007, Schenk et al., 2008).

Today, the combined market for microalgae and macroalgae products is estimated on the order of billions of dollars annually with ~20 commercial products and a growing demand for both existing commodities as well as potential biofuels and drugs (Hudek et al., 2014). The value of algal commodities varies markedly (**Table 1-1**), with the low price of fuels highlighting the difficulty in bringing these to market so far.

### 1.2.1 Human nutrition

Currently most commercial algal products are for human nutrition. The first to enter the market were the protein, vitamin and mineral-rich chlorophyte *Chlorella* in the 1950s and the cyanobacterium *Arthrospira platensis* (Spirulina) in the 1970s (Hudek et al., 2014). Unlike higher plants and animals, many algae synthesise *de novo* the long chain polyunsaturated fatty acids (PUFAs) docosahexaenoic acid (DHA) and eicosapentaenoic acid (EPA). Their importance in maintaining a healthy metabolism and disease prevention, in addition to concerns over the sustainable extraction of fish-based oils through over-fishing, have seen algal-based DHA and EPA grow to a reported value of $171.2 million in 2013 (~10% market share). Carotenoids and chlorophylls are increasingly recognised for their health benefits and powerful antioxidant effects. Some examples include the ketocarotenoid astaxanthin, which is associated with the prevention of skin, breast and prostate cancers, inflammation, ulcers and other age related diseases (Cardozo et al., 2007); the xanthophyll carotenoids zeaxanthin and lutein are known to lower the risk of age-related macular degeneration (Meyer and Sekundo, 2005); and β-carotene offers pro-vitamin A activity (Cardozo et al., 2007).

### 1.2.2 Aquaculture and animal feed

Depleting fisheries saw a rise in aquaculture to 45.71 million metric tons in 2000 (40% yield of wild fisheries) with a value at US$56.47 billion, up by 6.3% in production from 1999 (Cardozo et al., 2007). As the natural food source for many marine species, algae are used as feed for farmed prawns and mollusks, and to rotifers or pipis, which are then fed to crustaceans, salmon and other fish. Muller-Feuga (2000) estimated 1.5 million tonnes of dry weight algal biomass was consumed in mollusk farming alone in 1997. Live algae have higher nutritional value than frozen or dried sources (particularly fatty acids) and, as such, are often produced onsite. However, due to lack of algal cultivation expertise, some have estimated that 30-40% of hatchery costs are associated with algal

cultivation in Australia (Borowitzka, 1997). Algae are also increasingly fed to cattle to boost nutritional content (Hudek et al., 2014).

### 1.2.3 Wastewater treatment

Algae are used for the treatment of domestic, industrial and agricultural wastewaters as they are highly efficient at removing nutrients. For instance, *Chlorella sorokiniana* showed 100% uptake of nitrogen and phosphorous and high growth rates from blackwater (toilet water) (Vasconcelos Fernandes et al., 2015). In water treatment plants they are cultivated in high rate algal ponds which form part of an Advanced Pond System comprising anaerobic digestion pits, high rate algal production ponds, algal settling ponds and maturation ponds in series (Craggs, 2005). Park et al. (2011) reported that although the land requirements for Advanced Pond Systems were 50 times more than for activated sludge systems, the relative estimated capital and operational costs were less than one-half and one-fifth respectively.

### 1.2.4 Pharmaceuticals

Recent drug discovery efforts have focused on algae as a promising source of novel bioactive compounds (natural products) including steroids, polysaccharides, lectins, mycosporine-like amino acids, halogenated compounds, polyketides and toxins (Cardozo et al., 2007). The use of *Chlamydomonas reinhardtii* as a recombinant protein expression system for the production of vaccines, enzymes, bioactive proteins, antibodies, immunotoxins and hormones is also showing promise. Typically, these products have been produced with bacteria, particularly *Escherichia coli*, however, eukaryotic algae are capable of producing more complex larger proteins, with the added benefits, according to Rasala and Mayfield (2015) of being "safe, scalable, easy to genetically modify through transformation, mutagenesis, or breeding, and inexpensive to grow".

### 1.2.5 Biofuels

A concerted effort to use algae for fuels was made after the OPEC oil crisis in the 1970s with the creation of the Aquatic Species Program by the U.S. Department of Energy's Office of Fuels Development in 1978. The aim was to make biodiesel from high lipid producing strains using flue gas from coal fired power plants (Wijffels and Barbosa, 2010). However, after nearly two decades of research, the program was halted in 1996 due to technical challenges and a lack of funding. Despite the potential of algae to produce 10–30 times more oil per hectare than terrestrial soy, sunflower and canola crops (Schenk et al., 2008), up until now the relatively high capital and operational costs of algal cultivation for low-value fuels stifled the progress of the technology.

**Table 1-1.** Commodities from microalgae, common commercial species and current market value of products.

| Algal species | Product / Application | Description | Market Value (US$) | Ref. |
|---|---|---|---|---|
| *Haematococcus pluvialis* | Astaxanthin | Anti-oxidant, feed additive, seafood colourant | \$1,641-\$3,000 $kg^{-1}$ | (Hemaiswarya et al., 2011, Newswire, 2015). |
| *Isochrysis galbana*<br>*Thalassiosira pseudodonana*<br>*Tetraselmis* sp.<br>*Nannochloropsis* sp.<br>*Pavlova lutheri*<br>*Nitzschia and Navicula* sp. | Aquaculture Feed | Live, frozen, or dried cells | \$300-600 $kg^{-1}$ | (Borowitzka, 1997) |
| *Nannochloropsis* sp.<br>*Monodus subterraneus*<br>*Chlorella minutissima*<br>*Isochrysis galbana (DHA)*<br>*Phaeodactylum tricornutum (EPA)* | Eicosapentaenoic acid (EPA) docosahexaenoic acid (DPA) | Omega-3 long chain polyunsaturated fatty acid | \$ 19,312 $kg^{-1}$ | (Cardozo et al., 2007) (Carvalho et al., 2006b, Bernasconi, 2014) |
| *Arthrospira platensis* | Spirulina | High protein (60-70%) food supplement | \$56 $kg^{-1}$ | (Piccolo, 2012) |
| *Chlorella pyrenoidosa, C. vulgaris* | Chlorella | High protein, high vitamin food supplement | \$44 $kg^{-1}$ | (Oligae.com) |
| *Dunaliella salina* | β-carotene | Anti-oxidant, provitamin A supplement, pigment agent | \$1,000-2,000 $kg^{-1}$ | (März, 2011) |
| *Botryococcus braunii,*<br>*P. tricornutum*<br>*Chlorella* sp.<br>*Dunaliella tertiolecta*<br>*Tetraselmis* sp.<br>*C. reinhardtii* | Biofuels: biodiesel, biomass, biohydrogen, biogas | | \$2.50 $gallon^{-1}$ | (Barbosa and Wijffels 2013), www.eia.gov.au |
| *C. reinhardtii* | Antibodies<br>Immunotoxins<br>Other protein therapeutics | | >>\$1,000 $kg^{-1}$ | (Rasala and Mayfield, 2015) |

For instance, a joint venture between Synthetic Genomics and Exxon Mobil projected to invest $600 million over 10 years was terminated after four years and $100 million in 2013, due to concerns that algal fuel viability was greater than 25 years away.

In 2013, San Diego-based venture capital backed Sapphire Energy announced it would produce 1.5 million gallons crude oil per year, or 100 barrels per day by the end of 2014 on its 300 acre (121.4ha) capacity Green Crude Farm in New Mexico. However, as at December 2015, no announcements had been made as to whether this feat had been achieved and the company's website stated that the now 100 acre operational facility planned to produce 130 tonnes of omega 3 oils instead (1,600 tonnes of biomass.$yr^{-1}$, 39.6 $t.ha^{-1}.yr^{-1}$). Although most technologies advance down the cost curve from small high value to large low value markets, the large decline in crude oil prices during this period from ~US$100/bl to ~US$30/bl (EIA, 2015) may explain the strategic focus on higher value products and highlights the vulnerability of the technology to fluctuating oil prices.

On the contrary, the recent emergence of several algal-fuel start-up companies may hint that important technological and commercial advances are being made. Florida-based biotech Algenol has commenced operations and claims it will produce ethanol, gasoline, jet and diesel for as little as US$1.30 per gallon by 2016. Arizona-based Diversified Energy claim their expertise in systems engineering and project management could produce algal oils as low as $US0.18–0.26 $kg^{-1}$ (Ullah et al., 2014). In Australia, Aurora Algae successfully demonstrated productivities of up to 15 tonnes of dry biomass per month over a 2.5 year period on their 20 acre (~8.1 ha) open pond demonstration facility in Karratha with planned expansion of a commercial-scale facility in Texas after an initial six month trial surpassed growth expectations. South Australian-based biotechnology company Muradel launched their demonstration plant in Whyalla in 2014, with plans to produce 30,000 L green crude per annum using their five-step Green2Black™ technology. They forecast that this scalable technology would lead to 500,000 barrels of refinable green crude per annum on a 1,000 ha commercial facility.

Whether these projections prove realistic will ultimately be determined by the return on investment (ROI), and the energy return on energy invested (ERoEI), relative to that of fossil fuels and crop-based biofuels, both of which are often heavily subsidised by governments (Wagner et al., 2016). It will likely be necessary to couple algal-based fuels with existing applications, such as wastewater treatment plants, or by using a 'mild disentanglement' approach for extraction of discrete higher value feedstocks (lipids, proteins, starches, pigments) in order to co-produce cheap biofuels with higher value commodities.

A major reduction in biomass production efficiency and costs has been identified by techno-economic evaluations as being the critical factor to achieve commercially-viable algal fuel enterprises which would produce enough fuel to supplant conventional supplies (Stephens et al., 2010). This will involve both cost-effective systems in conjunction with increasing biomass yields.

### 1.3 Increasing photosynthetic productivity: challenges and opportunities

There is considerable scope for increasing current biomass yields achieved in outdoor systems. Photosynthetic conversion efficiency (PCE) is the whole-of-process conversion of photons to biomass energy (i.e. the percentage of intrinsic photon energy flux which is captured in the form of chemical energy (biomass enthalpy)). Reported PCEs are currently up to ~2%, yet the theoretical upper limits are estimated at 8–10% which could theoretically yield dry weight algal biomass of 77g.m$^{-2}$.day$^{-1}$ (280 ton.ha$^{-1}$.yr$^{-1}$, Melis (2009)).

Realisation of the potential of high microalgal yields in large scale outdoor production systems requires optimisation at many levels. Nutrient supply, $CO_2$ and $O_2$ exchange, temperature and pH are just some parameters that must be regulated to achieve high performance. The major limitation, however, lies in the poor light distribution and utilisation that typically occurs under mass culture conditions, which results in reduced PCE. Absorption by highly pigmented algal cells creates rapid attenuation of light at the surface, shading cells deeper in culture. The light gradient through the reactor depth is envisaged as creating four zones of growth as depicted in **Figure 1-1** (Grobbelaar, 2010). In the *photoinhibited* (PI) zone, cells at the surface receive higher light than the saturation irradiance ($I_k$) of photosynthesis. Here, some light is wasted by heat dissipation through non-photochemical quenching (NPQ) mechanisms to protect the cells from oxidative damage. However, beyond NPQ capacity, photodamage may also occur, reducing growth below its maximum capacity. In the *saturated* zone, light approaches optimal levels and growth is potentially near maximal ($\mu_{max}$). In the *limited* zone, light is below saturation and growth declines proportionally. In the *dead* zone (e.g. at the base of open ponds or the centre of two-sided PBRs) light is lower than the compensation irradiance of photosynthesis, $I_c$, where energy losses through respiration are higher than energy storage, necessarily resulting in net biomass loss.

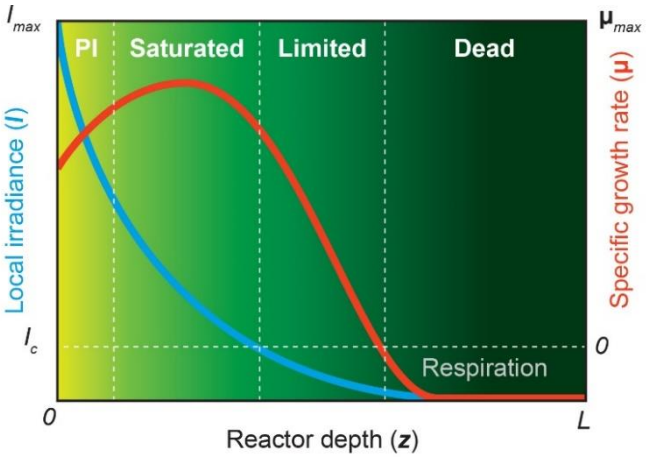


**Figure 1-1.** Schematic of the four growth zones within mass culture in response to local light intensities. Adapted from Grobbelaar (2010).

The relative proportion of each zone is dependent on the incident irradiance, reactor geometry, culture depth and density, and the biological properties of the algae (e.g. cell size and chlorophyll content). Clearly, design principles should maximise the *saturated* zone and minimise the *dead* and *PI* zones. Not surprisingly, the availability and intensity of light is the subject of intensive research efforts to enhance culture yields. This can be achieved at the level of systems design (engineering); strain selection, breeding or bioengineering (biological); or adjusting operating conditions (process control).

### 1.3.1 Systems design

Microalgae are cultivated in open ponds or closed PBRs (**Figure 1-2**). Open ponds are most widely used for commercial large-scale production, with ca. 98% of biomass produced in open ponds according to Park et al. (2011). The benefits are that they are cheaper to build and operate, and can be easily scaled to several hectares (Park et al., 2011). Open ponds usually have a pathlength between 0.1–0.5 m and are mixed with a paddlewheel or rotating arm at rates of 0.1–0.3 $m.s^{-1}$ (Borowitzka, 1999a, Craggs, 2005, Grobbelaar et al., 1995). The relatively poor illuminated surface area to volume (SA:V) ratio, slow mixing rates between light and dark zones, and increased risk of contamination from competitor algae, grazers and pathogens (Borowitzka, 1999a) typically yields lower productivities than PBRs as well as higher harvesting costs associated with water removal from dilute cultures. Reducing pond depth, increasing mixing rates and turbulence by sparging $CO_2$, or adding baffles are some strategies proposed to improve light distribution (Weissman and Goebel, 1987).

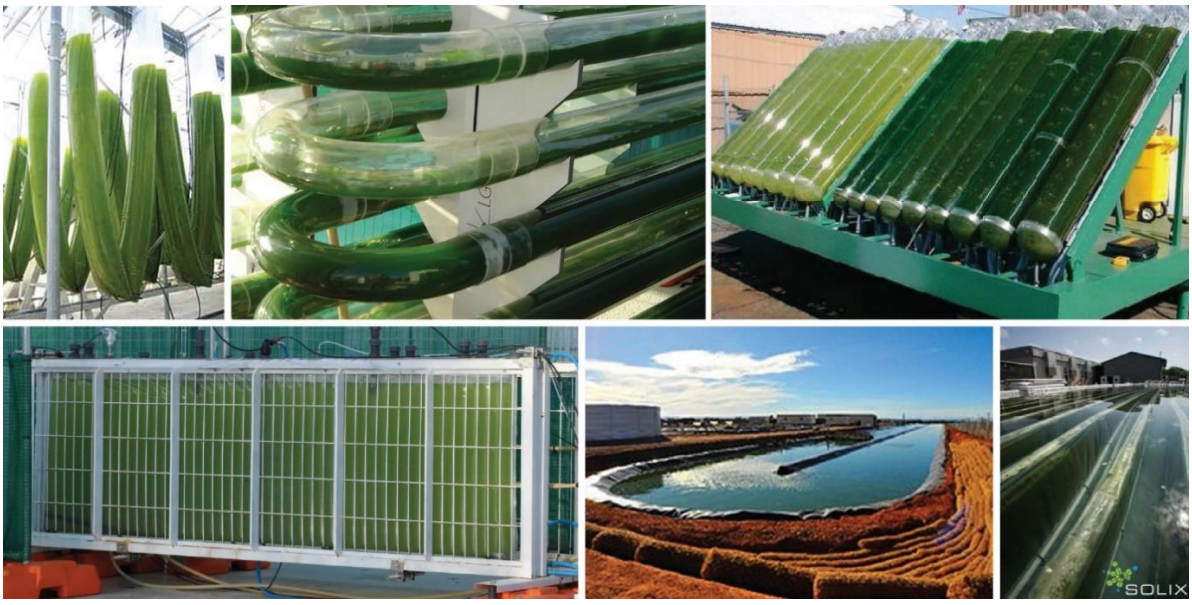


**Figure 1-2.** PBR configurations. A) V-shaped bags; B) vertically-stacked tubular systems; C) inclined column reactors (http://enfo.agt.bme.hu/drupal/en/node/9917); D) Flat panel reactors; D) Muradel's 4,000 $m^2$ open raceway pond; E) Solix Biofuels demonstration facility showing submerged flat panel plastic sleeves in water (Solix Biofuels 2010, Wilson 2010).

The short pathlength of PBRs is a key advantage over open ponds as it increases the SA:V ratio, improving light availability and permitting faster cycling of cells between light and dark zones. Several designs have been proposed, the most common being flat panel reactors, tubular reactors, column reactors and plastic V-shaped bags (**Figure 1-2**, Carvalho et al. (2006a)). More elaborate systems or add-ons include: thin-layer sloping reactors (Grobbelaar et al., 1995); the use of solar collectors (Ono and Cuello, 2006) or light guides (Lim et al., 2015); or the proposed use of pulsed light emitting diodes to create the 'flashing light' effect (Gordon and Polle, 2007). Higher cell densities can be maintained in PBRs thereby reducing water needs and harvesting costs, the latter being a major expense of algal cultivation. Parallel placement of flat panel or vertical tubular PBRs can be optimally spaced to create shading between adjacent reactors, creating a 'light dilution' effect that can lower photoinhibition at peak solar times (Slegers et al., 2011, Slegers et al., 2013). Other benefits of PBRs include: reduced evaporation and $CO_2$ losses; low contamination risk in closed systems; maintenance of axenic cultures; and tighter control of temperature, nutrient inputs and gas exchange (Dillschneider and Posten, 2013). Disadvantages include: a smaller thermal culture mass that can result in heating issues; problems with gas exchange in certain systems, particularly $O_2$ build up; surface fouling; and difficulties with scaling (Wolf J., 2016). The higher costs of PBRs have to date limited them to high value products such as astaxanthin or smaller volumes, such as for in-house production of aquaculture feed in hatcheries (Borowitzka, 1999b). However, a recent economic analysis by Barbosa (2014) on a range of algal production systems projected that flat panel reactors were the most economical, with potential production of algae forecast at €1.37 $kg.^{-1}$, while Algenol chose flat panel-like bag reactors over open ponds for production of low-cost fuels.

### 1.3.2 Strain selection and bioengineering

Microalgae are extremely diverse, with over 35,000 species known and up to 800,000 species estimated to exist in the wild (Cheng and Ogden, 2011). Despite this, only a few hundred have been screened, and a limited number of species are used for commercial applications (**Table 1-1**). Recent biodiscovery efforts have focused on collecting endemic cultures that may be better suited to local conditions (Jakob et al. 2015) or from unusual environments such as desert crusts (Treves et al., 2013). Depending upon the use of microalgae and the culture conditions, an 'ideal' strain for commercial cultivation should ideally possess a number of traits such as: high lipid content and quality; production of high value chemicals; fast growth; ability to outcompete competitors; flocculation for ease of harvesting; tolerance to high salinity; tolerance to shear stress; and tolerance to high nutrient loads and/or toxins for use of wastewater or industrial flue gas or for bioremediation.

In terms of light capture, and given that bioreactors are designed to operate under high light levels, ideal strains should possess optical properties which mean that they absorb only as much light as they need, so that excess light is transferred to cells deeper in culture. However, microalgae in nature have evolved selective advantages that may be disadvantageous to mass culture. Analogous to the 'selfish organism' approach, when algae cells perceive themselves to be under light limiting conditions, such is the case of high-density cultures, they increase their light harvesting capacity (see *1.6.7 Photoacclimation*). In doing so, they shade cells deeper in the culture and excess light absorbed is either wasted via NPQ or contributes to photodamage.

One solution is to engineer algal strains with permanently small light harvesting antenna systems. Polle et al. (2003) first isolated a truncated light-harvesting antenna mutant of *C. reinhardtii*, named *tla1,* via DNA mutagenesis and screening of light-green phenotypes. The *tla1* mutant exhibited a 50% and 65% reduction of LHCI and LHCII respectively and higher PCEs, whilst its sequencing revealed a novel gene involved in the regulation of antenna proteins. More targeted approaches followed, including RNA interference (RNAi) mediated down regulation of the entire LHC gene family in the *Stm3LR3* line (Mussgnug et al., 2007), which displayed a two-thirds reduction in chlorophyll, less photoinhibition and improved quantum yield under high light (**Figure 1-3**).

Beckmann et al. (2009) transformed a permanently active variant of the NAB1 repressor of LHC translation, resulting in a 50% increase in PCE at saturating light compared to the parental strain. In contrast, some studies reported lower productivities of antenna mutants in comparison to their wild-type counterparts in laboratory and outdoor conditions (de Mooij et al., 2014, Huesemann et al., 2009). Reasons postulated are possible higher respiration rates on a per chlorophyll basis, and lower photosynthetic rates on a per cell basis, particularly under low light; or higher susceptibility to photodamage due to compromised photoprotective mechanisms (Formighieri et al., 2012).

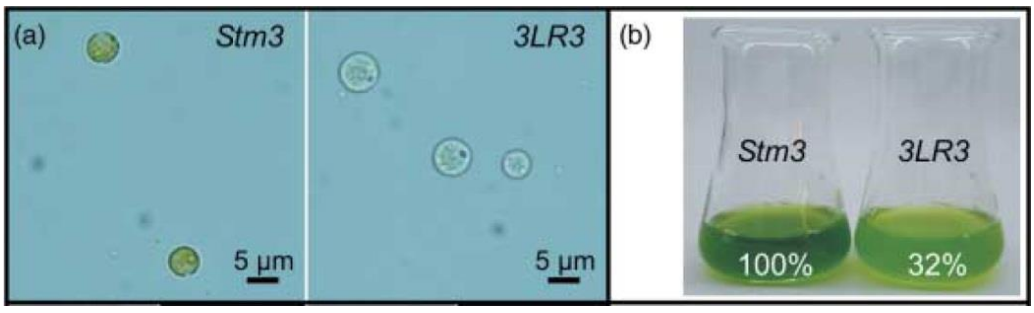


**Figure 1-3**. Phenotypic comparison of the high hydrogen producing *C. reinhardtii* strain *Stm3* and its truncated light harvesting antenna mutant *Stm3LR3*. a) Microscopy images of normally pigmented *Stm3* cells and reduced pigmented *Stm3LR3* cells. b) Cultures of *Stm3* and *Stm3LR3* adjusted to equal cell numbers. Relative chlorophyll concentrations are indicated. Reproduced with permission from Mussgnug et al. (2007).

Understanding the conditions and pathways that lead to high light acclimation in natural cells, and a better understanding of the complexity of light harvesting antenna systems is critical for the development of more strategically engineered mutants to fine-tune the photosynthetic apparatus in such a way that is best suited for biotech applications. Recent highly targeted approaches are offering promise, such as the triple knockdown of LHCBM1, LHCBM2, and LHCBM3 genes involved in expression of the outer antenna proteins (Oey et al., 2013)

## 1.4 The importance of light-limited photosynthetic models for algal biotechnologies

Mathematical models of light-limited photosynthetic growth have become a valuable tool for advancing algal biotechnologies. Several types of model exist, for different purposes. From a pure science level, mechanistic type models can help to support or refute hypotheses concerning the complex biological and metabolic processes involved in light-to-biomass conversion. Indeed, in order to model a system well, first requires a good understanding of it. At an applied level, output-based models are advantageous in two ways: firstly, they enable rapid assessments of different input criteria that can guide the development of advanced systems, optimise process control and select for suitable algal strains in order to maximise the desired output (in this case biomass). Secondly, robust models can provide realistic productivity estimates for techno-economic analyses (TEA) and life cycle analyses (LCA). To date, these studies have mostly extrapolated estimates from laboratory studies where algae are grown under near-optimal light conditions, or from other pilot or scale up facilities where conditions may vary significantly to those being assessed.

Whilst a variety of light-limited growth models have been described, most have been developed and validated for steady state irradiance where incident light flux and/or cell concentration is held constant (Bernardi et al., 2014, Geider et al., 1996). Some models have incorporated square wave or flashing light / dark cycles (Wu and Merchuk, 2001, Rubio et al., 2003, García-Camacho et al., 2012). Other models applicable to outdoor scale-up conditions have not been validated (Slegers et al., 2013, Slegers et al., 2011, Molina Grima et al., 1999). To this end, robust models that are applicable to and validated under light conditions representative of 'real world' systems are needed.

## 1.5 Thesis objectives and outline

The overall aims of this thesis study were to:

1. Develop a model that could accurately predict biomass productivities in conditions representing solar-illuminated algal production systems under both batch harvest and continuous modes of operation. In this context, the light regime is defined by daily and

seasonal variations in incident light, strong light gradients as cells are mixed through mass cultures, and, for batch harvest, changes in the optical properties as the culture density evolves;

2. elucidate the effect of the complex interaction of constantly changing light fluxes with the photosynthetic response of the cell (using the model alga *Chlamydomonas reinhardtii* as a reference); and
3. identify key opportunities that could enable higher biomass productivities in outdoor production systems.

Since algae have the potential to sequester high amounts of carbon and can be used for a range of different products, the focus was on increasing total biomass productivity, rather than a particular product (for instance, total lipids for biodiesel or pigments for nutraceuticals).

The remainder of Chapter 1 consists of a literature review on microalgal photosynthesis with a particular focus on responses under fluctuating light cycles, including photoregulation and photoacclimation processes, in addition to PCEs and productivities in comparison to cells under constant light. It should be noted that this literature review was conducted retrospectively, in light of the knowledge uncovered about these important mechanisms during this study. The remaining chapters are written chronologically, as follows:

Chapter 2 describes an initial development of a simple semi-predictive model. The model was designed as a decision-making tool to assess productivities in order to guide reactor design, process optimisation and strain selection as part of a larger pilot study at the group's Solar Biofuels Research Centre (SBRC), Pinjarra Hills, Qld. The model required a minimum number of inputs including: daily solar radiation data, local coordinates and system geometry, to calculate the amount of light captured at the reactor interface and its transfer through the liquid culture. Based on the 4-light zone model of Grobbelaar (2010) described above, it relies upon the prediction of local growth rates through the mass culture as a function of local light intensities using a static Haldane growth model. This requires a minimum number of parameters that are easily found from empirical growth-irradiance ($\mu$–$I$) response curves. Preliminary model simulations were performed to assess the theoretical upper limits of areal and volumetric biomass productivities in the sub-tropical location of Brisbane, Australia – the site of the Solar Biofuels Research Centre's pilot plant. The design criteria assessed were: reactor type (open ponds or flat panel reactors, FPRs); operating mode (batch or continuous); culture optical density, and for FPR systems, the spacing distance to reactor height ratio and the orientation. Three different strains were assessed including: *C. reinhardtii*, the low-chlorophyll *tla1* and a fast-growing *Chlorella* strain, 11_H5.

Chapter 3 describes experiments conducted to validate the growth behaviour of *C. reinhardtii* and *tla1* against model predictions. A novel laboratory-based environmental photobioreactor (ePBR) matrix was used that allowed for tight control of all other variables, such that light was the only limiting factor governing growth. Each ePBR was fitted with a programmable LED panel above that can simulate different diurnal cycles. To ascertain the model's capability to predict growth under a full year of light conditions, three 'typical' solar days in Brisbane were used for validation, representing relatively low, moderate and high light days. In addition to growth, supporting data collected including changes in pigment content, fluorescence kinetics, pH and dissolved $O_2$ throughout the 7–9 day cultivation periods. The experiments revealed that while it operated well within a defined set of conditions, the Haldane growth model could not satisfactorily predict long-term changes under batch harvest operation and a range of different incident light conditions. It was concluded that a problematic assumption underlying this model was that growth could be validly estimated in a light zone without reference to the local recent history of the cells.

In an effort to improve the quality of modelling, Chapter 4 consists of an experimental study to explore changes in photosynthesis in response to both relatively slow diurnal light cycles and relatively rapid cycles of cells mixing through mass cultures. To achieve a highly controllable fluctuation regime, an LED system was used to represent dynamic light fluxes over short timescales (10s) that would normally arise from mixing through a culture. Short cycles were superimposed over diurnal cycles representing changes in maximum irradiance over the course of the day. These two 'mixed' cycles were compared with 'non-mixed' cycles of the same average irradiance (and thus photon flux) to differentiate responses based on total quantity of photons versus light regime. The effects of photoacclimation and regulation under different light regimes and how these influence final biomass accumulation is discussed in the context of including these phenomena in future models.

Based on the experimental evidence obtained from Chapters 3 and 4, and from the literature review, Chapter 5 describes a more dynamic model aimed to incorporate the important affects of fluctuating light on photoacclimation and NPQ processes identified in Chapter 4. A preliminary estimation of model parameters showed a good correlation of the model to the validation data obtained in Chapter 3 under all light conditions.

Finally, Chapter 6 provides concluding remarks about the findings of this study and future perspectives.

## 1.6 Literature review: photosynthesis of microalgae and its regulation under fluctuating light

Photosynthesis is arguably the most important process for life on earth. This ancient (at least ~2.7 byr) process converts chemical $CO_2$ into organic carbon compounds that feed the biosphere. It is responsible for the atmospheric accumulation of $O_2$ that has enabled aerobic respiration and the subsequent evolution of more complex life forms. Light reactions involving $O_2$ in the stratosphere formed an ozone layer that absorbs 97–99% of harmful UV radiation and thus allowed plants and animals to emerge from the sea and colonise land approximately 500 myr ago. Over this same time period, the burial of a significant amount of fixed carbon has reduced the potent greenhouse gas $CO_2$ ~20-fold, resulting in a ~14$^{o}$C lower mild global mean temperature today (Retallack, 2002). Moreover, this buried storage of photosynthates is now the fossil energy that is used to fuel the global economy.

The photosynthetic machinery of plants and algae is a highly evolved, complex system designed to balance maximising light harvest for growth under low light whilst minimising its deleterious consequences when light supply exceeds photosynthetic capacity (Rochaix, 2011). Under optimal steady state light flux, a balance of mostly linear and some cyclic electron flows create a high ΔpH in the lumen needed to power ATP synthase and ensure the strict stoichiometry of ATP:NADPH required by the Calvin-Benson-Bassham (CBB) cycle such that carbon assimilation runs at near maximum efficiency (Strand et al., 2016, Cardol et al., 2011). In contrast, light fluctuations, particularly from light to total darkness and *vice versa*, disrupt the strong pH gradient of the thylakoid lumen and consequently slow down the ATP synthase upon returning into the light, relative to the rate of electron transfer (Rochaix, 2011). Consequently, a low ATP:NADPH ratio reduces carbon assimilation (Cardol et al. 2011). Upon transition from dark to light, linear electron flows proceed, but NADPH is not consumed fast enough by the CBB cycle because of a lack of ATP, running the risk of over-reducing the photosynthetic electron chain. Without sufficient electron sinks, highly charged electrons can react with molecular oxygen to form reactive oxygen species (ROS) that can damage photosystem II (PSII) or, worse still, photosystem I (PSI) which lacks an efficient repair system (Cardol et al. 2011).

Moreover, efficient photosynthetic energy conversion requires synchronisation of the light-driven PSI and PSII during extreme light fluctuations (Tikannen et al. 2012). Such rapid transitions from dark to light can imbalance the excitation energy distribution between the two photosystems. Abrupt shifts in light quality and quantity, as occur commonly in well-mixed algal production systems,

disrupt the redox poise of the photosynthetic machinery creating a situation that potentially is highly damaging, in addition to reducing photosynthetic productivity (Tikannen et al. 2012).

Not surprisingly, a large discrepancy exists between reported growth rates of algae grown under constant light in the laboratory and outdoor production systems (Melis 2009; Wolf et al. 2016). Partly this is explained by the fact that, in the former scenario, algae are able to *photoacclimate* to the steady state light conditions that they are subjected to by adjusting their light harvesting capacity to suit the given light conditions. In the latter scenario, algae are subjected to constant variations in light quality and quantity from diurnal and seasonal cycles, abrupt changes in weather (i.e. intermittent cloud cover or tropical afternoon storms), and rapid fluxes as they are mixed through dense cultures. Here, the relatively slow *photoacclimation* timeframe (several hours) required for changes in protein and pigment expression levels means that cells must continually attempt to acclimate to new light conditions but will unlikely reach an optimal state. It is also possible that light fluctuations may interfere with feedback signals involved in gene expression that are designed to acclimate the cell to its environmental conditions.

To this end, rapid *photoregulation* mechanisms, which operate on timescales of milliseconds to minutes have evolved to allow organisms to adapt to such changes in light fluxes. Such mechanisms will be most closely adapted to the situations in the natural ecology of algae which exert the highest selective pressure on the species (which may not necessarily be their most usual state). These mechanisms will play a critical role in the performance of well-mixed algal mass cultures, and include NPQ, alternative electron flows and regulation of enzyme activities, which aim to restore redox homeostasis in the cell. As reviewed below, a growing number of studies of knockout mutants devoid of various *photoregulation* mechanisms show that algae and plants are mostly able to cope or compensate under constant light (often even under high light), yet serious consequences to algal viability are observed under fluctuating light, or upon transitions from darkness to light or *vice versa*.

Understanding the consequences of fluctuating light on the photosynthetic machinery and the mechanisms that permit efficient photosynthesis under these conditions is vital from both a pure science perspective, to develop more robust models, and for practical reasons to increase photosynthetic productivities for foods, fuels and commodities. Here, photosynthesis, its regulation over long (*photoacclimation*) and short (*photoregulation*) timescales, and the cause and effect of *photoinhibition* is reviewed briefly below. A particular focus is given to these processes in the context of fluctuating light and where appropriate, to their effects on the model alga, *Chlamydomonas reinhardtii*, the subject of this study.

### *1.6.1 Chlamydomonas reinhardtii*

Whilst there are several algal species preferred for commercial cultivation (**Table 1-1**), *Chlamydomonas reinhardtii* was selected as the control species for this study because: 1) it is the target organism for most genetically modified cell lines aimed at improving photosynthetic productivity; 2) it is the model organism for photosynthetic research and there is a large body of information on its photosynthetic responses to various light conditions; and 3) its fully sequenced genomes (nucleus, chloroplast and mitochondria), expanding repertoire of transformation methods and ability to grow under heterotrophic conditions have allowed for investigation of the knockout or repression of a number of genes involved in photosynthesis without lethal consequences (Grossman et al., 2004). Studies of *C. reinhardtii* have been vital to elucidate the structure of photosynthetic complexes and key processes such as NPQ, cyclic electron flows, state transitions and circadian rhythms among others, in both algae and higher plants (Rochaix, 2002, Depège et al., 2003, Elrad et al., 2002, Fleischmann et al., 1999, Givan and Levine, 1967, Lavorel and Levine, 1968, Niyogi et al., 1997).

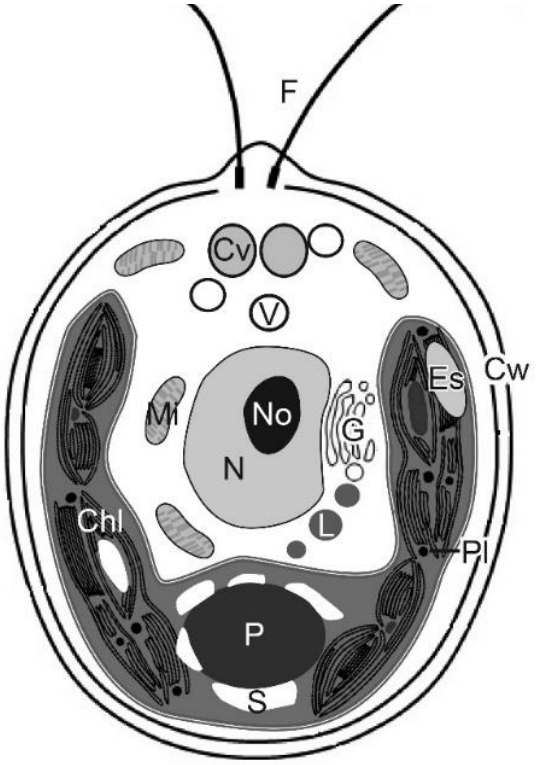


**Figure 1-4**. Schematic of a *Chlamydomonas reinhardtii* cell. Chl, chloroplast; $C_v$, contractile vacuole; Cw, cell wall; Es, eyespot; F, flagella; G, Golgi apparatus; L, lipid body; Mi, mitochondria; N, nucleus; No, nucleolus; P, pyrenoid; Pl, plastoglobuli, S, starch grain; v, vacuole (figure recreated with inspiration from Harris 2001 and Engel, Schaffer et al. 2015).

*C. reinhardtii* (class Chlorophyta) is a simple unicellular spheroid of approximately 10 µm originally isolated from soil (**Figure 1-4**). Its two anterior flagella enable phototaxis (movement toward or away from light), which employs photoreceptors within the so-called 'eyespot'. It has a large, single cup-shaped chloroplast that accounts for approximately half the cell's volume (Engel et al., 2015). At the base centre of the chloroplast resides a large body known as the pyrenoid surrounded by a starch sheath. The pyrenoid is the site of carbon fixation and contains a high concentration of Rubisco with associated proteins and a system of transporters which bring in $CO_2$ to form a carbon concentrating mechanism (CCM). *C. reinhardtii* has a relatively short life cycle and a rapid doubling time under ideal light of ~6-8 hours (Harris, 2001).

### 1.6.2 Structure of the photosynthetic apparatus

In eukaryotes, photosynthesis takes place in specialised double-membrane bound organelles known as chloroplasts, believed to be descendants of an ancient photosynthetic cyanobacterium that was engulfed by a eukaryote. The aqueous fluid that fills the inner space of the chloroplast is the stroma and contains chloroplast DNA, plastoglobuli, ribosomes, and other proteins. Suspended in the stroma is the network of thylakoid membranes, the site of the light reactions. The complex arrangement of thylakoids consists, in plants, of a number of tightly stacked membranes known as grana. In algae, thylakoid stacks are analagous to the grana in plant chloroplasts. Their arrangement creates internal pockets (lumenal spcaes) between layers that are separated from the inter-thylakoid stromal space and the chloroplast stroma (Engel et al., 2015).

Granal stacks are interconnected by longer thylakoids known as the stroma lamellae that wind around them in a helical manner and interconnect different regions. *In situ* cryo-electron tomography analysis on the native architecture of *C. reinhardtii* revealed thylakoid stacks were connected to the pyrenoid via cylindrical tubules and several associated minitubules (Engel et al., 2015). The authors suggested that these tubules may act as channels for the diffusion of small molecules between the stroma and pyrenoid, thereby connecting products from the light reactions and the CBB cycle. Embedded in the thylakoid membranes are the protein complexes that carry out the light reactions: PSII and PSI and their surrounding light harvesting complexes (LHCs) which form the supercomplexes PSII-LHCII and PSI-LHCI (**Figure 1-5**), cytochrome *b6f* (Cyt$b_6f$) and ATP synthase.

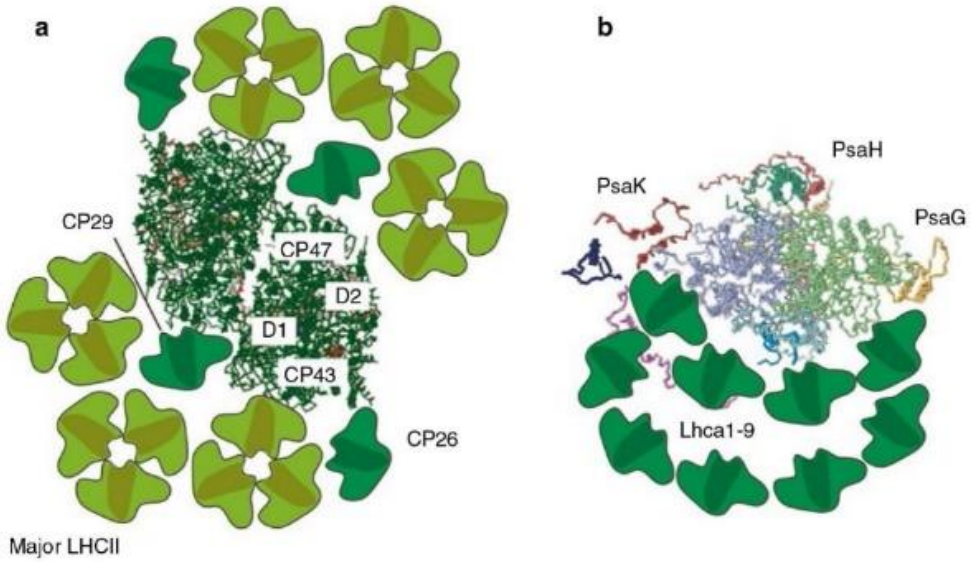


**Figure 1-5**. Supramolecular organization of a) PSII-LHCII and b) PS I-LHCI supercomplexes in *C. reinhardtii* based on the single-particle image analysis by Tokutsu et al. (2012) and Drop et al. (2011) respectively. Reproduced from Finazzi (2014).

PSII-LHCII and most of the mobile LHCII is enriched in granal stacks, while the bulky protrusion of PSI-LHCI and the ATP synthase confines them to the less appressed stroma lamellae. Cyt$b_6f$ is found in both regions (Austin and Staehelin, 2011). The mobile carriers plastoquinone (a small molecule quinone within the membrane) and plastocyanin (a globular protein within the lumen) shuttle electrons between PSII, Cyt$b_6f$ and PSI and the stromal-localised ferredoxin shuttles electrons from PSI to $NADP^+$ or other target molecules.

### 1.6.3 Light harvesting

Photosynthesis begins when photons are absorbed by pigment molecules. The precise distance between pigments and the highly organized arrangement of the LHCs and the photosystem subunits that bind them permit resonance energy transfer, funneling excitation energy toward the specialised chlorophyll dimers of P680 and P700 in the reaction centres of PSII and PSI respectively.

In *C. reinhardtii*, LHCs are arranged into outer major trimeric subunits that funnel captured light to the minor complexes (CP24, CP26 and CP29) and CP43 and CP47 that reside in the PSII core (**Figure 1-5**). The core antenna subunits contain chlorophyll *a* (Chl *a*), while the peripheral antenna combine Chl *a* and Chl *b* and accessory carotenoids (Car) (Dekker and Boekema, 2005), which have different action spectra, enabling a greater use of the broad solar spectrum (**Figure 1-6**).

Chl *a* and Chl *b* absorb strongly in the red and blue regions at 435 and 676 nm, and 475 and 650 nm respectively and Car absorbs in the blue region between 400–550 nm. The poorly absorbed region around 550 nm results, in plants and the Chlorophyte algae, in a characteristic green colour.

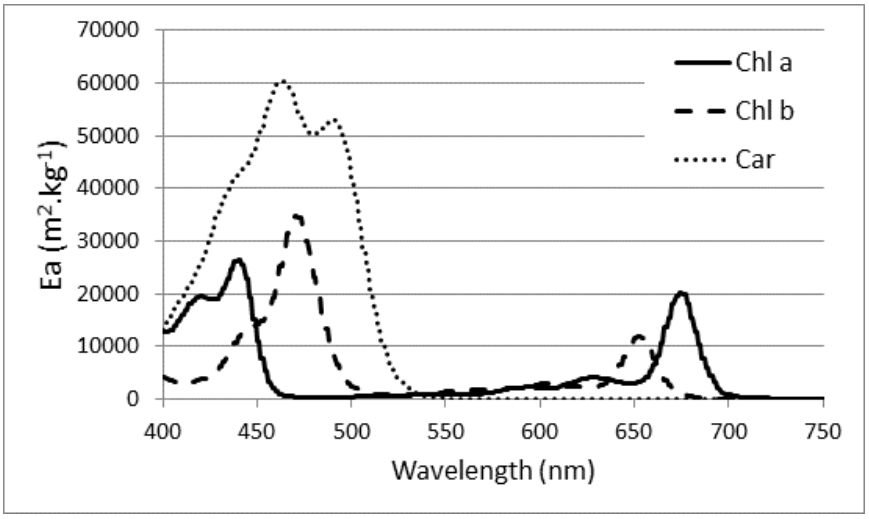


**Figure 1-6**. Absorption coefficient, $E_a$, of the major light harvesting pigments (pure) *in vivo* (Bidigare et al., 1990).

### 1.6.4 Linear electron flow: the 'Z' scheme of the light reactions

Linear electron flow (LEF) from an electron donor (water) to an electron acceptor (NADP+) results in the production of NADPH and ATP required to reduce $CO_2$ into organic compounds in the CBB cycle (**Figure 1-7**). Upon charge separation, the photochemically excited P680 chlorophyll dimer of PSII releases two electrons for every two photons absorbed to the bound plastoquinone $Q_A$, then to the mobile carrier plastiquinone $Q_B$, which is reduced, incorporating two protons from the stroma. Meanwhile, the lost electrons from P680 are replenished from the manganese cluster (also known as the oxygen evolving complex; OEC). After two further reactions, the fully oxidised Mg cluster catalyses the splitting of two $H_2O$, producing molecular oxygen and releasing four protons into the lumen. Reduced $Q_B$ undocks from PSII and docks to the $Q_O$ site of Cyt*b*$_6$*f*. Oxidation of $Q_B$ by Cyt*b*$_6$*f* releases two protons into the lumen, contributing to the buildup of a proton gradient that is used, along with the protons derived from $H_2O$, to drive the ATP synthase for ATP production. Of the two electrons absorbed by Cyt*b*$_6$*f*, one is shuttled through the high potential chain to the Rieski protein and Cyt*b*$_6$*f* and onto plastocyanin in the lumen, while the other is shuttled through the low potential chain to cytL and cytH onto a quinone at the $Q_i$ site to form a semiquinone (Rochaix, 2011). Plastocyanin is oxidised by the light-driven PSI complex and the electrons are passed through PSI's three internal 4Fe-4S centers ($F_X$, $F_A$, and $F_B$) to the mobile carrier ferredoxin, which shuttles the electrons to the Ferredoxin NADP Reductase (FNR) complex. After two electrons are transferred to FNR, NADPH is formed by combining the two electrons and one proton with $NADP^+$. Concurrently, the proton gradient created by the electron transport chain is utilised by ATP synthase to generate ATP from ADP and $P_i$ in a process homologous to that used in mitochondria. For a minima of 8 photons absorbed (4 by PSII and 4 by PSI), LEF yields $4e^-$ and 12 $H^+$ leading to 2 NADPH and ~2.57 ATP, or an ATP : NADPH ratio of ~1.28 (Rochaix, 2011) and the release of 1 $O_2$.

### 1.6.5 The Calvin-Benson-Bassham (CBB) cycle

The CBB cycle reduces $CO_2$ with $H_2O$ into sugars via 13 reactions carried out by 11 enzymes using the energy from ATP and NADPH. Broadly the cycle is divided into three phases: 1) carbon fixation; 2) reduction reactions; and 3) regeneration of ribulose 1,5-bisphosphate (RuBP). Carbon metabolism is initiated by ribulose-1,5-bisphosphate carboxylase/oxygenase (Rubisco) which catalyses the carboxylation of RuBP with atmospheric $CO_2$ to form two molecules of 3-phosphoglyceric acid (3-PGA). In the second step, 3-PGA is reduced to glyceraldehyde 3-phosphate (G3P). Lastly, regeneration of three RuBP occurs using in a complex series of reactions that rearrange five G3P, leaving a net gain of one G3P for the consumption of three $CO_2$, nine ATP and six NADPH.

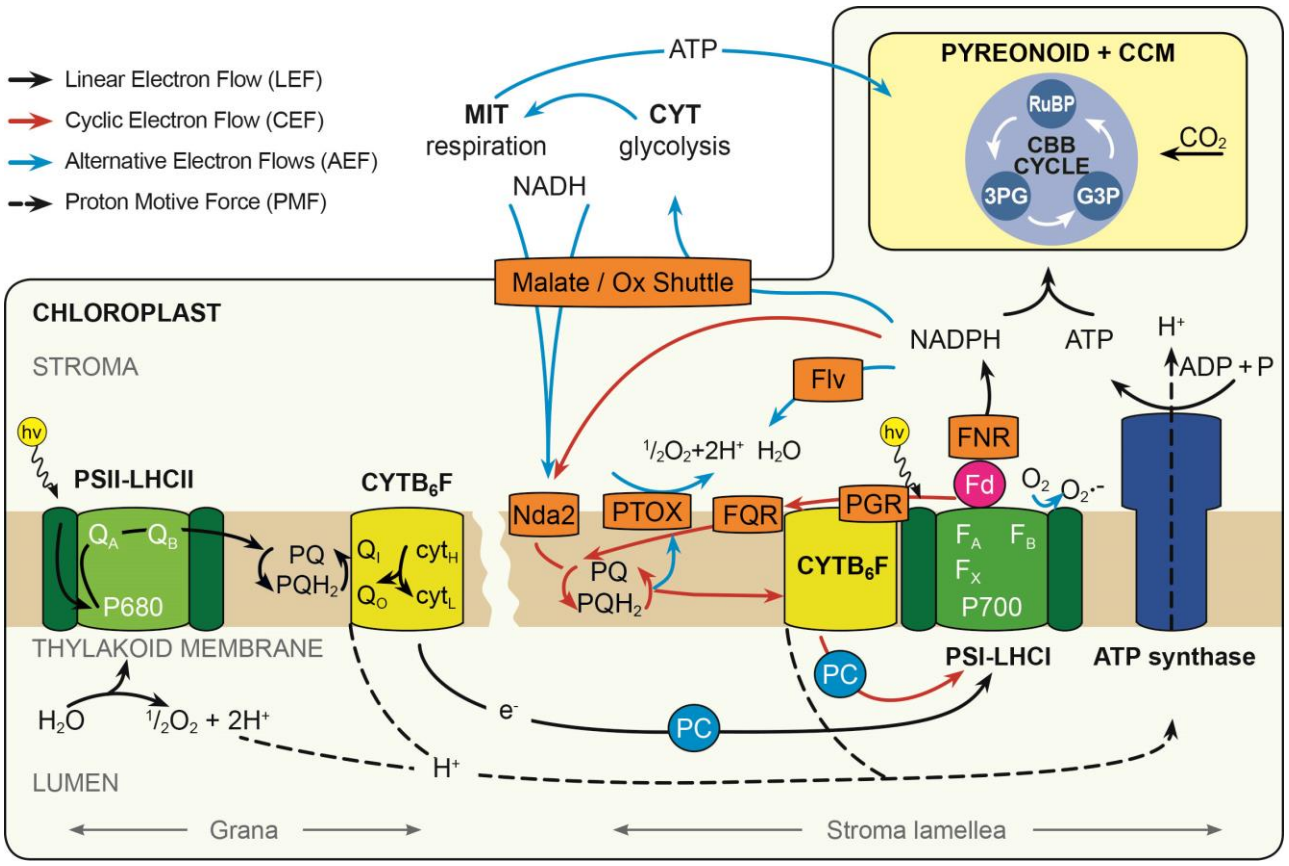


**Figure 1-7**. Schematic representation of the various electron flows of photosynthetic pathways in order to balance the requirements of ATP and NADPH. Black solid arrows depict linear electron flows (LEFs) that generate NADPH and ATP required to drive the CBB cycle; red arrows depict the two pathways of cyclic electron flows: the NDH pathway and the pgr5 pathway that produce ATP without the net production of NADPH. Note that the pgr5 pathway is proposed to involve formation of a supercomplex (not illustrated, see text for details). Blue arrows depict alternative electron flows including the Mehler reaction on the stromal side of PSI, Flv activity and plastid terminal oxidase (PTOX) activity which all result in $O_2$ reduction (water-water cycles). Reducing equivalents can be exported to the mitochondria via the Malate valve to form additional ATP i.e. for the CBB cycle, or can be imported to be used in the chlororespiratory pathway involving Nda2 and PTOX. Figure produced by author with inspiration from Cardol et al. (2011) and Rochaix (2011).

### 1.6.6 Too much of a good thing: light-driven production of Reactive Oxygen Species (ROS) and photoinhibition

The rate of LEF and carbon assimilation in *C. reinhardtii* is much slower than the photon flux densities (PFDs) encountered under full sunlight with photosynthetic saturation occurring ~80-200 $\mu mol.m^{-2}.s^{-1}$ depending on its acclimated state (cf an incident flux of ~2,000 $\mu mol.m^{-2}.s^{-1}$ in full sunlight). Excess light absorption and other environmental stresses (e.g. heat, high salinity, nutrient limitation) can lead to damaging ROS formation via two pathways. The first involves electron transfer to molecular oxygen at the acceptor side of either PSII or PSI, causing formation of the superoxide

radical ($O_2^-$), which can also react to form hydrogen peroxide ($H_2O_2$) or hydroxyl radicals (·OH). The second pathway occurs via triplet excited chlorophylls ($^3Chl^*$) which pass energy to molecular oxygen, leading to the formation of singlet oxygen ($^1O^*$) (Havaux and García-Plazaola, 2014). Notably, although harmful at higher concentrations, low levels of ROS play an important role in signaling for certain regulation mechanisms (Borisova-Mubarakshina et al., 2015, Iigusa et al., 2005, Apel and Hirt, 2004).

Algae possess several redox-regulated mechanisms to balance electron flows, however some ROS formation is inevitable, leading to photodamage at all light intensities. A noticeable decline in photosynthetic rates (i.e. photoinhibition), however, only occurs when the rate of photodamage exceeds the rate of repair (Adir et al., 2003). Mostly damage occurs to the D1 protein within the reaction centre of PSII, but photodamage can also occur to the oxygen evolving systems, electron carriers, D2 proteins, and the LHCII pigments and proteins (Adir et al., 1990). D1 damage triggers a repair process that involves migration of PSII to the stromal thylakoids where the D1 reaction centre protein is excised and degraded and a new D1 is inserted. The reconstructed PSII migrates back to granal membranes where other components of PSII are reassembled and become functional (García-Camacho et al., 2012).

The high efficiency of the PSII repair system results in photoinhibition only becoming evident when its rate exceeds that of repair, such as under long-term (> hours) high light exposure. In fact, Tikkanen et al. (2012) postulated that PSII photoinhibition is a major photoprotective mechanism because detached photoinhibited PSII centres and their LHCs slow down electron transfer, consequentially protecting PSI, which lacks an efficient repair system. This theory is supported by studies that found PSI damage was completely dependent on electron flow from PSII, as blocking LEF by 3-(3,4-dichlorophenyl)-1,1-dimethylurea (DCMU) prevented PSI damage (Sonoike and Terashima, 1994, Havaux and Davaud, 1994). Moreover, a study by Neale and Melis (1990) indicated that a 'reserve' pool of PSIIs exist in *C. reinhardtii* that are unable to reduce Qb under normal conditions, but convert to a Qb-reducing state when high levels of the majority pool of PSIIs become damaged in order to maintain photosynthetic rates.

Previously, the slowly-developing NPQ process (qI) that occurs on the order of minutes was thought to be due to heat dissipation occurring in detached photoinhibited PSIIs (Oja and Laisk, 2000). However, Sarvikas et al. (2010) showed that damaged PSIIs did not in fact protect the remaining PSIIs as photoinhibition continued to follow first-order kinetics with respect to light in lincomycin-treated pumpkin (*Cucurbita pepo* L.) and pepper (*Capsicum annuum* L.) leaves *in vivo*.

The *C. reinhardtii* mutant, *npq1* which lacks zeaxanthin showed no qI quenching, indicating that energy-dissipating xanthophylls were, in fact, the mode of action for qI (Baroli et al., 2003, Bonente et al., 2011). In green algae, the xanthophyll cycle occurs when violaxanthin is converted to zeaxanthin upon de-epoxidation via the intermediate antheraxanthin. This reversible reaction is driven by the light-driven splitting of water, via a response to ΔpH of the thylakoid lumen, ensuring that zeaxanthin only accumulates under high light (Jahns et al., 2009). In addition to energy dissipation, zeaxanthin plays a major role in ROS scavenging and detoxification (Dall'Osto et al., 2010). Additional ROS detoxification is mediated by glutathione peroxidases, peroxiredoxins and methionine sulfoxide reductases which are regenerated by thioredoxins (Michelet et al., 2013).

### 1.6.7 Photoacclimation

A major strategy to optimise light utilization and avoid photoinhibition is *photoacclimation*. Acclimation processes involve transcriptional changes induced by the surrounding light environment and typically occur on relatively slow timescales of 5 hours or more (Litchman, 2000, Neale and Marra, 1985). Light harvesting capacity is the most important and evident phenotype of photoacclimation, resulting in changes of cellular pigment content via adjustments of either LHC antenna size; the number of photosystems; PSII : PSI stoichiometries; or pigment stoichiometries (Bonente et al., 2012, Dubinsky, 2009). The increase in cellular absorption cross sections is not linear with pigment levels however, due to the so called 'packaging effect'. Since the cellular absorption cross section is the product of chlorophyll and the chlorophyll-specific cross section, the latter is reduced because of mutual shading of pigments with a concurrent increase in pigments or cell size (Kono et al., 2014, Dubinsky, 2009, Geider et al., 1996).

Under steady state light, Bonente et al. (2012) reported high light acclimation of *C. reinhardtii* led to a nearly 3-fold reduction in chlorophyll compared to low light treated cells, but a concomitant accumulation of relatively high amounts of zeaxanthin and lutein involved in photoprotection. The authors found the average antenna size of both photosystem I and II was, in fact, not modulated by acclimation; rather, the regulation affected the PSI : PSII ratio. In addition, high levels of LHCSR3 were accumulated, the primary protein involved in energy-dependent NPQ; and higher photosynthetic rates occurred on a per chlorophyll basis, despite Rubisco levels being similar.

A growing number of studies are providing insight into photoacclimation effects under fluctuating light, including those relevant to algal mass culture (sub-seconds to seconds cycle times) or for phytoplankton in natural water (hours cycles). In these studies, light fluxes are typically either performed as square wave light / dark cycles or sinusoidal curves. For algal biotech studies, evidence

suggests that several green algae including *C. reinhardtii*, *Nanochloropsis salina, Scenedesmus obliquus* and *Chlorella* sp. and other green algae acclimate to a lower perceived light level under light/dark fluctuations than under constant light of the same average irradiance (Grobbelaar et al., 1996, Janssen et al., 1999, Sforza et al., 2012, Takache et al., 2015). Under a light fraction of 0.67 and 13s cycle time, Janssen et al. (1999) reported *C. reinhardtii* increased its Chl *a* content two fold compared to continuous light of the same average irradiance ($I_{avg}$). Even under sub-second light/dark cycles, Sforza et al. (2012) showed Chl *a* contents were 2 and 5 times higher than cells under the same $I_{avg}$ under continuous moderate (120 $\mu mol.m^{-2}.s^{-1}$) and high (1,000 $\mu mol.m^{-2}.s^{-1}$) light respectively. Under slower vertical mixing cycles mostly related to phytoplankton studies (*in situ* or laboratory simulated), several algae also acclimated to a lower apparent state than the average irradiance including *Dunaliella tertiolecta, Phaeocystis globulosa*, *Thalassiosira weissflogii, Microcystis aeruginosa*, and *Planktothrix agardhii* (Havelková-Doušová et al., 2004, Ibelings et al., 1994, Fietz and Nicklisch, 2002, Flameling and Kromkamp, 1997), although some phytoplankton acclimated to the average (Vincent et al., 1994) or higher (Falkowski and Wirick, 1981, Denman and Marra, 1986) irradiance.

A study by Grobbelaar et al. (1996) using square wave light/dark fluctuations ranging from 0.1ms–10s found that photoacclimation was governed by the duty cycle time (or mixing frequency), rather than to a specific light/dark ratio, whereby rapid duty cycles caused cells to become acclimated to a higher perceived light than slower duty cycles in this range.

The molecular signals that lead to acclimated phenotypes appear to be governed by the redox state of different components in the electron transport chain (Escoubas et al., 1995) or ROS signalling (Borisova-Mubarakshina et al., 2015). For instance, the regulation of nuclear encoded *Lhcb* gene expression is shown to be regulated by changes in the redox state of the PQ pool (Durnford and Falkowski, 1997) and also by hydrogen peroxide ($H_2O_2$), which may act as an inhibitor (Borisova-Mubarakshina et al., 2015). Therefore, it is conceivable that low-light acclimation occurring in mixed dense cultures may result from both re-oxidation of the PQ pool upon constant transitions from light to darkness, and lower $H_2O_2$ production from short bursts of high light as the cells come to the surface.

The acclimation state of algae has dramatic consequences on photosynthetic rates and therefore should be a critical component of light-limited models. High light acclimated algae appear to be more beneficial to dense cultures as they have higher maximum photosynthetic rates. In fact, Melis (1999) showed 2–3 fold higher PCEs in high light acclimated *Duniella salina*. However, they also have higher respiration rates. Photosynthesis saturates at higher light intensities (higher $E_k$), while

photoinhibition ($\beta$) is reduced by a combination of higher NPQ and less absorption (Bonente et al., 2012, Grobbelaar et al., 1996, Grobbelaar et al., 1995, Melis, 1999). Furthermore, high light acclimation may be beneficial to energy storage (starches or lipids), as less energy is required for synthesis of light harvesting and other photosynthetic complexes (Geider et al., 1996).

### 1.6.8 Photoregulation

The rate of change in light fluxes encountered by microalgae in well-mixed mass culture occurs on the same sub-seconds to minutes scale as *photoregulation* mechanisms and as such, these processes are just as critical as acclimation processes. They are broadly divided into three categories: 1) non-photochemical quenching, which occurs primarily in the light harvesting complexes of PSII, 2) alternative electron flows, which regulate electron transport through the photosynthetic electron transport chain, and 3) redox-controlled post-translational modifications to photosynthetic enzymes, which modulates their activities.

#### *1.6.8.1 Non-photochemical quenching at the level of the light harvesting complexes*

According to Ebonhoe et al. (2014), collectively NPQ is defined as "*all processes that produce a difference between the chlorophyll fluorescence maximum of dark-adapted cells to that observed during subsequent illumination*". The simple model relating chlorophyll fluorescence of PSII shows that excitation energy absorbed by PSII's pigments of the LHCs is competed for by the processes of heat, fluorescence and photochemistry (Baker, 2008). Thus, chlorophyll fluorescence is either quenched via photochemical or non-photoochemical quenching processes. The latter mechanisms include those that either dissipate excess energy as heat or redistribute it to PSI. Therefore NPQ can be considered to be processes that occur in the light harvesting complexes of PSIIs (LHCIIs) to regulate the amount of light funneled to each photosystem's reaction centre. The three components of NPQ in *C. reinhardtii* are classified according to their relaxation times of chlorophyll fluorescence, as: 1) energy dependent quenching (qE); 2) state transitions (qT); and 3) xanthophyll activity (qI, as reviewed above).

#### *1.6.8.2 Energy dependent quenching (qE)*

The most rapid NPQ process is qE, which is activated in response to acidification of the thylakoid lumen. The molecular effectors responsible for qE and their mode of action differ in algae and higher plants. In *C. reinhardtii* and other chlorophytes, the ancient light harvesting complex stress-related protein LHCSR3 is the major effector, whereas in higher plants, it is the PsbS protein. PsbS is constitutively expressed, is linked to xanthophyll activity and involves a re-organisation of the

thylakoid membranes causing quenching sites in both the PSII antenna and the PSII reaction centre (Morosinotto and Bassi, 2014).

In contrast, LHCSR3 appears to be independent of xanthophyll activity despite its ability to bind pigments, as shown by *npq1* mutants deficient in zeaxanthin, which displayed similar qE activity to wildtype algae (Bonente et al., 2011). Liguori et al. (2013) showed that LHCSR3's unique dissipative ability lies in its unusual C-terminus sub-domain, which becomes protonated under acidic luminal conditions, reversibly altering its confirmation from a light harvesting to a dissipative state. Knockout mutants of the LhcbM1 subunit in *C. reinhardtii* show low qE capacity, indicating that this subunit may be the site of LHCSR3 activity (Ferrante et al., 2012). Notably, LHCSR3 is accumulated in response to high light (a *photoacclimation* response) and shows relatively high activation of qE in comparison to PsbS under low light (**Figure 1-8**). This high sensitivity, in conjunction with the phototactic ability of *C. reinhardtii* to move away from light, may explain the acclimation response of LHCSR3 levels to ensure it is synthesised only when needed.

Although qE is often cited as an important regulator under constant high light, recent studies suggest its greatest role is in fact under fluctuating light. For instance, Külheim et al. (2002) compared plant mutants defective in qE (*npq4*) and both qE and xanthophylls (*npq1*) under high light conditions or under 30s light fluctuations. Remarkably, no significant differences in fruit or seed production of the *npq4* and *npq1* mutants were found under high light, both mutants produced ~35% fewer fruits and seeds per plant under fluctuating light conditions. The authors hypothesised that rapid and irregular variations in excitation pressure probably result in greater damage to qE-defective mutants due to an inability to quickly adjust light harvesting.

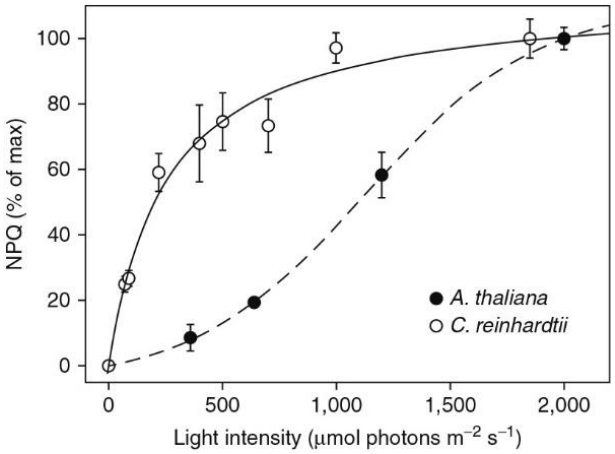


**Figure 1-8**. NPQ profiles of *C. reinhardtii* (open circles) and *A. thaliana* (black circles) in response to actinic light intensity. Both species were acclimated to high light for five days prior to measurements. Figure from Morosinotto and Bassi (2014) with data from Ballottari et al. (2007) and Bonente et al. (2012).

### *1.6.8.3 State transitions (qT)*

PSII and PSI must function in a coordinated manner to maintain efficient LEF and avoid over-reduction or over-oxidation of the PQ pool under changing light conditions. qT redistributes excitation energy between PSII and PSI via the migration of LHCIIs between the two photosystems and an ultrastructural reorganization of the thylakoid (Clowez et al., 2015). A transition from State 1 → State 2 occurs in response to an over-reduction of the PQ pool that is sensed via Cyt*b*$_6$*f*. Here, over excitation of PSII causes $PQH_2$ to bind to the luminal side of Cyt*b*$_6$*f* which activates the serine-threonine protein kinase *Stt7* in algae (homologous to *STN7* in higher plants). *Stt7* causes phosphorylation of LHCII, which dissociates from PSII, reducing its absorption cross section. This process is reversible upon over-excitation of PSI (State 2 → State 1), causing reduction of thioredoxins which act to dephosphorylate LCHIIs that then migrate back to the PSII complex (Finazzi and Minagawa, 2014).

qT is an important photoprotective process in algae, particularly under variable light conditions, as unlike higher plants, high qE requires acclimation to high light and may not be readily sufficient. It was often stated that up to 80% of LHCIIs in *C. reinhardtii* could detach from PSII, however, in variance to previous reports that all detached LHCIIs migrated to PSI, new evidence shows that only a small amount (~10%) attach to PSI (Ünlü et al., 2014). The exact portion of LHCIIs that detach is also unclear, although a large reduction of PSII antenna cross section is observed though this does not match a concomitant increase in PSI antenna size. Although qT was originally thought to be involved with cyclic electron flow, recent evidence of mutants devoid in qT shows that, while these two processes happen coincidentally in response to reducing pressure, they are in fact independent (Takahashi et al., 2013, Terashima et al., 2012).

State 2 transitions are higher in *C. reinhardtii* under low light than under high light (Bonente et al., 2012). Tikkanen et al. (2010) reason that the high dissipation capacity of qE under high light diminishes the need for qT. Under fluctuating light conditions, Tikkanen et al. (2012) reported 'severely stunted phenotypes' in STN7-deficient mutants (*stn7* and *stn7stn8*). The authors stated that "Coordination of excitation energy distribution between PSII and PSI from the common P-LHCII antenna is crucial in preventing the accumulation of electrons in ETC under low illumination phases of fluctuating growth light, and is therefore important for photoprotection of PSI in plant chloroplasts during the subsequent high light peak". In *C. reinhardtii*, an analysis of *npq4* and *stt7-9* mutants devoid in qE and qT respectively, and the double mutant *npq4 stt7-9*, revealed higher amounts of the ROS $H_2O_2$ accumulated in *Stt-7* and double mutants than *npq4* or *wt* cells upon transition from a dark to light period. Furthermore, exposure to high light followed by a dark period showed a transition

back to state 2 in the dark, perhaps due to anticipation of the cell to the onset of high light. This indicates that state transitions play an important protective role in algae under fluctuating light and that light/dark cycles may promote higher state 2 transitions.

### 1.6.9 Alternative electron pathways at the level of the electron transport chain

Efficient photosynthesis is mostly driven by the ATP and NADPH derived from linear electron flows. The strict ATP:NADPH stoichiometry of 1.5 required for carbon assimilation, is slightly higher than that produced in LEFs at ~1.28 (Dang et al., 2014). Moreover this stoichiometry may be further imbalanced by requirements for additional ATP and/or NADPH required for other metabolic pathways (i.e. CCM and protein, lipid and biosynthetic pathways, damage repair, photorespiration, reduction of $NO_x$ and $SO_x$).

In addition to NPQ mechanisms that aim to reduce energy reaching the photosystem reaction centres, algae and plants have evolved a number of rapid regulatory mechanisms operating within the electron transport chain. These alternative electron flows (AEFs) compete with LEFs to restore the ATP:NADPH balance, either by generating more of the former, consuming the latter, or both (**Figure 1-7**). In doing so, AEFs act to maintain high carbon assimilation rates, avoid over-reduction of the ETC and the consequential formation of ROS, and provide a high proton motive force across the thylakoid which also induces qE.

The influence of alternative electron pathways in the conversion of absorbed light into final biomass is indeed significant. Even under steady state optimal light, an estimated 25% of electrons produced by PSII are lost to alternative electron flows in *C. reinhardtii*, rather than used for $NADP^+$ reduction and this increases under light stress (Wagner et al., 2006, Jakob et al., 2007).

#### *1.6.9.1 Cyclic electron flows (CEF) and the role of proton gradient regulators (pgrs)*

CEF is the major competing electron pathway of LEF. It avoids PSII and instead recycles electrons around PSI (**Figure 1-7**), creating a light-driven proton pump across the thylakoid membrane that fuels ATP synthase without net reduction of $NADP^+$ (Breyton et al., 2006). CEF plays a major role in photo-protection by increasing reduction of the PQ pool. As the PQ pool becomes more reduced, mechanisms leading to PSII energy dissipation are engaged, reducing the rate of LEF.

Despite extensive research, the exact mechanisms and components of the CEF system are still debated, but current views support two pathways. In both, it is thought that electrons are transported from the PQ pool to PSI via the same mode as LEF. The return of electrons to PQ can occur via: 1) the pgr5 pathway whereby reduced ferrodoxin (Fd) is oxidised via ferrodoxin quinone reductase

(FQR) to reduce either Cyt*b*$_6$*f* or PQ (Munekage et al., 2002); or 2) NADPH is oxidised by the NAD(P)H dehydrogenase (NDH) complex to reduce PQ (Endo and Asada, 2008). In algae, CEF is proposed to involve the formation of a supercomplex which includes Cyt*b*$_6$*f*, PSI, and / or the FQR-related PGR5 and PRGL1 or NDH2, a type II NADPH dehydrogenase (Johnson et al., 2014). The FQR/pgr5 pathway is fast, generates a rapid proton motive force and is believed to be the main contributor to ATP production (Johnson et al., 2014). In contrast, the NDH pathway is relatively slow but is considered as a major stress response signaled by $H_2O_2$, such as in cases where large ATP deficiencies and / or redox imbalances occur (Strand et al., 2016).

In *C. reinhardtii*, Bonente et al. (2012) showed that CEF is up-regulated under low or moderate light conditions, relative to high light. Importantly, mutants devoid of either NDH or pgr5 (Kono et al., 2014) were found to be lethal under fluctuating light conditions compared to wild-type, suggesting that both CEF pathways are critical under frequent dark to light transitions which should include cells cycling between light and dark zones in high density cultures.

#### *1.6.9.2 Oxygen reduction processes (water-water cycles)*

The water–water cycles include the Mehler reaction, PTOX-mediated activity and flavodiiron (FLV) activity (Cardol et al., 2011). These processes act to restore the redox poise of an over-reduced electron transport chain by redirecting electrons toward molecular oxygen. The Mehler reaction transfers electrons at the PSI acceptor side to molecular oxygen, producing superoxide ($O_2^-$), which is converted to $H_2O_2$ by superoxide dismutase (SOD) and then, in turn, to water by ascorbate peroxidase and catalases (Cardol et al., 2011, Rochaix, 2011). Franck and Houyoux (2008) suggested that high rates of the Mehler reaction are likely to occur upon a transition from dark to light when CBB cycle enzymes are not fully activated, based on high rates of light-dependent $O_2$-uptake during photosynthetic induction. In contrast to the Mehler reaction which occurs downstream of PSI, $O_2$ reduction by PTOX activity occurs downstream of PSII. Its role here is to oxidise the PQ pool and may act as a safety valve by slowing the rate of electron transfer to Cyt*b*$_6$*f*, thereby avoiding an over-reduced ETC and too much reducing power during photosynthetic induction (i.e. dark to light transition) when the CBB cycle is not fully activated; it may also increase ATP production by allowing a rapid generation of proton motive force (PMF) to take place (Cardol et al., 2011, Rochaix, 2011, Alric et al., 2010). PTOX is also a factor involved in the elusive chloro-respiratory chain. The chloro-respiratory pathway is thought to involve the oxidation of reducing equivalents (either from the stroma or transported from mitochondria or glycolysis) to the NDH complex, through the PQ pool and then onto PTOX where $O_2$ is reduced to water (Rochaix, 2011).

The Flv pathway, typically found in cyanobacteria water-water cycles, has also recently been confirmed as an alternative electron route in *C. reinhardtii* (Jokel et al., 2015) following speculation about its role in green algae based on the high homology of Flv genes among organisms (Peltier et al., 2010). Jokel, et al. (2015) found that Flv-mediated $O_2$ reduction in *C. reinhardtii* occurs just before the onset of anaerobiosis with electrons extracted from NADPH. Flv accelerates induction of ETR on transition from light to dark, and acts as an electron sink and a safety valve.

#### *1.6.9.3 Mitochondrial respiration (light-enhanced dark respiration) and photorespiration*

Mitochondrial respiration in the light also plays a role in balancing the reducing and phosphorylating power when more ATP is required or the chloroplast stroma becomes over-reduced (Dang et al., 2014, Lemaire et al., 1988, Cardol et al., 2009). Excess NADPH can be exported from the chloroplast to the cytosol and then to the mitochondria via the malate/oxaloacetate shuttle (Shen et al., 2006, Hoefnagel et al., 1998). There NADPH is used for the synthesis of ATP which can be transported to the pyrenoid and used for carbon fixation.

Photorespiration occurs under high $O_2$:$CO_2$ ratios where Rubisco binds $O_2$ instead of $CO_2$, increasing ATP demand and incurring biomass loss as fixed carbon is converted back to $CO_2$ (Kliphuis et al., 2011). Many cyanobacteria and microalgae including *C. reinhardtii* possess a CCM to limit photorespiration, however this also requires additional ATP (Dang et al., 2014). Furthermore, Kliphuis et al. (2011) found that under $O_2$:$CO_2$ ratios typically found in PBRs biomass yields were lowered by suspected photorespiration by 20–30%.

### 1.6.10 Redox regulation of photosynthetic enzyme activity

Redox cascades generated by light regulate the activity of a number of photosynthetic proteins via reversible post-translational modifications. These processes are mostly mediated by thioredoxins (via the ferrodoxin/thioredoxin (**Figure 1-9**) or the NADP/thioredoxin systems) and glutaredoxins (via the glutathione/glutaredoxin system, involving glutathione and a glutaredoxin, Buchanan and Balmer (2005)). The multiple thioredoxins reported in plants, algae and bacteria serve different functions. Many are specific to their taxonomic group, including six identified in *C. reinhardtii* (Michelet et al., 2013). Key enzymes regulated by thioredoxins include four directly involved in the CBB cycle (phosphoribulokinase, glyceraldehyde-3-phosphate dehydrogenase, fructose-1,6-bisphosphatase, and sedoheptulose-1,7- bisphosphatase); ATP synthase; Acetyl-CoAcarboxylase, involved in initial steps of fatty acid synthesis, and three enzymes involved in starch metabolic pathways (ADP-glucosepyrophosphorylase, glucan:water dikinase and beta-amylase BAM1 (Michelet et al., 2013).

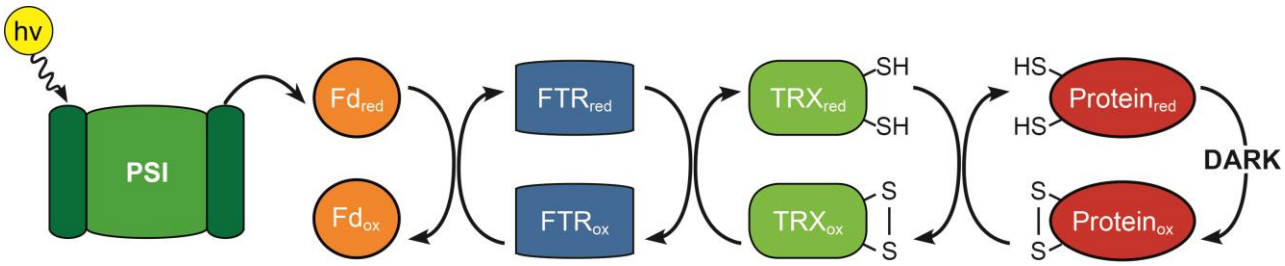


**Figure 1-9**. Redox regulation of the ferrodoxin/thioredoxin system. During the light reactions, some electrons from reduced Fd ($Fd_{red}$) are shuttled to ferrodoxin-thioredoxin reductase (FTR), which then acts to reduce thioredoxins (TRX). Reduced TRXs act to reduce disulphide bonds of regulatory cysteine residues on target photosynthetic proteins, changing their confirmation and function into a catalytic state (reproduced from Michelet et al. (2013)).

Moreover, a proteomics study revealed a total of 55 possible protein targets of thioredoxins in *C. reinhardtii*, highlighting the versatility and importance of redox-signaling in various metabolic pathways (Lemaire et al. 2004).

Despite being traditionally referred to as the 'dark reactions' of photosynthesis, importantly, the CBB cycle is tightly coupled to light-driven redox processes and does not operate at night. Deactivation of CBB cycle enzymes is thought to prevent photorespiration of carbon in the absence of NADPH, which would waste ATP in the process. In fact, recent biochemical and proteomic studies have indicated that all 11 enzymes as well as several associated regulatory proteins of the CBB cycle may be redox regulated (Michelet et al., 2013).

Whilst many photosynthetic proteins are transcribed at levels determined by light-acclimation responses, the relative cellular concentration of Rubisco in chlorophytes seems to be unaffected by light conditions (Bonente et al., 2012, Sukenik et al., 1987). However, the activity state of the Rubisco pool is tightly controlled by the nuclear-encoded chloroplast protein Rubisco activase, which is in itself, activated via both thioredoxin under reducing conditions and ATP availability. In the dark, Rubisco is inhibited by the substrate RuBP bound to an uncarbamylated lysine residue, thereby blocking the binding of $CO_2$. Upon photosynthetic induction from a dark to light transition, the increase in ATP:ADP ratio permits the ATP hydrolysis reaction of Rubisco activase, which carbamylates the Rubisco lysine, removing the RuBP inhibitor. Its activity is further increased by thioredoxin-f. In addition, a $Mg^+$ released from the thylakoid upon a drop in the luminal pH also requires binding to the lysine to fully activate Rubisco (Zhang and Portis, 1999).

In higher plants, Rubisco activation upon photosynthetic induction and deactivation after light has been reported to occur on a timescale of minutes (Gross et al. 1991). Regulation of Rubisco activity

has not been studied in algae, although Gontero et al. (2014) speculate that it is probably similar to plants (Gontero et al. 2014). Importantly, deactivation of photosynthetic enzymes is thought to be mediated by oxidized thioredoxins, molecular oxygen and accumulation of oxidants (Schürmann and Buchanan, 2008, Dangoor et al., 2012). Thus, Nikkanen et al. (2014) state that the enzymes under thioredoxin control are not permanently active in light but rather sensitive to changes in electrons flows from light reactions. Therefore, cells under mixing cycles in high density cultures subject to constant alterations in redox potential and ATP:ADP ratios may likely have a portion of the enzyme pool deactivated (Nikkanen et al. 2014). This could explain the variations in photosynthetic-irradiance response curves of algae under different acclimation states, where high light acclimated cells or those in dilute culture show markedly higher maximum photosynthetic rates, $P_{max}$, then low-light acclimated cells or those in dense cultures (Grobbelaar et al 1995; Grobbelaar et al. 1996; Bonente et al. 2012). The activation state of photosynthetic enzymes under fluctuating conditions, particularly Rubisco which is the rate-limiting step of photosynthesis, may therefore be a critical component of PBR modelling.

## 1.7 Linking photoacclimation and photoregulation with reported productivities under fluctuating light conditions

Given the importance of regulatory and acclimatory mechanisms in protecting the cell from redox imbalances occurring under fluctuating light, there is an urgent need for more in-depth empirical and modelling studies relating the extent of these processes under second to minute timescales to their effects on final biomass accumulation. To date, existing studies of mixing cycles on green algae in photobioreactors have focused mainly on productivity or biomass yield on light energy, $Y_{x,E}$. The key influences of the light regime considered were: the light fraction of the culture, mixing cycle time, $t_c$; average irradiance, $I_{avg}$, and incident irradiance, $I_0$, the latter of which usually also defines the maximum irradiance, $I_{max}$.

In general, the light fraction was reported to be the most prominent factor influencing light-to-biomass efficiency (measured as PCE, biomass yield on light energy, or proportion of growth to proportion of light received relative to controls under continuous illumination). Light-to-biomass efficiency was reduced as the light fraction decreased (i.e. as cultures became more dense) (Barbosa, 2003, Grobbelaar, 1994, Janssen et al., 2000, Janssen et al., 1999). Barbosa et al. (2003) found cultures with a light fraction <0.23 could not be maintained, resulting in a culture crash. In contrast, the biomass yield on light energy for high light fractions (>0.8) was either similar or slightly higher than under continuous light (Barbosa, 2003, Janssen et al., 2000, Wu and Merchuk, 2001), suggesting that a

small dark zone does not pose serious redox imbalances and may also give reprieve from photoinhibition under high light conditions (Grobbelaar et al., 1996, Janssen et al., 2000).

In *C. reinhardtii*, a light fraction of 0.5 resulted in 26–43% lower biomass yields on light energy than under continuous light of the same $I_{avg}$ under square-wave light/dark cycles of 6–24s (Janssen et al., 2000). In this study the maximum specific photosynthetic activity, $P_{max}$ (measured as $O_2$ evolution) decreased by ~30% which may infer changes in Rubisco activity, and the quantum yield of photochemistry was less than half that under continuous illumination. Furthermore, growth rates declined more than proportional to the relative amount of light received under mixed cycles for the fast-growing *C. sorokiniana*.

With regard to mixing rates, cycle times greater than ~10 s seemed to have little effect on productivity, while shorter cycle times showed some improvements in biomass productivity (Barbosa, 2003, Grobbelaar, 1994, Janssen et al., 2000, Janssen et al., 1999, Grobbelaar et al., 1996, Takache et al., 2015). A relationship between cycle time and light fraction may also exist. For instance in *D. tertiolecta*, more rapid mixing improved productivity for light fractions ~0.5, yet longer cycles were beneficial under a light fraction of 0.86 and high incident light (Barbosa et al., 2003). In any case, achieving higher biomass yield on light energy than under continuous light requires extremely rapid 'flashing' light cycles typically in the range of 100 ms or less. For *D. tertiolecta*, a 94/94 ms light/dark cycle was required (Janssen et al., 2001). For *N. salina*, smaller light fractions of 0.1 and 0.33 using irradiances of 1,200 and 350 $\mu mol.m^{-2}.s^{-1}$ required cycle times of 100 and 33 ms respectively (Sforza et al., 2012).

In contrast to most of the above mentioned studies which simulated culture conditions by manipulating the external light source, a study by Grobbelaar et al. (1995) revealed changes in the shape of photosynthetic irradiance (*P–I*) curves of *Scenedesmus obliquus* and some *Chlorella* sp. under an actual evolving batch culture. As culture density increased, $P_{max}$ decreased but photosynthetic efficiency (alpha) increased. The specific productivity decreased rapidly with an increase in the biomass concentration, but the yield remained linear during the batch production cycle, even at high areal densities. Remarkably, a further study by Grobbelaar et al. (1996) found that after time in lower light : dark ratios of 0.33, the light/dark compensation ratio (i.e. where respiration and photosynthesis are equal such that $O_2$ evolution is nil), was decreased, indicating that cells become more efficient at light utilisation in dense cultures.

## 1.8 Mathematical models describing photosynthetic growth in mass culture

Several mathematical models describing the light-dependent growth of algae of varying complexities and at different timescales exist, depending on the hypotheses they set out to test for (for excellent recent reviews see Zonneveld (1998a), Béchet et al. (2013) and Matuszyńska and Ebenhoeh (2015)). At the complex end of the spectrum are large-scale genome-wide metabolic models that attempt to account for all known biochemical reactions of the cell (Fell et al., 2010, de Oliveira Dal'Molin et al., 2011). These models analyse large '-omics' data sets to reconstruct metabolic pathways and are useful to identify metabolic bottlenecks, resource allocation responses and areas for genetic design. One drawback, however is that they are usually limited to a particular state of the cell in response to a fixed condition. A group of mechanistic 'physiological' models are also complex, but have the added benefit of examining the dynamics of the cell to changing conditions (**Figure 1-10C**). The aim of these physiological models is to understand and explain fundamental biological processes. As such, they typically include large numbers of parameters, some of which may be difficult, if not impossible, to measure (García-Camacho et al., 2012).

In contrast, the aim of most light-limited growth models for process engineering optimisation is to predict biomass productivities and/or cell composition (i.e. lipid, starch and protein). The purpose of these models is not to describe physiological processes *per se*, but rather to rapidly assess the upper limits of biomass outputs in solar-illuminated outdoor systems that could be achieved under different environmental and design scenarios (e.g. reactor type or location). These simulations can be used to guide the design of advanced production systems, define optimal operating conditions, and to assess the performance of different algal strains. For example, simulations of a range of operating biomass concentrations can establish the optimal concentration at different times of the year (i.e. winter *vs.* summer). Furthermore, these predictions can be coupled to LCAs and TCAs to evaluate the energy, resources and expenses required for optimizing biomass yields to establish the 'sweet spot' between maximizing production and minimizing resources that will deliver the highest return on investment (ROI) or energy return on energy invested (EROEI). To this end, a reductionist approach is desired to develop simple expressions with a minimum number of parameters that can be easily estimated.

One strategy to reduce parameter numbers is to simplify systems into conceptualized schemes. An example is the popular class of '3-state' models that are based on the concept of the so-called photosynthetic unit (PSU) (Eilers and Peeters, 1988, García-Camacho et al., 2012, Rubio et al., 2003, Wu and Merchuk, 2001, Zonneveld, 1998b, Bernardi et al., 2014)).

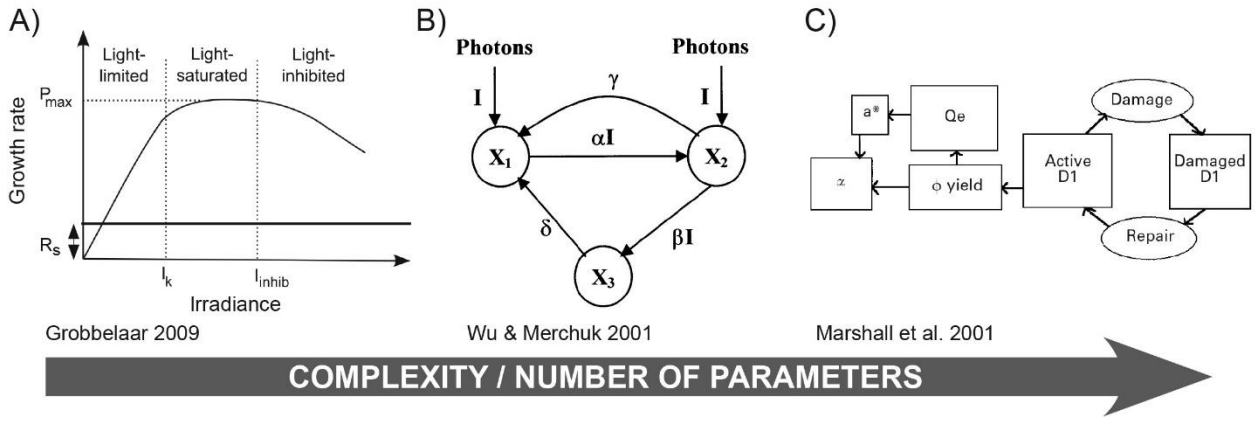


**Figure 1-10.** Example of three popular modelling approaches for light-limited algal growth based on their level of complexity and number of parameters required. A) Static models based on empirical growth-irradiance (μ–I) response curves; B) dynamic 3-state models based on the concept of the phosynthetic unit (PSU); and C) mechanistic physiological models describing key processes.

The PSU is considered to encompass one entire photosynthetic apparatus, comprised of the major complexes (PSI, PSII, $Cyt_{b6f}$, ATPase), and all associated proteins that allow for photosynthesis to take place. These dynamic models use a system of ordinary differential equations to monitor the relative proportions of PSUs that are considered to be in one of three states: a 'resting' state, whereby the PSU is ready to receive a photon for photosynthesis; an 'activated' state, whereby the PSU has undergone charge separation after photon absorption but is unable to receive another photon; or an 'inactivated' state, whereby the PSU is non-functional due to photodamage (**Figure 1-10B**) but capable of repair (or replacement). Growth is then estimated from the proportion of 'activated' PSUs of the cell. These '3 state' models account for both instantaneous light responses as well as considering the light history of the cell. One drawback of these models is that they require knowledge of the cell trajectory and travel time through the mass culture. This necessitates either rigorous computational fluid dynamics analysis, or measured or estimated flow rates, adding further variability and complexity to the model.

A popular class of minimal models are based on the relationship between growth and irradiance, represented by the well-known growth-irradiance ($\mu$–$I$) response curve (or $P$–$I$ curve for photosynthesis measurements, **Figure 1-10A**). These models require a minimum number of parameters that represent the lumping of a number of physiological processes and can be easily fit to empirical data. They are typically based on Monod-type kinetics of growth rates commonly used for bacterial growth in response to a limiting substrate (in this case light),

Eq.1-1 $$\mu = \frac{\mu_m I}{K_s + I}$$

Where $\mu$ is the specific growth rate, $\mu_m$ is the maximum potential growth rate, $I$ is irradiance, and $K_s$ is the half saturation irradiance. Several other formulas have been used for $\mu$–$I$ relationships including Poisson or tangent hyperbolic functions (Bechet et al. 2013). Since light can be both limiting and inhibiting, the Haldane's growth model better represents the growth kinetics to light, particularly to the high incident irradiance of outdoor mass cultures (Kumar et al., 2005),

Eq. 1-2 $$\mu = \frac{\mu_m I}{K_s + I + (I^2/K_i)} - R_s$$

Where $\mu$ is the specific growth rate, $\mu_m$ is the maximum potential growth rate, $I$ is irradiance, $K_s$ is the half saturation irradiance, $K_i$ is the coefficient for the irradiance of photoinhibition and $R_s$ is the respiration rate. The resulting curve from Eq. 2-1 is represented by four regions of growth: 1) negative growth below a critical irradiance ($I_c$) where respiration losses exceed photosynthetic growth; 2) a light limited region where growth increases linearly to increases in light; 3) a saturating region where photosynthesis approaches its maximum ($\mu_{max}$) and 4) a photoinhibited region where too much light diminishes growth due (**Figure 1-10A**).

For the above considerations, a review by Béchet et al. (2013) of over 40 productivity models concluded that static growth models which couple instantaneous growth rates to local and temporal light intensities within the mass culture offered the best compromise between accuracy and practicability. However, it is realized that these models are based on key assumptions that cells instantly acclimate to a given irradiance at a particular point in the culture media and do not account for changes in the acclimation state of the cell.

With increasing model complexity comes an increasing amount of uncertainty, yet simple models may fail to explain important phenomena. Therefore, a suitable productivity model must ideally find a compromise between the two.

## 1.9 Conclusion

In conclusion, this review has revealed that photoacclimation and photoregulation affects the plasticity of the photosynthetic-irradiance response. These processes, as well as the effects of redox imbalances and carbon assimilation, must be better understood under fluctuating light conditions typical of mass cultures in order to develop more representative models that account for dynamics of the parameters that define the shape of the *P-I* curve.

# 2 Development of a simple light-to-biomass model and simulations comparing productivities of three algae in outdoor open ponds and flat panel reactors in a sub-tropical location.

*"Everything should be made as simple as possible, but not simpler" – Albert Einstein*

## 2.1 Abstract

Here a semi-predictive light-to-biomass model is described, based on a refinement of published models, with the purpose of identifying opportunities and constraints for process optimisation at scale-up. The model estimated time-dependent incident irradiance from daily solar radiation obtained by local meteorology stations. Local light within the mass culture is predicted using a two-flux approximation to solve the radiative transfer equation. A simple Haldane growth model was used to predict local growth rates coupled to the local distribution of light within the mass culture volume. The parameter values required for the growth model were established from empirical growth-irradiance ($\mu$-$I$) curves obtained under a range of constant light intensities. Preliminary simulations were performed to assess productivities under open pond and parallel placed flat panel reactors (FPRs) on a theoretical scaled-up facility (1 ha) over a 'typical' year of solar conditions in a sub-tropical climate (Brisbane, Australia). Three algal strains were compared under a number of design scenarios: the model alga *C. reinhardtii* (*wt*) ('base case'), its truncated light harvesting antenna mutant *tla1,* with improved optical properties; and a fast-growing endemic strain *Chlorella* sp. (Strain 11_H5) currently being used for pilot scale trials. Model predictions showed that under optimised conditions, the improved light distribution of FPR systems could permit up to 10-11 fold increases in volumetric productivities and 2-3 fold increases in areal productivities than open ponds. For biological considerations, the improved properties of *tla1* and *Chlorella* sp. could achieve ~40% and 80% higher productivities respectively than *C. reinhardtii*. These results show that productivities are highly susceptible to system configuration, strain selection and operating conditions and that predictive models provide a powerful tool to optimise production processes and increase the feasibility and net energy returns of algal production systems.

## 2.2 Introduction

The development and successful scale up of industrial algal production facilities requires rigorous techno-economic and life cycle analyses (TCA and LCA respectively) based on realistic inputs of algal productivities. Long-term productivity data under local environmental conditions and mass

production is usually unavailable, and subsequently, estimates are often extrapolated from small scale laboratory experiments, or at best, pilot scale trials over short time periods. Given the cost of construction for large scale facilities, mathematical models that can reliably estimate productivities in response to the complex temporal and spatial light regimes of outdoor production facilities are a valuable tool for identifying opportunities and constraints to improve the viability of this technology.

Consequently, this research study began with the development of a light-to-biomass model that can be used to analyse various design, operational and biological criteria in order to identify areas for optimisation and the upper theoretical productivities of light-limited growth in outdoor solar conditions. The model uses a static $\mu$–$I$ mathematical expression coupled to local light intensities (mapped across the culture using the radiative transfer equation, RTE) that are summed to estimate algal productivity at a given instant of time.

This model was then subjected to dynamic light regimes (based on empirical weather data) over a 'typical' 1-year period representing all solar conditions. The aim was to analyse improvements at the level of reactor and systems design (an engineering consideration); operating conditions (biomass concentration and harvest mode) and algal strain selection (biological). In this respect, the 'base case' scenario used the model alga *C. reinhardtii* under batch cultivation in an open pond system, for which typical productivities are known.

The model considers reactor geometries in terms of Cartesian coordinates. Two common bioreactor designs were employed, namely high-rate open raceway ponds (referred hereafter as 'open ponds') and flat panel reactors (FPRs, **Figure 2-1**). The mode of operation can be assigned as continuous or batch harvest. The model can be applied to any geographical location and for cultivation of different algal species. For simulations, the sub-tropical location of Brisbane Australia was selected as it is the site of the Solar Biofuels Research Centre where pilot scale trials are being conducted, and additionally, its high solar radiation makes it an ideal location for algal production.

As discussed in Chapter 1, increasing productivities can be achieved by way of systems design, operating conditions or strain selection. Low-cost reactors and high density cultures are desired to reduce capital and operating costs respectively but typically result in reduced productivity. Improving the biology of a particular strain to achieve the above constraints is a desired strategy with little expense. Two major characteristics of an algal strain for high productivity are: fast growth and enhanced optical properties (i.e. better light utilization). For the former, we used a *Chlorella* sp. (strain 11_H5) which was endemically isolated (Jakob et al., 2013) and identified as one of the best growing of 100 strains analysed in a high-throughput screening that also achieved high PCEs in

outdoor pilot scale trials (Wolf et al., 2015). For enhanced optical properties, we used a genetically engineered strain of *C. reinhardtii* termed *truncated light harvesting antenna 1* (*tla1*) that displays ~63% less pigmentation than its wildtype parent (Polle et al., 2003, Mitra and Melis, 2008). A numerical study by Murphy and Berberoğlu (2011) based on the empirical data of Mitra and Melis (2008) predicted that *tla1* could improve reactor productivity by 30% under full sunlight, despite a higher saturation irradiance ($I_k$). Based on this work, this project was focused on exploring whether enhanced light penetration from a reduction in absorption capacity, combined with its consequential changes on growth responses to different irradiances, could theoretically improve productivity in outdoor cultures over an *entire* year of 'typical' solar conditions, including, for instance, during low light periods (i.e. early morning or high cloud cover), when photosynthetic rates may be lower than for the wildtype. The model alga *C. reinhardtii* (CC125) was used as a wildtype control.

## 2.3 Model approach

In the light-limited growth model presented here, a minimal number of inputs are required: location coordinates; total daily radiation data; the growth parameters of the algal species/strain; and the radiation characteristics of the alga. A number of decision variables pertaining to reactor configuration and system layout can be input at the users' discretion according to **Table 2-1**. The growth response of algae is considered instantaneous and as a function of the local light encountered within the culture mass. The light regime within the mass culture is highly dynamic and must be calculated temporally and spatially. For reliable predictions, the model calculation scheme considers the following (depicted in **Figure 2-1**): 1) Horizontal solar irradiance (i.e. ground radiation) as a function of location, hour, day and local weather data; 2) Incident irradiance received into the reactor culture volume as a function of the reactor configuration including its geometry, dimensions, orientation, spacing distance between neighboring reactors, and surface material properties; and 3) Light transfer through the mass culture as a function of the optical properties of the cell, operation mode (continuous or batch), cell concentration at a given time and the reactor pathlength.

### 2.3.1 System description & decision variables used for simulations

For an assessment of scale-up, a theoretical one-hectare microalgal production facility was considered. The facility was comprised of either 10 large open ponds or *n* parallel placed FPRs (where *n* depends on the spacing distance between FPRs) as illustrated in **Figure 2-1** (inputs defined in **Table 2-1**). Variables analysed included: reactor type (open pond *vs* FPRs); strain selection (*wt, tla1, Chlorella* sp.); operating concentration; operation mode (batch *vs* continuous); and for FPRs, reactor orientation, spacing distance between FPRs.

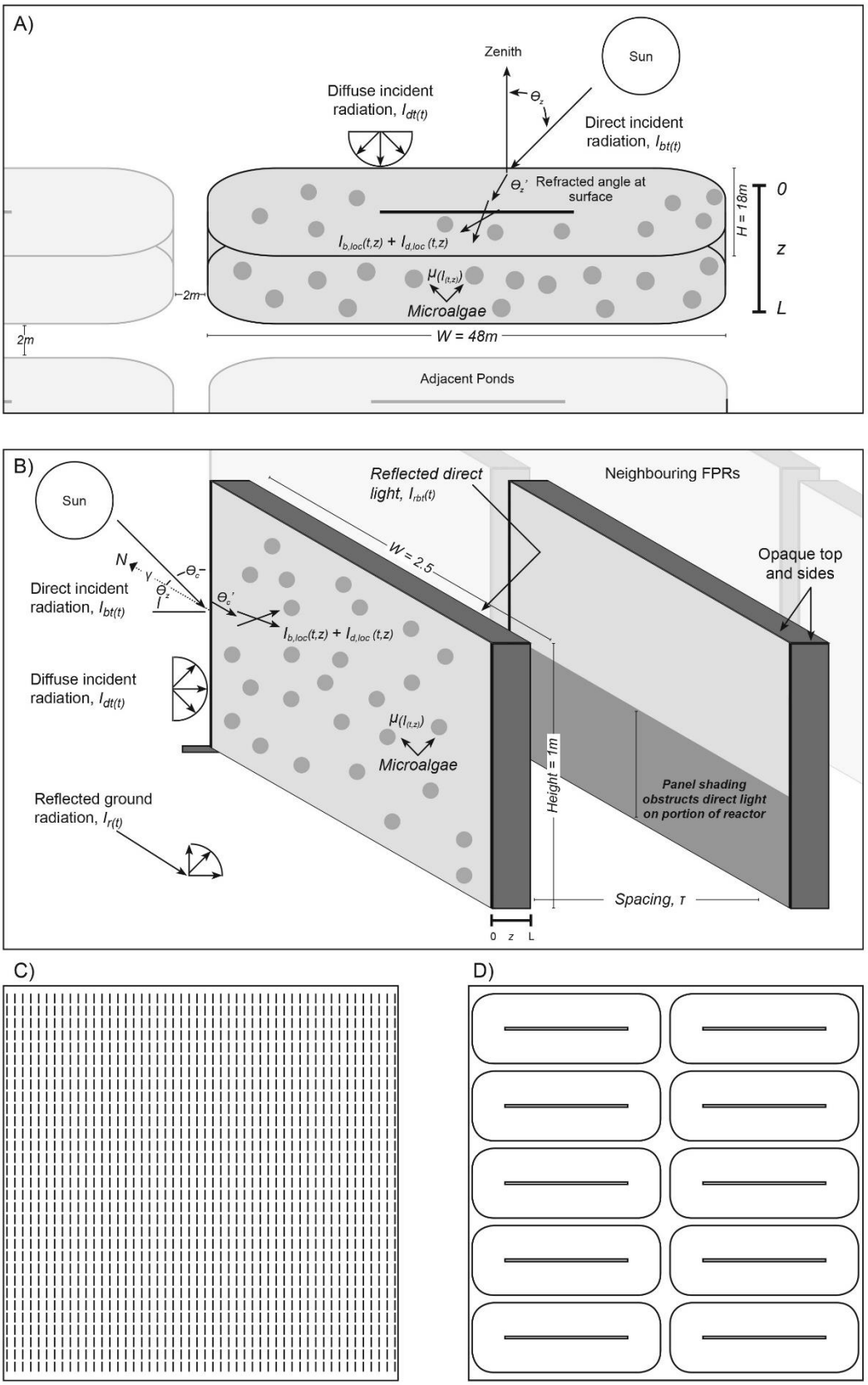


**Figure 2-1**. Schematic of the geometries of the A) open pond systems; and B) vertical closed flat panel reactors (FPRs) and the various angles and coordinates required for modelling light-limited growth. Areal schematic of a theoretical one-hectare microalgal production facility with: C) parallel placed FPRs; or D) 10 large open pond systems.

**Table 2-1.** Input values and decision variables used for model simulations analysis.

| Description | Parallel FPRs | Open Ponds |
|---|---|---|
| ***Fixed inputs used for simulations*** | | |
| Cultivation location, $\varphi$ | Brisbane, Australia | Brisbane, Australia |
| Local coordinates | 27.5° S, 153° E | 27.5° S, 153° E |
| Time interval for hours in day, $\hbar$ | 0.5 (30 mins) | 0.5 (30 mins) |
| Time interval for days in year, $N$ | 1:365 | 1:365 |
| Height illuminated area, $h$ (m) | 1.0 | 18 |
| Width illuminated area, $w$ (m) | 2.5 | 48 |
| Reactor depth, $L$ (m) | 0.05 | 0.25 |
| No. of illuminated sides | 2 | 1 |
| Illuminated area ($m^2$.reactor$^{-1}$) | 5.0 | 820 |
| Reactor volume ($m^3$.reactor$^{-1}$) | 0.125 | 205 |
| Surface area : volume ratio ($m^{-1}$) | 40 | 4 |
| Tilt angle, $\chi$ (degrees) | 90° | 0° |
| Ground reflectivity, $\rho$ | 0.5 | n/a |
| Surface material | 2 mm PMMA | n/a |
| Refractive index of surface material, $n_2$ | 1.49 | n/a |
| ***Adjusted variables used for simulations*** | | |
| Spacing distance (m) | 0.2–3.0 | n/a |
| Spacing distance : reactor height ratio | 0.2–3.0 | n/a |
| Reactor areal footprint ($m^2$) | 0.47–5.96 | 0.82 |
| Areal illuminated surface area, $SA_{areal}$ ($m^2$.$m^{-2}$ footprint) | 0.73–8.05 | 0.82 |
| No. of reactors (hectare$^{-1}$) | 1242–13657 | 10 |
| Inoculating concentration, $C_x$ | 0.25–2.5g.$L^{-1}$ | 0.05–0.5$L^{-1}$ |
| Culture optical thickness ($C_xL$) | 0.00125–0.0125 | 0.00125–0.0125 |
| Surface azimuth angle (degrees, orientation) | 0° (NS), 90° (EW) | n/a |
| Harvest method | Continuous | Batch, Continuous |
| Algal species | *C. reinhardtii* (*wt*), *tla1*, *Chlorella* sp. (11_H5) | |

### 2.3.2 Model assumptions

The model assumed only a light-limited state, with optimised temperature, replete nutrients, stable pH; sufficient $O_2$ removal and $CO_2$ supplied at ~1%. The systems were assumed to be well-mixed (via paddle wheels for open ponds or gas sparging for FPRs) and cells distributed homogenously throughout. Mixing rates were assumed to have no effect on growth between open ponds and FPRs.

The portion of photosynthetically active radiation (PAR) was assumed to be 43% of total solar radiation. Incident diffuse radiation was assumed to be isotropic (Perez et al., 1987). The liquid culture was considered to be non-absorbing, emitting or scattering for photosynthetically active radiation (PAR, 400–700nm). Bubbles created by mixing were considered small and the liquid medium to be non-scattering or absorbing such that these variables had negligible effects on light transfer (Berberoglu et al., 2007). Shading effects at the edge of reactors were assumed to be negligible, as was validated for reactors >2m in length (Lee et al., 2013). For simulations of FPRs: the number of reactors per hectare was sufficiently large so that differences in the incident illumination profiles of reactors along the boundary lines (i.e. less shading effect) were ignored; the horizontal spacing distance between panels was small, such that shadow effects are considered to occur only along the height of the panels and were assumed to be constant over the width of the panels; light was assumed to penetrate only through the front and rear surfaces – no light penetrated through the edges (top or side). For simulations of open ponds: the ponds were considered to be unlined so that no reflection occurs at the base, since pond linings increase capital costs.

## 2.4 Governing equations

### 2.4.1 Modelling light-limited biomass productivity

During the growth phase, the volumetric biomass productivity of the system, $P_{vol}$ (reported as kg.m$^{-3}$) is determined by the rate of change of the algal biomass concentration, $C_x$ over time is:

Eq. 2-1 $$P_{vol(t)} = \frac{dC_x}{dt} = \bar{\mu} C_x$$

Where $\bar{\mu}$ is the mean specific net growth rate at a given time, $t$, (accounting for cell death, which is factored from empirical parameter values), integrated at all points, $z$ over the reactor depth, $d$ (and for stacked FPRs at all points, $y$, over the reactor height, $h$,

Eq. 2-2 $$\bar{\mu}(t) = \frac{1}{h \cdot d} \int_0^h \int_0^d \mu(y, z, t) C_x \, dz dy$$

Eq. 2-1 and 2-2 are valid for cultivation under batch mode and continuous mode, however for the latter, the dilution rate, $D = \bar{\mu}$ and $C_x$ will remain at a pseudo steady state.

The areal productivity at a given time, $P_{areal}$ is,

Eq. 2-3 $$P_{areal(t)} = \frac{P_{vol(t)} * PBR_{vol}}{PBR_{area}}$$

Where $PBR_{vol}$ is the volume of the open pond or FPR and $PBR_{area}$ is the system's areal footprint, including the area of the system and spacing distances between adjacent reactors.

Light distribution through the microalgal culture is highly heterogeneous due to absorption and scattering of the cells in the medium. Therefore growth rates $\mu_{z,t,y}$ are modelled locally along the depth (and height for stacked FPRs) of the reactor pathlength as a function of the local photon fluence rate averaged for PAR, $I_{loc}$ experienced by the cell at a given instant using the Haldane's growth model,

Eq. 2-4 $$\mu(t,z,y) = \mu_m \frac{I_{loc}(t,z,y)}{K_s + I_{loc}(t,z,y) + \frac{I_{loc}(t,z,y)^2}{K_i}} - R_s$$

The parameters $\mu_m$, $K_i$, $K_s$ and $R_s$ are fitted to empirical growth-irradiance response curves ($\mu - I$ curve) as described in Section 2.5.1. From Eq. 2-4, further useful parameters of the $\mu - I$ curve can be found, including the realised maximum growth rate (Versyck et al., 1997),

Eq. 2-5 $$\mu_{max} = \mu_m \frac{1}{1+2(K_s/K_i)^{1/2}}$$

which occurs at the saturating (or optimal) irradiance,

Eq. 2-6 $$I_k = (K_s K_i)^{1/2}$$

and the photosynthetic efficiency in the light limited region of the $\mu - I$ curve (i.e. the initial slope) is,

Eq. 2-7 $$\alpha = \mu_{max}/I_k$$

### 2.4.2 Calculation of local light intensities through the mass culture

Irradiance through a culture with microorganisms is highly variable due to absorption and scattering of the cells in the medium. The local PAR-averaged PPFR, $I_{loc}(z,\hat{s})$ at a given location, $z$, travelling along a particular path, $\hat{s}$, through a suspension of microorganism can be found by solving the radiative transfer equation. The total irradiance is the sum of the direct and diffuse components (Murphy and Berberoğlu, 2011).

For direct (collimated), $I_{dir,\lambda}(z,\hat{s})$, the RTE is defined as follows:

Eq. 2-8 $$\frac{\partial I_{dir,\lambda}(z,\hat{s})}{\partial z} = -\beta_{eff,\lambda} I_{c,\lambda}(z,\hat{s})$$

While the steady state radiative transfer for diffuse, $I_{dif,\lambda}(z,\hat{s})$ light is found by:

Eq. 2-9 $$\frac{\partial I_{dif,\lambda}(z,\hat{s})}{\partial z} = -\beta_{eff,\lambda} I_{d,\lambda}(z,\hat{s}) + \frac{\sigma_{eff,\lambda}}{4\pi} \int_{4\pi} I_{d,\lambda}(z,\hat{s}) \Phi_\lambda(\hat{s}_i,\hat{s}) d\Omega_i$$

$$+ \frac{\sigma_{eff,\lambda}}{4\pi} \int_{4\pi} I_{c,\lambda}(z, \hat{s}) \Phi_{\lambda}(\hat{s}_i, \hat{s}) d\Omega_i$$

In Eq. 2-8 and 2-9, $\beta_{eff,\lambda}$, is the extinction coefficient expressed as,

Eq. 2-10 $$\beta_{eff,\lambda} = \kappa_{eff,\lambda} + \sigma_{eff,\lambda}$$

Here, $\kappa_{eff,\lambda}$ and $\sigma_{eff,\lambda}$ are the spectral absorption and scattering coefficients of the microorganism respectively.

The scattering phase function of the microorganism, $\Phi_{\lambda}$, represents the probability that light travelling in the solid angle, $d\Omega i$ around the direction $\hat{s}_i$ will be scattered into the solid angle $d\Omega$ around the direction ŝ. The first integral term corresponds to the in-scattered diffuse radiation and the second accounts for the in-scattered collimated radiation.

Several solutions of the RTE equation exist of varying complexity (Lee et al., 2013, Murphy and Berberoğlu, 2011, Acién Fernández et al., 1999). The most simple is the often used Beer-Lambert law,

Eq. 2-11 $$I_{loc,\lambda}(z) = I \cdot exp(-E_{ext,\lambda}\, z)$$

where $E_{ext,\lambda}$, is the spectral mass extinction coefficient expressed as,

Eq. 2-12 $$E_{ext,\lambda} = E_{a,\lambda} + E_{s,\lambda}$$

and $E_{a,\lambda}$ and $E_{s,\lambda}$ are the spectral mass absorption and scattering coefficients of the microorganism respectively.

The Beer-Lambert law, however, fails to consider in-scattering and can reduce accuracy, particularly for thick cultures where multiple scattering events occur (Pilon et al., 2011). By contrast, more exact numerical methods are computationally intensive (Lee et al., 2013, Pottier et al., 2005). A practical compromise may be found using an analytical solution of the Schuster-Schwarzchild two-flux approximation method (Viskanta and Menguc, 1989), that has been used to model light transfer in PBRs (Pottier et al., 2005, Cornet et al., 1992, Lee et al., 2013, Pruvost et al., 2011). This approach consists of solving two coupled ordinary differential equations obtained by integrating the one-dimensional RTE over two complementary hemispheres. It accounts for both in-scattering and anisotropic scattering but assumes it is confined to the front or back directions. On the assumption of a one-dimensional light field, Pottier et al. 2005 validated the two-flux approximation for *C. reinhardtii*. The model was further extended by Pruvost et al. (2011) to outdoor solar conditions,

taking into consideration non-normal incidence dependent on the position of the sun, as well as treating direct (i.e. beam or collimated) and diffuse radiation components separately. From this, Lee et al. (2013) found estimates of $I_{loc}$ varied by 2-13% to predictions obtained from a numerical solution of the RTE (discontinuous Galerkin method) over simulated day cycles for open ponds and FPRs.

In Cartesian coordinates, the irradiance field for direct radiation is (Pruvost et al., 2011),

Eq. 2-13 $$\frac{I_{loc,dir}(z)}{I_{0,dir}} = I_{0,dir}\, 2\sec(\theta)\, \frac{(1+\alpha_1)\exp[-\delta_{dir}(z-L)] - (1-\alpha_1)exp[\delta_{dir}(z-L)]}{(1+\alpha_1)^2\exp[\delta_{dir}L] - (1-\alpha_1)^2\exp[-\delta_{dir}L]}$$

And for diffuse radiation (Pruvost et al., 2011),

Eq. 2-14 $$\frac{I_{loc,dif}(z)}{I_{0,dif}} = I_{0,dif}\, 4\, \frac{(1+\alpha_{\lambda 1})\exp[-\delta_{dif}(z-L)] - (1-\alpha_1)\exp[\delta_{dif}(z-L)]}{(1+\alpha_1)^2\exp[\delta_{dif}L] - (1-\alpha_1)^2\exp[-\delta_{dif}L]}$$

Where $\Theta$ is the angle of the direct beam radiation, $z$ is the local position, $L$ is the reactor depth, and the two flux extinction coefficients, $\delta_{dir}$ and $\delta_{dif,}$ for direct and diffuse respectively are,

Eq. 2-15 & 2-16 $$\delta_{dir} = \frac{\alpha C_x}{\cos\theta}\,(E_a + 2bE_s), \text{ and } \delta_{dif} = 2\alpha_1 C_x\,(E_a + 2bE_s),$$

In Eq. 2-15 and 2-16, $E_a$ and $E_s$ are the PAR-averaged mass absorption and scattering coefficients, $b$ is the backward scattering fraction, and $\alpha,$ is the linear scattering modulus (Pruvost et al., 2011),

Eq. 2-17 $$\alpha = \sqrt{\frac{E_a}{(E_a+2bE_s)}}$$

For open ponds with a non-reflecting, opaque base, total local irradiance is found by summing the direct and diffuse components:

Eq. 2-18 $$I_{loc}(z) = I_{loc,dir}(z) + I_{loc,dif}(z)$$

For two sided vertical FPRs, $I_{loc}(z)$ is the sum of direct radiation received on one side of the reactor and diffuse radiation received on the front and back sides,

Eq. 2-19 $$I_{loc}(z) = I_{loc,dir}(z) + I_{loc,dif(front)}(z) + I_{loc,difback}(z)$$

### 2.4.3 Predictive determination of cellular optical properties.

Solving the two-flux approximation of radiative transfer above requires calculation of three parameters that define the optical property of the cell ($E_a$, $E_s$ and $b$). These are calculated below and are closely based on the method described by Pottier et al. (2005). This semi-predictive approach

requires only experimental determination of cellular pigment fraction, cell size distribution and the cell's refractive index.

First the complex refractive index of the particle is found,

Eq. 2-20 $$m = n \pm i\kappa_\lambda$$

where $n$ and $\kappa_\lambda$ are the real and imaginary parts of the refractive index of the cell, representing scattering and absorption phenomena respectively. The real part, $n$, is mainly involved with scattering. Scattering is wavelength dependent, but varies minimally within the 400–750 nm range (Lee et al., 2012). For ease of experimental determination, a reasonable average of $n$ can be determined by measuring transmittance at a non-absorbed wavelength (i.e. 750 nm).

The predictive determination of the imaginary part of the refractive index $\kappa_\lambda$, which is mainly responsible for absorption, is based on electromagnetic theory and dependent upon the absorption coefficient of the cell material $a_{cm}$,

Eq. 2-21 $$\kappa_\lambda = \frac{a_{cm}\lambda}{4\pi}$$

Here, $a_{cm}$ is a function of both the pigment's *in vivo* spectral mass absorption coefficient, $Ea_{pig.i}(\lambda)$, and its concentration, and $i$ is a pigment in the cell, $C_{pig.i}$, with a total of $n$ pigments,

Eq. 2-22 $$a_{cm} = \sum_{i=1}^{n} Ea_{pig.i}(\lambda) \cdot C_{pig.i}$$

In Eq. 2-22, $C_{pig.i}$ can be found by determining the mass fraction of each pigment, $w_{pig.i}$, and knowing the density of the dry material $\rho_{dm}$ and the *in vivo* fraction of water, $x_w$,

Eq. 2-23 $$C_{pig.i} = \rho_{dm}\frac{1-x_w}{x_w} \cdot w_{pig.i}$$

Electromagnetic theory states that cellular absorption efficiency, $q_{abs}$ does not vary linearly with wavelength, but varies according to the dimensionless efficiency factor for packaging is, $Q^*_\lambda$,

Eq. 2-24 $$Q^*_\lambda = \frac{3}{2\xi}\left[1 + \frac{2e^{-\xi}}{\xi} + 2\frac{e^{-\xi}-1}{\xi^2}\right]$$

Where $\xi$ is the particle optical thickness, combining the size parameter ($2\pi r/\lambda$) and $\kappa_\lambda$, giving,

Eq. 2-25 $$\xi = 4\frac{2\pi r}{\lambda}\kappa_\lambda$$

For instance, as $\xi \rightarrow 0$, the particle does not exist and $Q^*$ is equal to one, corresponding to the molecular absorption of the pigments themselves. However, as $\xi$ increases, $Q^* \rightarrow 0$ as a result of the so-called packaging effect from mutual shading of pigments (Pottier et al. 2005).

A better estimate of the true absorption index is then found by taking into account the imaginary part of the refractive index at a given wavelength with its efficiency factor at same wavelength,

Eq. 2-26 $$\kappa_\lambda = \kappa_\lambda \cdot Q^*{}_\lambda$$

Knowing the real, $n$ and imaginary, $\kappa$ parts of the particle refractive index, $m$, the predictive calculation of the radiative properties can be calculated based on the Lorenz-Mie theory for spherical particles of a given size distribution with a mean radius. Here a freely available numerical MATLAB code for Mie theory adapted from Bohren and Huffman (2008) was downloaded and used (Maetzler 2002). The outputs of this code are the wavelength-dependent absorption, scattering and extinction efficiencies of the cell ($q_{abs,\lambda}$, $q_{sca,\lambda}$, $q_{ext,\lambda}$) which are used to compute the mass absorption and scattering coefficients $E_{a,\lambda}$ and $E_{s,\lambda}$, as well as the scattering phase function $p(\theta,\theta')$, which is used to compute the backward scattering fraction, $b_\lambda$ (Morel and Bricaud, 1981; Maetzler 2002; Pottier et al. 2005).

The extinction and scattering cross-sections ($C_{ext,\lambda}$ and $C_{sca,\lambda}$) are then derived from the following,

Eq. 2-27 & 2-28 $C_{ext,\lambda} = q_{ext,\lambda}\pi r^2$ and $C_{sca,\lambda} = q_{sca,\lambda}\pi r^2$,

While the absorption cross section, $C_{abs,\lambda}$, is deduced,

Eq. 2-29 $$C_{abs,\lambda} = C_{ext,\lambda} - C_{sca,\lambda}$$

Now, the mass and volumetric absorption and scattering coefficients ($E_{a,\lambda}$, $E_{s,\lambda}$, and $a_\lambda$, $s_\lambda$ *respectively*) can be calculated from their respective cross-sections by the following equations,

Eq. 2-30 & 2-31 $E_{a,\lambda} = \frac{C_{abs,\lambda}}{V_p\, \rho_{dm}(1-x_w)}$, $E_{s,\lambda} = \frac{C_{sca,\lambda}}{V_p\, \rho_{dm}(1-x_w)}$

Eq. 2-32 & 2-33 $a_\lambda = E_{a,\lambda}C_x$, $s_\lambda = E_{s,\lambda}C_x$

Where $V_p$ is the mean particle volume calculated from the Sauter mean diameter, $\rho_{dm}$ is the density of the dry biomass and $x_w$ is the water fraction of the cell.

Finally, the mean mass absorption and scattering coefficients of the particle ($E_a$ and $E_s$) and the mean backscatter coefficient, $b$ are found by integrating over all wavelengths in the PAR,

Eq. 2-34, 2-35, 2-36 $E_a = \int_{700}^{400} E_{a,\lambda}\, d\,\lambda, \quad E_s = \int_{700}^{400} E_{s,\lambda}\, d\,\lambda, \quad b = \int_{700}^{400} b_\lambda\, d\,\lambda$

### 2.4.4 Incident light received by the reactor

Determination of local light through the reactor requires knowing the amount of incident direct and diffuse solar irradiance received by the reactor ($I_{0,dir}$ and $I_{0,dif}$ respectively). For open ponds comprising only one horizontal illuminated surface, this is a function of time, location, and cloud cover. For FPRs, $I_{0,dir}$ and $I_{0,dif}$ is also defined by the reactor geometry, orientation, surface materials and reflective characteristics of the ground and adjacent panels.

Local solar data provided by an on-site weather station or metrological bureau over short time intervals (≤1 h) are most desired. If unavailable, however, predictions can be made using commercial software integrating solar models or using a set of equations widely adopted in solar engineering applications (Duffie & Beckman, 1980) that have been previously applied to photo-bioreactor modelling (Molina Grima, et al. 1999). For this study, the only available meteorological data for Brisbane, Australia was total daily global radiation, $H$ (Station number: 040193, www.bom.gov.au).

Daily radiation, $H$, can then be converted to hourly incident PAR irradiance, $I_o$ (μmol.m$^{-2}$.s$^{-1}$, Molina Grima, et al. 1999), by,

Eq. 2-37 $$I_0 = \frac{\pi H E_f}{24 \cdot 3600} \cdot \left(1 + 0.033 \cdot \cos\left(\frac{360N}{365}\right)\right)\left(\frac{\cos(\omega) - \cos(\omega_s)}{\sin(\omega_s) - \omega_s} \cdot \cos(\omega_s)\right)$$

In Eq. 2-37, $E_f$ is the photosynthetic efficiency factor ($E_f$ = 1.98), converting W.m$^{-2}$ to PAR (μE.m$^{-2}$.s$^{-1}$), where 1 W = 4.6 μmol.m$^{-2}$.s$^{-1}$ and PAR is ~0.43 of the total solar spectrum (Morel and Smith, 1974). The second term relates to fluctuations in solar radiation due to variations in distance between the earth and the sun of around +/– 3% based on the day of year, $N$. The solar hour angle, $\omega$, is defined as the east to west angular displacement of the sun in relation to the local meridian (Duffie & Beckman, 1980),

Eq. 2-38 $$\omega = 15(t_{solar} - 12)$$

where solar time, $t_{solar}$, is corrected for the difference in longitude between the observer's meridian location and the meridian on which the local standard time is based,

Eq. 2-39 $$t_{solar} = hour + 4(L_{st} - L_{loc}) + E$$

Here, $L_{st}$ is the Standard meridian, and $L_{loc}$ is the longitude. The sun takes 4 minutes to traverse 1° of longitude, while $E$ is the equation of time (Duffie & Beckman, 1980).

Eq. 2-40 $$E = 9.87 \sin 2B - 7.53 \cos B - 1.5 \sin B$$

and

Eq. 2-41 $$B = \frac{360(N-81)}{364}$$

From Eq. 2-47, $\omega_s$ is the sunset hour angle,

Eq. 2-42 $$\omega_s = cos^{-1}(\tan\varphi \tan\delta)$$

Where $\varphi$ is the latitude and $\delta$ is the declination ($-23.45 < \delta < 23.45$),

Eq. 2-43 $$\delta = 23.45 \sin\left(360 \frac{284+N}{365}\right).$$

*2.4.4.1 Diffuse and direct radiation*

The relative amounts of direct, $I_{0,dir}$ and diffuse, $I_{0,dif}$ radiation need to be distinguished from $I_0$ in order to solve the two-flux RTE (Eq. 2-13 & Eq. 2-14). Collares-Pereira and Rabl (1979), established the following correlations for the proportion of diffuse to total radiation,

Eq. 2-44 $$I_{dif} = \begin{cases} 0.99\, I_0, & K_t \leq 0.17 \\ \left(1.188 - 2.272K_t + 9.473{K_t}^2 - 21.865{K_t}^3 + 14.648{K_t}^4\right)I_0, & 0.17 < K_t \leq 0.75 \\ (-0.54K_t + 0.632)I_0, & 0.75 < K_t \leq 0.8 \\ 0.17\, I_0, & K_T > 0.8 \end{cases}$$

Then direction incident radiation is deduced,

Eq. 2-45 $$I_{dir} = I_0 - I_{dif}$$

In Eq. 2-43, $K_t$ is the daily average atmospheric clarity index, which is predominantly a function of cloud cover and, to a much lesser degree, of aerosols and other atmospheric particulates. Thus at low $K_t$ there is high cloud cover which increases light scattering and the proportion of diffuse radiation. $K_t$ is estimated from the fraction of daily extraterrestrial radiation, $H_o$, reaching a horizontal surface after attenuation through air:

Eq. 2-46 $$K_t = \frac{H}{H_0}$$

And $H_o$ is,

Eq. 2-47 $$H_0 = \frac{24 \cdot 3600\zeta}{\pi} \cdot \left(1 + 0.033 \cdot \cos\left(\frac{360N}{365}\right)\right)\left(\cos(\delta)\cos(\varphi) \cdot \sin(\omega_s) + \frac{2\pi\omega_s}{360}\sin(\varphi)\sin(\delta)\right)$$

where, $\zeta$ is the universal solar constant, 1,353 W m$^{-2}$.

### 2.4.5 Incident light on single standing flat panels

Equations 2-44 and 2-45 estimate diffuse and direct radiation on horizontal surfaces such as open ponds. For tilted surfaces such as FPRs, the ratio of direct radiation to that on horizontal surface, $I_{dir,t}$, is a function of the geometric factor, $R_b$,

Eq.2-48 & 2-49 $I_{dir,t(front)} = I_{dir} \cdot R_{b(front)}$ and $I_{dir,t(back)} = I_{dir} \cdot R_{b(back)}$

Where $R_b$ considers the angle of incidence, $\theta$ and the solar zenith angle, $\theta_z$ (Duffie & Beckman, 1980):

Eq. 2-50 & 2-51 $R_{b(front)} = \frac{\cos\theta_{(front)}}{\cos\theta_z}$ and $R_{b(back)} = \frac{\cos\theta_{(back)}}{\cos\theta_z}$

In Eq. 2-50 & 2-51, $\theta_z$ is the solar zenith angle being the angle between the sun and a horizontal surface for direct radiation (Duffie and Beckman 1980),

Eq. 2-52 $$\theta_Z = \cos^{-1}(cos(\delta) \cdot cos(\varphi) \cdot cos(\omega) + sin(\delta) \cdot sin(\varphi)),$$

The angle of incidence on a tilted surface, $\theta$, accounts for the tilt angle, $\chi$ (i.e. the slope relative to the ground), and the surface azimuth angle, $\gamma$, between the normal of the reactor surface (where south = 0° in the northern hemisphere or north = 0 ° in the southern hemisphere) (Duffie and Beckman, 1980),

Eq. 2-53 $$\theta = cos^{-1}\ [sin(\delta)\,sin(\varphi)\,cos(\chi) - sin(\delta)\,cos(\varphi)\,sin(\chi)\,cos(\gamma) + cos(\delta)\,cos(\varphi)\,cos(\chi)\,cos(\omega) + cos(\delta)\,sin(\varphi)\,sin(\chi)\,cos(\gamma)\,cos(\omega) + cos(\delta)\,sin(\chi)\,sin(\gamma)\,sin(\omega)]$$

For two-sided illuminated reactors, $\theta$ is found for the front ($\theta_{front} = \theta$) and the reverse side, $\theta_{back}$ by modifying the reverse slope angle, $\chi_{(back)}$ and surface azimuth, $\gamma_{(back)}$ (Slegers, et al., 2011),

Eq. 2-54 $\chi_{(back)} = 180 - \chi_{(front)}$ and $\gamma_{(back)} = 180 + \gamma_{(front)}$

$\cdot R_{b(front)}$

Diffuse radiation is considered isotropic (Perez et al., 1987) and thus the geometric factor is not dependent upon the solar zenith angle, so for FPRs becomes, diffuse radiation becomes,

Eq.2-55 & 2-56 $I_{dif,t(front)} = I_{0,dif} \cdot \left(\frac{1+cos\chi_{(front)}}{2}\right)$ and $I_{dif,t(back)} = I_{0,dif} \cdot \left(\frac{1+cos\,\chi_{(back)}}{2}\right)$

For vertical flat plate collectors, radiation received by the ground and reflected onto panels can be high, particularly for light coloured surfaces such as white painted concrete (Hunn and Calafell,

1977). For single standing panels unaffected by shading, $I_{ref,}$ is found for front and the back sides (Grima et al. 2009),

Eq.2-57 & 2-58 $I_{ref(front)} = I_0\rho\frac{1-cos\chi(front)}{2}$, and $I_{ref(back)} = I_0\rho\frac{1-cos\chi(back)}{2}$

Where the albedo, $\rho$, is the ratio of reflected flux over the incoming flux and is a function of the colour and surface properties of the ground material.

### 2.4.6 Light direction, transmission and reflection at the reactor surface

Transmittance, reflectance and refraction of direct light at the reactor interface are dependent on the angle of incidence and the refractive indices between the air to water (for open ponds) or to the surface material (for FPRs), then to water. At small incident angles relative to the surface normal, for example, the angle of the sun at midday relative to the surface of an open pond, reflection is minor and most light is transmitted. At large angles, for example the angle of the sun at midday on a vertically titled FPR, reflection becomes more prominent (Duffie and Beckman, 1980a). Transmission is assumed to be independent of wavelength, which is acceptable for highly transmissive surfaces such as those used for PBRs (i.e. glass, low density polyethylene (LDPE) and rigid acrylic (PMMA)).

For open ponds the fraction of total reflected direct light is,

Eq. 2-59 $$r_{dir} = \frac{1}{2}\left(r_{||} + r_{\perp}\right)$$

where, $r_{\perp}$ and, $r_{||}$, are the perpendicular and parallel components of polarized reflected light respectively,

Eq. 2-60 and 2-61 $r_{\perp} = \frac{sin^2(\theta_2-\theta)}{sin^2(\theta_2-\theta)}$ $and$ $r_{||} = \frac{tan^2(\theta_2-\theta)}{tan^2(\theta_2-\theta)}$

And $\Theta_2$ is the refracted angle of $\Theta$ after passing from one from one medium with a refractive index, $n_1$ to another medium with a second refractive index, $n_2$, defined by Snell's law:

Eq. 2-62 $$\theta_2 = sin^{-1}\left|\frac{n_1 sin\theta}{n_2}\right|$$

For FPRs, Eq 2-59 is modified to account for transmission through the surface material, such that the fraction of reflected light is,

Eq. 2-63 $$r_{dir} = \frac{1}{2}\left(r_{||}\left(1+\tau_a\tau_{||}\right)^2 + r_{\perp}(1+\tau_a\tau_{\perp})^2\right)$$

Here, $\tau_a$, is the transmittance of a surface material, considering losses by absorption, defined as:

Eq. 2-64 $$\tau_a = e^{-KL_{surface}/cos\theta_2}$$

Where $L_{surface}$ is the thickness of the surface material and $K$ is the extinction coefficient of the surface material, and $\tau_{||}$ and $\tau_{\perp}$ are the perpendicular and parallel components of polarized transmitted light respectively,

Eq. 2-65 and 2-66 $$\tau_{\perp} = \frac{\tau_a(1-r_{\perp})}{(1+r_{\perp})}\frac{(1-r_{\perp})^2}{(1-\tau_a r_{\perp})^2} \; and \; \tau_{||} = \frac{\tau_a(1-r_{||})}{(1+r_{||})}\frac{(1-r_{||})^2}{(1-\tau_a r_{||})^2}$$

For isotropic diffuse radiation, the fractions of transmitted and reflected light are found the above equations but by substituting $\theta$ with a fixed angle of 60$^o$ (Duffie and Beckman, 1980).

### 2.4.7 Incident light for parallel placed FPR systems

Parallel placement of FPRs can create the so-called 'light dilution effect'. This may benefit cultures by distributing light over a greater surface area and avoiding photoinhibiting light at the surface during peak solar hours. Parallel-stacked flat panel reactors creates shading from direct radiation on a portion of a neighbouring reactor depending on sun's angle (over time) and the spacing distance to height ratio of the FPRs (**Figure 2-1B**). Subsequently, the shaded portion receives only diffuse radiation, while the illuminated portion receives diffuse and direct. In addition, smooth materials such as glass and Perspex cause specular reflection of direct light which may be reflected to the reverse side of an adjacent reactor or to the ground. Thus, these effects divide the reactor height into three fractions based on the light received: 1) illuminated ($f_{illum}$) receiving direct and diffuse on the front side and diffuse on the back, 2) shaded ($f_{shaded}$), receiving only diffuse radiation on both sides, and 3) shaded with specular reflection on the reverse side ($f_{refl}$). For flat panel reactors with an opaque top, shading below the surface occurs, however, with a small reactor pathlength to height ratio, these shading effects are small.

The height of the illuminated fraction of the reactor is (Slegers et al., 2011),

Eq. 2-67 $$h_{illum} = \frac{\varrho \cdot \tan(90-\theta_z')}{\sin(\psi)}$$

Where $\varrho$ is the spacing distance between panels, $\theta_z'$ is the projection of $\theta_z$, and $\psi$ is the angle between the sun's rays and the reactor,

Eq. 2-68 $$\psi = \left|90 - |\gamma - \gamma_s|\right|$$

The illuminated fraction of the FPR is then,

Eq. 2-69 $$f_{illum} = \begin{cases} 1 & h_{light} > h_{reactor} \\ \frac{h_{illum}}{h_{reactor}} & 0 > h_{light} < h_{reactor} \\ 0 & h_{light} \leq 0 \end{cases}$$

Where $h_{reactor}$ is the height of the FPR.

Specular reflection is the mirror reverse of the direct beam radiation, and therefore the fraction of the panel height receiving specular reflection is equal to the illuminated fraction, except during times when some or all of the reflected light is directed to the ground,

Eq. 2-70 $$f_{refl} = \begin{cases} 0 & n_r < 1 \\ f_{illum}\,(n_r - 1) & 1 \leq n_r < 2 \\ f_{illum} & n_r \geq 2 \end{cases}$$

Where $n_r$ is the total number of possible reflections ($n_r = \frac{h_{reactor}}{h_{illum}}$)

The portion of the panel receiving no direct or specular reflected radiation is then the shaded fraction receiving only diffuse radiation,

Eq. 2-71 & 2-72 $f_{shaded(front)} = \frac{1-f_{illum}}{2}$ and $f_{shaded(back)} = \frac{1-f_{refl}}{2}$

*2.4.7.1 Diffuse radiation gradients between stacked panels*

Parallel placement of FPRs causes the so-called 'canyon effect' for diffuse radiation in which a gradient of light occurs along the height axis, decreasing to the bottom of the reactor. Thus, for parallel placed FPRs, Eq.2-55 and Eq. 2-56 and modified according to Slegers et al. (2011),

Eq. 2-73 and 2-74 $I_{dif(front),s} = I_{dif}\left(\frac{1+\cos(\chi_{(front)}+u)}{2}\right)$ & $I_{dif(back),s} = I_{dif}\left(\frac{1+cos(\chi_{(back)}+u)}{2}\right)$

Where,

Eq. 2-75 $$u = tan^{-1}\left(\frac{y}{\vartheta}\right)$$

Where $y$ is the position along the height axis of the reactor, measured from the top (Slegers et al. 2011) and $\vartheta$ is the spacing distance between the panels.

Some direct and diffuse radiation received at the ground will be reflected back onto panels in a diffuse manner due to the rough surface properties of the ground material. Therefore total diffuse radiation is the sum of diffuse radiation and reflected ground radiation.

The portion of ground receiving direct radiation will vary depending on the solar angle (i.e. hour of the day), spacing distance and orientation of panels, such that the fraction of ground receiving direct light, $I_{r,Hb}$ is found by:

Eq. 2-76 $$fI_{r,Hb}(t) = \vartheta - h_{reactor} \cdot \tan(\theta_z) \cdot sin(\psi)$$

With the following conditions:

Eq. 2-77 $$\begin{cases} fI_{r,Hb} > 1, & fI_{r,Hb} = 1 \\ fI_{r,Hb} < 0, & fI_{r,Hb} = 0 \end{cases}$$

Making the total amount of reflected direct radiation,

Eq. 2-78 $$I_{r,Hb}(t) = fI_{r,Hb} \cdot I_{dir}$$

while the amount of diffuse radiation received by the ground is equal to the amount of diffuse radiation calculated at the bottom of the reactors,

Eq. 2-79 $$I_{r,Hd(front)} = I_{dt(front)} \; and \; I_{r,Hd(back)} = I_{dt(back),} \; where \;\; y = y_{end}$$

Finally, the total adjusted reflected ground radiation received by the panels is,

Eq. 2-80 $$I_{ref,g} = (I_{r,Hb} + I_{r,Hd})\rho \cdot u'$$

Where u' is the inverse of u, such that the diffuse gradient decreases from bottom to top.

For simplicity, since the gradient of diffuse radiation and the gradient of reflected diffuse ground radiation between stacked panels is small, the gradients are averaged over the panel height axis, *y*, such that the mean diffuse radiation between stacked panels in the shaded portion, $f_{shaded(front)}$ and $f_{shaded(back)}$ are,

Eq. 2-81 $$I_{dif(front),s} = \frac{1}{y}(\int_y I_{ref,g}\, dy + \int_y I_{dif(front),s}\, dy)$$

Eq. 2-82 $$I_{dif(back),s} = \frac{1}{y}(\int_y I_{ref,g}\, dy + \int_y I_{dif(back),s}\, dy)$$

The irradiance received at the illuminated fraction of panels, $f_{illum,}$ is,

Eq. 2-83 $$I_{illum} = I_{dir,t} + I_{dif(front),s}$$

And for the specular reflected fraction $f_{refl,}$ is,

Eq. 2-84 $$I_{refl} = r_{dir}\, I_{dir,t} + I_{dif(back),s}$$

## 2.5 Determination of algal characteristics

### 2.5.1 Growth parameters

For each algal strain, the parameter constants $\mu_m$, $K_s$, $K_i$, and $R_s$ of the Haldane growth model (Eq. 2-4) were established from experimentally derived $\mu$–$I$ curves (**Table 2-2**). The strains were cultivated in 100 ml flasks in triplicate in photoautotrophic media (TAP minus acetate) under 100 µE.m$^{-2}$.s$^{-1}$ on a shaker for 5 days prior to experimentation. Cells were adjusted to the same dilute optical density at 750 nm ($OD_{750}$) of 0.1 (~1-2 x $10^6$ cells.ml$^{-1}$) to avoid cell shading. $OD_{750}$ was measured in a 1 ml cuvette using a SmartSpec spectrophotometer (Bio-Rad Laboratories, Inc., CA, USA). For each strain and replicate, 120 µl of culture (~3 mm depth) was inoculated onto a 96 well microtitre plate. A total of 10 plates were each subjected to a different irradiances ranging from 0–1,200 µmol.m$^{-2}$.s$^{-1}$ (where negative growth at 0 µmol.m$^{-2}$.s$^{-1}$ was used to determine the respiration rate) using a customised light emitting diode (LED) lighting system designed by Jennifer Yarnold, Ian Ross, and John Srnka on a Tecan® robot.

Briefly, this system consists of one individual LED positioned under each individual well on a 96 well plate to provide a near identical irradiance for each well. Each plate was connected to a microcontroller (Arduino$^{TM}$), with a custom-designed program that allows individual settings of irradiance and duration for each plate. An integrating spherical light sensor was used to correlate the power voltage to actual PAR. To avoid light shock, samples were acclimated to their respective light intensities for 1 h prior to starting the experiment by increasing light from 50 µmol.m$^{-2}$.s$^{-1}$ up to the given irradiance at 10 min intervals. The Tecan® robot was programmed to measure $OD_{750}$ every 3 h to monitor growth over the 48-hour cycle. Each plate was incubated on a shaker at 480 rpm for 48 h at 25°C, while the entire enclosed TECAN system was enriched with 1.2% atmospheric $CO_2$ and 3.5 L.min$^{-1}$ air.

Growth was monitored as the change in $OD_{750}$. The cells were grown through log phase to establish the specific hourly growth rate, $\mu$, at each irradiance level, using the equation:

Eq. 2-85 $$\mu = \frac{\ln(OD_{750,end}) - \ln(OD_{750,start})}{T_1 - T_0}$$

where $OD_{750,end}$ and $OD_{750,start}$ are the optical density readings at the end and beginning of the log phase of growth, and $T_1$ and $T_0$ are times at the end and start of the log phase respectively.

**Figure 2-2** shows the empirical data fitted to the growth model (Eq. 2-4) using the Levenberg-Marquardt non-linear least squares algorithm (MATLAB® Curve Fitting Toolbox).

Parameter values and their goodness of fit are listed in **Table 2-2**. The maximum growth rate, $\mu_{max}$ was approximately the same for *C. reinhardtii* and its antenna mutant *tla1,* and was ~35% higher for the fast-growing *Chlorella* sp. (0.192). The irradiance at which saturation occurs, $I_k$, varied markedly between the strains: *Chlorella* sp. was ~40% lower and *tla1* was ~80% higher than *C. reinhardtii*. A similar pattern was observed for the irradiance at which photoinhibition became apparent, $K_i$, but was remarkably ~225% higher in *tla1* indicating that less absorption should reduce photoinhibition. The respiration rate, *M* was similar among all strains.

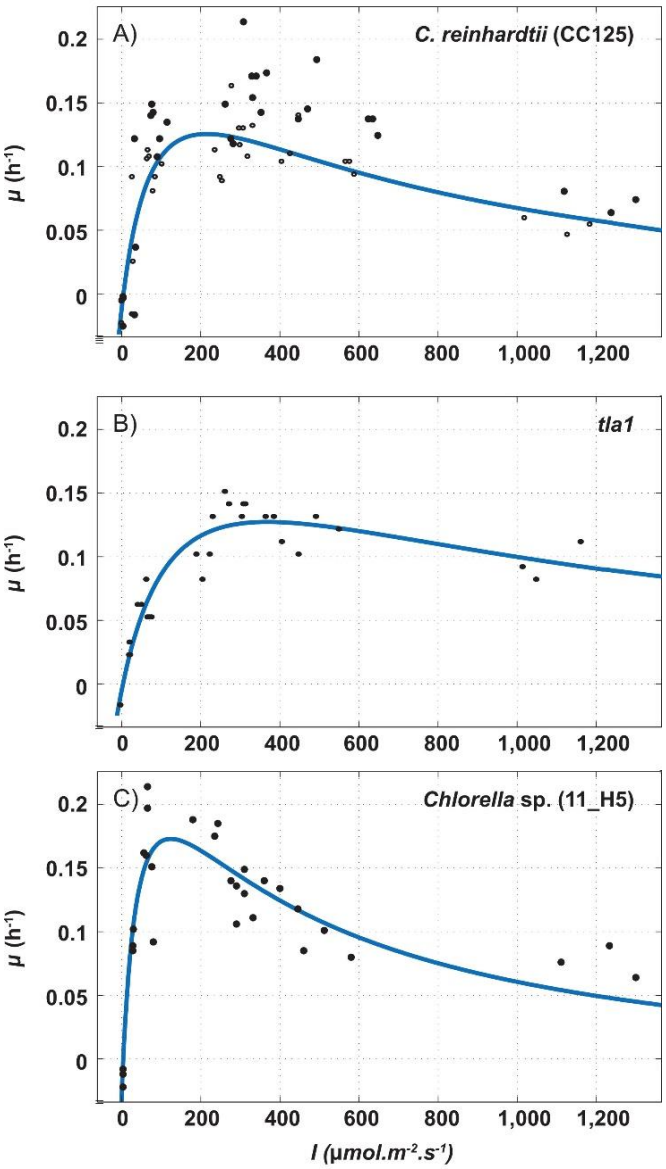


**Figure 2-2**. Growth-irradiance response curves for a) *C. reinhardtii*; b) *tla1* and c) *Chlorella* sp. Black dots are empirical measurements. Blue lines are the Haldane model (Eq. 2-2). fitted with the parameter values listed in **Table 2-2**.

### 2.5.2 Algal optical properties

Values of optical parameters of the cell ($E_a$, $E_s$, and $b$) required to solve the two-flux approximation for *C. reinhardtii* CC125 *wt* and *tla1* were used from a comprehensive experimental study of radiation characteristics by Berberoglu et al. (2008). For *Chlorella* sp. 11_H5, estimation of $E_a$, $E_s$, and $b$ were found using the semi-predictive approach described in Section 2.4.3.

This approach requires empirical determination of the cellular fraction of the pigments Chl *a*, Chl *b* and Car as well as the cell size distribution. This method is beneficial because firstly, experimental determination of $E_a$ requires the use of an integrating sphere photometer which was unavailable, and secondly, for more advanced models that are capable of predicting changes in acclimation (pigments content, cell size), the method can be fully-predictive. The optical properties revealed a ~34% reduction in the mass absorption coefficient for *tla1* in comparison to *C. reinhardtii*, consistent with the reduced levels of chlorophyll reported.

**Table 2-2.** Algae strain specific growth parameter values

| **Paramater** | ***C. reinhardtii (wt)*** | ***tla1*** | ***Chlorella* sp.** |
|---|---|---|---|
| *Growth parameters* | | | |
| $R_s$ | -0.012 | -0.013 | -0.014 |
| $u_m$ | 0.259 | 0.258 | 0.329 |
| $K_s$ | 86 | 147 | 44 |
| $K_i$ | 483 | 908 | 347 |
| $u_{max}$ | 0.141 | 0.143 | 0.192 |
| $I_k$ | 204 | 365 | 124 |
| $\alpha$ | $1.3x10^{-3}$ | $7.1x10^{-4}$ | $2.6x10^{-3}$ |
| Goodness of fit: | | | |
| SSE: | 0.014 | 0.007 | 0.020 |
| R-square: | 0.787 | 0.091 | 0.801 |
| Adjusted R-square: | 0.762 | 0.090 | 0.778 |
| RMSE: | 0.023 | 0.016 | 0.027 |
| *Radiation characteristics* | | | |
| $E_a$ | 174[a] | 114[a] | 178[b] |
| $E_s$ | 672[a] | 795[a] | 1740[b] |
| $b$ | 0.02[a] | 0.01[a] | 0.065[b] |

[a]Values were compiled as the taken from Pilon tables compiled using an integrated sphere photometer and reported by Berberoglu 1998. [b]Values calculated from mass pigment fraction and cell size distribution using Mie theory as described in appendix A.

## 2.6 Simulation results and discussion

To illustrate the capabilities of the model as a tool for analysing microalgal production facilities, simulations were performed using Matlab R2013a.

### 2.6.1 Effects of reactor type and system layout on incident light capture

A key consideration of reactor design is light capture and distribution. Subsequently, the surface area to volume ratio (SA:V) is an important parameter considered in reactor design. For the dimensions considered in this study, the SA:V ratio is 10-fold higher in thin two-sided FPRs in comparison to open ponds at 40 $m^{-1}$ and 4 $m^{-1}$ respectively (**Table 2-1**). A further important parameter in scaled up facilities is the areal illuminated surface area ($SA_{areal}$), considering the area of illuminated surface on the same area of land. For open ponds, this value is fixed for a given depth, but for parallel placed

FPRs of a fixed depth, $SA_{areal}$ can be increased by lowering the spacing distance to height ratio between stacked FPRs. For instance, open ponds have a fixed areal illuminated surface area of 1 square meter per square metre footprint, but when considering the proposed 1-ha facility of 10 ponds and the spacing distances surrounding them, $SA_{areal}$ is reduced to 0.8 $m^2.m^{-2}$. For FPRs, a spacing distance to panel height ratio of 2.2 gives approximately the same $SA_{areal}$ as open ponds. Reducing the spacing distance to height ratio to 0.4 increases $SA_{areal}$ to 4.0 $m^2.m^{-2}$. As $SA_{areal}$ increases, the captured light will be dispersed over a wider area, creating the so-called 'light dilution' effect which is postulated to increase reactor productivity by reducing photoinhibitory irradiances and dark zones.

**Figure 2-3** compares the light profiles of the incident irradiance (as photosynthetic photon flux density, PPFD) received by an individual reactor averaged over the total illuminated surface for open ponds and FPRs (left panels); and the total daily areal radiation intercepted by all reactors on a 1-ha facility (right panels) and a summary is presented in **Table 2-3**.

### *2.6.1.1 Incident light profiles of open ponds*

Open ponds receive highest radiation during summer (Dec to Feb) and during the middle of the day, where extreme irradiances of up to ~2,000 $\mu mol.m^{-2}.s^{-1}$ can be received (**Figure 2-3A**). The total daily radiation received by open ponds in comparison to total daily radiation received on a horizontal surface is proportional to its $SA_{areal}$ (0.8 $m.m^{-2}$), i.e. the portion of lost radiation is simply due to that falling on the surrounding spaces between the ponds (**Figure 2-3A**).

### *2.6.1.2 Incident light profiles of FPRs – effects of spacing distance and panel orientation*

For FPRs, the profiles of incident irradiance at the reactor surface and the total radiation captured by the system are more complex due to the spacing distance to height ratio between vertically placed panels and the orientation of the panel (where orientation refers to the wide illuminated panel face).

**Table 2-3.** Mean daily radiation recovered by different system configurations over a 1-ha facility.

| | *Open ponds* | | *Stacked FPRs* | | | ***H*** |
|---|---|---|---|---|---|---|
| $SA_{areal}$ ($m^2.m^{-2}$) | 0.82 | 0.82 | 0.82 | 3.5 | 3.5 | |
| Orientation | n/a | NS | EW | NS | EW | |
| Mean radiation ($MJ.day^{-1}$) | 14.7 | 7.0 | 7.9 | 13.0 | 13.5 | **17.9** |
| Total radiation recovered by system (%) | 82% | 39% | 44% | 72% | 75% | **100%** |

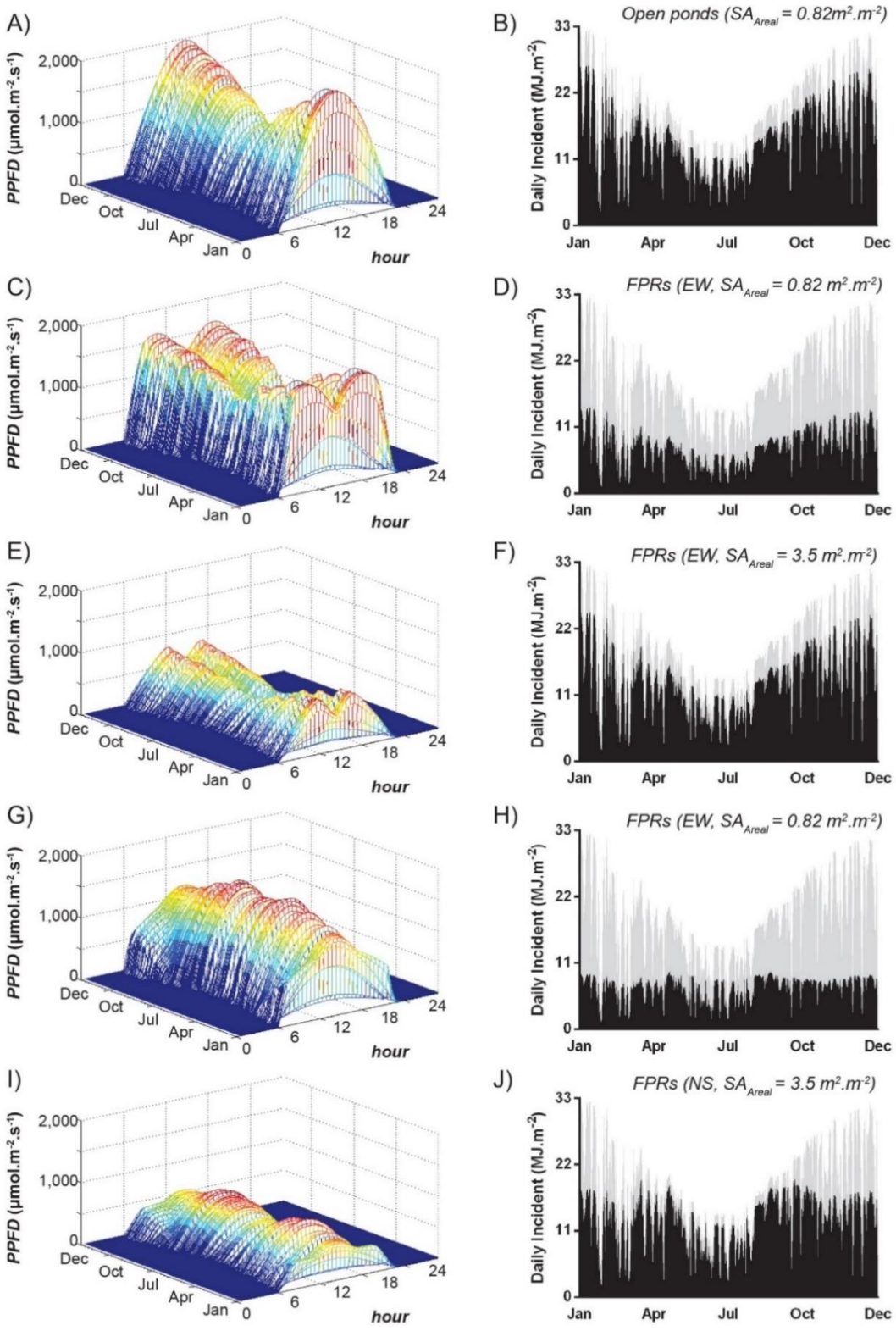


**Figure 2-3.** Incident light capture of different system configurations. Left panels: averaged total incident irradiance (PPFD) received at the reactor surface over time. Right panels: daily radiation captured by the 1-ha system (black lines) relative to total radiation (grey). A, B) open ponds; C, D) widely spaced east-west facing FPRs (spacing:height ratio = 2.2); E, F) tightly spaced east-west facing FPRs (spacing:height ratio = 0.5); G, H) widely spaced north-south facing FPRs (spacing:height ratio = 2.2); I, J) tightly spaced north-south facing FPRs (spacing:height ratio of 0.5).

East-west oriented FPRs (**Figure 2-3C & E)** receive highest light in summer during mid-morning and mid-afternoon. Around midday, the steep solar angle relative to the vertical panels reduces much of the direct radiation because of reflection, while some radiation is received by the ground. The opposite occurs for north-south oriented FPRs, with higher radiation received at midday and during winter months (**Figure 2-3G & I)**.

For widely spaced FPRs with a similar $SA_{areal}$ as open ponds, some reduction in photoinhibitory light occurs at the reactor surface, relative to open ponds. However, the total areal radiation captured (**Figure 2-3D & H**) is drastically reduced to just 39 and 44% of total available radiation for NS and EW orientations respectively because much light being lost to the ground and/or reflected to space, rather than being received by the reactor surface. For tightly spaced FPRs with increased $SA_{areal}$ (**Figure 2-3 E, F & I, J)**, light dilution and shading between panels avoids the high photo-inhibitory irradiances at the surface as seen in open ponds (**Figure 2-3 E & I**). In addition total radiation intercepted by the 1-ha facility is high (and similar to that of open ponds) due to larger numbers of panels and less light being lost to the ground or reflection (**Figure 2-3F & I).** The amount of radiation recovered by the reactors for east-west and north-south oriented panels is 72 and 75% respectively, slightly less than for open ponds (82%, **Table 2-3**).

### 2.6.2 Reactor design: radiative transfer

For the same culture optical thickness (being the product of biomass concentration, absorption and pathlength, $\chi = C_x E_a L$), **Figure 2-4** demonstrates the improvement in light distribution of two-sided FPRs through the culture mass over the day. Unlike open ponds, the surfaces of which are exposed to extreme light at midday and dark zone deeper down, FPRs have reduced direct and diffuse light entering on one side, plus diffuse and specular reflected direct light received on the opposite side. This, combined with the tilt angle, creates more optimal light close to the front and back surfaces and removes large dark zones in the culture (**Figure 2-4**).

### 2.6.3 Comparison of productivities under different design scenarios

A total of 780 simulations were performed to ascertain best case productivities achievable under light limited conditions over a one year period of typical solar radiation for Brisbane, Australia. The variables analysed were reactor type (open pond and FPR), algal strain (*wt, tla1, 11_H5*), harvest method (continuous or 5-day batch harvest); and a range of operating biomass concentrations under continuous operation, $C_x$. For FPRs, productivities were assessed at 15 different spacing distances (ranging from 0.2–3m) and for the illuminated area of the panels oriented in either a north-south (NS) or east-west (EW) direction.

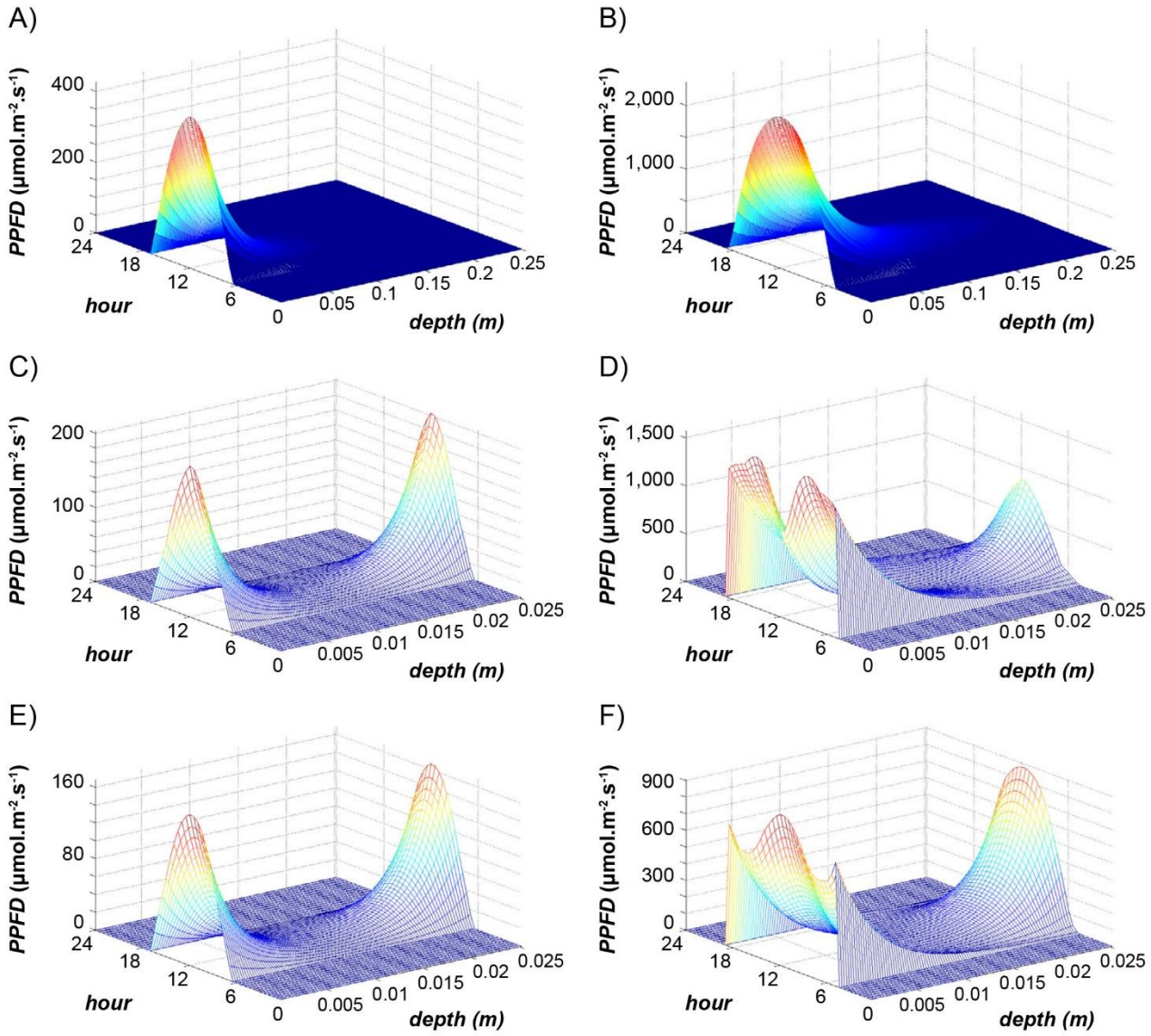


**Figure 2-4.** Radiative transfer profiles over the day and culture depth. Left and right panels are simulated on the Southern Hemisphere's Winter (June 21) and Summer (December 21) solstice days respectively in A, B) open ponds; C, D) unshaded FPRs east-west facing orientation; and E, F) unshaded FPRs north-south orientation. FPRs: pathlength = 0.025m, $C_x$ = 1 g.L$^{-1}$; Open ponds: pathlength = 0.25m, $C_x$ = 0.1 g.L$^{-1}$. Simulations were performed for cultivation of *C. reinhardtii* (*wt*).

From these simulations, the maximum areal and volumetric productivities ($P_{areal}$ and $P_{vol}$) and the optimal conditions at which they occur were identified, as summarised in **Table 2-4**. The model predictions highlight that for a given location, productivities can vary by an order of magnitude, ranging from 29 t.ha$^{-1}$.yr up to 176 t.ha$^{-1}$.yr$^{-1}$ under optimised operating conditions, depending on the reactor, system layout, and the strain. This is in agreement other actual or model-predicted values reported, where productivities have ranged from 10.5–110 ha$^{-1}$.yr$^{-1}$ in open ponds and 36–180 t.ha$^{-1}$.yr$^{-1}$ in photobioreactors (Lardon et al., 2009, Wigmosta et al., 2011, Slegers et al., 2011).

In open ponds, maximum $P_{areal}$ and $P_{vol}$ occurs under the same conditions. For a given strain cultivated in open ponds of a fixed depth, this maximum is a function of the operating biomass concentration, either under steady state, $C_x$ for continuous operation (**Figure 2-5A**) or the initial inoculating concentration, $C_{x0}$ for batch harvest (**Figure 2-5B**). Productivity predictions under batch harvest show a higher sensitivity to $C_{x0}$ than $C_x$ under continuous culture, with a narrow optimal range found at very low biomass concentrations, after which rapid declines are observed (**Figure 2-5B**).

For all strains, maximum productivities under continuous mode predicted ~15% higher yields than under 5-day batch harvest (**Table 2-4**). A comparison of growth profiles under batch harvest shows final yields in summer are nearly twice that of winter conditions (**Figure 2-6**).

For FPRs, the situation is complicated by the spacing distance between panels and an inverse relationship exists between $P_{areal}$ and $P_{vol}$ (**Figure 2-7**). Typically, higher $P_{areal}$ is achieved at smaller spacing distances, mostly due to the increased volume achieved through the use of greater numbers of FPRs per hectare, despite each FPR producing a lower $P_{vol}$. An exception can occur at extremely low spacing to panel height ratios (~0.2), where light limitation can decrease productivity to such an extent that greater numbers of FPRs do not compensate for the low $P_{vol}$ realised per reactor, reducing $P_{areal}$.

**Table 2-4.** Predicted maximum productivities under optimized conditions for different scenarios.

| **Reactor type (harvest method)** | **Strain** | **$C_x$ (g.L-1)** | **$SA_{areal}$ ($m^2.m^{-2}$)** | **Orientation** | **Spacing Distance (m)** | **$P_{vol}$ ($g.L^{-1}.day^{-1}$)** | **$P_{areal}$ ($t.ha^{-1}.yr^{-1}$)** |
|---|---|---|---|---|---|---|---|
| Open ponds (Batch) | *C. reinhardtii* | 0.05[a] | 0.8 | – | – | 0.04 | 29 |
| | *tla1* | 0.05 [a] | 0.8 | – | – | 0.05 | 40 |
| | *Chlorella* sp. | 0.05 [a] | 0.8 | – | – | 0.07 | 50 |
| Open ponds (Continuous) | *C. reinhardtii* | 0.10 [b] | 0.8 | – | – | 0.05 | 34 |
| | *tla1* | 0.15 [b] | 0.8 | – | – | 0.06 | 47 |
| | *Chlorella* sp. | 0.10 [b] | 0.8 | – | – | 0.08 | 60 |
| FPRs optimised for $P_{areal}$ (Continuous) | *C. reinhardtii* | 0.50 [b] | 4.0 | NS | 0.4 | 0.3 | 95 |
| | *tla1* | 0.50 [b] | 4.0 | NS | 0.4 | 0.3 | 100 |
| | *Chlorella* sp. | 0.50 [b] | 4.0 | NS | 0.4 | 0.5 | 178 |
| FPRs optimised for $P_{vol}$ (Continuous) | *C. reinhardtii* | 0.75 [b] | 0.6 | EW | 3 | 0.5 | 29 |
| | *tla1* | 1.00 [b] | 0.6 | EW | 3 | 0.6 | 37 |
| | *Chlorella* sp. | 0.75 [b] | 0.6 | EW | 3 | 0.8 | 47 |

[a] Initial inoculating biomass concentration. [b] steady state biomass concentration

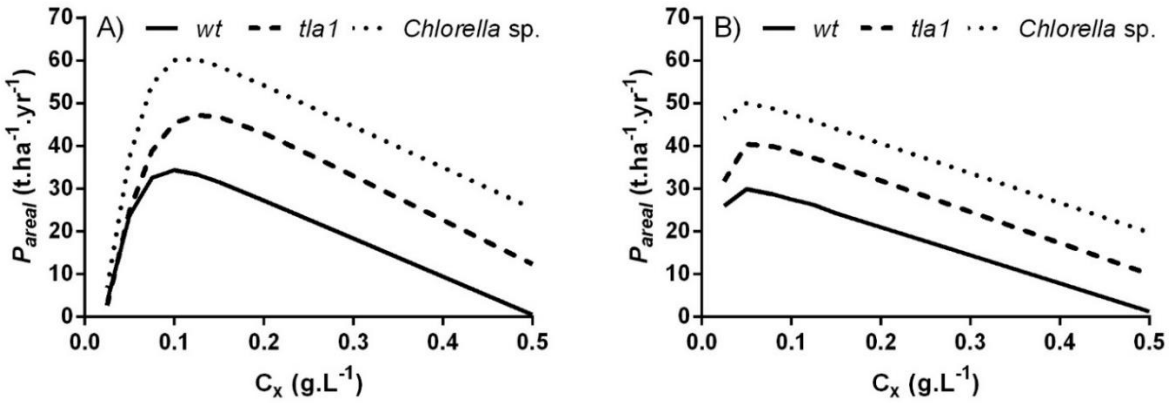


**Figure 2-5** Comparison of $P_{areal}$ in open ponds for three strains as a function of operating biomass concentration under A) continuous operation; and B) batch harvest.

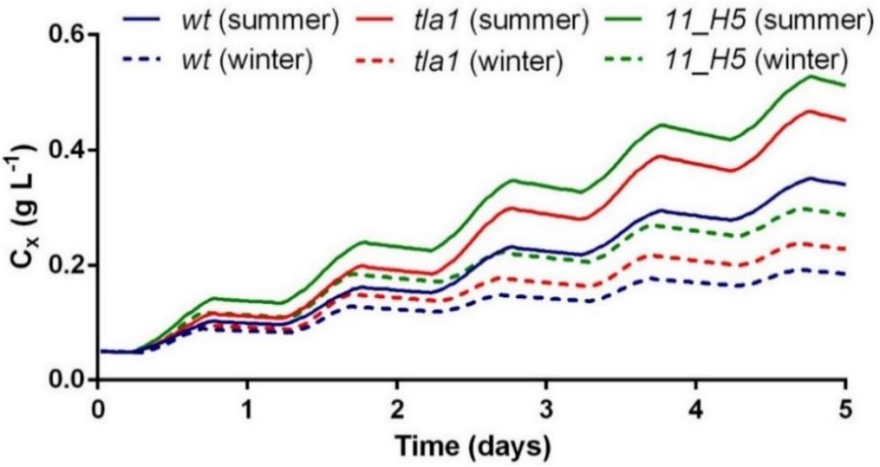


**Figure 2-6.** Predicted evolution of biomass under a 5-day batch cultivation in open ponds during summer ($N$ = 6–10) and winter ($N$ = 156–160).

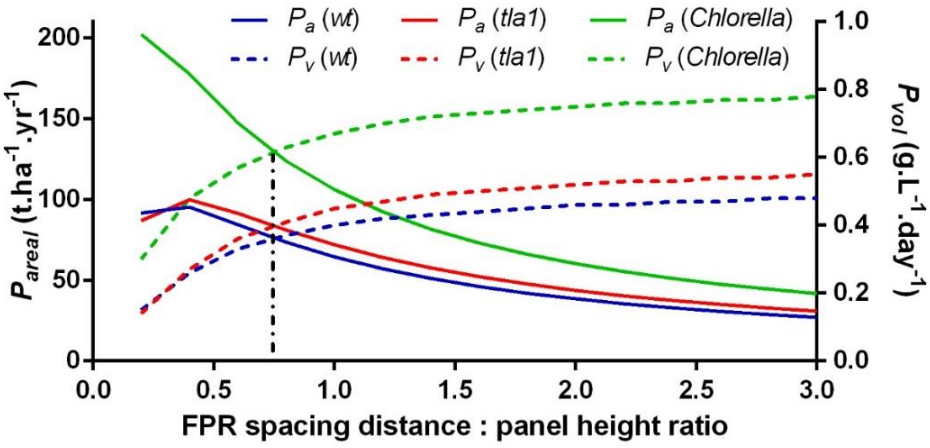


**Figure 2-7** Change in annual areal and mean volumetric productivities ($P_a$ and $P_v$ respectively) in FPRs as a function of spacing between panels. Simulations above are for north-south facing reactors at a continuous biomass operation of 0.5 g.L$^{-1}$. Solid lines = $P_{areal}$; dashed lines = $P_{vol}$. Blue = *C. reinhardtii wt*; red = *tla1*; green = *Chlorella* sp. 11_H5.

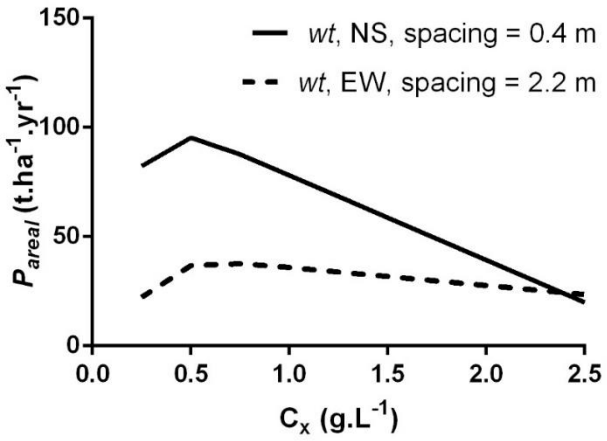


**Figure 2-8** $P_{areal}$ in FPRs as a function of operating biomass concentration at different spacing distances.

The opposite occurs as spacing distance between FPRs increases. Here, $P_{vol}$ increases in a hyperbolic manner toward a maximum, where wider spacing adds little gain in yields (**Figure 2-7**).

For consideration of a commercial scale facility of FPRs, it is therefore paramount to decide on what productivity is most desired: $P_{areal}$ or $P_{vol}$. In this regard, a true assessment of the most 'ideal' system must be coupled with LCA and TCA studies. For instance, higher $P_{areal}$ will reduce land costs but increase capital and operating costs associated with additional FPRs, in addition to higher water demands and harvesting costs as tightly spaced FPRs required dilute cultures and attain lower $P_{vol}$. Assuming land costs per ha are considerably less than bioreactor construction costs, volumetric productivity would be the more appropriate measure for flat panel reactors.

Considering open ponds under continuous operation as a base case, widely spaced FPRs optimised for $P_{vol}$ showed a 10–11 fold improvement in $P_{vol}$, despite a 14–22% reduction in $P_{areal}$ (**Table 2-4**). This will drastically reduce costs associated with harvesting, in particular dewatering. Furthermore, under this design scenario, the water volume of the 1-ha system is just 155 m$^3$ as compared to 2,050 m$^3$ for open ponds, further reducing costs for water demands.

Even tightly spaced FPRs optimised for $P_{areal}$ resulted in a ~4–6 fold increase in $P_{vol,}$ as well as a ~2–3 fold increase in $P_{areal}$, depending on the strain. For FPRs, both the optimal panel orientation and operating biomass concentration were affected by spacing distance. For tightly spaced FPRs, a north-south orientation of the panel's illuminated surface yielded slightly higher productivities, while for widely spaced FPRs, east-west orientations performed better. For tightly spaced FPRs, optimal biomass concentrations were 50-100% lower than for widely spaced FPRs (**Table 2-4**) and productivities were more sensitivity to changes in $C_x$ (**Figure 2-7**). This is due to the lower incident light received at each reactor, thus requiring more dilute cultures to avoid dark zones.

### *2.6.3.1 Comparison of productivities between three algal strains*

As summarised in **Table 2-4**, each algal strain showed large differences in predicted productivities, where their performance was also dependent on the system design. In consideration of *C. reinhardtii* as a base case algal strain, the engineered small antenna mutant *tla1*, with reduced absorption capacity showed a 38% productivity increase when cultivated under continuous operation in open pond systems. To achieve this, *tla1* required a higher culture density, with an optimised operating concentration 50% higher than *wt* and 11_H5 (**Table 2-4**). In addition, *tla1* showed less sensitivity to changes in biomass concentration with a broader peak productivity range than the other two strains (**Figure 2-5**).

In FPRs, the advantages of the small antenna system of *tla1* were less beneficial than open ponds, where only a modest 5% gain was realised in tightly spaced FPRs, increasing to a 25% gain in widely spaced FPRs in comparison to *C. reinhardtii*. These results are not surprising since the reduction in cellular light absorption is most advantageous for open ponds with large dark zones, whereas predictions suggest that the higher saturating irradiance required of *tla1* is not suitable for low light conditions, such as those found in tightly spaced FPRs. Remarkably, the fast-growing *Chlorella* sp. 11_H5 gave the highest improvement in modelled productivities, yielding 76% gains in open ponds and 60–86% gains in FPRs in comparison to *C. reinhardtii*. In fact, tightly-spaced light limited FPRs showed the highest productivity gains for *Chlorella* sp., with model predicted yields of 178 $t.ha^{-1}.yr^{-1}$. The optimal operating biomass concentration to achieve maximum productivities were the same for *C. reinhardtii* and *Chlorella* sp.

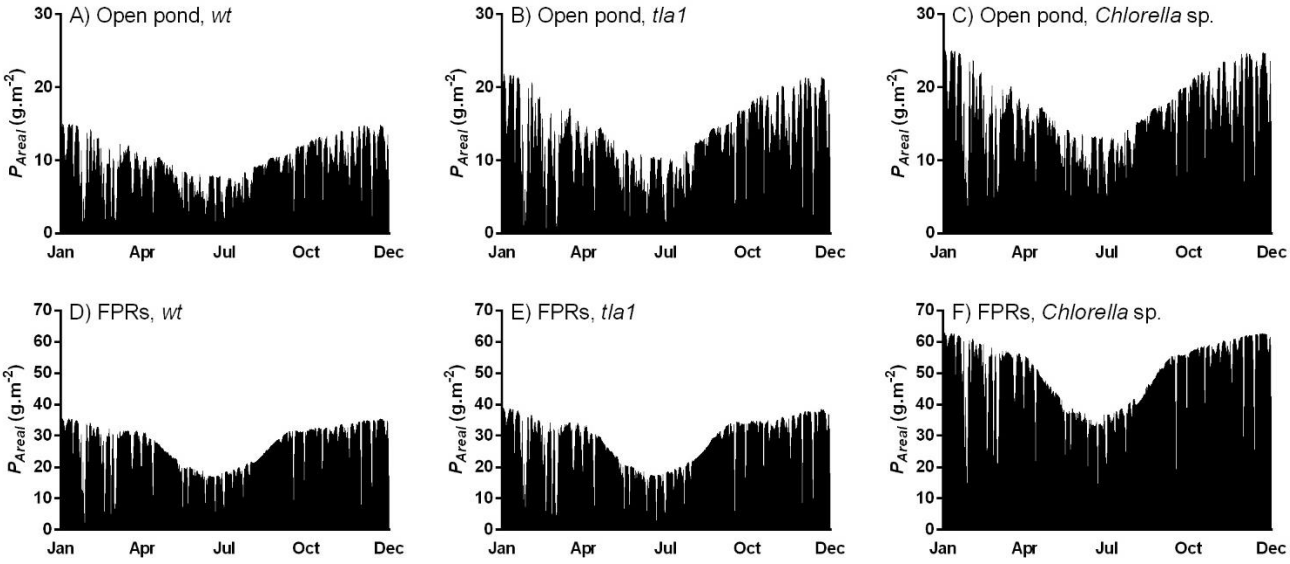


**Figure 2-9.** Maximum daily $P_{areal}$ under continuous cultivation and optimized conditions in open ponds and tightly spaced (0.4m) NS oriented FPRs for each strain.

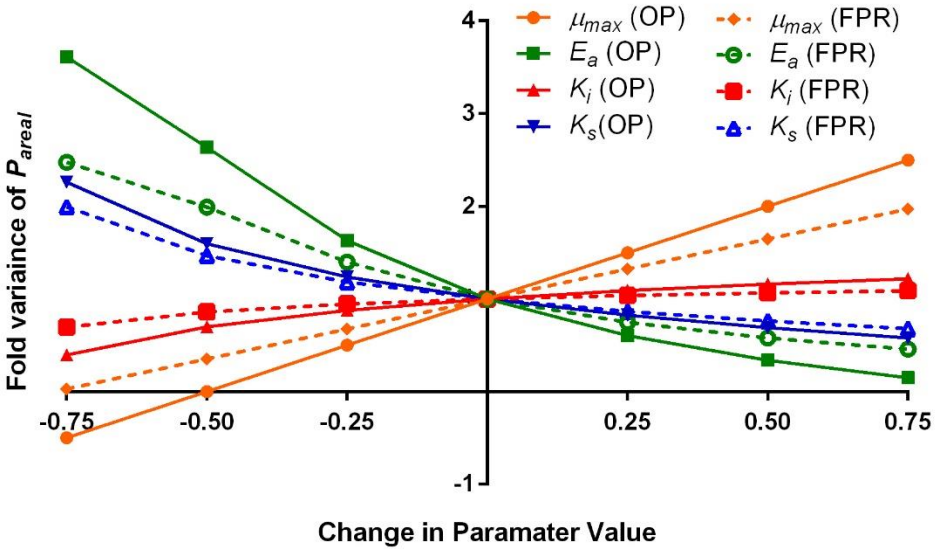


**Figure 2-10** Sensitivity plot showing fold variance in $P_{areal}$ in open ponds (solid lines, denoted above as 'OP') and FPRs (dashed lines) as a function of changes in algae-specific model parameter values ($\mu_{max}$, $K_i$, $K_s$, $E_a$).

### *2.6.3.2 Sensitivity analysis of algal properties*

For a given reactor design and operating condition, algal productivity is influenced by the growth parameters of a particular strain (maximum growth rate, $\mu_{max}$, the irradiance of saturation, $K_s$ and the irradiance of photoinhibition, $K_i$) as well as its optical properties (in particular the mean mass absorption coefficient, $E_a$). Therefore, a sensitivity analysis was performed to assess changes in these parameter values to predicted productivities, in order to assess the precision required for their estimation and to gain insight into which properties are most desired to select a high-productivity algal strain. Simulations were performed using *C. reinhardtii* for cultivation in both open ponds and FPRs at optimised continuous biomass concentrations (**Figure 2-10**). Parameter values were modified at 0.25 intervals to a range of ±0.75 of the original value.

All parameters showed that less sensitivity to changes in productivities occurred in FPRs than in open ponds due to the extreme light gradients of the latter. $E_a$ showed the highest sensitivity to change, with an approximate ± 60% fold variance in $P_{areal}$ in open ponds for a change of ±25% in its estimated value. Further reductions in $E_a$ resulted in a larger positive fold variation in $P_{areal}$, yet further increases in $E_a$, resulted in less change. This suggests that light distribution has a larger bearing on $P_{areal}$ than the growth properties of the strain and that a high precision of radiative transfer is required to give reliable productivity estimates. It should also be noted that a relationship exists between $E_a$ and the growth parameters, particularly $K_i$ and $K_s$, as demonstrated by the parameters fitted to experiment data of *tla1*. On the one hand, a low $E_a$ will be accompanied by less photoinhibition, resulting in $P_{areal}$ improvements associated with higher $K_i$, but on the other hand, will require higher light for saturation

($K_s$), reducing $P_{areal}$. Indeed, a reduction of $K_s$ predicted greater improvements in $P_{areal}$ than the same increase in $K_i$, but still, its positive effects were small compared to the combined effects of $E_a$ and $K_i$. The estimation of $\mu_{max}$ was the most sensitive growth parameter, showing a linear relationship and was most sensitive to decreases in its value.

## 2.7 Conclusion

In summary, these simulations show the potential of mathematical models to predict the optimal operating conditions to maximise productivities and how essential it is to determine them; otherwise systems could very well operate far below the maximum achievable production levels. Furthermore, these rapid assessments save time and cost of large scale experiments and trial and error, which is critical to advance this technology.

It should be noted that the above simulations provide an upper limit based solely on light, and do not consider other variables that may reduce productivity. Ideally, nutrients, pH and gas exchange should be optimised. Importantly, the model considered here does not account for temperature variations, which will no doubt affect productivities through the modulation of enzyme kinetics and will be incorporated into a later model.

However, this model does highlight the variables that can be optimised to achieve better photosynthetic efficiencies. For instance, traditional open pond systems offer more limited options for improvements in gains and the model suggests that it is essential to optimise biomass concentration to realise maximal yields. The results also suggest that FPRs positioned carefully can demonstrate a significant potential for maximising both $P_{areal}$ and $P_{vol}$. Moreover, the choice of a suitable strain is paramount to increasing feasibility and energy returns as, unlike design factors, there are no (or relatively little) costs associated with the selection of an algal species. An ideal species should possess both a low absorption cross section and high photon conversion efficiency.

# 3 Model validation and analysis of *C. reinhardtii* and *tla1* productivity using a novel environmental PBR matrix to simulate outdoor conditions.

## 3.1 Abstract

In this chapter, validation of the model proposed in Chapter 2 was attempted using a matrix of laboratory-scale environmental photobioreactors (ePBRs) fitted with programmable LED arrays that enabled light simulations of diurnal solar cycles. The ePBRs are designed to emulate solar conditions in outdoor ponds while controlling other parameters including temperature, pH, $CO_2$ and mixing. To assess the robustness of the model under a wide range of incident solar conditions and culture densities, experiments were run under batch mode to simulate three different light cycles representing 'typical' days in Brisbane Australia: 1) winter clear sky (i.e. no cloud cover); 2) spring/autumn clear sky; and 3) cloudy (low light) day. Growth was monitored for 7–9 days for *C. reinhardtii wt* (all light regimes) and 9 days for *tla1* (spring/autumn regime only) and compared against model predictions. In addition, an analysis of $O_2$ evolution, photoacclimation processes via changes in cellular pigment composition; and photoregulation processes via changes in photosystem II (PSII) activity of chlorophyll fluorescence were performed. It was found that the model could accurately predict growth under some, but not all diel light cycles and under an evolving culture. This was mostly attributed to the model's failure to account for dynamic acclimation processes. Additionally, as culture density increased, respiration and/or photoinhibition type processes appeared to decrease. The model was subsequently modified to account for the observed changes and the revised predictions showed good agreement to measured changes in biomass.

## 3.2 Introduction

Predictive models of algal growth are essential tools to assess the upper limits of productivity without the time and costs associated with large-scale experiments. However, models require rigorous validation under the conditions they set out to test to ensure that they are robust and reliable. For light limited models, all other variables must be tightly controlled to the model assumptions, ensuring that the final productivity is solely a function of the light regime. In outdoor systems, these requirements are challenging due to the large number of variables that may affect productivity, such as rapid changes in solar irradiance from intermittent cloud cover, unforeseen weather events, temperature and pH fluxes, gas exchange rates, contamination, predator grazing and sub-optimal nutrient supply, to name a few. For this reason, many models are validated under tightly controlled laboratory conditions where algal cultures are subjected to steady state conditions in chemostat or turbidostat

mode (i.e. continuous operation) and under constant incident irradiance. These lighting regimes are far from most outdoor mass cultures which are operated under batch or semi-continuous mode and under a range of diel solar cycles.

Lucker et al. (2014) introduced a novel laboratory-scale environmental photobioreactor (ePBR) matrix "designed to replicate the environmental conditions in algal production ponds and natural systems that impact algal physiology, energy capture, and life cycle". The ePBR matrix allows simulation of diel light and temperature cycles more representative of outdoor cultures whilst allowing tight control of other variables. This system was used for validation experiments of the model presented in Chapter 2. Growth of CC125 and its truncated antenna mutant, *tla1* (Mitra et al. 2012) was monitored under batch mode with simulation of three representative diel cycles of solar radiation in Brisbane, Australia.

## 3.3 Methods and Experimental Design

### 3.3.1 Microalgae culture and medium

*C. reinhardtii* strains CC125 (*wt*) and its truncated light antenna mutant, CC4169 (*tla1*) were purchased from Chlamy Collection (www.chlamycollection.org). Stock cultures were grown in flasks for two weeks under moderate light (~100 µmol.$m^{-2}$.$s^{-1}$) at room temperature and shaken by hand twice daily. Cells were cultured in photoautotrophic media (TAP minus acetate media).

### 3.3.2 Photobioreactor matrix setup

Biomass productivity of *C. reinhardtii* (strain CC125) was monitored using a novel matrix of photobioreactors (ePBR, Phenometrics, Langsing MI USA) as described by Tamburic et al. (2014) in collaboration with the research group of Prof. Peter Ralph, University of Technology Sydney. Each ePBR is cylindrical with a light path of 0.25 m and a working volume of 450 mL (**Figure 3-1**). Temperature was maintained with a Peltier controlled temperature jacket at 25$^{o}$C, since the growth parameters derived from $\mu$-$E$ curves were established at this temperature. Cultures were sparged with ambient air through a gas dispersion tube and 1,100 ppm $CO_2$. Dilute suspensions ($OD_{750}$ = 0.1) were inoculated into the cylindrical ePBRs. The suspension was cultivated in the ePBR for 48 h to pre-acclimate cells, then re-diluted to an $OD_{750}$ of 0.05–0.1. Each treatment was performed in duplicate.

### 3.3.3 Light regimes and treatments

In order to mimic outdoor conditions in open ponds or single sided horizontal FPRs, a one-directional light source was positioned above the cultivation chamber of the ePBR using a panel array of white

light emitting diodes (LEDs) collimated through a molded plastic optical component so that the irradiance can be considered almost exclusively direct (Lucker et al. 2014).

The LEDs have a spectral composition similar to daylight (Tamburic et al., 2014, Appendix 8.2). The LEDs were programmed with a sinusoidal irradiance profile and day length ranging from 0 to a maximum irradiance, ($I_{max}$, μmol.m$^{-2}$.s$^{-1}$) with light intensities changing at 1 minute intervals. The three irradiance cycles, referred hereafter as 'cloudy', 'winter' and 'spr/aut', represent relative low, moderate and high light days for Brisbane, Australia (27.5$^{o}$S 153$^{o}$E). These were compiled from model predictions using actual meteorological daily solar radiation data as an input (as described in Chapter 2). Light intensities were averaged over the season for winter and spring/autumn under clear sky conditions (i.e. no cloud cover, $K_t \geq 0.75$). For the 'cloudy' treatment, irradiance values were averaged for days of high cloud cover throughout the year that had a $K_t$ index <0.2. It should be noted that since the LEDs provided almost only direct irradiance, model predictions were also simulated on the assumption of direct irradiance only.

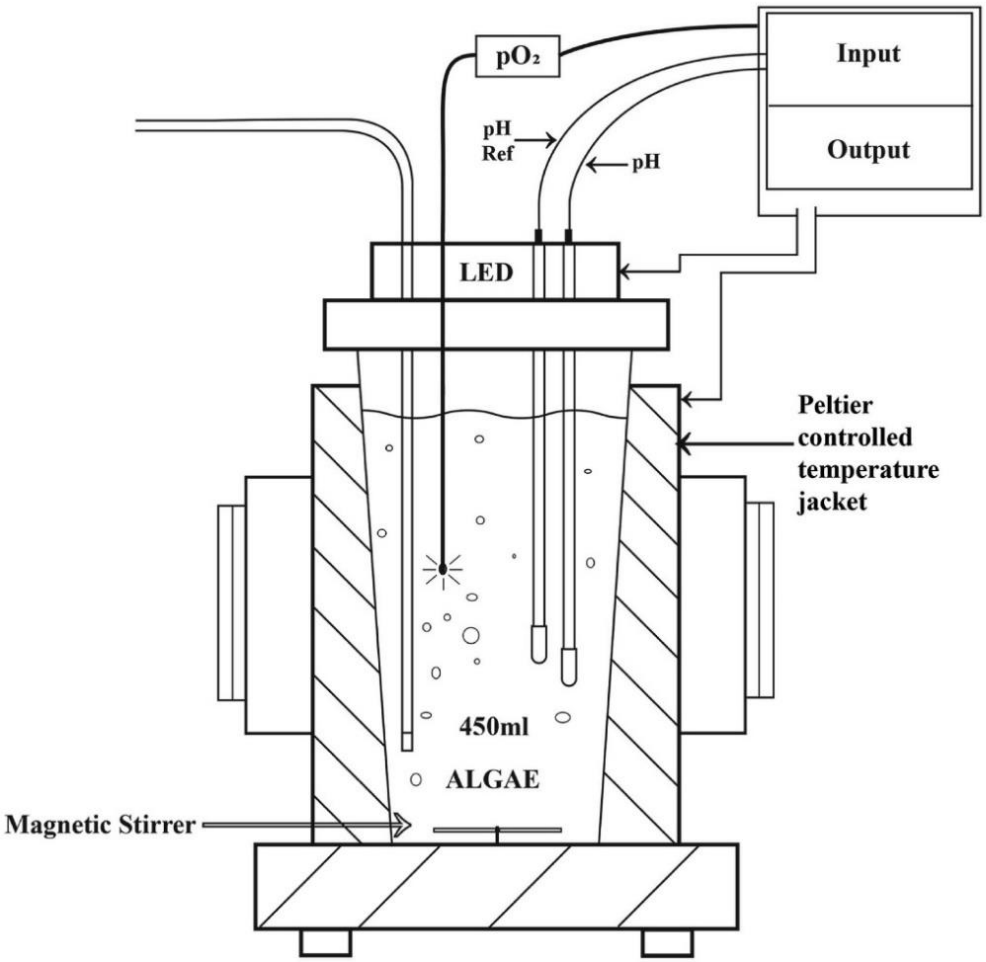


**Figure 3-1.** Schematic diagram of a single ePBR that forms part of a matrix of ePBRs (source: Tamburic et al. 2014. doi:10.1371/journal.pone.0086047.g001).

Four experimental treatments were analysed in duplicate reactors over two time periods. The first two experiments were performed over a 7-day period using winter and cloudy light regimes, both with cultivation of *wt*. The third and fourth experiments were performed for two treatments over a 9-day period, both using the spr/aut light regime but with cultivation of *wt* and *tla1* respectively. The key variables defining the light regimes and treatments are summarised in **Table 3-1**.

### 3.3.4 Estimation of biomass production from $OD_{750}$ measurements

Biomass dry weight (BDW) measurements are the 'gold standard' for analysing changes in biomass. However, the substantial sample volume required to be taken from the culture for BDW would result in changes in the light profile and pathlength over the cultivation period or would require replacing sampled volume with media, thereby diluting the culture. Subsequently BDW measurements were taken at the beginning ($t_0$) and end ($t_{end}$) of each experiment and a calibration of BDW versus $OD_{750}$ was established for each treatment. For BDW, triplicates of a given volume of sample of known $OD_{750}$ were filtered onto pre-weighed and pre-combusted glass fibre filters (Whatman G/F) and dried at 90°C until no further change in weight occurred.

During the cultivation period, 1 ml samples were taken from each PBR and measured at one or two time points each day at 680, 750 and 940 nm in a spectrophotometer. Additionally, growth was monitored continuously *in situ* with an optical density probe at 940 nm and compared with external $OD_{940}$ measurements for verification. BDW was estimated from the correlation values to 750 nm, as reported in **Table 3-2**.

**Table 3-1.** Experimental treatments and description of light regimes. $I_{0,max}$ = maximum incident irradiance at noon, $I_{0,avg}$ = daily averaged incident irradiance. Each experiment was performed in duplicate ($N$ = 2). Experiments 1 and 2 were conducted 16–23 October 2014 and Experiments 3 and 4 were conducted 9-18 December 2016.

| Expt | Strain | Light regime | Light regime description | Expt. Duration (days) | Light hours ($day^{-1}$) | Daily $I_{0,max}$ (µE) | Daily $I_{0,avg}$ (µE) |
|---|---|---|---|---|---|---|---|
| 1 | *wt* | winter | Mean irradiance for winter clear sky days, Brisbane | 7 | 12 | 1,262 | 394 |
| 2 | *wt* | cloudy | Mean irradiance for high cloud cover days ($K_t$ < 20%), Brisbane | 7 | 12 | 435 | 138 |
| 3 | *wt* | spr/aut | Mean irradiance for spring and autumn clear sky days, Brisbane | 9 | 14 | 1,416 | 515 |
| 4 | *tla1* | spr/aut | Mean irradiance for spring and autumn clear sky days, Brisbane | 9 | 14 | 1,416 | 515 |

**Table 3-2.** BDW ($g.L^{-1}$) versus $OD_{750}$ calibration. Values are the mean of triplicate samples taken from each of two reactors at the beginning and end of the experiment. Standard deviation is reported as the combined error of BDW and $OD_{750}$ values.

| **Light regime (strain)** | **BDW ($kg.m^{-3}$) at $OD_{750}$ = 1** | **$R^2$** |
|---|---|---|
| winter (*wt*) | 0.43 ± 0.04 | 0.96 |
| cloudy (*wt*) | 0.45 ± 0.08 | 0.98 |
| spr/aut (*wt*) | 0.40 ± 0.05 | 0.97 |
| spr/aut (*tla1*) | 0.22 ± 0.16 | 0.95 |

A similar correlation of BDW and $OD_{750}$ occurred for *wt* under all light regimes. Remarkably, the correlation of BDW and $OD_{750}$ for *tla1* was approximately half that of *wt* (0.22 ± 0.16) suggesting a high amount of cell scattering, possibly due to changes in its refractive properties, size or number. Furthermore, the large standard deviation of *tla1* occurred mostly from the final BDM measurement of R2 which was almost twice that of R1 and remarkably similar to *wt* (0.40 ± 0.004). Growth and pigment analyses between R1 and R2 for *tla1* also differed markedly, suggesting a possible reversal of the *tla1* mutant back to its wildtype phenotype in R2, as discussed in the Results section.

### 3.3.5 Pigment composition

The cellular mass fractions of Chl *a*, Chl *b* and Car ($kg.kg^{-1}$) were determined using a spectrophotometer. A volume of 1 ml of cells were filtered onto glass fibre filters (Whatman G/F), cut into strips and placed into Eppendorf tubes with an equal volume of 90% acetone de-acidified with saturated $MgCO_3$. Tubes were placed in a sonication bath on ice then incubated at 4°C in the dark for 4 h, vortexed and centrifuged at 13,000rpm for 5 min to remove debris from the supernatant. Concentrations were found according to Strickland and Parsons (1972):

Eq. 3-1 $$C_{Chl\ a} = 11.6(\mathrm{OD}_{665} - \mathrm{OD}_{750}) - 1.31(\mathrm{OD}_{645} - \mathrm{OD}_{750}) - 0.14(\mathrm{OD}_{630} - \mathrm{OD}_{750})$$

Eq. 3-2 $$C_{Chl\ b} = 20.7(\mathrm{OD}_{645} - \mathrm{OD}_{750}) - 4.34(\mathrm{OD}_{665} - \mathrm{OD}_{750}) - 4.42(\mathrm{OD}_{630} - \mathrm{OD}_{750})$$

Eq. 3-3 $$C_{Car} = 4.0(\mathrm{OD}_{480} - \mathrm{OD}_{750})$$

The mass fraction of each pigment was found by dividing the above concentrations by the BDW.

### 3.3.6 Quantum yield of photosystem II (ΦPSII)

The quantum yield of photosystem II ($\Phi_{PSII}$) measures the PSII operating efficiency in the light, i.e. the portion of absorbed light that is used for $Q_A$ reduction (Baker 2008):

Eq. 3-4 $$\Phi_{PSII} = (F_m' - F) / F_m'$$

Where $F_m'$ is the light-adapted maximum fluorescence of PSII and $F$ is the steady state minimum fluorescence in the light. $\Phi_{PSII}$ was determined for the winter and cloudy regimes during the first experimental period at seven daily timepoints using a handheld pulse-amplitude modulated fluorometer (Pocket PAM, Walz, Effeltrich, Germany). The Pocket PAM was placed against the outside of each PBR chamber at 8 cm along the height axis. Measurements were taken on non-dark adapted cells at: 05:45 (pre-dawn), 06:15 (shortly after the onset of light); 09:00 (mid-morning), 11:45 (midday), 15:00 (mid-afternoon), 17:45 (pre-dusk) and 18:15 (shortly after the onset of dark). Pocket PAM settings were: measuring irradiance = 0.2 µmol photons $m^{-2}$ $s^{-1}$ PAR; saturation pulse irradiance = 2600 µmol photons $m^{-2}$ $s^{-1}$ PAR; saturation pulse width = 0.8 s.

### 3.3.7 Dissolved Oxygen (pO2) Profiles

*In situ* $pO_2$ profiles were measured optically using mini sensors (PyroScience).

## 3.4 Results & Discussion

### 3.4.1 Assessment of batch growth via changes in optical density

The evolution of biomass was monitored by changes in optical density at 940 nm both *in situ* using an optical density probe ($OD_{940,in\ situ}$) and externally by taking triplicate 1 ml aliquots from each reactor and measuring photospectrometrically in a 10mm pathlength cuvette ($OD_{940,spec}$). **Figure 3-2A & B** reveals that errors with *in situ* probe readings occurred, resulting in large variations in $OD_{940,in\ situ}$ measurements between reactors 1 and 2 (R1 and R2 respectively) for both winter and cloudy treatments, as well as large anomalies on days 3 and 7 in the cloudy treatment (**Figure 3-2B**).

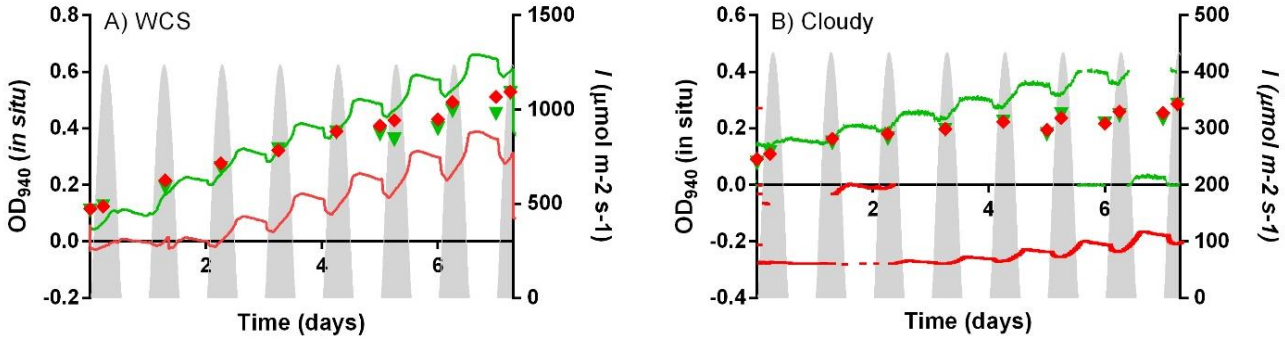


**Figure 3-2.** Change in biomass as monitored by changes in optical density at 940 nm using an *in situ* optical density probe ($OD_{940,in\ situ}$: green lines (R1); red lines (R2)) and comparison with external $OD_{940}$ readings on 1 ml aliquots using an external photospectrometer ($OD_{940,spec}$: green triangles (R1); red diamonds (R2)). $OD_{940,spec}$ values for each reactor are the mean of three technical replicates.

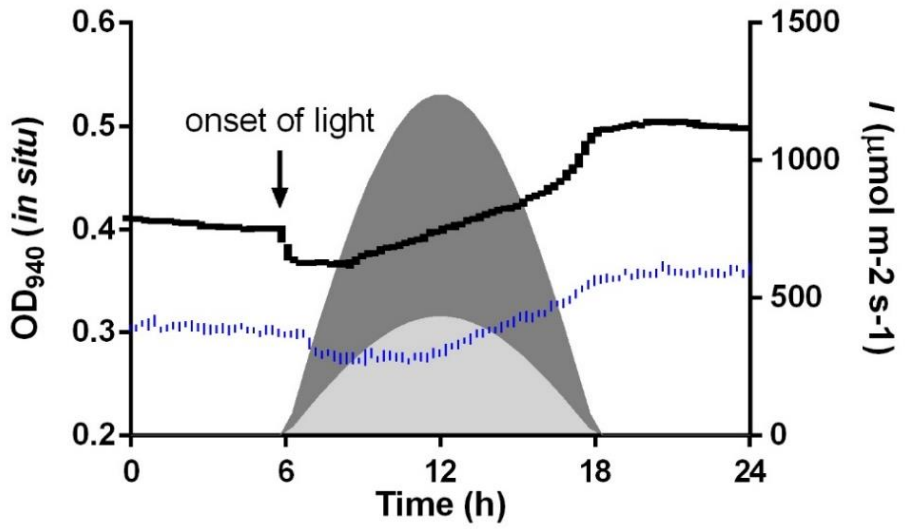


**Figure 3-3.** Daily profile of *in situ* measurements of $\Delta OD_{940}$ as an indicator of biomass growth (day 4 used as an example) for WCS (black line) and cloudy (blue line) in response to their respective irradiances (WCS = dark grey; cloudy = light grey). Errors encountered with the optical density probe may show artefacts in the data (see text for further details).

These problems also occurred during Experiment 2 for spr/aut regime and cultivation of *wt* and *tla1* (data not shown). Furthermore, the *in situ* probe errors also resulted in differences in absolute values of $OD_{940,in\ situ}$ and $OD_{940,spec}$ measurements (red diamonds and green triangles), the latter being highly consistent between the replicate reactors. Therefore, external OD measurements were used for calibration against BDW to estimate changes in biomass concentration ($\Delta C_x$).

Despite the problems encountered with $OD_{940,in\ situ}$ measurements, the pattern observed from their daily profiles was relatively consistent throughout each experiment and among the different treatments, providing insight into the daily growth pattern of *C. reinhardtii*. **Figure 3-3** shows a typical day midway through the cultivation period (day 4) for winter (black line) and cloudy (blue line) treatments. At the onset of light, a decline in $OD_{940}$ occurs until mid-morning (~9.30am). This coincides with increases in dissolved $O_2$ profiles with a peak in $O_2$ at ~9.30am for winter treatment, but continued increase until ~12pm for cloudy treatment (**Figure 3-8**). Growth occurs throughout the remainder of the light period, with a sharp increase occurring toward the end of the light period. A slight increase continues at the onset of dark before a consistent decline occurs attributable to dark metabolism. Importantly, in all regimes the net hours of $OD_{940}$ increases (i.e. growth) were approximately the same as the number of light hours, as predicted by the model. The remarkable decline in $OD_{940}$ at light onset may due to metabolic changes that occur to ready the cell for photosynthesis. For example stored energy reserves (starch or lipids) may be metabolised to synthesise photosynthetic proteins, explaining the drop in biomass.

The high peak of $OD_{940}$ toward the end of the light period may signal a reduction in light-enhanced dark respiration in response to lower light levels (Xue, Gauthier, Turpin, & Weger, 1996) or a lag between the light reactions and biosynthetic pathways. In any case, further investigations are required to establish the underlying cause of these $OD_{940}$ patterns, which may also reflect changes in cell aggregation or scattering in response to circadian rhythm or cell cycling patterns.

### 3.4.2 Photoacclimation: changes in cellular pigment composition

The model presented in Chapter 2 assumed that optical properties of the cell remained constant. To validate this assumption, cellular pigment contents were monitored throughout the evolution of the batch cultivation in each treatment by spectroscopic analysis.

Cultivation of *wt* under cloudy and winter light regimes showed similar acclimation trends (**Figure 3-4A & B**). Upon commencement of the experiment, a sharp decline in pigments was observed from pre-dawn to noon on day 1. This suggests that pre-cultures may have been low-light acclimated and also shows the speed at which cells can reduce their absorption capacity in response to sudden increases in light. From days 1–4, pigment contents remained fairly stable and were reasonably similar between treatments (mean Chl *a* concentration of ~24 and ~25 $g.kg^{-1}$ for winter and cloudy respectively). On day 5 a shift occurred, resulting in a dramatic increase in pigments from day 6 onwards with Chl *a* content rising to ~34 and ~42 $g.kg^{-1}$ for winter and cloudy respectively. This pattern of shifting from high- to low-light acclimation from the start to the end of a batch culture is consistent with other reports as reviewed in Chapter 1.

In contrast to winter and cloudy treatments, cultivation of *wt* under the high light spr/aut treatment showed relatively consistent pigment levels throughout the cultivation, with mean Chl *a* concentrations also ~25 $g.kg^{-1}$ (**Figure 3-4C**). The culture appeared to remain high light acclimated throughout the 9-day cultivation period, despite reaching higher culture densities than winter and cloudy. This is likely because the higher incident irradiance and longer light hours of spr/aut resulted in a higher average irradiance, $I_{avg}$ over the depth of the culture and time.

Winter and cloudy pigment measurements were taken once daily, while spr/aut were taken at pre-dawn and at the end of the day. Here, daily fluctuations in pigment contents were also observed. As the spr/aut culture stabilised, these fluctuations showed a typical pattern of an increase between ~8-17% in pigment fraction from the start to the end of the day. Although rapid acclimation processes can occur, particularly from a shift of low- to high-light acclimation, as seen on day 1 of the cloudy and winter treatments, it seems that this may happen upon a sudden disruption to the culture (for instance, after a batch harvest when are highly re-diluted).

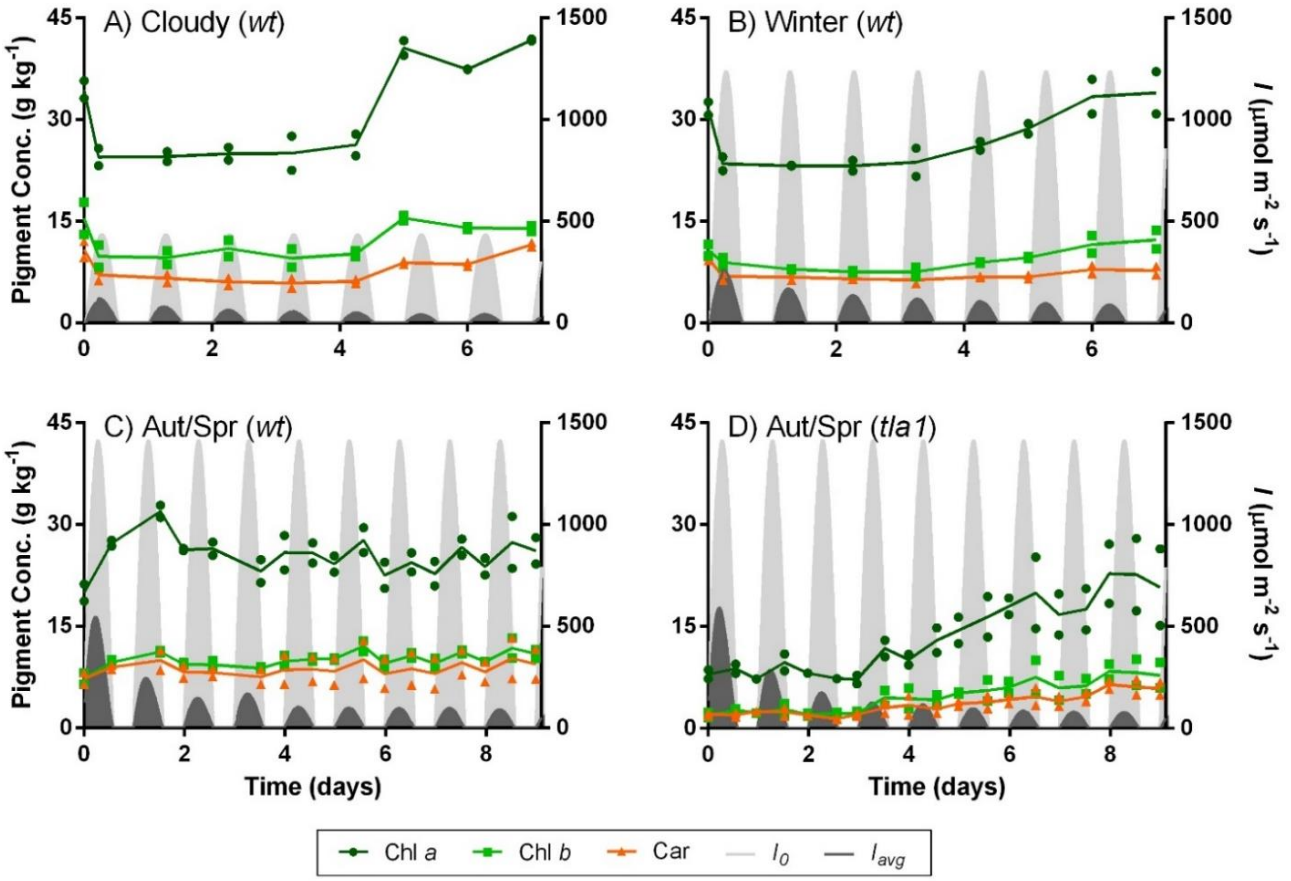


**Figure 3-4**. Changes in mass cellular pigment concentrations of Chl *a* (dark green), Chl *b* (light green) and Car (orange) during batch cultivation. Incident irradiance ($I_0$ = light grey) and locally averaged irradiance through the culture depth ($I_{avg}$ = dark grey) are shown.

For the most part, the relatively similar pigment levels of *wt* seen under all treatments for at least days 1-4 (Chl *a* ~25g.kg$^{-1}$) suggests that acclimation processes may be slower under more constant conditions (i.e. the same daily light cycles used here), remaining relatively stable up until a critical point at which a signal occurs to switch from a low-light phenotype (days 5$^{+}$ in winter and cloudy). In fact, Takache et al. (2014) investigated *C. reinhardtii* under 1:1 light/dark fractions of duty cycles ranging from 3–360s and also found Chl *a* levels similar to that reported here (~22–25 g.kg$^{-1}$) and slightly lower for more rapid cycles (~20 g.kg$^{-1}$ where $t_c$ = 0.5–1 s).

Remarkably, the 'low chlorophyll' strain *tla1* appeared to revert back to a wildtype phenotype over the cultivation period (**Figure 3-4D**). Initially *tla1's* Chl *a* concentration was ~40% to that of *wt* at ~18 g.kg$^{-1}$ (similar to that reported by Berberoglu, Pilon, and Melis (2008) at 18.98 ± 1.36) However toward the end of the culture the pigment concentration in R2 was similar to *wt* (up to 28.31± 0.41 g.kg$^{-1}$). The same trend occurred in R1, but with lower pigment levels, however, this culture also crashed. Remarkably, growth of *tla1* was poor until the increase in pigment levels occurred,

suggesting that genetic modifications to light harvesting antenna systems can have unexpected detrimental consequences on photosynthesis.

### 3.4.3 Validation of the static μ–I Haldane growth model

The model's assumption of constant optical properties was invalidated by these results, with the above reported pigment mass fractions showing up to 80% variation over the cultivation period. For a start, this will change the optical properties of the cell and affect light transfer through the culture. Subsequently, to provide a more accurate prediction of radiative transfer in order to validate the growth component of the model, daily-averaged optical parameter values ($E_a$, $E_s$, and $b$) were re-calculated from actual pigment concentrations reported below using the semi-predictive method based on Mie theory as described in Section 2.4.3. These values were input into the model for the simulations below.

**Figure 3-5** compares actual and model-predicted changes in biomass concentration using the modified optical properties. Model predictions for *wt* under the winter light treatment varied within an acceptable range of 8%. However, the model overestimated final biomass in the low-light cloudy treatment by 10% and underestimated final biomass in the high-light spr/aut treatment by 27%. A refit of the model parameters continually showed an overestimation under low incident light (cloudy) and underestimation under high incident light (spr/aut).

Regressional and residual analyses (**Figure 3-6A & B** respectively) further revealed in all light treatments that modelled predictions overestimated growth at low cell densities during early cultivation (at least the first 4–5 days) then underestimated growth at higher cell densities. In retrospect, one limitation of these validation experiments was the short duration of cultivation (7–9 days) and the residual plot analysis (**Figure 3-6B**) suggests that longer cultivation periods resulting in higher cell densities may have produced even larger discrepancies.

A similar two-part study by Fouchard et al. (2009) and Degrenne et al. (2009) also modelled growth of *C. reinhardtii* under batch cultivation using the Haldane growth model and a similar method of estimating model parameters by exposing different cell samples to a range of steady-state irradiances. The difference in their study was that for validation experiments they used constant incident irradiances rather than diurnal cycles. In their studies, the same phenomenon of higher modelled predictions occurred during the start of batch cultures and a re-estimation of parameter values resulted in a large decline in both $\mu_{max}$ and $R_s$. The authors attributed the errors to photosynthetic differences arising from the so-called 'kinetic regime' occurring under constant light conditions used to establish

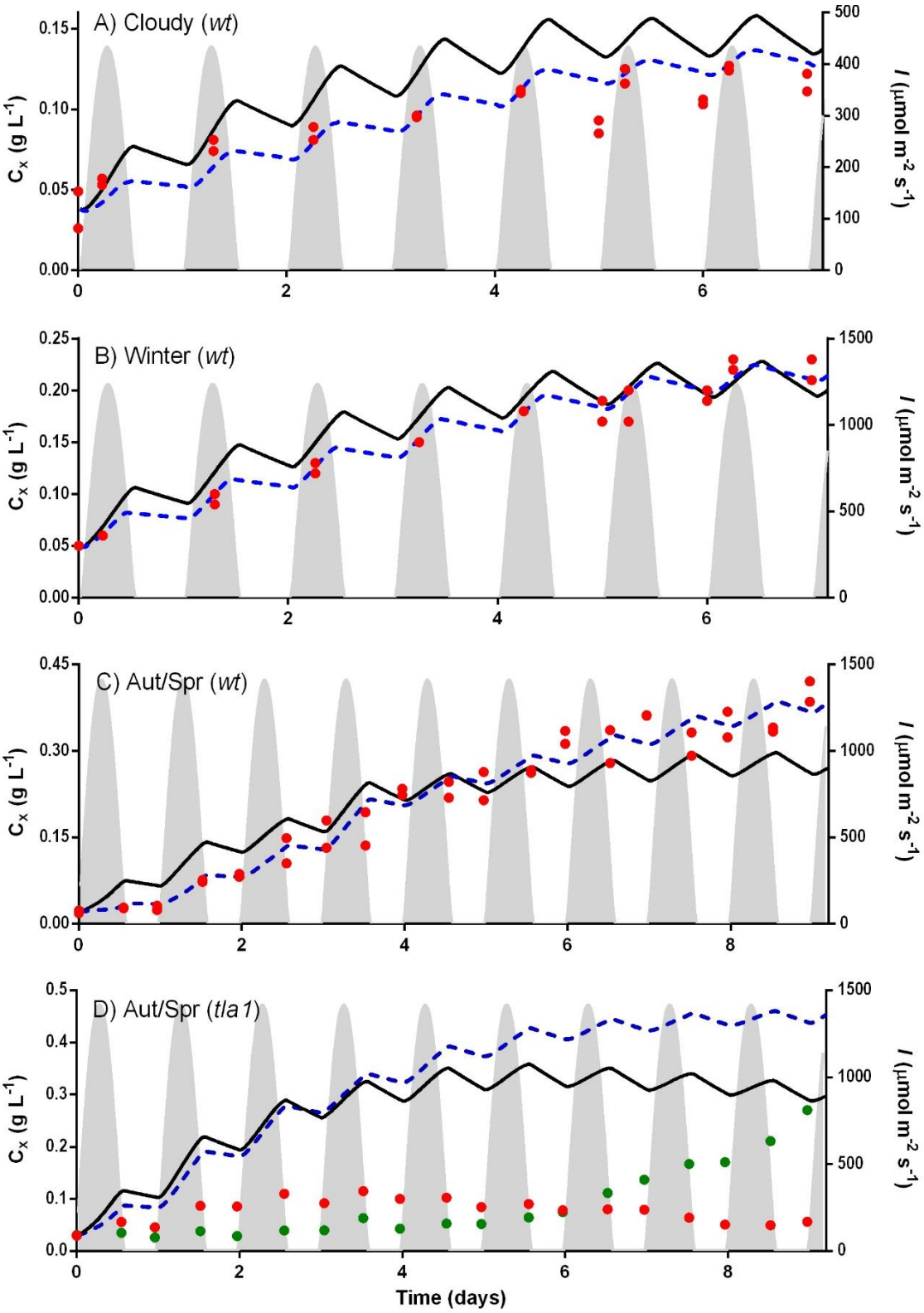


**Figure 3-5.** Comparison of experimental and model-predicted changes in biomass over a batch cultivation for the following treatments: A) winter, cultivation of *wt*; B) cloudy, cultivation of *wt*; C) spr/aut, cultivation of *wt*; and D) spr/aut, cultivation of *tla1*. Black solid line = original Haldane model (Eq. 2-4); Blue dashed line = modified Haldane model with new respiration rate, $R_s$ (Eq. 3-5); red dots = measured biomass from two individual reactors ($n$ = 2). Note: in D), red dots and green dots are shown to differentiate reactors, due to remarkable differences in growth patterns.

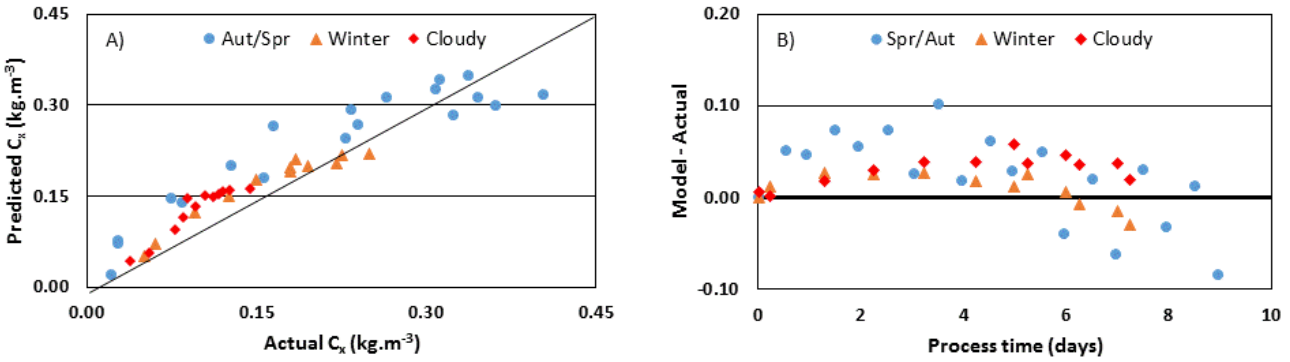


**Figure 3-6** A) linear regression of actual *versus* model-predicted biomass concentrations (kg.m$^{-3}$); and B) residual plot analysis over time.

the $\mu$–$I$ curves for parameter estimation and the 'physical limitation by light' that arises from cells mixing in optically dense batch cultures. These results imply that the static Haldane growth model is not capable of accurately predicting growth under dynamic light regimes that occur from changes in both incident and local light intensities.

### 3.4.4 Performance of *tla1*

Remarkably, *tla1* grew poorly in the spr/aut light regime (**Figure 3-5D**) and a complete culture crash occurred in R2. A long lag phase was also encountered in R1 followed by exponential growth from day 6 and this coincided with an increase in cellular pigment concentration suggesting a reversal to its wildtype phenotype (**Figure 3-4D**).

### 3.4.5 Adjustment of the Haldane model to account for observed changes

Unexpectedly, although the model over-predicted growth under low incident light (i.e. cloudy), it underestimated growth as the density of the culture increased for cultivation of *wt* in the relatively higher light treatments of winter and spr/aut, despite higher densities having a lower integrated $I_{avg}$. This suggests that respiration and/or the propensity for photoinhibition declined as the culture density increased. A decrease in photoinhibition could occur in dense cultures because of less exposure to photoinhibiting irradiances. Furthermore, more time spent in dark zones will result in more cells being in an 'open' state (i.e. an oxidised PQ pool), where they are ready to receive a photon, as seen by higher $\Phi_{PSII}$ toward the end of the cultivation period (**Figure 3-7**). A decrease in respiration processes over time may occur because of lower growth rates per cell, resulting in reduced light-enhanced respiration processes associated with carbon storage metabolic pathways, the malate shuttle and repair of photosystems.

To this end, a correction factor for the respiration term, $R_s$ was added as a function of culture density:

Eq. 3-5 $$R_s = M + \frac{C_{Rs}}{C_x}$$

Where $C_{Rs}$ is a fitted coefficient, $M$ is the term for basal metabolism in the dark and $C_x$ is the biomass concentration. Using parameter values of $2.0 \times 10^{-3}$ for $C_{Rs}$ and 0.005 for $M$, the new model-predictions (**Figure 3-5**, blue dashed lines) show a good correlation with actual productivity values under all light regimes and over the duration of the batch culture.

Although the adjusted respiration rate produced a good fit for the experimental conditions presented here, it is unknown whether this model is robust for other scenarios or even fundamentally accurate.

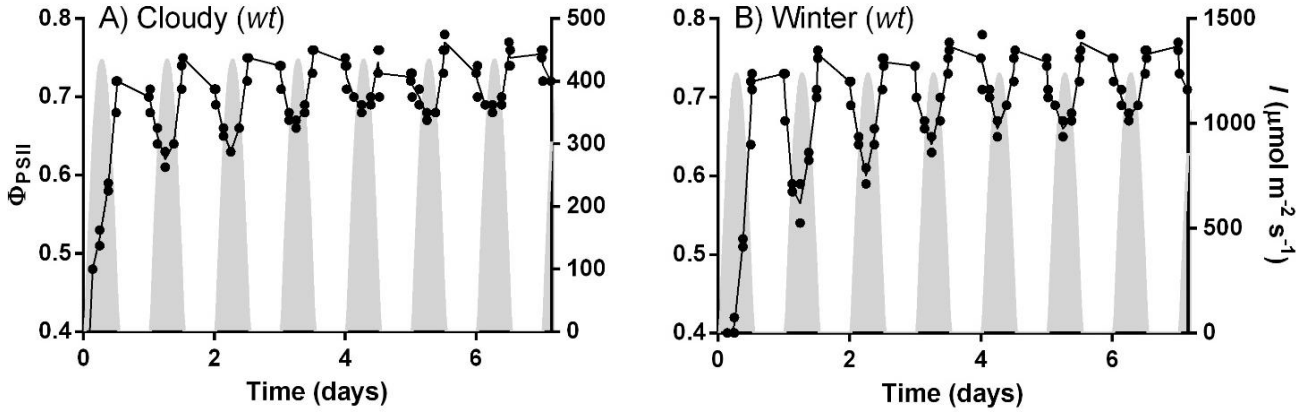


**Figure 3-7.** Changes in the quantum yield of photosystem II ($\Phi_{PSII}$) during batch cultivation under A) cloudy and B) winter treatments. Dots are the mean of two replicate reactors ($n$ = 2). Connecting lines are for visual purposes.

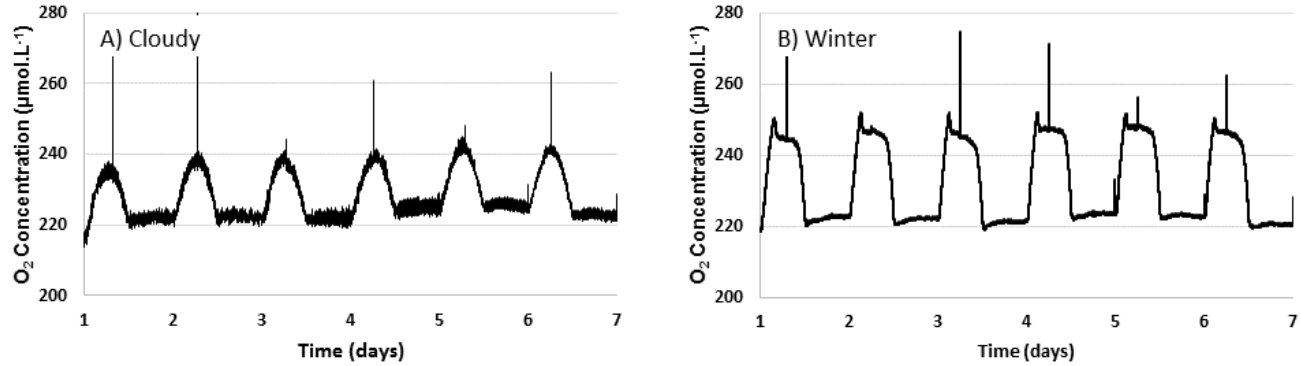


**Figure 3-8** *In situ* dissolved oxygen profiles of *C. reinhardtii* under A) cloudy and B) winter treatments for one representative reactor ($n$ = 1). Note: ePBRs were continually sparged with air.

Furthermore, the parameters that define the current model provide little information about the underlying mechanisms that are occurring. Subsequently, the next part of this study entailed a deeper examination of dynamic changes occurring under simulated outdoor mixed production systems in order to provide insight into which phenomena best explain the observed changes in photosynthetic productivities.

## 3.5 Conclusions

This chapter focused on validation of the model presented in Chapter 2. It was found that the model could not satisfactorily predict biomass production for a variety of incident light regimes typical of outdoor conditions as well as changes in biomass concentration over a batch culture. Further investigations into the photoacclimation, photoregulation and growth response of algae under dynamic mixing cycles are therefore needed in order to develop a more advanced model capable of explaining the growth phenomena.

# 4 Research paper: Photoacclimation and productivity of *Chlamydomonas reinhardtii* grown under fluctuating light regimes which simulate outdoor algal culture conditions

**Authors:** Jennifer Yarnold, Ian L. Ross and Ben Hankamer

## 4.1 Overview

*The manuscript below was published in Algal Research, January 2016 (doi: 10.1016/j.algal.2015.11.001). After the development of a simple model, we recognised the need to better understand how mixing cycles influence algal physiology and photosynthetic regulation. We therefore designed this experiment to explore the differences between light regimes that simulate algal cells circulating in mass cultures in outdoor light conditions, against 'non-mixed' light cycles under constant light of the same average irradiance.*

## 4.2 Abstract

Outdoor microalgae systems are a promising platform for fuels and chemicals, but are currently limited by relatively low productivities. This study investigated the effects of photoacclimation on the productivity of *Chlamydomonas reinhardtii* grown under fluctuating light regimes which simulate well-mixed cultures in outdoor reactors. Simulations represented cells cycling between high light and dark zones in high-density ($HD_{Fluc}$, light fraction (LF) = 0.5) and low-density ($LD_{Fluc}$, LF = 0.9) cultures. Each fluctuating treatment was controlled by cultures grown under non-fluctuating light of the same hourly average irradiance ($HD_{Avg}$ and $LD_{Avg}$) to differentiate between light dosage and regime. The large dark fraction of $HD_{Fluc}$ resulted in a low-light acclimated phenotype displaying up-regulation of light harvesting pigments and low NPQ caused by reduced levels of the dissipative protein LHCSR3. All other treatments led to high-light acclimation phenotypes. $HD_{Fluc}$ showed an estimated three-fold lower biomass yield relative to light absorbed and significant reductions in the quantum yield of PSII compared to $HD_{Avg}$. This suggests that during high light periods of fluctuating cycles, higher absorption and an inability to safely dissipate excess light, resulted in greater photodamage and respiration required for repair. A framework for including these findings in predictive modelling of mass cultures is presented.

## 4.3 Introduction*

Forecasts indicate that by 2050 we will require 70% more food (FaAOoUN, 2009), 50% more fuel (IEA, 2010), 50% more fresh water (OECD, 2014), and ~50-80% $CO_2$ emissions reductions (IPCC, 2014) to sustain a population of ~9.6 billion (United Nations, 2013). Algae biotechnologies are positioned at the nexus of these challenges as they can be located on non-arable land, tap into the huge energy resource of the sun (~2600x global energy demand, Smil (2008)), and use $CO_2$ to produce food, fuels and clean water. Techno-economic analysis has revealed biomass productivity as a critical factor in increasing the economic competitiveness of algal technologies (Stephens et al., 2010). While high-rate outdoor microalgae production systems are already achieving photon conversion efficiencies (PCE) of ~2% (Stephens et al., 2010, Melis, 2009), which is an order of magnitude higher than those of field trials for switchgrass and sugarcane of ~0.2%, (Formighieri et al., 2012, Macedo et al., 2008, Schmer et al., 2008), this remains far below the theoretical upper limits of ~8–10%, which could yield up to 77g biomass dry weight.$m^{-2}$.$day^{-1}$ (Melis 2009). The focus of this study is on bridging the gap between the current and theoretical PCE in outdoor mass cultures.

In well-mixed, high-density mass cultures, cells are subjected to dynamic light fluxes in which they are repeatedly cycled between photoinhibitory high light levels at the illuminated surface (up to ca. 2,000 μmol photons.$m^{-2}$.$s^{-1}$) and light-limited dark zones where respiration dominates.

Rapid light/dark cycles on the millisecond timescale, result in the so called 'flashing light' effect and can improve PCE. This is because photosynthesis approaches total light integration through which the cells perceive the average irradiance (Kok, 1956, Grobbelaar et al., 1996, Sforza et al., 2012). In contrast, medium-duration light/dark cycles (seconds to minutes) typical of algae production systems have been reported to yield lower PCE than under continuous illumination for *Chlamydomonas*

* **Abbreviations:** BDW, biomass dry weight; $E_a$, average mass absorption coefficient 400-700 nm ($m^2$.$kg^{-1}$); $E_k$, minimum saturating irradiance; $E_s$, average mass scattering coefficient 400-700 nm ($m^2$.$kg^{-1}$); ETR, electron transport rate; $ETR_{max}$, maximum relative electron transport rate; F, fluorescence yield; $F_m$, maximum fluorescence yield of dark-adapted cells; $F_m$', maximum fluorescence yield of light-adapted cells; $F_0$, minimum fluorescence of dark-adapted cells; $F_v/F_m$, maximum quantum yield of PSII; $HD_{Fluc}$, Fluctuating light cycle simulating a high-density culture; $HD_{Avg}$, Non-fluctuating control for $HD_{Fluc}$; $I_{avg}$, average irradiance; $LD_{Fluc}$, Fluctuating light cycle simulating a low-density culture; $LD_{Avg}$, Non-fluctuating control for $LD_{Fluc}$; NPQ, non-photochemical quenching; P, biomass productivity (g.$m^{-2}$.$d^{-1}$); PAR, photosynthetically active radiation; PCE, photon conversion efficiency; P–E, photosynthesis–irradiance; $P_m$, photosynthetic capacity at saturation; $P_s$, photosynthetic scaling factor; PSII, photosystem II; PPFD, photosynthetic photon flux density; $Q_A$, primary electron acceptor; $Q_{abs}$, cellular absorption efficiency; ROS, reactive oxygen species; RLC, rapid light curve; Rubisco, Ribulose-1,5-bisphosphate carboxylase/oxygenase; TAP: Tris acetate phosphate medium; $Y_{X,E}$, biomass yield i.e. biomass per unit light energy absorbed (g biomass.mol photons absorbed$^{-1}$); α, photosynthetic rate in light-limited region of RLC; β, slope decline of RLC due to photoinhibition; ΦPSII, effective quantum yield of PSII

*reinhardtii*, *Chlorella sorokiniana*, *Dunaliella tertiolecta* and *Nannochloropsis salina* (Janssen et al., 2000, Janssen et al., 1999, Barbosa et al., 2003, Sforza et al., 2012), highlighting the importance of the illumination profile on biomass productivity. In these studies, the illuminated fraction of the culture (representing culture density) and cycle time (representing mixing rate and culture depth) were analysed. The authors found that the illuminated fraction influenced productivity most greatly, and that cells which spent more time in the light relative to the dark achieved higher biomass conversion efficiencies. Cycle times <12s yielded modest productivity improvements with increased frequencies (partial light integration). Little to no effect occurred for cycle times >12s as light integration was not achieved. Under longer illumination cycles, the photosynthetic response to the local irradiance received by the cell can be considered instantaneous (Janssen et al., 1999, Barbosa et al., 2003, Takache et al., 2015).

Reduced yields under the extreme light gradients of mass culture are due to both photoinhibition under high photon flux at the illuminated surface and light limitation in dark zones, relative to continuous light of the spatially integrated average irradiance, $I_{avg}$. Yet lower than expected yields observed under actual cultivation cannot be explained entirely by the light regime alone. Grobbelaar et al. (1996) concluded that under longer light / dark cycles the cell perceives itself to be under lower light than in faster cycles of the same $I_{avg}$. This suggests that high-density cultures do not acclimate to the average integrated light level, but to some apparent below-average light level, yet there appears to be no theory that accurately predicts this target. This would explain for instance, the reported two-fold increase in cellular Chl *a* levels in *C. reinhardtii* and *N. salina* under certain light/dark cycles in comparison to continuous light of the same $I_{avg}$ (Janssen et al., 1999, Sforza et al., 2012).

Photoregulation and in particular non-photochemical quenching (NPQ), is also rapidly induced and occurs on similar timescales as the mixing cycles of cells circulating through cultures, but is poorly understood in mass culture. Despite these changes, current predictive light models of algal growth are based on relatively simple 3-state models of PSII responses and do not typically include NPQ as a dynamic process in the range of second-to-minute light fluctuations (Eilers and Peeters, 1988, Rubio et al., 2003, Zonneveld, 1998). NPQ is essential to protect against photodamage as it dissipates light energy in excess of photosynthetic capacity. The three components of NPQ include energy dependent quenching (qE), state transitions (qT) and a slowly developed quenching (qI) that has been linked to photoinhibition and/or xanthophyll activity. In *C. reinhardtii*, qE is most rapidly induced by acidification of the thylakoid lumen upon illumination, and this results in protonation of the stress-related light harvesting complex protein LHCSR3 (Peers et al., 2009, Bonente et al., 2011). Unlike the quenching amplifier PsbS in higher plants which signals pH changes and activates the xanthophyll

pigments bound to it, in algae LHCSR3 is directly involved in heat dissipation, while xanthophyll pigments are thought to be primarily involved in scavenging of reactive oxygen species (ROS) (Bonente et al., 2012, Peers et al., 2009, Allorent et al., 2013). Furthermore, LHCSR3 is not constitutively expressed like PsbS, but accumulates under high light. Thus high levels of qE require both induction (a slow acclimation response) and activation (a rapid regulation response).

In this study, we first compared the effects of low- and high-density cultures under fluctuating ($LD_{Fluc}$ and $HD_{Fluc}$) and non-fluctuating ($LD_{Avg}$ and $HD_{Avg}$) light conditions on photoacclimation, photoregulation and efficiency of light utilisation by photosystem II (PSII) in the model organism *Chlamydomonas reinhardtii*; and second, we developed a framework to explain the effect of the above responses on the final biomass accumulation. This study extends on previous systems modelling based on simple square-wave light / dark cycles (Grobbelaar et al., 1996, Janssen et al., 2000, Janssen et al., 1999, Sforza et al., 2012) or light gradients lacking diurnal fluctuations (Barbosa et al., 2003). This was achieved by applying light regimes which simulated both rapid cycling through a culture (10s cycles) and gradated hourly changes in maximum irradiance to reflect daily cycles (**Figure 4-1**). The inclusion of a diurnal cycle is critical to accurately assess acclimation and circadian rhythm processes, and to avoid light-shock and stress caused by an abrupt switch from a long dark period to high light.

A particular question that we sought to resolve was, the extent to which LHCSR3 would be both expressed and activated under fluctuating light cycles with supraoptimal and photolimiting irradiances and to estimate the efficiency of biomass accumulation which acts as an integrated signal for photosynthetic activity over longer timescales. Based on these results, a modelling framework was developed to describe the effects of light history on photoacclimation, light regulation, and the combined effects of the light history and cellular response on the final photosynthetic productivities of cells in mass culture. It is envisaged that this study will support predictive modelling efforts and guide engineering of cell lines and systems for the delivery of high-efficiency microalgae cultures. These factors are important to delivering necessary gains in economics, energy balance and greenhouse gas emissions required for commercial scale up.

## 4.4 Materials and methods

### 4.4.1 Culture Conditions

*C. reinhardtii* CC125 was purchased from Chlamydomonas Resource Centre (St Paul, USA). Pre-cultures were grown in 20 ml of photoautotrophic medium (TAP minus acetate, Harris (2001)) in 100 ml flasks with gas-permeable lids, and maintained on shakers (200 rpm) in an enclosed system

(TECAN, Melbourne), as described by Radzun et al. (2015). The atmosphere of the enclosed system was purged with 1.2% $CO_2$ and 4 $L.min^{-1}$ air. Pre-cultures were acclimated to their respective light regime for 7 days and diluted every 48 h to an $OD_{750}$ of 0.15 or ~$6.0 \times 10^5$ cells to minimise cell shading. After 7 days in flasks, more precise acclimation of each light regime was obtained by inoculating 7 ml of pre-culture into each well of a 6-well plate (Nunc) and diluted every 24 h to an $OD_{750}$ of 0.15 (pathlength = 6 mm). Plates were raised 30 mm from the light source and a diffuser sheet was placed below each plate to provide homogenous light to each culture well.

### 4.4.2 Light simulation and experimental setup

The enclosed TECAN system provided three shakers designed to hold six microwell plates per shaker (18 total) and is described in Radzun et al. (2015). Each plate was custom-fitted with 96 uniformly distributed warm white light-emitting diodes (LEDs) that are controlled by user-defined scripts using an Arduino® integrated circuit controller and software, allowing coding of 18 different light conditions. The spectral distribution of the LEDs in the PAR region is shown in Appendix 8.2. Light measurements were calibrated using a light sensor (Heinz Walz GmbH, Germany). The 'dark' periods of the light cycle measured <1 $\mu mol.m^{-2}.s^{-1}$.

To simulate the illumination pattern experienced by cells circulating in well-mixed outdoor mass cultures, thin dilute cultures with minimal self-shading were cultivated in 6 well plates in an enclosed $CO_2$-enriched apparatus equipped with a programmable LED lighting array. In this experimental design, the light regime imposed on the cells was almost exclusively a function of the external LED array rather than through adjustments in culture density and/or mixing rate, enabling tight control of the light level and period. This had the added benefit of maintaining equal mixing rates between light treatments, and separating the confounding effects of light from turbulence which is reported to enhance productivity through improved gas and nutrient exchange (Grobbelaar, 1994). Moreover, each well is considered an individual culture, allowing parallel analysis of multiple treatments and biological replicates. All analyses were performed on three individual wells per light regime. Nutrients were non-limiting and temperature was maintained at a constant 25°C.

**Figure 4-1** illustrates the four light treatments of this study and **Table 4-1** defines their respective parameters. The two fluctuating regimes coupled 'slow' and 'rapid' illumination cycles to model changes in light occurring due to diurnal shifts (slow) and cell mixing (rapid) through low-density ($LD_{Fluc}$) and high density ($HD_{Fluc}$) mass cultures. The slow 13:11 h day/night cycle (**Figure 4-1C & F**) was established through the use of a sinusoidal illumination pattern based on hourly changes in incident irradiance. The daily maximum photosynthetic photon flux density (PPFD) at midday ($I_{max}$) for both $HD_{Fluc}$ and $LD_{Fluc}$ regimes was set at 1,416 $\mu mol\ photons.m^{-2}.s^{-1}$, which represents near

optimal sub-tropical operational conditions based on average Spring and Autumn clear sky days in Brisbane, Australia.

The rapid light cycle (**Figure 4-1B & E**), simulating light fluctuations experienced by cells mixing between the illuminated and dark zones of a culture, was set to a periodicity of 10 s, which represents the cycle typical of a shallow high rate pond or long pathlength photobioreactors (Grobbelaar et al., 1996). Although an accurate representation of cell trajectories requires rigorous computational analysis of fluid dynamics, for simplicity a cyclic mixing regime was assumed as a first approximation which gives rise to a sinusoidal fluctuation (Wagner et al., 2006, Ibelings, 1994).

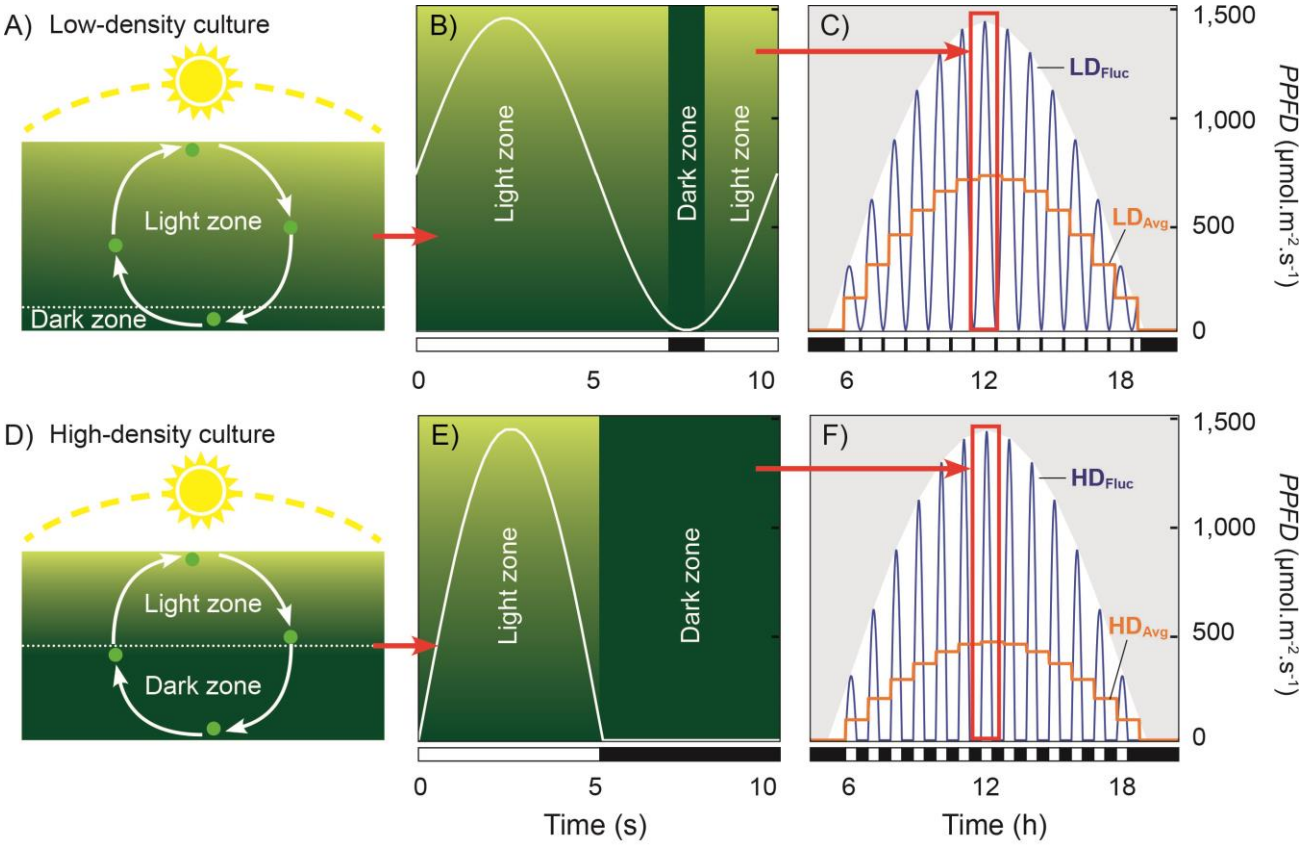


**Figure 4-1.** Illumination profile and simulation of low and high density cultures. A & D, Schematic of the light history of a cell as it is mixed though low-density and high-density cultures respectively. B & E, Rapid illumination cycles of $LD_{Fluc}$ and $HD_{Fluc}$ respectively, simulating the cyclical motion of cells through culture were achieved via programmed changes in PPFD (example at midday). C & F, Daily changes in irradiance. These combine slow diurnal cycles (white background shading) via hourly changes as well as rapid (10 s) cell mixing cycles. Note: The rapid cycles shown in C & F are purely schematic and are not drawn to scale. Red lines = non-fluctuating constant light regimes ($LD_{Avg}$ and $HD_{Avg}$) lacking the rapid cycles. These were set to the hourly average irradiance of $LD_{Fluc}$ and $HD_{Fluc}$ regimes respectively. Bottom bars: black = dark period; white = light period.

**Table 4-1.** Variables of light regimes. ε = illuminated fraction, $c_t$ = cycle time, Daily $I_{avg}$ = daily integrated mean irradiance; Daily $I_{max}$ = maximum daily irradiance.

| Sample | Description | ε | $c_t$ [s] | Daily $I_{avg}$ [μmol.m$^{-2}$.s$^{-1}$] | Daily $I_{Max}$ [μmol.m$^{-2}$ .s$^{-1}$] |
|---|---|---|---|---|---|
| $HD_{Fluc}$ | High density culture, fluctuating light | 0.5 | 10 | 165 | 1,416 |
| $HD_{Avg}$ | Hourly continuous light, $I_{avg} = HD_{Fluc}$ | 1.0 | – | 165 | 450 |
| $LD_{Fluc}$ | Low density culture, fluctuating light | 0.9 | 10 | 272 | 1,416 |
| $LD_{Avg}$ | Hourly continuous light, $I_{avg} = LD_{Fluc}$ | 1.0 | – | 272 | 708 |

Algae circulating in high-density mixed cultures are likely to be exposed to a light limiting or dark zone for a substantial fraction of the cultivation period, reducing the illuminated fraction. In contrast, in a low-density mixed culture cells do not experience as steep an illumination gradient and there is either no truly dark zone (i.e. the light flux supports photosynthesis) or it is brief in duration, relative to residence in the illuminated zone. Consequently, the variations in culture density resulted in an illuminated fraction of 0.9 for $LD_{Fluc}$ and 0.5 for $HD_{Fluc}$. It is important to note that both of the fluctuating light regimes simulate cultures exposed to the same daily solar conditions (i.e. incident radiation 0-1,416 μmol photons.m$^{-2}$.s$^{-1}$).

However, individual cells in a high-density mixed culture experience a reduced total net photon flux compared to cells in a low-density culture, due to cell shading. To separate light dosage and acclimation effects, two control light regimes ($HD_{Avg}$ and $LD_{Avg}$) were exposed to continuous light with the same hourly average irradiance as that experienced by each of the fluctuating light cultures (**Figure 4-1 C & F** & **Table 4-1**). It should also be noted that although high-density culture simulations received less total light than low-density culture simulations, the daily $I_{avg}$ of 165 μmol photons.m$^{-2}$.s$^{-1}$ is still considered high in many studies.

### 4.4.3 Biomass Dry Weight (BDW) and optical density

BDW was determined by filtration of 5 ml culture onto a pre-dried and twice pre-weighed glass-fibre filter (Whatman GF/F). The filter was rinsed three times with 5 mL Milli-Q $H_2O$, dried in an oven for 5 days at 95° C, cooled in a desiccator then measured twice on a precision scale. BDW was correlated to optical density measurements at 750 nm ($OD_{750}$) performed on a spectrophotometer (BioRad SmartSpec 3000, Hercules CA, USA) in a cuvette of 1cm pathlength and blanked with culture media.

### 4.4.4 Cellular pigment content

A volume of 1 ml of cell suspension was recovered on glass fibre filters (Whatman GF/F). The filter was cut into ~5 mm strips and placed in a 1.5 mL microcentrifuge tube with 1 mL of 90% acetone (v/v) deacidified with saturated $MgCO_3$. Tubes were wrapped in aluminium foil to avoid light exposure, sonicated in an ice water bath for 5 min, vortexed and incubated overnight at 4° C. After 5 min centrifugation at 13,000 rpm, the concentration (µg.ml$^{-1}$) of chlorophyll *a* ($C_{Chl\text{-}a}$) chlorophyll *b* ($C_{Chl\text{-}b}$) and total photoprotective carotenoids ($C_{Car}$) (comprising neoxanthin, loroxanthin, violaxanthin, antheraxanthin, zeaxanthin, lutein, and β-carotene) was determined spectrophotometrically as follows (Pottier et al., 2005):

Eq. 4-1 $$C_{Chl-a} = [11.6(OD_{665} - OD_{750}) - 1.31(OD_{645} - OD_{750}) - 0.14(OD_{630} - OD_{750})]$$

Eq. 4-2 $$C_{Chl-b} = [20.7(OD_{645} - OD_{750}) - 4.34(OD_{665} - OD_{750}) - 4.42(OD_{630} - OD_{750})]$$

Eq. 4-3 $$C_{Car} = [4.0(OD_{480} - OD_{750})]$$

The mass fraction of each pigments was determined by relation to BDW.

### 4.4.5 Cellular morphology

Sample aliquots were taken in triplicate and stored in a 1:1 volume of fixative solution (1% glutaraldehyde; 1% paraformaldehyde; 30mM HEPES pH 7.4; 0.5M sucrose). Images were compiled using a (Nikon Ti-U microscope fitted with a Nikon Digital Sight DSU2, 5mp colour head; 40x magnification). Particle analysis was performed using Image J software (National Institutes of Health, USA) on a minimum of 70 cells per sample.

### 4.4.6 Chlorophyll fluorescence

Fluorescence measurements were performed in triplicate on whole cells, gently stirred at room temperature using an FL3500 Dual Modulation Kinetic Fluorometer (Photon Systems Instruments Ltd (PSI), Drasov, Czech Republic). A low cell concentration (1.0–2.0 x $10^5$ cells.ml$^{-1}$) ensured minimal reabsorption of fluorescence and light scattering from cells. The instrument employs a red LED with a peak emission at 625 nm as the measuring light, saturating flash and actinic light. Chlorophyll fluorescence was detected at wavelengths above 710 nm. PFFD was calibrated using a micro-quantum sensor (Walz GmbH, Effeltrich, Germany) placed in the centre of the cuvette holder. FluorWin (PSI, Czech Republic) software was used to control settings.

To assess changes in PSII photochemistry and regulation, two chlorophyll fluorescence techniques were used as described below.

#### *4.4.6.1 Dark adapted measurements*

Dark-adapted quenching was performed on aliquots of each treatment to assess potential levels of stress and photoinhibition (by measurement of $F_v/F_m$); to correlate LHCSR3 levels with qE-mediated NPQ; and to measure the quantum yield of PSII (*ΦPSII*). Samples were first dark adapted for 20 mins under aerobic conditions to allow re-oxidation of the PSII primary quinone electron acceptor ($Q_A$), in order to determine the minimum and maximum dark fluorescence levels ($F_0$ and $F_m$ respectively). Cells were pulsed with far red light prior to analysis to promote transition of cells into State 1. A high actinic light intensity (800 μmol photons.$m^{-2}$.$s^{-1}$) was used to maximise NPQ. Aliquots were taken in triplicate of each sample, placed into cuvettes and dark adapted for 20 mins. The *Quenching Analysis* protocol of FluorWin was performed with the following settings: measuring light: 20% V; saturating pulse: 0.9s, 80% V; actinic light: 200 s, 26.69% V. Pulses of weak far-red light (730 nm) were applied prior to measurement to remove electrons from $Q_A$ by preferential excitation of photosystem I (PSI).

#### *4.4.6.2 Rapid Light Curves*

RLC were performed in triplicate on fresh aliquots of each sample using a modified *Quenching Analysis* script. Samples were quasi-dark adapted for 30 s before analysis. Cells were exposed to 25 s periods of eight actinic irradiances increasing stepwise from 0 – 1,600 μmol photons.$m^{-2}$.$s^{-1}$ with a 30 s dark interval between each irradiance. Three saturating pulses were averaged for each irradiance for estimation of $F_m'$. For calculation of NPQ, the quasi-dark $F_m$ and $F$ values obtained during the first measurement without actinic light (PFFD = 0 μmol photons.$m^{-2}$.$s^{-1}$) were corrected by –10 and +10% respectively to estimate $F_0$ and $F_m$ of dark adapted samples in which $Q_A$ is maximally oxidised and all PSII reaction centres are in a so-called 'open' state, according to the method of Ralph and Gademann (2005). Rapid light response curves were then performed on fresh aliquots of cells from each treatment. These provided *P–I* curves based on linear electron transport rates (ETR), which in the absence of photorespiration and under ideal conditions, have been shown to provide a good correlation to $O_2$ evolution and $CO_2$ assimilation rates (Beer and Björk, 2000). From this analysis, NPQ-irradiance response curves were also established. Cells were briefly dark adapted for 30 s prior to analysis, providing a quasi-dark measurement. In contrast to dark-adapted quenching measurements, rapid light response curves performed directly on acclimated cells taken from a given light regime demonstrate the efficiency of PSII to utilise various levels of irradiance for linear electron transport or to dissipate excess energy as heat, without allowing time for relaxation of NPQ to occur (Ralph and Gademann, 2005). Thus, they may more accurately model the photosynthetic responses of cells that occur *in situ*.

### 4.4.7 Growth & Productivity

Growth was monitored at four time points over a 24 h period by measuring the change in $OD_{750}$ (corrected for $OD_{750}$ on media without sample) on triplicate wells of a 6 well plate using the high-throughput system's in-built absorbance plate reader (11 - Tecan Infinite M200 PRO, Tecan Group Ltd., Männedorf, Switzerland). Growth rates were calculated as:

Eq 4-4. $$\mu = \frac{ln\ OD_{750(t2)} - ln\ OD_{750(t2)}}{t_2 - t_1}$$

Where $t_1$ and $t_2$ are times at measured points of $OD_{750(t2)}$ and $OD_{750(t1)}$ respectively. The biomass yield on light, $Y_{X,E}$ was calculated from Equation 6 and by approximating DW from $OD_{750}$ correlations.

### 4.4.8 Western blot analysis of LHCSR3 and RbcL

The LHCSR3 and large Rubisco subunit (RbcL) were determined by western blot analysis. A volume of 1 mL culture was pelleted by centrifugation (1,700*g* for 5 min), resuspended in 50 µL 20 mM HEPES buffer pH 7.5, snap frozen in liquid nitrogen, then stored at -80° C until analysis. Protein concentration was quantified using a Nanodrop 2000c spectrophotometer (Thermo Fisher Scientific) and an aliquot of sample taken for 90% acetone extraction to estimate chlorophyll as previously described. Dilutions were prepared for final concentrations of 3.0, 1.5 and 0.75 µg protein in Milli-Q $H_2O$ and 1x standard SDS denaturing buffer (60 mM DTT, 60 mM $Na_2CO_3$, 2% [v/v] SDS, and 12% [w/v] sucrose), then heated at 95° C for 5 min for lysis and protein denaturing. Proteins were separated on 4–12% Bis-Tris denaturing polyacrylamide gels (Bolt, Life Technologies) using 120 V for 80 min. Proteins were blotted onto polyvinylidene fluoride membranes using an XCell II transfer apparatus (Life Technologies). The membrane was stained with Ponceau Red S and imaged on a flat bed scanner (Epson) to verify protein estimation, washed and blocked overnight with 5% skim milk in TBST buffer (100 mM Tris-Cl pH 7.5, 1.5M NaCl, 0.05% v/v Tween 20). The membrane was incubated with anti-LHCSR polyclonal antibody (Agrisera) diluted 1:5,000 for 1 hour and then rinsed three times for 10 min each before incubation with 1:2,500 dilution of goat anti-rabbit horse radish peroxidase conjugate secondary antibody (Abcam) for a further 1 hour then rinsed three times for 10 min. Chemiluminescent detection was performed using the ECL system (BioRad, California) with development on medical x-ray films (FujiFilm Corporation, Japan).

## 4.5 Results and discussion

Photoacclimation

### *4.5.1.1 Cellular pigment content*

Changes in cellular pigment concentrations and composition affect light absorption capacity and are the most recognisable phenotype of photoacclimation. Changes are associated with expression levels of photosystems and/or their light harvesting antenna proteins in response to light (Bonente et al., 2012), while intrinsic circadian rhythms have also been shown to down-regulate Chl *a*/*b* binding proteins during the night (Falkowski and LaRoche, 1991, Jacobshagen and Johnson, 1994). To monitor these changes in acclimation at the extremes of the day, total concentrations of chlorophyll *a*, chlorophyll *b* and carotenoids, as well as cellular chlorophyll *a*/*b* ratios were determined spectrophotometrically before the onset of light (predawn) and after exposure to maximum midday illumination levels (sampled at ~1pm).

Cells under the $HD_{Fluc}$ light regime showed an up-regulation of all pigments between pre-dawn and midday (**Figure 4-2**) with chlorophyll *a* content rising from 24.9 ± 4.3 to 35.4 ± 1.6 g.kg$^{-1}$. Moreover, these cells had more than twice the cellular concentration of chlorophylls *a* and *b* and carotenoids in comparison to the levels observed under $HD_{Avg}$ and had a lower relative chlorophyll *a*/*b* ratio than other treatments, indicative of larger light harvesting complexes typical of low light acclimation.

In contrast, pigment concentrations of the $HD_{Avg}$, $LD_{Fluc}$ and $LD_{Avg}$ treatments were quite similar to each other and typical of high light acclimation. Between pre-dawn to

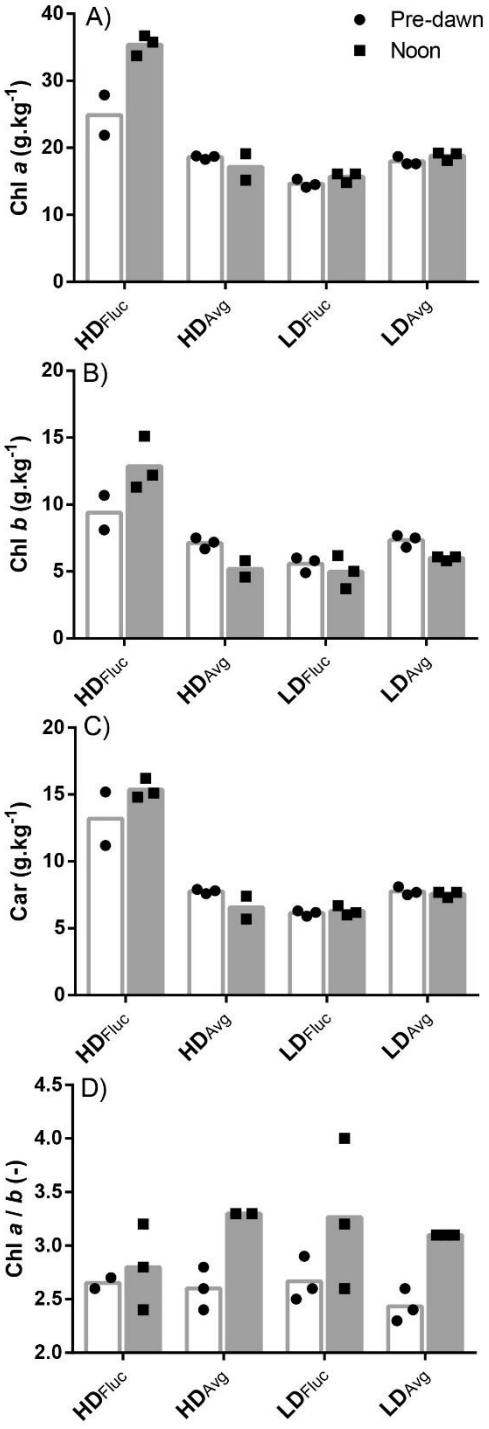


**Figure 4-2.** Cellular pigment concentrations (g kg$^{-1}$ dry biomass) of A) chlorophyll *a;* B) chlorophyll *b;* C) Carotenoids; D) Chlorophyll *a*/*b* ratio. Individual data points shown. The bars represent the sample mean (White = pre-dawn measurements (5.30am); Grey = midday (approx. 1pm)). *n* = 3.

midday, minor reductions (<10%) of chlorophyll *a* (**Figure 4-2A**) and a greater down regulation of chlorophyll *b* by ~26%, 10% and 17% respectively (**Figure 4-2B**) were observed, which resulted in an increased chlorophyll *a/b* ratio (**Figure 4-2D**). Considerably higher levels of carotenoids were observed in cells in the $HD_{Fluc}$ (**Figure 4-2C**) treatment and the chlorophyll *a* : carotenoid ratio was lower relative to all other treatments and were up-regulated through the day. Paradoxically, although the $HD_{Fluc}$ regime results in *lower* average light levels than $LD_{Fluc}$, the accumulation of certain carotenoids such as zeaxanthin is typically associated with cells under *high light* stress during which free oxygen radical scavengers are required (Bonente et al., 2012). These observations may indicate an increased stress response resulting from constant shifts between over-saturated and light-limiting irradiance levels.

#### *4.5.1.2 Cellular optical properties*

Acclimation affects the PAR-averaged mean mass absorption and scattering coefficients ($E_a$, and $E_s$ respectively), which influences the amount of light transfer through the culture medium. These parameters were estimated from the cell shape and size (**Table 4-2**) and the above pigment concentrations using a semi-predictive approach based on Lorenz-Mie theory for spherical particles, according to the method of Pottier et al. (2005).

In accordance with increased pigment content and a ~15% smaller mean radius to other treatments, cells under $HD_{Fluc}$ showed a ~60% larger $E_a$ than $HD_{Avg}$ and a slight increase in $E_s$ (**Table 4-2**). Cells under $HD_{Avg,}$ $LD_{Fluc}$ and $LD_{Avg}$ had similar $E_a$ values, while cells grown under $LD_{Avg}$ showed a reduction of $E_s$ due to a larger particle size. These results indicate that, in addition to cellular responses, radiative transfer under $HD_{Fluc}$ will also be adversely affected, increasing the extent of the dark zone due to additional cell shading.

**Table 4-2.** Cell size, shape and estimated optical properties*. *n = 3.*

| | $HD_{Fluc}$ | $HD_{Avg}$ | $LD_{Fluc}$ | $LD_{Avg}$ |
|---|---|---|---|---|
| ***Cellular morphology*** | | | | |
| Average major diameter (μm) | 8.9 (3.0) | 10.3 (1.4) | 10.7 (1.9) | 10.3 (1.5) |
| Average minor diameter (μm) | 6.9 (2.5) | 8.2 (1.2) | 8.1 (1.9) | 8.7 (1.5) |
| Circularity (–) | 0.73 (0.16) | 0.81 (0.06) | 0.74 (0.11) | 0.79 (0.09) |
| Mean cell radius (μm) | 4.0 | 4.6 | 4.7 | 4.7 |
| Mean particle volume ($m^3$) | $2.6e^{-16}$ | $4.2e^{-16}$ | $4.3e^{-16}$ | $4.4e^{-16}$ |
| ***Estimated optical properties*** | | | | |
| PAR absorption coefficient $E_a$ ($m^2.kg^{-1}$) | 355 (7) | 219 (21) | 212(8) | 236 (4) |
| PAR scattering coefficient $E_s$ ($m^2.kg^{-1}$) | 858 (5) | 814 (19) | 811 (7) | 774 (3) |

**Values in parentheses are +/- one standard deviation*

### *4.5.1.3 LHCSR3 and Rubisco accumulation*

Photosynthesis requires a balance between absorbed light energy and $CO_2$ assimilation. The latter is limited by $CO_2$ concentration and the levels and turnover rate of Rubisco, while energy exceeding this capacity must be redirected or dissipated as heat to avoid photodamage, and is highly dependent on the accumulated amount of the stress protein LHCSR3 (Peers et al., 2009). Changes in LHCSR3 and Rubisco abundance were therefore investigated just after maximum light exposure at ~1pm. Specific polyclonal antibodies against LHCSR3 and the large Rubisco subunit RbcL were employed in western blot analyses of whole cell extracts normalised to chlorophyll content (**Figure 4-3**). Blotting membranes were stained with Ponceau Red S as a control for protein loading (**Figure 8-3**). It has been reported that LHCSR3 expression increases under high light (Bonente et al., 2012, Peers et al., 2009) and this was supported by our results which showed higher levels of LCHSR3 in the higher light treatment of $LD_{Avg}$ in comparison to $HD_{Avg}$ treated cells. Remarkably, we also found lower levels of LHCSR3 under both fluctuating light treatments ($HD_{Fluc}$ and $LD_{Fluc}$) relative to their respective non-fluctuating regimes of the same $I_{Avg}$ ($HD_{Avg}$ and $LD_{Avg}$,). This was particularly evident between the low-light acclimated $HD_{Fluc}$ and the high-light acclimated $HD_{Avg}$ treatments. These trends were also observed on western blots normalised to cellular protein content (**Figure 8-4**), indicating that the differences were not simply due to a greater chlorophyll content in $HD_{Fluc}$ cells.

These findings suggest that dark zones disrupt the signals that regulate LCHSR3 expression, even when peak irradiance is high. To our knowledge, this is the first report showing that light gradients typical of mixed cycles in outdoor mass cultures lead to a reduction of the photoprotective LHCSR3 protein in comparison to non-fluctuating controls exposed to the same $I_{avg}$.

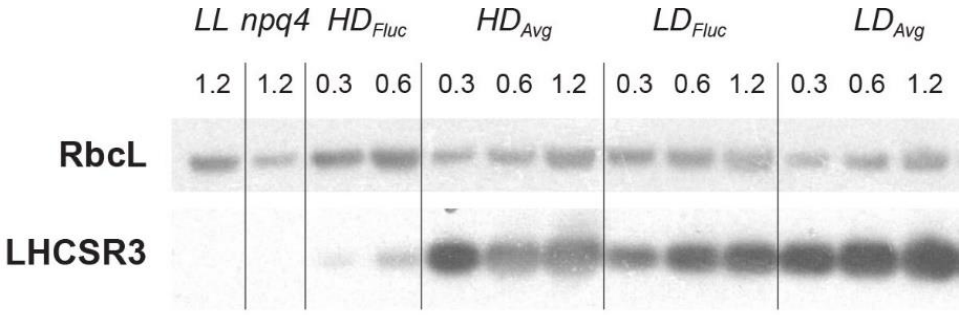


**Figure 4-3.** Western blot analysis of LHCSR3 and the large subunit of Rubisco (RbcL) normalised to total chlorophyll. The amount of chlorophyll loaded into each lane is in micrograms. *LL = C. reinhardtii* cells cultivated in TAP under external low light levels (25 μmol.$m^{-2}$.$s^{-1}$) and *npq4* = the LHCSR3 deficient mutant (Peers et al., 2009). Both *LL* and *npq4* were used as negative controls.

No apparent variations in RbcL abundance were observed between the different light treatments (**Figure 4-3**). Although transient suppression of RbcL has been shown in *C. reinhardtii* cells subjected to abrupt light-shock from a low to high irradiance (Shapira et al., 1997) our results correspond to other studies that found cellular Rubisco levels to be mostly independent of irradiance (Bonente et al., 2012, Sukenik et al., 1987).

In summary, these results indicate that despite high bursts of supersaturating irradiances and a reasonably high daily light dosage ($I_{avg}$ = 165 μmol photons.m$^{-2}$.s$^{-1}$), high-density cultures in which cells are exposed to fluctuating light photoacclimate in a way which is typically produced by, and appropriate for, a low light state. This seems to be influenced by the fraction of time spent in the dark rather than total light, since $HD_{Avg}$ showed a high light acclimation state. Importantly, the low light acclimation state of $HD_{Fluc}$ leads to an increase in absorption capacity due to increased light harvesting pigment levels. This affects light response at the cellular level as well as the optical properties of the culture, resulting in enhanced cell shading and further reduced light penetration into the culture. Paradoxically, the light regime simulating mixed low-density cultures (i.e. $LD_{Fluc}$) led these cells to acclimate towards a similar apparent light state than if they were exposed to the same $I_{avg}$ ($LD_{Avg}$) with respect to absorption capacity, probably because the dark fraction was small enough not to result in antenna up-regulation. In other words, in low density mixed cultures, the maximum light level appears to be the dominant regulatory factor while in the high density cultures the dark fraction appears to be the more dominant effect.

### 4.5.2 Photoregulation and PSII efficiency

#### *4.5.2.1 Dark adapted chlorophyll fluorescence analysis*

$NPQ_{800}$ is the relative difference between the maximum fluorescence in the dark and in the light (at 800 μmol photons.m$^{-2}$.s$^{-1}$), induced by heat loss from PSII ($NPQ_{800} = F_m/F_{m'} - 1$). At pre-dawn, $NPQ_{800}$ was found to be minimal under all four light treatments tested. In contrast at noon, $NPQ_{800}$ levels increased in all treatments (**Figure 4-4 E–H**). Most noticeably however, cells under fluctuating cycles showed only around half the $NPQ_{800}$ capacity at midday relative to those under non-fluctuating treatments of the same $I_{Avg}$. The highest $NPQ_{800}$ level was observed under $LD_{Avg}$ (0.92 ± 0.03), which was more than twice that of $LD_{Fluc}$ (0.44 ± 0.04). Similarly, $HD_{Avg}$ showed nearly twice the $NPQ_{800}$ as $HD_{Fluc}$ (0.35 ± 0.02 and 0.18 ± 0.04 respectively), and $HD_{Avg}$ was slightly lower than $LD_{Fluc}$. The relative differences of $NPQ_{800}$ levels correlated with LHCSR3 accumulation across all four light treatments (**Figure 4-3**).

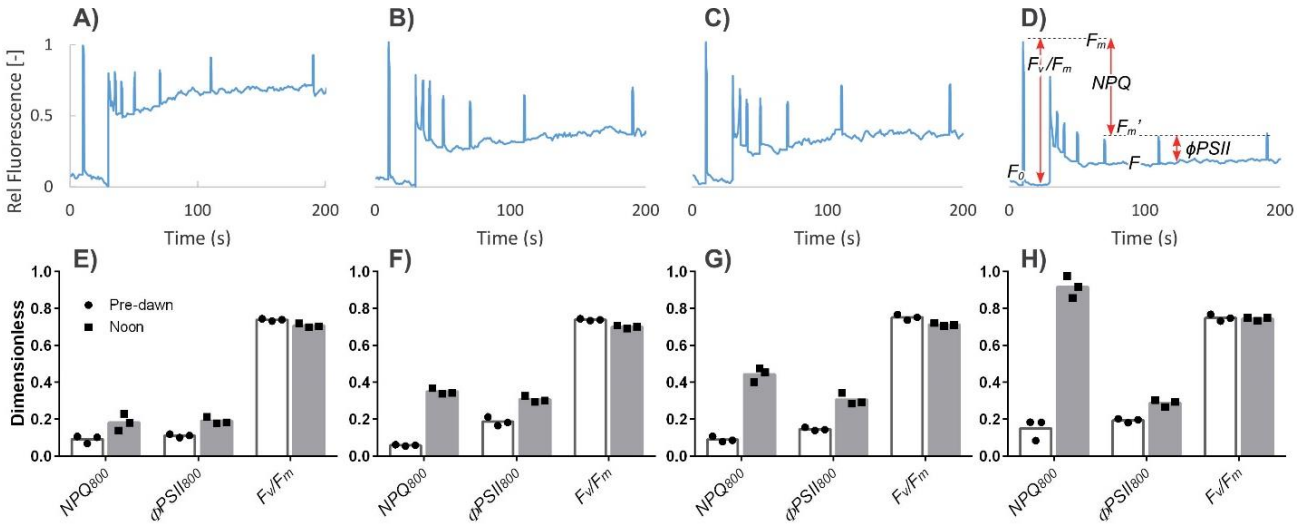


**Figure 4-4.** Chlorophyll fluorescence dark-adapted quenching analysis. A–D Fluorescence traces of $HD_{Fluc}$ $HD_{Avg}$ $LD_{Fluc}$ and $LD_{Avg}$ at midday, respectively. E–H $NPQ_{800}$ and $\Phi PSII_{800}$ (at 40 s exposure to actinic light) and $F_v/F_m$. Samples were dark adapted for 20 mins. Actinic light = 800 µmol.m$^{-2}$.s$^{-1}$. Individual data points shown. The bars represent the sample mean (White = pre-dawn measurements (5.30am); Grey = midday (approx. 1pm)).

$\Phi PSII_{800}$ is the effective photochemical quantum yield at 800 µmol photons.m$^{-2}$.s$^{-1}$. It provides an estimation of the efficiency with which absorbed photons are used for linear electron transport, based on the change in minimum and maximum fluorescence in the light over the maximum fluorescence in the light ($\Phi PSII_{800} = F_m – F_m'/ F_m$) (Baker, 2008). At noon, $LD_{Fluc}$ and $LD_{Avg}$ treatments showed a very similar $\Phi PSII_{800}$ (0.29 ± 0.03 and 0.31 ± 0.03), despite large differences in $NPQ_{800}$ (**Figure 4-4E–H**). In contrast, low-light acclimated $HD_{Fluc}$ cells showed a reduction of $\Phi PSII_{800}$ of ~36% in comparison to other treatments (**Figure 4-4 E–H**).

$F_v/F_m$ is the maximum quantum efficiency of PSII, and is measured by exposing a dark adapted culture, in which all photosystems are assumed to be in an open state and plastoquinone (PQ) acceptors fully oxidised, to a saturating light pulse. In healthy plant leaves, $F_v/F_m$ values are remarkably similar (ca. 0.83), and thus low $F_v/F_m$ is an indicator of stress or damage to photosystems (Baker, 2008). Under low light pre-dawn conditions, $F_v/F_m$ was similar for all treatments tested (0.74 ± 0.01 – 0.75 ± 0.01), in agreement with maximum values reported elsewhere for *C. reinhardtii* (Bonente et al. (2012); **Figure 4-4 E–H**).

At midday high light conditions, both $LD_{Avg}$ and $LD_{Fluc}$ had been exposed to a long period of photoinhibiting irradiance. Despite this, virtually no reduction in $F_v/F_m$ in $LD_{Avg}$ (0.74 ± 0.01) was observed, indicative of a high photoprotective capacity. Similarly only a small reduction in $F_v/F_m$ was seen in $LD_{Fluc}$ (0.71 ± 0.01) and the $F_v/F_m$ values of $HD_{Fluc}$ (0.71 ± 0.01) and $HD_{Avg}$ (0.70 ± 0.01)

treatments exposed to high midday irradiance levels only resulted in a ~4% reduction compared with $LD_{Avg}$. Interestingly, $F_v/F_m$ for $HD_{Fluc}$ and $HD_{Avg}$ treatments were virtually the same despite their differences in NPQ and $\Phi_{PSII}$ which may be explained by the fact that $HD_{Fluc}$ cells are in the dark 50% of the time, allowing adequate time for repair of photosystems.

The differences in $NPQ_{800}$, $\Phi PSII_{800}$ and $F_v/F_m$ at midday are visualised in raw fluorescence traces (**Figure 4 A–D**). Despite the relatively high fluorescence saturation peaks of $HD_{Fluc}$ (**Figure 4-4 A**), $\Phi PSII_{800}$ was diminished because the minimum fluorescence level in the light, *F*, was extremely high (**Figure 4-4A**), demonstrating an inability of the photosynthetic apparatus to oxidise $Q_A$ sufficiently rapidly, nor to dissipate excess energy as heat. This inability to oxidise $Q_A$ is the combined result of light oversaturation and low NPQ. The high pigment levels of $HD_{Fluc}$ may be the result of an up-regulation of the LHC antenna systems or a change in PSII-LHCII/PSI-LHCI complexes, however the low $\Phi_{PSII}$ in addition to the lower chlorophyll *a*/*b* ratio suggests that an up-regulation of the LCHII antenna complexes has occurred, leading to greater photon absorption per photosystem. The absorbed photons are either dissipated as heat by NPQ or used to drive photochemistry through linear electron transport (i.e. photochemical quenching, qP). Since qP is limited by $CO_2$ (and the rate of carbon fixation by Rubisco) and the availability of alternative electron routes, and since NPQ is mostly effected by LHCSR3, the levels of which are low in $HD_{Fluc}$, there is limited sink capacity for electrons, and this results in photoinhibition, which even if quickly repaired will still contribute to the reduction of $\Phi_{PSII}$ of $HD_{Fluc}$.

### *4.5.2.2 Instantaneous Rapid Light Response Curves*

Next rapid light response curves were determined for both *relative* and *absolute* electron transport rates (ETR) as well as for NPQ at eight irradiance levels from 0–1,600 μmol photons.$m^{-2}$.$s^{-1}$. *Relative ETR* ($ETR_r$) provides insight into the efficiency with which photosystems use absorbed photons for linear electron transport, being the product of the effective quantum yield of photochemistry (ΦPSII) and the photosynthetic photon flux density (PPFD, μmol photons.$m^{-2}$.$s^{-1}$) at a given wavelength (λ) as shown in Equation 4-1.

Eq. 4-5 $$ETR_r = \Phi PSII \cdot PPFD_{(\lambda)}$$

*Absolute* ETR ($ETR_{abs}$) estimates the total number of electrons used for photochemistry, by measuring the absorption efficiency of the cell at a particular wavelength (in this case, 625 nm).

Eq. 4-6 $$ETR_{abs} = \Phi PSII \cdot PFFD_{(\lambda)} \cdot Q_{ABS(\lambda)} \cdot 0.5$$

Where $Q_{ABS(\lambda)}$ is the absorption efficiency of the cell at a particular wavelength ($\lambda$), and 0.5 assumes two photons per electron transferred from water to $NADP^+$ (one photon per PSII and one photon per PSI charge separation event) (Schreiber, 2004).

To estimate the parameters that define the shape of the rapid light response curves for each light regime, we used a least-squares non-linear curve fit of the double exponential decay model (Platt et al., 1980) to the empirical data,

Eq. 4-7 $$ETR = P_S(1 - e^{-(\alpha \cdot PFFD/P_S)})\, e^{-(\beta \cdot PFFD/P_S)}$$

where $P_s$ is the scaling factor for the maximum potential ETR, $\alpha$ is the initial slope at low PFFD, which reflects the maximum photosynthetic quantum yield, and $\beta$ is the slope decline due to photoinhibition.

From equation 4-7, the maximum ETR, $ETR_{max}$ was found.

Eq. 4-8 $$ETR_{max} = P_S(\alpha/[\alpha + \beta])(\beta/[\alpha + \beta])^{\beta/\alpha}$$

And the minimum saturating irradiance, $I_k$ is defined as:

Eq. 4-9 $$I_k = \frac{ETR_{max}}{\alpha}$$

A comparison of $ETR_r$ $ETR_{abs}$ and NPQ-irradiance curves between fluctuating and non-fluctuating light regimes is presented in **Figure 4-5**.

### 4.5.3 Relative electron transport rate ($ETR_r$)

**Figure 4-5A** shows that the low-light acclimated cells ($HD_{Fluc}$) had a 40% lower maximum *relative* ETR ($ETR_{r,max}$ = 151 μmol photons.$m^{-2}$.$s^{-1}$) and a noticeable lower initial slope, ($\alpha$ = 0.57) compared to those of the $HD_{Avg}$ culture ($ETR_{r,max}$ = 251 μmol photons.$m^{-2}$.$s^{-1}$; $\alpha$ = 0.72;). In comparison, the high-light acclimated ($LD_{Fluc}$) cells showed less variation compared to $LD_{Avg}$ (**Figure 4-5B**) with a slightly higher initial slope, but lower $ETR_{r,max}$. Interestingly, despite different light dosage and different light regimes, $HD_{Avg}$ and $LD_{Fluc}$ showed very similar parameters (α, $E_k$, $ETR_{max}$). Collectively these results indicate that PSII efficiency is significantly reduced in $HD_{Fluc}$ treated cells either because of excess light transfer from the LHC antenna systems of PSII, increased levels of inactive PSII or a combination of both.

### 4.5.4 Absolute electron transport rate ($ETR_{abs}$)

Although cells under the $HD_{Fluc}$ regime showed much lower $ETR_r$ in comparison to $HD_{Avg}$ little variation was found in terms of $ETR_{abs}$ between these treatments (**Figure 4-5C**). This is because the

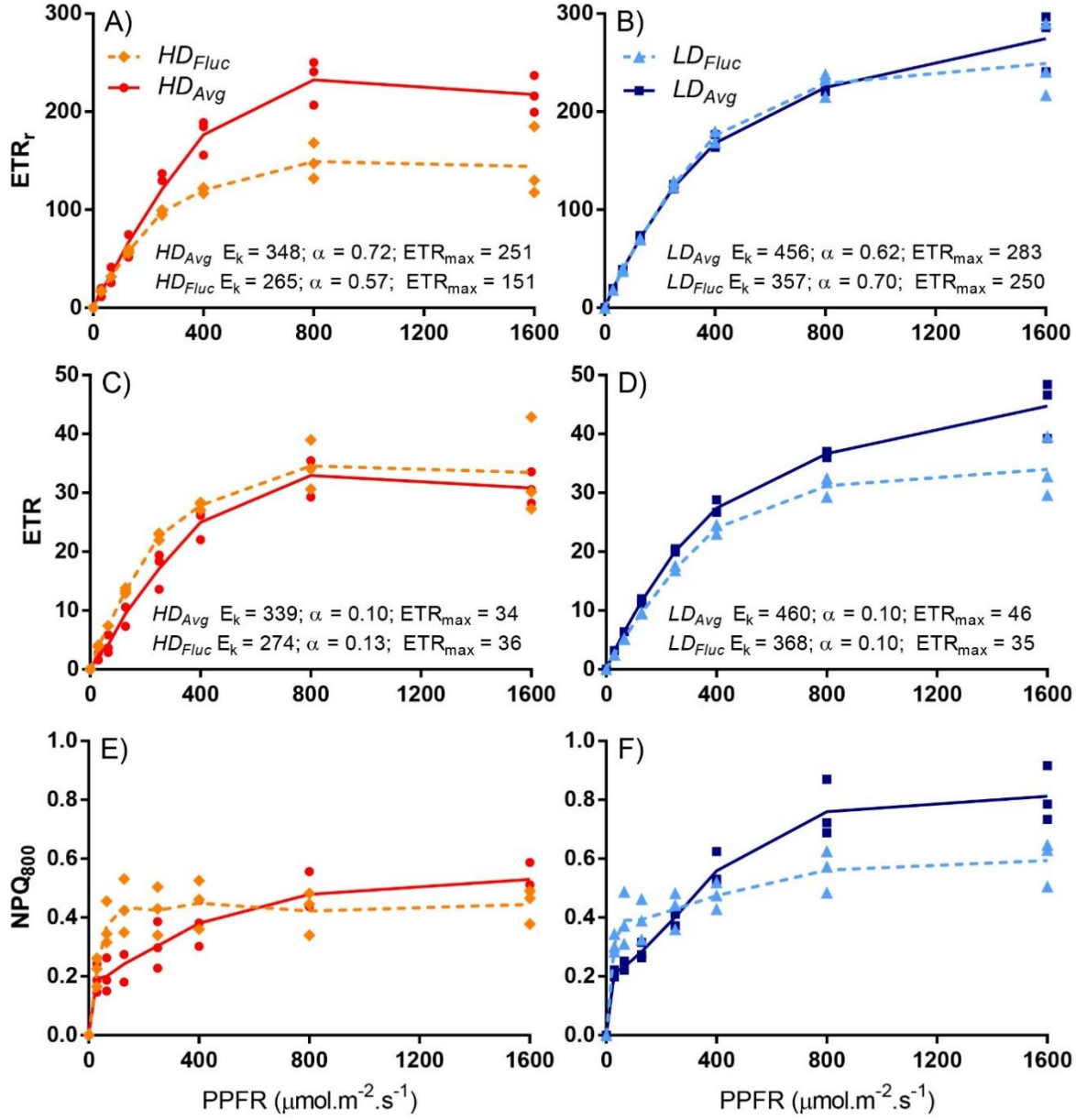


**Figure 4-5.** Rapid Light Curves of samples analysed at noon. A, $ETR_r$ of $HD_{Avg}$ and $HD_{Fluc}$ B, $ETR_r$ of $LD_{Avg}$ and $LD_{Fluc}$ C, $ETR_{abs}$ of $HD_{Avg}$ and $HD_{Fluc}$ D, $ETR_{abs}$ of $LD_{Avg}$ and $LD_{Fluc}$ E, NPQ-irradiance curves of $HD_{Avg}$ and $HD_{Fluc}$ F, NPQ-irradiance curves of $LD_{Avg}$ and $LD_{Fluc}$. Individual data points shown. Lines are the mean.

high absorption capacity of $HD_{Fluc}$ compensates for the low $\Phi_{PSII}$ (**Figure 4-5C**). In fact, $ETR_{max}$ was virtually the same for all treatments (34–36 µmol photons.$m^{-2}$.$s^{-1}$), except $LD_{Avg}$, which was ~31% higher (46 µmol photons.$m^{-2}$.$s^{-1}$, **Figure 4-5D**). The similar $ETR_{abs}$ among light treatments agrees with findings that the rate of linear electron transport is ultimately limited by $CO_2$ availability, the rate of carbon fixation by Rubisco and the concentration of Rubisco (Bonente et al., 2012, Dang et al., 2014, Sukenik et al., 1987), the latter also being similar between different light treatments (**Figure 4-3**). Despite similar $ETR_{abs}$ among all four light treatments, the $ETR_r$ values reveal that the

underlying reasons for these similar rates are not the same. In high light acclimated cells (*HD*$_{Avg}$, *LD*$_{Fluc}$ and *LD*$_{Avg}$) $\Phi_{PSII}$ is high and absorption is low, likely due to down-regulation of the antenna proteins; while in low light acclimated cells (i.e. *HD*$_{Fluc}$), an up-regulation of the antenna proteins results in higher light absorption, which is, however, used less efficiently for photosynthesis. This implies that the energy of the remaining photons does not enter the electron transport chain and must be lost as either chlorophyll fluorescence or heat, or will contribute to photodamage. Since dark adapted fluorescence of *HD*$_{Fluc}$ cells showed little capacity to dissipate energy as heat and high fluorescence (**Figure 4-5A**), it is a reasonable assumption that the remaining photons contribute to photoinhibition.

### 4.5.5 NPQ-irradiance curves

In general, some NPQ was observed for all conditions even under low light (30 μE.m$^{-2}$.s$^{-1}$) consistent with reports that a limited amount of excess energy can be dissipated by LHCSR3 under non-protonating conditions (Peers et al., 2009). The amplitude of NPQ was also consistent with levels of LHCSR3, showing highest NPQ under the *LD*$_{Avg}$ regime, then similar maxima for *LD*$_{Fluc}$ and *HD*$_{Avg}$, while the lowest NPQ was found under *HD*$_{Fluc}$ (**Figure 4-5E** & **F**).

Remarkably, NPQ-irradiance curves of fluctuating and non-fluctuating light regimes showed very different trends (**Figure 4-5E** & **F**). Under non-fluctuating light (*HD*$_{Avg}$ and *LD*$_{Avg}$), *NPQ* increased with irradiance in a light dose-dependent manner. The shape of this NPQ trend corresponded to that observed for ETR at each irradiance, suggesting that, under the non-fluctuating light treatments, NPQ was mediated by increased lumen acidification resulting from linear electron transport that caused protonation of LHCSR3, while the amplitude of NPQ was determined by the level of LHCSR3 expression.

In contrast, cells under *HD*$_{Fluc}$ and *LD*$_{Fluc}$ exhibited a relatively high NPQ at low irradiance (30-250 μE.m$^{-2}$.s$^{-1}$), which was considerably higher than *HD*$_{Avg}$ and *LD*$_{Avg}$ respectively. The *HD*$_{Fluc}$ cells with high absorption and low LHCSR3, shows a rapid rise in NPQ which plateaus at ~128 μE.m$^{-2}$.s$^{-1}$. *LD*$_{Fluc}$ with lower absorption and higher LHCSR3, also showed a large initial increase, and then entered a second stage of a biphasic response which was light dependent.

The high levels of NPQ observed at low incident light intensities in the cells subjected to fluctuating light regimes (i.e. "mixed cultures") suggests that a rapid change in thylakoid luminal pH occurs from dark to light transitions. Studies have shown that proton gradient regulation is essential for the health of plants and algae under low and fluctuating light conditions (Tikkanen et al., 2012). This allows a rapid proton motive force across the thylakoid membrane from dark to light transitions and has been

connected to increased rates of both cyclic electron flow (Alric et al., 2010, Bonente et al., 2012, Johnson et al., 2014) and the water-water cycle (Asada, 1999). Apart from being necessary to initiate linear electron transport, an important benefit of a rapidly developing proton motive force under fluctuating light is to slow down the electron transfer from cytochrome $b_6f$ to protect PSI, and to induce NPQ to prevent overexcitation of PSII (Tikkanen et al., 2012). Therefore, it is likely that the rapid increase in NPQ with incident irradiance observed under fluctuating light conditions is due to increased protonation of LHCSR3 (**Figure 4-5E** & **F**), by the rapid development of a luminal pH gradient. Although outside the scope of the current work, the underlying mechanisms are being further investigated.

## 4.6 Growth & biomass accumulation efficiency

### 4.6.1 Estimation of biomass yield on light energy

To determine the effects of the extrinsic light regime and the biological photoacclimation and regulation response on the biomass productivity of *C. reinhardtii*, growth was monitored by changes in optical density at 750 nm ($OD_{750}$) for the four light regimes over a 24 h period.

Each light treatment was first adjusted to a similar low $OD_{750}$ value to avoid cell shading (**Figure 4-6A**, $OD_{750}$ = 0.15 $cm^{-1}$). Remarkably, $HD_{Fluc}$ which most closely mimics typical operational mass culture conditions showed a ~63% reduction in the mean growth rate, relative to $HD_{Avg}$ (0.7 ± 0.1 and 1.9 ± 0.1 $day^{-1}$ respectively, **Figure 4-6**). In contrast, $LD_{Fluc}$ had a similar mean growth rate to $LD_{Avg}$ over the 24 h period (1.7 ± 0.1 and 1.7 ± 0.1.$day^{-1}$ respectively).

Since low- and high-density treatments received different amounts of light, biomass yield (**Figure 4-6B**) was next estimated on the basis of available light energy ($Y_{X,E}$ = g dry biomass $mol^{-1}$ photons absorbed (Eq. 6) to assess the relative efficiency of each culture condition to utilise light for biomass productivity.

Eq 4-10. $$Y_{X,E} = \int \frac{C_x - C_{x0}}{I_{avg}{}^{-6}(t) \cdot 3{,}600 \cdot E_a \cdot C_{x0}(1+\mu(t))}\, dt$$

In equation 4-6, $C_x$ and $C_{x0}$ are the final and initial biomass concentrations respectively ($kg.m^{-3}$), $I_{avg}$ is the hourly averaged PPFD (μmol $photons.m^{-2}.s^{-1}$), and 3,600 is the conversion factor from seconds to hours.

$C_x$ and $C_{x0}$ were estimated from the final and initial $OD_{750}$ measurements (**Figure 4-6A**). Due to the small dilute sample volumes used in this study, the relationship between $OD_{750}$ and biomass dry weight (BDW) was calibrated at a single time point for each light treatment and this value was used

to calibrate the other $OD_{750}$ measurements on the assumption that cellular characteristics would not change significantly over the time course. Using this approach, Griffiths et al. (2011) established an error range of 5–13% under normal conditions over a 17-day growth period and up to 25% error under nitrogen starved conditions for four algal species. We therefore acknowledge uncertainty in the calculation of $Y_{X,E}$ and to be cautious, have therefore conservatively reported differences greater than 25% as significant.

An approximate three-fold higher $Y_{X,E}$ was estimated for cells in the $HD_{Avg}$ regime (0.29 ± 0.02) compared to those in the $HD_{Fluc}$ treatment (0.10 ± 0.02 respectively), despite the fact that the two regimes received the same total light dosage (**Figure 4-6B**). In contrast, no significant difference in $Y_{X,E}$ of cells grown under $LD_{Fluc}$ and $LD_{Avg}$ conditions was observed. These results suggest that light-to-biomass conversion is highly affected by the illuminated fraction of the culture: cells exposed to dark periods for a large proportion of time may not utilise light efficiently for biomass accumulation, while those subjected to a small dark fraction may obtain similar yields than cells under continuous irradiance. These findings are in agreement with previous studies (Janssen et al., 2000, Janssen et al., 1999).

### 4.6.2 Biomass accumulation efficiencies varies under different light regimes

A large discrepancy in biomass yield was observed between $HD_{Fluc}$ and $HD_{Avg}$ treatments (**Figure 4-6B**) in response to the light energy ($Y_{X,E}$) received. This demonstrates high energy losses between the initial light absorption and the final biomass storage stage under $HD_{Fluc}$ conditions. There are several steps in the light-to-biomass pathway where these losses may occur (**Figure 4-7**). First, losses occur at the level of PSII when absorbed photons exceed the capacity of electron transport. This energy is either lost via NPQ-mediated heat dissipation, or contributes to photodamage via formation of ROS. Second, electrons in the electron transport chain may be diverted to alternative electron pathways that do not result in NADPH formation. These include the water-water cycle (Mehler reaction), photorespiration, and PSI-mediated cyclic processes (Wilhelm and Selmar, 2011). Third, ATP and reducing equivalents produced by the light reactions may be used in metabolic processes that do not contribute to growth (including nutrient assimilation and repair). Finally, some fixed $CO_2$ is used for respiration.

The fluctuating and non-fluctuating treatments received the same average light dosage as their respective controls. However the light gradients of the fluctuating regimes included super- and sub-saturating irradiance levels which result in reduced photosynthetic rates during the light-limiting periods and zero photosynthetic rates during dark periods.

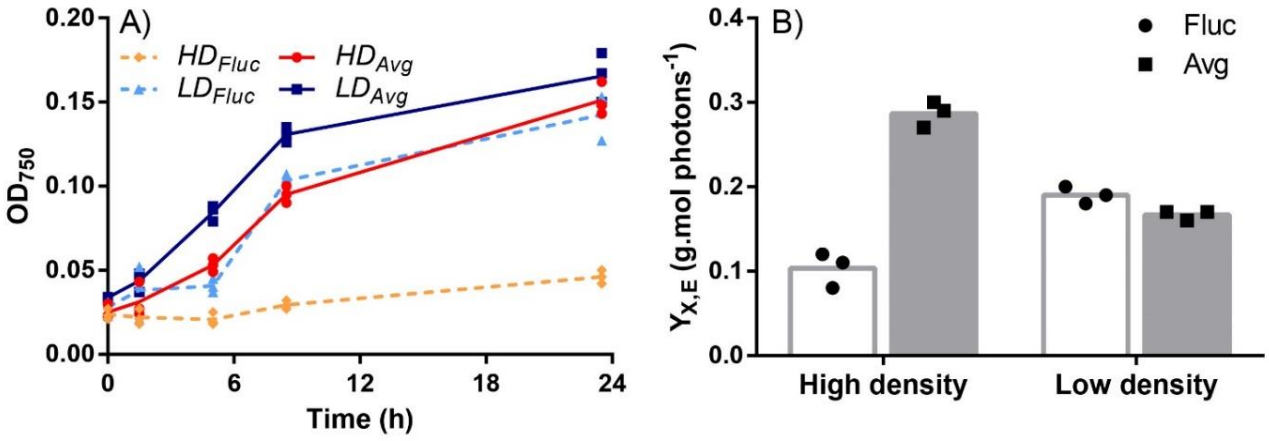


**Figure 4-6.** Effect of light regime on culture productivity: A $OD_{750}$ growth curves of 7-day acclimated samples over a 24 h light regime period. B Biomass yield on available light energy $Y_{X,E}$ (g biomass per mol photons). Individual data points shown. The bars represent the sample mean. Note: Variations in data points are due to deviations in $OD_{750}$ measurements and do not include potential error in OD : BDW correlations (see results).

Furthermore during the highest light periods, the limited ETR capacity will prevent full utilisation of this energy and under extreme conditions photoinhibition. Therefore it is unlikely that the total usable photon flux (and hence electron transport rate, ETR) in the supersaturating period of the light regime will compensate for the loss of electron transport during the dark period and so overall biomass accumulation will be compromised.

To establish whether differences in biomass accumulation were due to the light regime itself or the photosynthetic response of cells based on their acclimated state, we compared the relative proportions of electron transfer rates from PSII (i.e. gross photosynthesis in response to local light) and the relative proportions of biomass accumulation among treatments (i.e. net photosynthesis after respiration load for maintenance and repair are subtracted). Using Equation 4-3 and the parameters fitted to the ETR curves for each light regime (**Figure 4-5C** & **D**, **Table 4-3**), we modelled the mean photosynthetic rates to the respective daily irradiances of each light treatment. The modelled rates were integrated over the day to estimate the mean daily ETR (**Table 4-3**).

Not surprisingly, the light gradients of fluctuating regimes estimated a 32% reduction of daily mean ETR in $HD_{Fluc}$ in comparison to $HD_{Avg}$, and a 30% reduction of $LD_{Fluc}$ relative to $LD_{Avg}$. These reductions account for all losses at the level of PSII. This would lead us to expect at least a 30% reduction in biomass accumulation efficiency under fluctuating light relative to their respective non-fluctuating controls. However, this does not happen in either case.

**Table 4-3.** Model fitted parameters of equation 4-3 and comparison of modelled mean daily photosynthetic rates (ETR) and estimated biomass accumulation efficiencies ($Y_{X,E}$).

| **Model Parameters** | $HD_{Fluc}$ | $HD_{Avg}$ | $LD_{Fluc}$ | $LD_{Avg}$ |
|---|---|---|---|---|
| $P_s$ | 44 | 54 | 35 | 46 |
| α | 0.13 | 0.1 | 0.01 | 0.1 |
| $ETR_{max}$ | 36 | 34 | 35 | 46 |
| $I_k$ | 274 | 339 | 368 | 460 |
| $R^2$ | 0.9993 | 0.9981 | 0.9987 | 0.9984 |
| **Daily Mean ETR** | **7.5** | **11.0** | **10.7** | **15.3** |
| **Fluc as % of Avg** | **68%** | **100%** | **70%** | **100%** |
| **$Y_{X,E}$ (g biomass.mol photons.$^{-1}$)** | **0.09** | **0.29** | **0.18** | **0.17** |
| **Fluc as % of Avg** | **32%** | **100%** | **108%** | **100%** |

Low density cultures ($LD_{Fluc}$) show no significant difference in $Y_{X,E}$ between fluctuating and non-fluctuating conditions, while the lower ETRs of $HD_{Fluc}$ cells only account for half of the losses of $Y_{X,E}$ relative to $HD_{Avg}$ cells (**Figure 4-6B**). In the case of $LD_{Fluc}$ no net reduction is evident in $Y_{X,E}$ in comparison to $LD_{Avg}$, despite ~30% lower ETR. This is likely because both $LD_{Avg}$ and $LD_{Fluc}$ populations are under considerable light stress (daily $I_{avg}$ 272 μmol photons.m$^{-2}$.s$^{-1}$). In the $LD_{Fluc}$ regime, with its short dark zone, photosynthetic losses will be low and may be balanced by the accompanying reduction in light stress during the intermediate parts of the light cycle where conditions are close to optimal during the times of highest daily photon flux. In contrast, $LD_{Avg}$ under long durations of continually high light stress would likely suffer greater photoinhibition.

The idea that a small dark fraction provides reprieve from photoinhibition experienced under continuous high light is supported by observations that high light fractions (0.8–0.85) achieved higher biomass conversion efficiencies than under continuous high light (Barbosa et al., 2003, Janssen et al., 2000, Wu and Merchuk, 2001). $LD_{Fluc}$ and $LD_{Avg}$ also had lower biomass yields per light energy absorbed (i.e. lower $Y_{X,E}$) than $HD_{Avg}$, despite similar growth rates among these three treatments. This is therefore due to an inability to utilise the higher average photon flux ($I_{avg}$ ~65% higher than $HD_{Avg}$) experienced by these cultures. In contrast to the low-density regimes, the estimated ~67% relative reduction in $Y_{X,E}$ for $HD_{Fluc}$ cannot be explained by lower mean ETR alone. Additional losses occurring after photons have entered the electron transport chain are either the result of alternative electron flows, or increased metabolic load. Under $HD_{Fluc}$, we found that NPQ capacity was diminished, light absorption was high, minimum fluorescence ($F$) increased and low $\Phi_{PSII}$ efficiencies were observed (**Figure 4-5**).

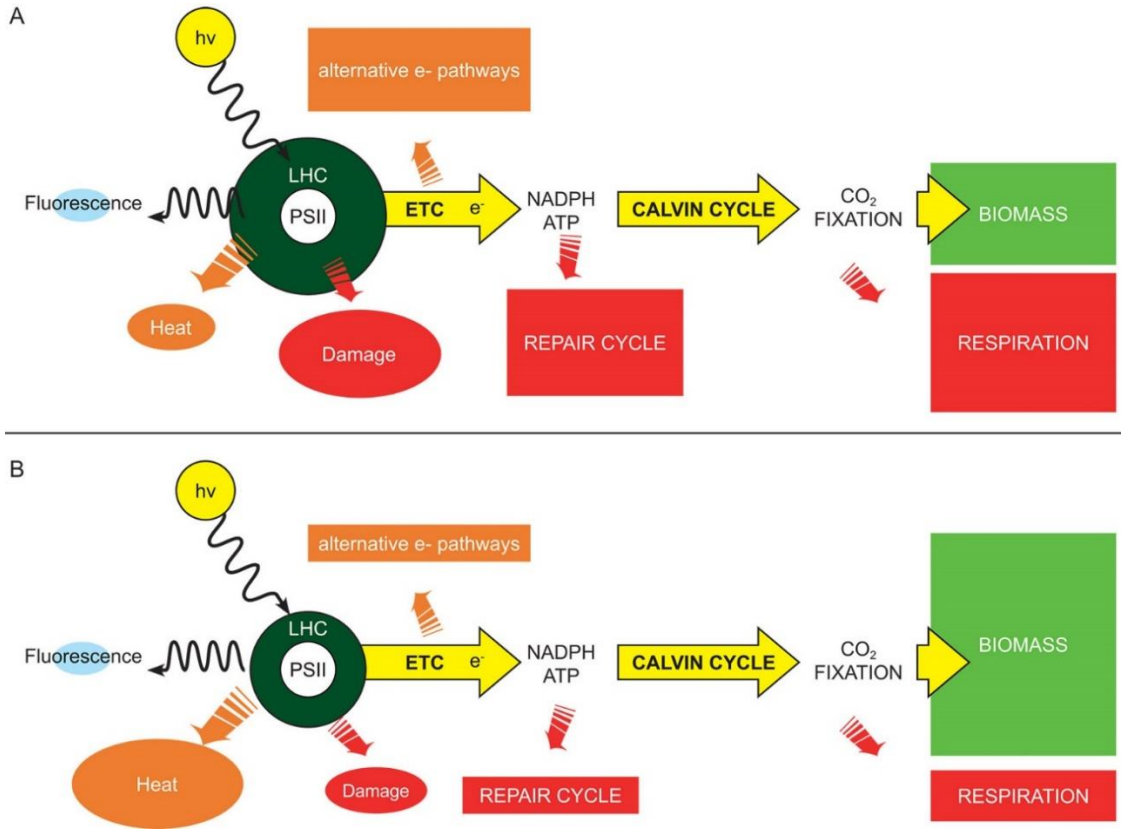


**Figure 4-7.** Schematic diagram of energy flows from light absorption to biomass accumulation for A Low-light acclimated cells under fluctuating light (i.e. $HD_{Fluc}$) and B High-light acclimated cells under non-fluctuating moderate light ($HD_{Avg}$).

All these factors strongly indicate that substantial photodamage occurs in $HD_{Fluc}$, increasing metabolic load for energy directed toward repair. In addition, it has been shown that fluctuating light induces alternative electron flows such as the water-water cycle (Asada, 1999) and therefore these may also contribute to a reduction in light-to-biomass conversion. In conclusion, our modelled estimations suggest the poor productivity of $HD_{Fluc}$ can be attributed almost equally to both the sub-optimal light conditions and the cell's low-light acclimation response, which is inappropriate to these light conditions. Based on these findings, **Figure 4-7** compares the potential energy flows of $HD_{Fluc}$ and $HD_{Avg}$.

## 4.7 General discussion

Of the four treatments, the $HD_{Fluc}$ light regime, with its extensive dark zone and medium-duration 10 s cycle time, most closely represents the light history of cells cultivated under high density outdoor microalgae cultivation systems. Indeed, widely used production systems such as high rate ponds often have a much smaller light : dark zone ratio (e.g. ~10 mm light: 240 mm dark in high rate ponds). Yet the $HD_{Fluc}$ conditions yielded by far the worst biomass accumulation efficiencies, in line with

previous reports. Assuming as a first approximation that $HD_{Fluc}$ productivities represent a baseline for many current mass culture systems, our data suggest that up to a three-fold increase in light to biomass conversion efficiencies could be achieved by improving both the light distribution and the biological response of *C. reinhardtii*.

Theoretically improved light distribution can be achieved by biological (e.g. light harvesting antenna engineering) and engineering (increasing SA:V ratio) means. As the capital costs of photobioreactors are proportional to the material required to build them, increasing the SA:V ratio will likely increase capital costs and reduce economic returns unless offset by the achieved efficiency gains. In contrast genetically engineered fit-for-purpose cell lines which are programmed to be high-light adapted could result in significant efficiency gains with minimal capital outlay.

A critical conclusion of this study is that the $HD_{Fluc}$ conditions resulted in the cells acclimating to low light levels, despite the fact that they were exposed to periods of extremely high light (up to 1,416 μmol photons.$m^{-2}$.$s^{-1}$) and received a high daily average irradiance which caused high light acclimation under non-fluctuating conditions (i.e. $HD_{Avg}$). In particular, low-light acclimation in $HD_{Fluc}$ induced both an up-regulation of the light harvesting antennae and a down-regulation of the major NPQ component LHCSR3.

Under true light-limiting conditions when the rate of electron transport exceeds the rate of photon absorption, low-light acclimation is beneficial to maximise light capture and minimise energy spent on unrequired dissipation mechanisms. However, under the extreme light gradients of mass culture, this low light acclimation response has detrimental consequences both on the photosynthetic-irradiance response curve when combined with the light history of a fluctuating cycle and light transfer through the culture because of higher absorption and scattering. Based on the results of this study, a model illustrating the effects of low- and high-light acclimated cells on culture productivity under the same mass culture conditions (i.e. cell concentration, pathlength) is proposed in Figure 4-8.

Under low light acclimation (**Figure 4-8A**), the dual effect of high light absorption and the lack of LHCSR3 mediated-NPQ results in a synergistic reduction of the irradiance level at which photoinhibition occurs ($I_b$) as well as an increased sensitivity to photoinhibition, as evidenced by a higher slope decline (β). Increased light absorption results in a higher initial slope of the growth curve (α) and a lower saturation irradiance ($E_k$); but these effects are partly reversed by inactivated photosystems from accumulated photodamage during periods of high light of the fluctuating regime. Moreover, photodamage and potentially higher alternative electron flows result in a reduction in maximum growth ($\mu_{max}$), while a higher dark respiration rate occurs ($R_s$) as energy is directed toward

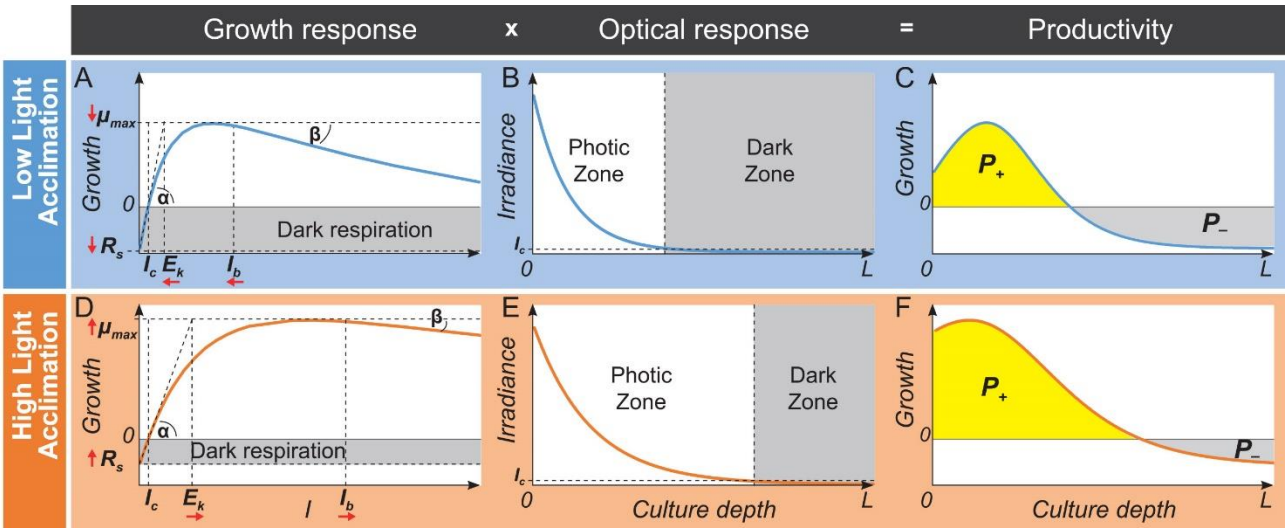


**Figure 4-8.** Growth response model. The effects of low- (A–C) and high-light acclimated (D–F) cells under fluctuating light on culture productivity. A & D *P–I* response curve. B & E Irradiance through the culture depth. C & F Biomass productivity is the integrated growth rate through the reactor. See Section 3 for details.

repair. The irradiance compensation point at which photosynthetic growth exceeds respiration loss ($I_c$) is reduced from higher absorption, but also increased from higher respiration.

Figure 4-8B shows that an increase in absorption and scattering coefficients of low-light acclimated cells reduces light penetration through the culture, resulting in a larger dark zone. The combined effects of growth response (**Figure 4-8A**) and local light exposure in the culture (Figure 4-8B) result in low productivity in algal systems. In contrast Figure 4-8D shows the *P–I* curve of high light acclimated cells under fluctuating light. High levels of LHCSR3 mediated-NPQ lowers β and increases $I_b$. Reduced photodamage and higher PSII efficiency lowers $R_s$ and increases $\mu_{max}$.

Lower absorption per photosystem reduces α but this is partly offset by a higher proportion of functional photosystems within the total culture. **Figure 4-8E** shows that cell shading and light scattering are reduced because of lower absorption and larger cell size, increasing the photic zone of the culture**.** Consequently in **Figure 4-8F**, the combined effects of growth response (**Figure 4-8D**) and local light exposure (**Figure 4-8E**) on productivity lead to a larger zone of productivity, higher yields at the surface and a smaller zone of respiration losses.

Whilst this model framework is based on our study of *C. reinhardtii*, the similar productivity responses between light/dark cycles and continuous light for *C. sorokiniana*, *D. tertiolecta* and *N. salina* suggest that this framework may also be applicable for other commercially relevant strains. Moreover, Quaas et al. (2015) found that NPQ responses in six algal species were based on an acclimated response.

It should also be noted that the above responses do not consider the potential effects of temperature variations. Temperature stresses will doubtless affect these responses in a nonlinear way and will require additional modelling to take these environmental effects into account.

Clearly, an understanding is required of the physiological mechanisms by which low light acclimation is inappropriately induced in cells exposed to medium-duration fluctuating light such as occurs during mixing cycles. This would provide the opportunity to engineer strains which do not behave in this way. To date, molecular efforts have focused on truncating the light harvesting antenna of algae with the aim of reducing light absorption per cell, thereby increasing light availability to cells deeper in the culture (Beckmann et al., 2009, Mitra et al., 2012, Mitra and Melis, 2008, Mussgnug et al., 2007, Oey et al., 2013, Perrine et al., 2012). As yet, antenna mutants have not been adopted at pilot or industrial scales, and some reports suggest lower productivities than wild type strains (Chow and Thung, 2015, de Mooij et al., 2014). de Mooij et al. (2014) and others associated the lower yields to a higher light sensitivity of these antenna mutants, suggesting that photoprotective mechanisms were compromised. Thus more targeted engineering modifications of the LHC systems should not only focus on reducing absorption capacity, but also maintaining photoprotective mechanisms.

## 4.8 Conclusion

The development of high performance microalgal systems would benefit from more accurate predictive light-to-biomass modelling tools. Our results suggest that this is possible if the effects of fluctuating light regimes are included in the modelling, which would require equations able to predict the effect of the light regime on the *P–I* curve, such that the parameters ($\alpha$, $\beta$, $\mu_{max}$, $R_s$) become variables; and also on the optical properties of the cell required to estimate radiative transfer through the culture. We anticipate that an improved understanding of the effects of low- or high-light acclimation in mass culture will guide the development of more accurate predictive models to improve the feasibility of algal biotechnology systems.

# 5 A dynamic model of algal behaviour under outdoor batch cultivation.

## 5.1 Abstract

The data obtained from this thesis study so far, including the batch cultivation experiments performed in the ePBR matrix (Chapter 3) and the light simulations performed on dilute microwell cultures (Chapter 4), indicated that several interconnected photosynthetic processes change dynamically over time in response to both diel incident light fluxes and changes in culture density. The static Haldane growth model, although fitted against the existing data by adjusting the respiration rate, does not provide sufficient information about the underlying mechanisms occurring as a batch culture evolves to model the biological response properly. Moreover, a review of the literature, carried out retrospectively, reveals that the *P–I* response curve of algae is highly plastic, in response to changes in light dose and light pattern. This final research chapter presents a more realistic, empirically founded mechanistic growth model that attempts to explain some important underlying biological phenomena of outdoor algal production systems. Based on a dynamic 3-state model of the so-called photosynthetic unit (PSU) described in the literature, the model is here refined to describe changes in photoacclimation, non-photochemical quenching and carbon assimilation efficiency as a function of key elements of the light regime that were found to influence these processes. These key elements include the local irradiance, spatially-averaged irradiance through the culture depth, the illuminated fraction of the culture, and consideration of the light history of the cell. It should be noted that further experiments are required to accurately estimate model parameters and validate the model structure. However, preliminary validation with parameter values based on the literature and available data shows a good correlation between predicted and measured changes in biomass, cellular pigment content and fluorescence kinetics for three different daily light conditions.

## 5.2 Introduction

Whilst static models are desired for simplicity, in reality, biological systems are governed by complex feedback loops (Flynn, 2005), often necessitating dynamic models except under steady state conditions. The results obtained from this study as well as those reviewed in the literature revealed some important insights about the behavior of algae under batch cultivation. Firstly, the findings of Chapter 4 and by Grobbelaar et al. (2005), Janssen et al. (2000) and Takache et al. (2015) suggest that cellular absorption capacity increases as culture density increases and appears to be influenced, not just by the average or local irradiance, but also by the proportion of time spent in so-called dark zones. For example, a dense culture (i.e. large dark fraction) with relatively high incident and spatially-averaged light may be as likely to become low-light acclimated as a dilute culture (low dark

fraction) under relatively low incident and spatially-averaged light (see Chapter 4). The impact of the dark zone suggests that changes in photoacclimation (referred hereafter as 'acclimation') may be signalled by changes in the redox poise of the photosynthetic apparatus that occur from constant light-to-dark transitions (e.g. state transitions). In conjunction, the maximum capacity for NPQ seems to lessen in response to an increased dark to light ratio (i.e. higher culture density) in *C. reinhardtii* because of reduced accumulation of the dissipative protein LHCSR3 (Yarnold et al. 2016). Since LHCSR3 is found in other Chlorophyta, including one of the earliest lineages, *Ostreococcus* (Peers et al., 2009), this suggests that this qE mechanism is highly conserved and therefore applicable to many other green algae. In spite of reduced photoprotection, the batch cultivation in ePBRs (Chapter 3) revealed that although cellular growth rates diminished as the culture dark fraction increased, growth was still higher than predicted by the static Haldane growth model. This implied a possible decline in photoinhibition and/or respiration type processes. A reduction of photoinhibition may simply occur as a result of either higher numbers of 'open' reaction centres (i.e. oxidised $Q_A$) from longer periods in the dark. Reduced respiration could arise from lower light-enhanced dark respiration associated with reduced photosynthetic production on a per cell basis. Finally, a further dynamic change that seems likely in an evolving culture is the activation state of the Rubisco pool, which may decrease under higher cell densities due to reduced ATP production and oxidation of the ETC under light-to-dark transitions (Gontero et al. 2014). This could lead to oxidation of Rubisco activase and consequentially, a higher proportion of deactivated Rubisco, thereby diminishing the capacity for carbon assimilation which will ultimately affect maximum photosynthetic and growth rates ($P_{max}$ and $\mu_{max}$ respectively) – a factor that was revealed from a sensitivity analysis to have a high impact on productivity estimates (Chapter 2). This assumption is supported by literature studies that reported high plasticity in measured *P–I* curves over time under batch cultivation where dilute cultures showed a high $P_{max}$ which decreased as culture density increased (Grobbelaar et al., 1996, Grobbelaar et al., 1995).

In light of the above situation, this final research chapter develops and tests a theoretical model that endeavors to account for dynamic feedbacks of relatively slow processes occurring on tens-of-minutes to hours timescales including: acclimation (e.g. protein and pigment expression), the activation state of the Rubisco pool, and the D1 repair cycle; and relatively rapid processes occurring on sub-seconds to minute timescales including: photoproduction, NPQ and photoinhibition. The model is based on the dynamic three-state PSU model of Wu and Merchuk (2001) and refined to incorporate the abovementioned acclimation and regulation effects. In addition to growth, the three state model can predict changes in the state of PSII over time as monitored by chlorophyll

fluorescence data (Ebenhöh et al., 2011). This model is useful to investigate whether the general assumptions of photosynthetic growth modelling assigned in this study have been reasonable.

## 5.3 Model approach

### 5.3.1 The dynamic 3-state 'PSU' model of Wu and Merchuk (2001)

The class of models based on the concept of the so-called photosynthetic unit (PSU), also referred to as 'photosynthetic factories' was first proposed by Kok (1956) and later refined by others (Bernardi et al., 2014, Eilers and Peeters, 1988, García-Camacho et al., 2012, Han, 2002, Rubio et al., 2003, Wu and Merchuk, 2001, Zonneveld, 1998, Zonneveld et al., 1997). According to Wu and Merchuk (2001), the PSU is defined as "the sum of the light trapping system, reaction centres and associated apparatus, which are activated by a given amount of light energy to produce a certain amount of photo-product".

In the model of Eilers and Peeters (1988) and modified by Wu and Merchuk (2001), the PSU at any given instant is assumed to be in one of three excitation states: the open (resting), termed $x_1$, active (closed), termed $x_2$, or damaged (inhibited), termed $x_3$ (**Figure 5-1**). When a photon is received by an open PSU it becomes active ($x_1 \rightarrow x_2$) based on a first order rate of activation in response to light, $k_a$. For a PSU in the activated state, two possibilities can occur: if another photon is received, it will become inhibited ($x_2 \rightarrow x_3$) at another first order reaction rate, $k_i$. Otherwise, photochemical quenching by carbon assimilation occurs at a rate $k_d$, and the PSU is then open to receive another photon ($x_2 \rightarrow x_1$). Finally, inhibited reaction centres are repaired by the D1 repair process at a further rate constant, $k_r$ ($x_3 \rightarrow x_1$). The rates of $k_d$ and $k_r$ are of zero order as they are independent to light (the so-called 'dark reactions' of carbon assimilation and the D1 repair system). Accordingly, the probability of the fraction of the PSU pool in each of the three excitation states at any given time is represented by the following system of linear ordinary differential equations:

Eq. 5-1. $$\frac{dx_1}{dt} = -k_a I x_1 + k_d x_2 + k_r x_3$$

Eq. 5-2. $$\frac{dx_2}{dt} = k_a I x_1 - k_d I x_2 - k_i x_2$$

Eq. 5-3. $$\frac{dx_3}{dt} = k_i I x_2 - k_r x_3$$

where,

Eq. 5-4. $$x_1 + x_2 + x_3 = 1$$

and the specific growth rate, $\mu$ ($s^{-1}$) is defined as,

Eq. 5-5. $$\mu(t) = k_p k_d x_2(t) - R_s$$

In Eq. 5-5, $k_p$ (–) is a proportionality constant between the rate of photochemical quenching and biomass accumulation and $R_s$ ($s^{-1}$) accounts for all maintenance losses.

### 5.3.2 Model enhancement with dynamic acclimation and regulation

In addition to photoproduction and photoinhibition included in the original 3-state model above, the model is modified to include photoregulation (referred to hereafter as 'regulation') and acclimation processes calculated at timescales of seconds and hours respectively. The new model calculation scheme predicts that under an evolving batch culture in outdoor light cycles, these processes will be highly dynamic and will create feedbacks on both photosynthetic rates and the optical properties of the culture (**Figure 5-1**). Acclimation processes are calculated at a timescale of one hour and include: absorption capacity (as affected by pigment content); and the maximum capacity for NPQ due to LHCSR3 accumulation. Regulation processes are calculated at a timescale of seconds, and include: the realised rate of NPQ, which is considered to be mostly affected by energy dependent quenching (qE) and to some extent, state transitions (qT). An exception is the realised maximum rate of photosynthesis, $P_{max}$, which is modelled from changes in Rubisco activity – although this is strictly a regulatory process, it occurs on the order of tens to minutes (Gross et al., 1991) and the model predicts it will reach a pseudo-steady state under a given incident irradiance, $I_0$ and cell density, $C_x$, where small changes in $I_0$ and $C_x$ under shorter (< hours) timescales will have a negligible effect on $P_{max}$. Greater detail of the modelling of these processes is presented next.

### 5.3.3 Available light for photochemistry as governed by the light harvesting complexes

When light falls on a chloroplast surface, the rate at which photons reach the PSU reaction centres (i.e. the amount available for photosynthetic electron transport) to the rate of incident light flux is in part governed by the light harvesting complexes – the site where absorption and dissipation of light energy occurs. Many models assume growth as a function simply of the irradiance that the cells are subjected to, but this tells little about the amount of light available for photochemistry, that is, the irradiance reaching the electron transport chain, $I_{ETC}$. Zonneveld (1998) proposed that the rate of photosynthesis was based on the photon absorption rate, rather than on irradiance. However, this does not take into account light that is dissipated by non-photochemical quenching processes within the light harvesting complexes before reaching the reaction centre. The recently elucidated biology of LHCSR3 makes it clear that in fact, both the induction of this protein and its dynamic regulation by

the proton gradient affect the behaviour of the system. In particular, the majority of light dissipation occurs prior to, and not after, absorption by PSII, but only if LHCSR3 has already been induced during acclimation. Consequently the model proposed here accounts for this by introducing a term $(1 - q_{NPQ})$ to modulate the fraction of absorbed light that is actually transferred to the photochemical reaction centre (Figure 5-1):

Eq. 5-6. $$I_{ETC} = I_{loc}\, q_{abs}\, (1 - q_{NPQ})$$

In Eq. 5-6, $q_{abs}$ is the absorption efficiency factor, being the fraction of light energy absorbed to the light energy received by its geometrical cross-section (Morel and Bricaud, 1981), and $q_{NPQ}$ is the fraction of light energy that is lost by all NPQ processes (Nikolaou et al., 2015).

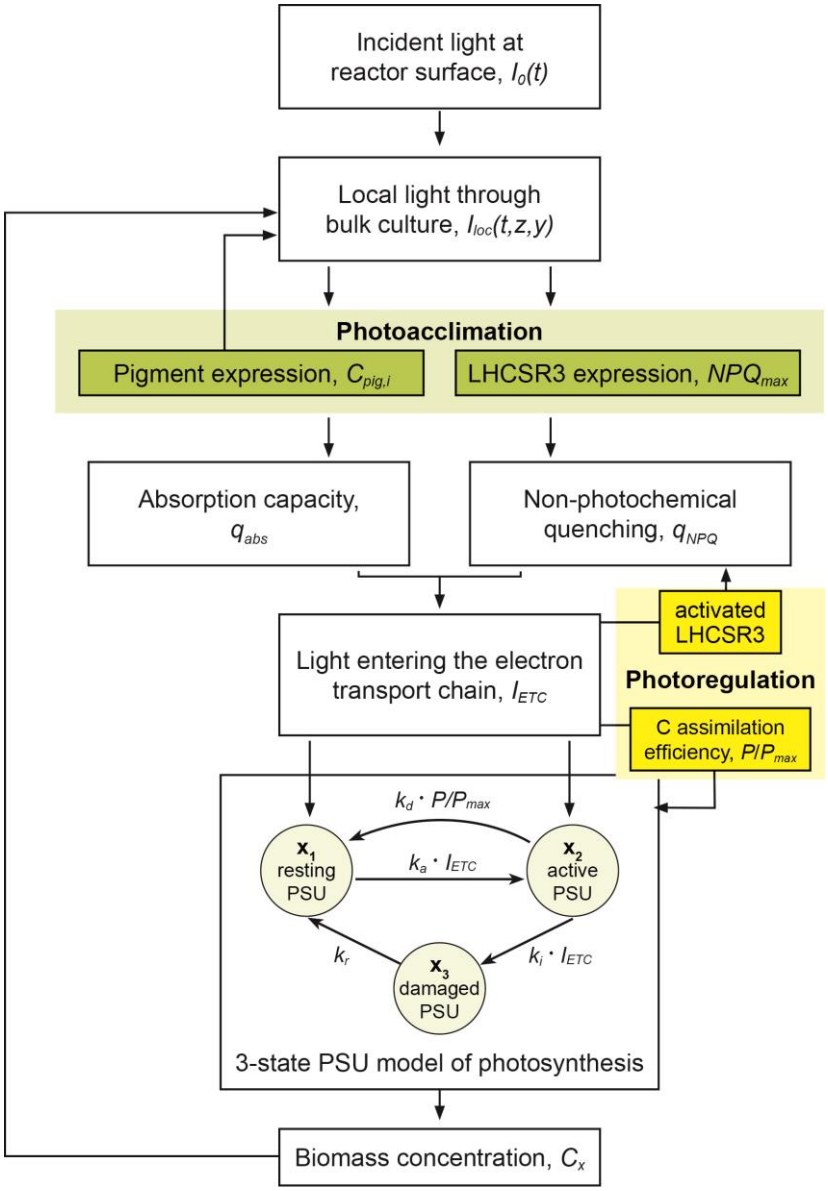


**Figure 5-1.** Model calculation scheme of the modified 3-state PSU model with incorporation of dynamic acclimation and regulation feedbacks.

As depicted in **Figure 5-1**, $q_{abs}$ is affected by changes in pigment expression levels, while $q_{NPQ}$ is affected by both the magnitude of NPQ ($NPQ_{max}$), and its activation state, as affected by local irradiance, $I_{loc}$ and the activation state of the PSU based on its light history. Initially, many models neglected NPQ or did not consider it a dynamic process, although more recent models are now incorporating NPQ dynamics (Nikolaou et al., 2015, Bernardi et al., 2014). Uniquely here, the magnitude of NPQ in algae, $NPQ_{max}$ is modelled using the assumption that it is governed by expression levels of LHCSR3, which has been experimentally demonstrated by several groups (Bonente et al., 2011, Peers et al., 2009, Quaas et al., 2015, Yarnold et al., 2016).

### 5.3.4 Predicting photoacclimation under fluctuating light

Zonneveld (1998) and others assumed algae acclimate to the spatially averaged amount of light integrated over the culture depth, $I_{avg}$ received by the cell,

Eq. 5-7. $$I_{avg}(t) = \frac{1}{L}\int_L I_{loc}(t)dz$$

Where $L$ is the culture depth and $I_{loc}$ is the local irradiance.

A key finding of this study, including the results of Chapter 4 and literature studies reviewed in Chapter 1, suggests however, that cells under seconds-to-minutes fluctuating light cycles (typical of mass culture with significant dark fractions) acclimate to a lower irradiance than $I_{avg}$. Therefore, a unique term is introduced here to account for the 'perceived' light level of algae, $I_{p,}$ where $I_{avg}$ is modified by a proportionality constant, ε, such that,

Eq. 5-8. $$I_p(t) = I_{avg}(t)\,\varepsilon(t)$$

where ε is the illuminated fraction of the culture,

Eq. 5-9. $$\varepsilon(t) = \frac{L_c}{L}$$

and $L_c$ is the compensation depth where $I_{loc} = I_c$ – the compensation irradiance where gross photosynthesis and respiration losses are equal (i.e. zero net photosynthesis).

#### *5.3.4.1 Absorption capacity, $q_{abs}$*

Under the hypothetical situation of a fluctuating light cycle where $I_{avg}$ and ε remained constant, it is assumed that a pseudo-steady state concentration of the major pigments would be reached as an inverse hyperbolic function of 'perceived' irradiance, $I_p$ using the modified equation of García-Camacho et al. (2012),

Eq. 5-10. $$C_{pig.i} = C_{\max.i} - (C_{\max.i} - C_{\min.i}) \frac{I_p}{K_{pig} + I_p}$$

In Eq. 5-10, $C_{pig,i}$ is the concentration of pigment *i* in the cell, and $C_{max(i)}$ and $C_{min(i)}$ are the upper and lower cellular concentrations of pigment *i* (*pig*.*i* = Chl *a*, Chl *b* and Car).

Under dynamic light regimes imposed by changes in both culture density and diel incident light fluxes, it is assumed that acclimation does not reach steady state, but changes from one light regime, $I_{p,0}$ to another, $I_{p,f,}$ by first order logistic-type kinetics, (García-Camacho et al., 2012),

Eq. 5-11. $$C_{pig.i}(t) = \frac{C_{pig.i}(I_{p,f})}{1+[(C_{pig.i}(I_{p,f}) - C_{pig.i}(I_{p,0}))/C_{pig.i}(I_{p,0})]e^{-k_{acc}\,t}}$$

Here, $k_{acc}$ is the apparent rate constant of acclimated changes of cellular pigments (García-Camacho et al., 2012). Importantly, Eq. 5-11 predicts a faster rate of decline in pigment concentrations than to an increase. This is supported by experimental evidence of the ePBR experiments in Chapter 3, and from studies that found faster acclimation from low light to high light than *vice versa* (Tomaselli et al., 1997, García-Camacho et al., 2012), suggesting that degradation of light harvesting pigments is more rapid than biosynthesis.

Knowing the estimated concentrations of pigments predicted by Eq. 5-11, and the size distribution of cells, the PAR-averaged absorption coefficient of the cell, $q_{abs}$, as well as the optical parameters required to solve the two-flux approximation for radiative transfer ($E_a$, $E_s$ and *b* respectively) were calculated using the adapted code for Mie theory, as outlined in **Section 2.4.3**. Although equations 5-10 and 5-11 require empirical determination of seven constants (the minimum and maximum concentrations of each pigment as well as the acclimation rate, $K_{acc}$), a major benefit of this model is that once these values are established for a given species, changes in the optical properties of a culture and of $q_{abs}$ become fully predictive (with only initial inputs required).

#### *5.3.4.2 NPQ capacity ($NPQ_{max}$)*

In Chapter 4, it was found that levels of LHCSR3, the dominant protein responsible for energy dependent quenching (qE), was reduced under fluctuating light cycles in comparison to non-fluctuating light of the same $I_{avg}$, supported also by Quaas et al. (2015) who showed that the amplitude of NPQ was a result of acclimation to different light intensities for six algae species. Thus the work in Chapter 4 suggests that the molecular switches responsible for inducing this protein also appear to be affected by the light fraction and the 'perceived' rather than average light, in a similar manner to acclimation of pigment concentrations, such that under steady state conditions, $NPQ_{max}$ at steady state is found by Monod-type kinetics,

Eq. 5-12. $$\mathrm{qNPQ_{max}} = \left(\mathrm{qNPQ_{max,abs}} - \mathrm{qNPQ}_{min,\mathrm{abs}}\right)\frac{I_p}{K_{NPQ,max}+I_p}$$

Similarly to pigment concentrations, levels of LHCSR3 will be transient under dynamic light cycles, therefore, we use, Eq. 5-11 to calculate $NPQ_{max}$ under non-steady state incident light cycles as,

Eq. 5-13. $$\mathrm{qNPQ_{max}}(t) = \frac{\mathrm{qNPQ_{max}}(I_{p,f})}{1+[(\mathrm{qNPQ_{max}}(I_{p,f})-\mathrm{qNPQ_{max}}(I_{p,0}))/\mathrm{qNPQ_{max}}(I_{p,0})]e^{-k_{acc}\,t}}$$

#### *5.3.4.3 Maximum photosynthetic rate ($P_{max}$) as affected by carbon assimilation efficiency*

One aspect that is often neglected in models is the maximum rate of photosynthesis or growth, ($P_{max}$ or $\mu_{max}$), which changes in response to both $I_{avg}$ and ε and therefore, also to $I_p$. Since the activation state of the Rubisco pool and other key photosynthetic enzymes is highly modulated by redox-regulation processes (i.e. the thioredoxin system) and / or ATP (as reviewed in Chapter 1), it is theorised that $P_{max}$ will decline as culture density increases and average light is reduced. To the author's knowledge, no models accounting for changes in carbon assimilation efficiency of algal exist, although several models describe this process for higher plants. According to Gross et al. (1991) and based on the models of Farquhar and Von Caemmerer (1982), a further Michaelis-Menten equation is introduced to describe the maximum proportion of photosynthesis to its upper limit $P$ / $P_{max}$ that will be used to adjust the rate of deactivation, γ of active reaction centres $x_2$, based on the activation state of the Rubisco pool and other enzymes involved in carboxylation,

Eq. 5-14. $$\frac{P}{P_{max}} = \frac{\alpha_v I_{avg}(1-V_0)}{\alpha_v I_{avg}+1-V_0}$$

Where P is the level of activation giving a maximum growth rate at a particular irradiance, and $\alpha_v$ and $V_0$ are dimensionless parameters (Gross et al., 1991). Although this is a redox regulation process in response to the thioredoxin system, it occurs on the order of tens to minutes and to reduce computational load, is therefore calculated hourly.

### 5.3.5 Predicting NPQ under fluctuating light

Based on the results of the acclimation study of Chapter 4, (**Figure 4-5E & F**), the steady state realised amount of light dissipated, $q_{NPQ}$ is a square hyperbolic function of irradiance. Its magnitude is based on the acclimated maximum capacity for NPQ, $NPQ_{max}$ (Eq. 5-12 and 5-13). Its realised value is dependent on the activation state of LHCSR3, which is a function of absorbed irradiance at a given time and the pH of the thylakoid lumen from photosynthetic activity, which is implicit in the proportion of activated PSUs, $x_2$,

Eq. 5-15. $$q_{NPQ} = \mathrm{qNPQ}_{\max} \frac{I\, q_{abs}\, x_2}{K_{NPQ} + I}$$

Remarkably, for cells grown under fluctuating light cycles, much higher levels of NPQ occurred at low actinic irradiance than for cells grown under constant light, despite a relatively lower magnitude of NPQ from low LHCSR3 expression (**Figure 4-5E & F**). It was therefore proposed (Yarnold et al., 2016) that this induction must be due to increased lumen acidification independent of linear electron flows. From this it was concluded that higher amounts of cyclic electron flows or other alternative electron flows could be responsible for the relatively high qE under low light, as these process are known to be up-regulated from light to dark transitions (as reviewed in Chapter 1).

As an initial starting point, a fit to the data of **Figure 4-5E & F** shows the half saturation constant for $I_p$, $K_{NPQ}$ is a second order function of ε,

Eq. 5-16. $$K_{NPQ} = \varepsilon^2 I_{NPQ}$$

### 5.3.6 Predicting changes in respiration

Finally, the static maintenance term has been modified to include a factor for additional metabolic costs associated with the repair of damaged PSUs as proposed by Bernardi et al. (2014),

Eq. 5-17. $$R_s = M + k_m \delta x_3$$

Where $M$ is the basal metabolic rate, $k_m$ is a rate constant of respiration associated with repair of damaged reaction systems, $x_3$ and their rate of repair, δ.

### 5.3.7 Modified 3-state model accounting for dynamic regulation and acclimation

From the original model of Wu and Merchuk (2002), Eq. 5-1–5-5 are modified such that,

Eq. 5-18. $$\frac{dx_1}{dt} = -\, k_a I_{ETC} x_1 + \frac{P_{eq}}{P_{max}} k_d x_2 + \, k_r x_3$$

Eq. 5-19. $$\frac{dx_2}{dt} = \, k_a I_{ETC} x_1 - \, k_i {I_{ETC}}^2 x_2 - \frac{P_{eq}}{P_{max}} k_d x_2$$

Eq. 5-20. $$\frac{dx_3}{dt} = k_i {I_{ETC}}^2 x_2 - \, k_r x_3$$

Eq. 5-21. $$x_1 + x_2 + \, x_3 = 1$$

Eq. 5-22. $$\mu = k_p \frac{P_{eq}}{P_{max}} k_d x_2 - (M + k_m k_r x_3)$$

## 5.4 Parameter estimation and justification

Parameter values were estimated from the literature or fitted to available empirical data (**Table 5-1**). The parameters related to the original 3-state model ($\alpha$, $\beta$, $\gamma$, $\delta$, $k_p$, $R_s$) are based on those reported by Wu and Merchuk (2001) as a reference point and are modified where indicated **Table 5-1.**

**Table 5-1.** Parameter description and estimated values used in the model.

| Code | Value | Description | Units | Ref |
|---|---|---|---|---|
| α | $1.94 \times 10^{-3}$ | Kinetic rate constant of activation | $m^2/\mu mol.s^{-1}$ | [1] |
| $\beta$ | $2.78 \times 10^{-08}$ | Kinetic constant of inhibited reaction rate | $m/\mu mol.s^{-1}$ | Modified from [1] |
| γ | 0.175 | Kinetic rate constant of deactivation | $s^{-1}$ | Modified from [1] |
| $\delta$ | $4.80 \times 10^{-4}$ | Kinetic constant recovery rate of inhibited reaction centres | $s^{-1}$ | [1] |
| $k_p$ | $3.65 \times 10^{-4}$ | Proportionality factor between photochemical quenching and biomass growth rate | – | Modified from [1] |
| $k_M$ | $8.0 \times 10^{-3}$ | Proportionality factor for metabolic losses due to repair of damaged PSUs | – | Estimate |
| $M$ | 0.01 | Maintenance factor (dark respiration) | $h^{-1}$ | Estimate |
| **Constants related to photoacclimation and photoregulation** | | | | |
| $Chl\text{-}a_{min}$ | 16 | Maximum chlorophyll *a* concentration | $g\ kg^{-1}$ | Estimate from data |
| $Chl\text{-}a_{max}$ | 50 | Minimum chlorophyll *a* concentration | $g\ kg^{-1}$ | Estimate from data |
| $Chl\text{-}b_{max}$ | 5 | Maximum chlorophyll *b* concentration | $g\ kg^{-1}$ | Estimate from data |
| $Chl\text{-}b_{min}$ | 18 | Minimum chlorophyll *b* concentration | $g\ kg^{-1}$ | Estimate from data |
| $Car_{max}$ | 4 | Maximum carotenoid concentration | $g\ kg^{-1}$ | Estimate from data |
| $Car_{min}$ | 12 | Minimum carotenoid concentration | $g\ kg^{-1}$ | Estimate from data |
| $K_{pig}$ | 20 | Half saturation irradiance for pigments | $\mu mol.m^{-2}.s^{-1}$ | Modified from [2] |
| $k_{acc}$ | $4.9 \times 10^{-5}$ | Acclimation rate constant | $s^{-1}$ | Modified from [2] |
| $q_{NPQmax,upper}$ | 0.71 | Maximum upper capacity of NPQ | – | Empirical fit |
| $q_{NPQmax,lower}$ | 0.19 | Minimum upper capacity of NPQ | – | Empirical fit |
| $K_{NPQmax}$ | 180 | Half saturation irradiance for maximum NPQ | $\mu mol.m^{-2}.s^{-1}$ | Empirical fit |
| $K_{NPQ}$ | 148 | Half saturation irradiance for realised NPQ | $\mu mol.m^{-2}.s^{-1}$ | Empirical fit |
| $q_{NPQ,min}$ | 0.10 | Minimum realised NPQ | – | Empirical fit |
| $a_v$ | 0.04 | Michaelis rate constant for Rubisco activity | – | [3] |
| $V_0$ | 0.16 | Rubisco activity at 0 PFD | – | [3] |

[1] Wu and Merchuk (2002) [2] García-Camacho et al. (2012) [3] Gross et al. (1991)

The rate of deactivation is slightly higher than reported by Wu and Merchuk (0.146 $s^{-1}$) since it is modified by $P/P_{max}$ and thus represents an upper limit. The parameters relating to carbon assimilation efficiency are based on a study of higher plants (Gross et al. 1991), since no data for algae is available. The parameters of minimum and maximum pigment concentrations are estimated from measured pigment levels as reported in this thesis and other experiments conducted in this study. The rate of change of acclimation, $k_{acc}$, was modified from García-Camacho et al. (2012). Constants relating to NPQ are from experimental work as described below.

A preliminary experiment was performed to determine the parameters required for the maximum capacity of NPQ, $NPQ_{max}$ as a function of $I_p$. Cells in dilute culture were cultivated in triplicate under 12 different light regimes representing varying combinations of average irradiances ($I_{avg}$ = 100, 250 and 500 µmol.$m^{-2}$.$s^{-1}$) and light fractions (ε = 0.4, 0.7 or 1) to obtain a range of 'perceived' irradiance values ($I_p$ = 40–500 µmol.$m^{-2}$.$s^{-1}$). In addition, two different cycle times were tested ($c_t$ = 40s and 10s) to determine whether $c_t$ affected the capacity for LHCSR3 accumulation. After 6 h of incubation, chlorophyll fluorescence measurements were performed in triplicate on whole cells dark adapted for 20 min, as described in section 3.7.6 and 3.7.6.1, and applying a high actinic light intensity (AL = 1600 µmol.$m^{-2}$.$s^{-1}$) for a duration of 216 s to ensure maximum NPQ activity.

According to Nikolaou et al. (2014), the proportion of light dissipated by all NPQ processes, $q_{NPQ}$ can be established via the differences in the dark- and light-adapted maximum fluorescence values ($F_m$ and $F_m$' respectively), and via scaling the difference to $F_m$ in order to provide an index between 0 and 1,

Eq. 5-23 $$q_{NPQ} = \frac{F_m - F_m'}{F_m}$$

The curve obtained for empirical fluorescence values of $q_{NPQ,max}$ as a function of $I_p$ (**Figure 5-3B)** were fitted to Eq. 5-23 using a non-linear least squares fit Levenberg-Marquardt fit (MATLAB curve fitting toolbox) to establish the parameters $q_{NPQmax,upper}$, $q_{NPQmax,lower}$ *and* $K_{NPQmax}$ (**Table 5-1**).

## 5.5 Model behavior and preliminary validation

### 5.5.1 Changes in photoacclimation under an evolving batch culture

#### *5.5.1.1 Predicted changes in absorption capacity*

**Figure 5-2** compares model-predicted changes in cellular pigment levels of Chl *a*, Chl *b* and Car. The model predicts daily fluctuations in pigment contents, showing a decline at noon when irradiance is high. **Figure 5-2A & B** shows agreement with empirical data (compiled from model validation

experiments, Chapter 3) where a rapid decline from initial pigment levels from pre-dawn to noon is observed on Day 1 for cloudy and winter clear sky light treatments. Changes in pre-dawn and noon pigment levels were also found in the acclimation study (**Figure 4-2**). Overall, the model predicts a gradual increase in pigments over the cultivation period. This relates reasonably well to changes in pigments over time for the cloudy and winter treatments, although more noise was observed in measured spr/aut pigments where unusually high pigment levels were measured early in the cultivation period (**Figure 5-2C**).

Based on predicted cellular pigment concentrations, **Figure 5-3A** shows the change in two key model variables as a function of the 'perceived' irradiance of the cell: $E_a$, being the dominant factor response for light transfer through the culture, and $q_{abs}$, used to calculate the portion of light absorbed by the cell,. The model predicts a sharp decline in $E_a$ and $q_{abs}$ below $I_p$ = 100 µmol.m$^{-2}$.s$^{-1}$, suggesting most acclimation to fluctuating light regimes occurs in this region of $I_p$ before approaching a minimum.

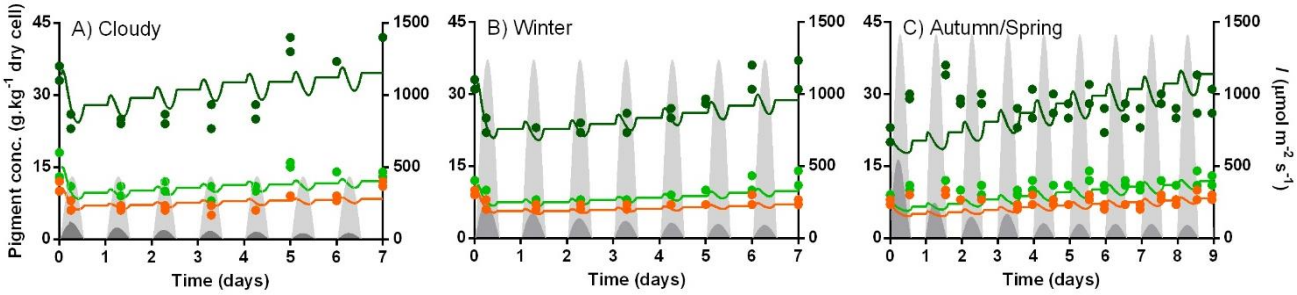


**Figure 5-2.** Predicted (lines) *versus* measured (dots) changes in cellular concentrations of Chl *a* (dark green), Chl *b* (light green) and total Car (orange) over an evolving batch culture for: A) cloudy; B) winter; and C) spr/aut light regimes (see Chapter 3 for methods). Light grey = incident irradiance, $I_0$, Dark grey = $I_{avg}$.

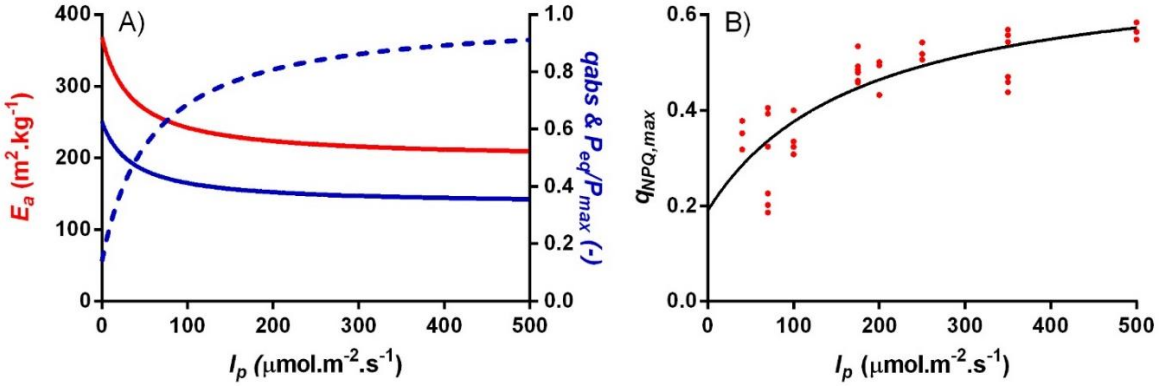


**Figure 5-3**. Predicted changes in acclimation as a function of 'perceived' irradiance, $I_p$ A) PAR-averaged mass absorption coefficient, $E_a$ (red solid line); cellular absorption efficiency, $q_{abs}$ (blue solid line); proportionality constant of maximum photosynthetic rate, $P/P_{max}$. B) Maximum NPQ capacity, $q_{NPQ,max}$ as governed by acclimated changes in LHCSR3 expression, measured (red dots) *versus* model fitted data as a function of $I_p$ (black line).

#### *5.5.1.2 Predicted changes in maximum capacity for NPQ ($NPQ_{max}$).*

**Figure 5-3B** shows reasonable agreement between model predictions and the actual maximum capacity of NPQ as a function of $I_p$, Some noise and an indication of sub-populations within the data occurred such that the correlation between the model fit and the experimental data gave an $R^2 = 0.75$. This suggests that not all factors may be accounted for by the model and will require further investigation, but in any case, it provides a reasonable basis for future refinement.

#### *5.5.1.3 Predicted changes in $P_{max}$.*

As previously discussed, the Rubisco pool remains unaffected by irradiance, however changes in ATP production due to light-dark transitions and the redox state of thioredoxins concertedly act on Rubisco activase to determine the active state of the redox pool. There is a lack of data on carboxylation activity in algae (Gontero and Salvucci, 2014). However notable studies have shown dramatic changes of $P_{max}$ or $\mu_{max}$ under varying steady state irradiance levels as well as to changes in culture density. Therefore, the parameter values of $a_v$ and $V_0$ required for $P/P_{max}$ (Eq. 5-14) were obtained from studies of higher plants as reported in Gross et al. 1991. Concordant with other acclimation changes, the model predicts a dramatic change in $P/P_{max}$ for $I_p < 100$ µmol.m$^{-2}$.s$^{-1}$, suggesting that carbon assimilation rates will be much slower in dense cultures.

### 5.5.2 Validation of PSU kinetics and change in biomass

#### *5.5.2.1 Predicted changes of PSUs as compared to fluorescence measurements*

Chlorophyll fluorescence measurements from the ePBR validation experiments (Chapter 3) were used to validate changes in the state of the PSU as predicted by the model. The ratio of the effective PSII operating efficiency in the light ($\Phi_{PSII}$) to the maximum quantum efficiency of PSII ($F_v/F_m$) in non-damaged dark-adapted samples indicates the light-adapted fraction of reaction centres able to reduce $Q_A$ (i.e. 'open' PSUs, $x_1$).

In healthy *C. reinhardtii* cells, a maximum $F_v/F_m$ value of 0.76 ± 0.01 was found during dark periods in the ePBR experiments for cloudy and winter treatments (**Figure 5-4**), in agreement with that reported in Chapter 4 ($F_v/F_m = 0.75 \pm 0.01$) and other literature studies (Bonente et al., 2012, Falk and Samuelsson, 1992). Subsequently, the $\Phi_{PSII}$ measurements taken at a culture depth of 17 cm were normalised to 0.76 (maximum $F_v/F_m$) to estimate the fraction of $x_1$, and compared with model predicted changes over time at the same depth (**Figure 5-4**).

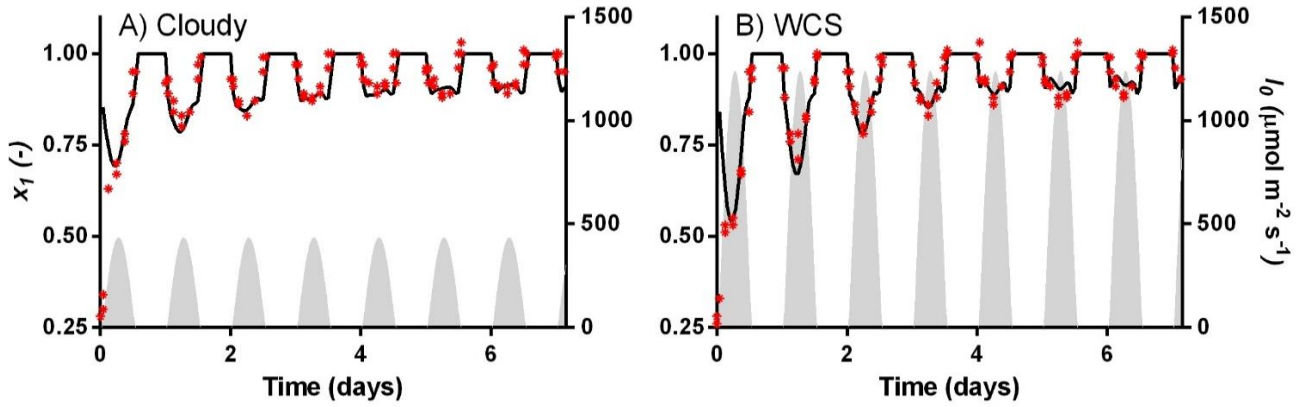


**Figure 5-4.** Changes in the fraction of open PSUs ($x_1$) during batch cultivation for A) cloudy and B) winter light regimes. Red stars = measured $\Phi_{PSII}$ normalised to $F_v/F_m$ ($n$ = 2); black lines = predicted fraction of $x_1$. Light grey shaded = incident irradiance, $I_0$.

**Figure 5-4** shows good correlation between predicted and measured changes in the fraction of open PSUs in both cloudy and winter treatments over the course of the experiment. An exception occurred in estimation of initial values upon commencement of the experiment where measured $x_1$ was extremely low, possibly due to a stress response of cells after re-dilution. From the available data, it was not possible to distinguish the fractions of $x_2$ and $x_3$.

### *5.5.2.2 Estimation of growth and biomass*

**Figure 5-5** shows predicted changes in growth and respiration (left panels) and both predicted and measured changes in the evolution of biomass under batch culture (right panels). Unlike the static growth model, results show that the dynamic model with acclimation and regulation features well represents biomass growth under all light regimes and changes in culture density. The model predicts both high growth and respiration under the relatively high light treatments (winter and spr/aut). A noticeable decline in net growth rates are observed at noon from both inactivated reaction centres and high respiration rates, causing a hysteresis effect of lower growth for the remainder of the day, as compared to morning hours. Under the relatively low light cloudy treatment, very little net reduction in growth occurs as here photoinhibition is low, however substantially lower mean growth rates over the culture depth are observed.

## 5.6 Discussion

The light-limited model presented above includes some novel features that, to my knowledge, have not been described previously, and which can help to advance predictive light-limited models for microalgal biotechnologies. Most notable is the inclusion of the influence of the locally 'perceived' rather than average or incident irradiance, by incorporating the effect of the illuminated fraction as

well as average irradiance on acclimation processes (pigment and LHCSR3 expression and maximum carbon assimilation). Additionally, the shift from a static to a dynamic 3-state model allows for a more accurate estimation of photoinhibition effects on productivity. Since this is the net result of the rate of damage *versus* the rate of repair, empirical measurements of photoinhibition will overestimate its magnitude if measured over long periods, and *vice versa* if measured over short periods.

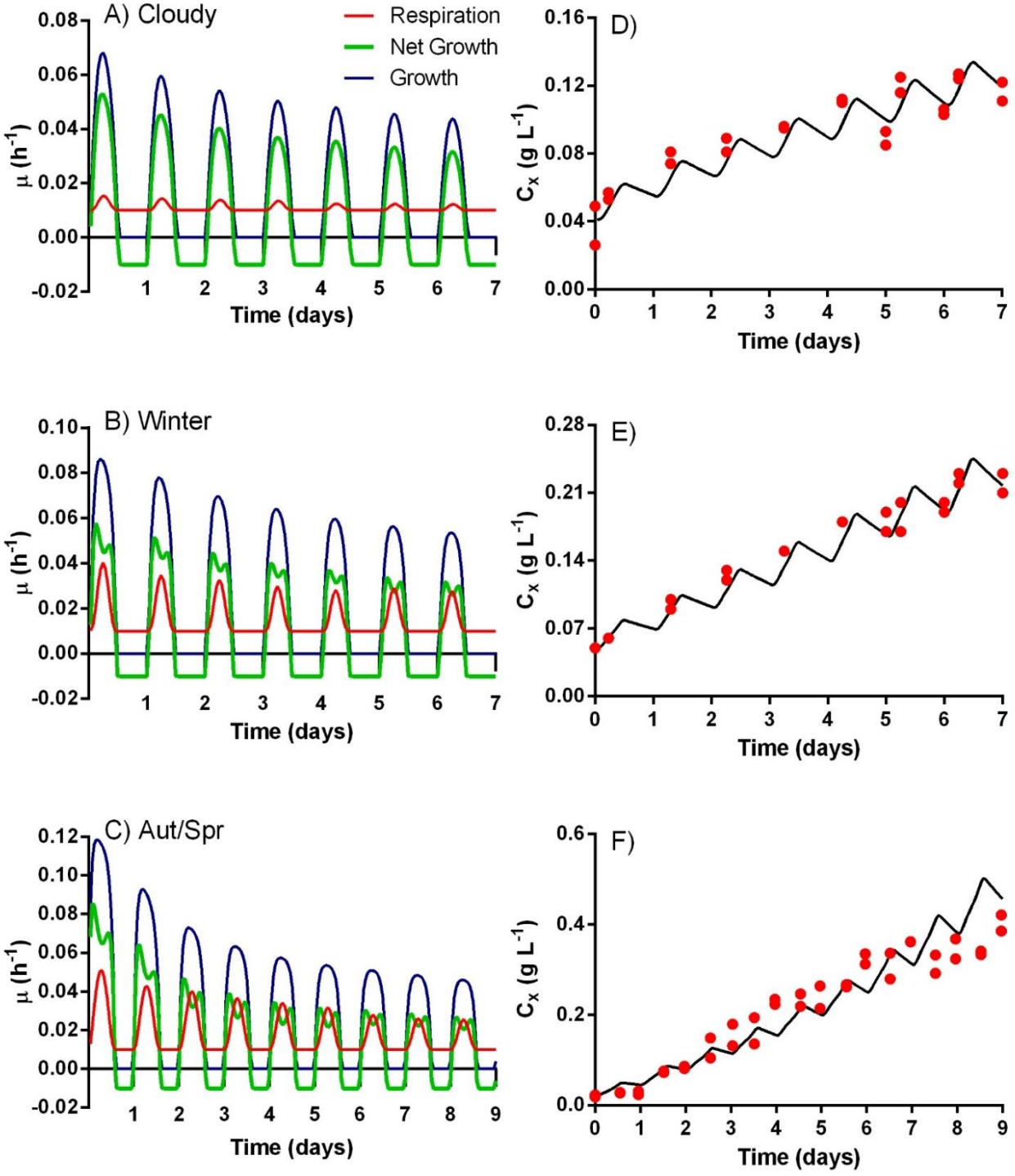


**Figure 5-5.** A–C) Changes in mean growth and respiration rates over time and with evolving biomass, and D–F) Predicted (black lines) and measured (red dots) changes in biomass ($n$ = 2).

Due to the late development of this model and the time constraints imposed on this thesis study, it is realised that the parameter values estimated from the literature and the existing data obtained during this study may not be entirely accurate, but as shown in Figure 5-6 the model is capable of providing a good fit the experimental test data. Future work is planned with experiments designed to practically and accurately identify model parameters, validate the model against a wider range of conditions and test the necessity or redundancy of its features. The latter is particularly important to simplify the model in order to provide an easy-to-implement tool for predictive assessments of productivities, which was the initial goal of this study.

## 5.7 Conclusions

To date, few studies have attempted to model the complexity of cells mixing through strong light gradients, and most are confined to very limited steady state incident light fluxes or even steady state operating conditions. The final chapter of this study attempts to describe the important phenomena that change under non-steady state conditions, i.e. where cells never reach a true steady-state. So many biological variables are in fact more complex than this model provides for; indeed, the above approach may be difficult to implement at large scale. Nevertheless, this is the system that is most typical of real-world conditions and as such, is what must be modelled. As a preliminary assessment, we demonstrated the behavior of the proposed model to fit well with data obtained in the various diel light cycles under batch cultivation. Further experimental data under a broader range of experimental conditions and for longer times will test the limits of the model.

# 6 Conclusions and future directions

This thesis study began with the aim to develop a mathematical tool that could be used to guide the design of high-efficiency algal production systems. It became apparent, however, that in order to truly increase productivities, a deeper understanding was needed of the complexity of biological responses from algae circulating through light gradients imposed by mixed mass cultures. Thus, what began as a process of deduction (model development to validation), became a process of induction (empirical data to model). Subsequently, the final result is a combination of mathematical modelling, algal physiology and photosynthesis with some novel insights.

Although the number of studies on fluctuating light conditions relevant to algal bioreactors is growing, significant knowledge gaps still exist, particularly with regard to redox imbalances associated with fluctuating light, the regulatory mechanisms to overcome these problems and their timescales, and the energetic costs that affect final photosynthetic productivities. The empirical results, model development and literature review of this thesis have provided a more comprehensive interpretation of the important elements of the light regime that influence photosynthetic responses, and the important photosynthetic responses that, in turn, influence productivity.

Following are the final conclusions drawn from this study, and future directions needed to advance modelling efforts as well as strategies to optimise biomass yields in outdoor production systems.

## 6.1 Light gradients in dense mass cultures reduce photosynthetic efficiency

Chapter 4 showed that *C. reinhardtii* cells grown under steady state light, acclimate to the level of irradiance they experience in order to balance light harvesting, ATP and NADPH production. This enables high carbon assimilation rates, except under long exposure to high irradiances that overcome NPQ processes, where rates of photodamage are faster than repair. In contrast, it is evident that the strong light gradients and seconds-to-minutes mixing cycles of outdoor mass cultures typically prevent the high level of photosynthetic efficiency realised under constant light.

These detrimental effects of light fluctuations were attributed, first, to redox imbalances that increase ROS and photoinhibition, reduce carbon assimilation efficiency, and waste more energy from alternative electron flows (and NPQ under sub-saturating light) in an effort to restore homeostasis. Second, this study highlighted the sub-optimal acclimation state of the cell in response to light regimes typical of mass culture. The selective pressures that have evolved to cope with different light fluxes in the natural environment seem unsuited to the artificial light regimes imposed in densely populated algal production systems, opening up the opportunity to develop *fit-for-purpose* cell lines

for high-performance cultivation systems. In nature, dense cultures (e.g. pond scum) are generally static, while flowing water typically has low algal culture densities. Consequently, an oxidised electron transport chain for long periods will signal true light limitation, causing an increase in photosynthetic components such as light harvesting complex proteins and pigments in order to increase photoproduction (Durnford and Falkowski, 1997). However, oxidation which occurs upon constant mixing from light to dark zones in bioreactors at seconds to minutes timescales seems to also drive algal responses toward a low-light acclimation state. The main consequences of this are higher cellular light absorption, which further hinders light distribution through the culture, and reduced photoprotection which increases susceptibility to damage during the high light periods.

To this end, what is desired for cells in dense mixed bioreactor cultures is to switch from a photosynthetic light harvesting state during low-to-moderate light periods to a protective state, to safely dissipate excess energy during high light periods. Accordingly, the high light acclimated phenotypes of low light absorption, high NPQ capacity, high throughput rates of electron transport, and greater energy directed toward storage molecules (i.e. lipids and starches) are most beneficial for maximising biomass at the cellular level. It should be emphasised that, although technically NPQ 'wastes' light energy, it does so mostly in response to feedback from an over-acidified lumen when electron transport rates exceed carbon assimilation. Consequently its role is photo-protective. Therefore, the tight regulation of NPQ ensures it is only 'turned on' as needed, and will reduce energy losses from photoinhbition and repair processes. It is, in fact, the absorption of excess light that causes light wastage. In contrast to the abovementioned benefits of high light acclimation at the cellular level, from the perspective of the entire culture, the results from this study showed that high density cultures, despite having lower cellular growth rates and causing low light acclimation of cells, may have advantages in terms of reducing photoinhibition and/or respiration-type processes.

In the light of these findings, it is therefore postulated that an ideal scenario to increase biomass productivity might occur by producing a high-light *acclimated* state in the culture, despite the cells being grown at high density. In this case, cells with low light absorption, high photoprotection, and high carbon assimilation would be cultivated in dense cultures where photoinhibition and/or respiration are reduced.

### 6.1.1 Opportunities and future directions

For consideration of process optimisation and systems design, the usual strategy to promote high light acclimation of cells and reduce the severity of redox changes is to operate cultures at low cell densities and thereby minimise 'dark zones', however this comes with additional water requirements, mixing

energy and potential increases in respiration and/or photoinhibition. A second strategy is to increase mixing frequencies so that duty cycles are <10 s, as literature studies showed this improved productivity for the same light fraction and light dose (Grobbelaar et al., 1996, Takache et al., 2015). However, increasing mixing frequencies via pumping, sparging, paddlewheels or other means requires additional energy inputs and associated costs. Therefore, the most feasible and simple design strategy recommended is to minimise the reactor pathlength. This will both reduce the optical thickness of the culture and increase the mixing frequency between light and dark zones, without additional energy requirements.

From a biological perspective, how can algal cells in dense cultures become high light acclimated? To answer this, a detailed understanding is needed of the chloroplast signalling pathways and molecular mechanisms that influence expression levels of genes involved in light harvesting complexes and other photosynthetic components. Clearly cells do not acclimate to the "average irradiance" as has been previously suggested, but the mechanisms that actually calibrate the cellular response to light are not well understood. As these mechanisms are revealed, the engineering of high-efficiency cell lines can be achieved by using a more targeted approach (e.g., through RNAi or the CRISPR/Cas9 system), to refine the LHCs in such a way that not only minimises absorption (as has been the primary focus to date) but without affecting the essential NPQ and regulatory mechanisms that protect the chloroplast. Conversely, understanding acclimation pathways could help to find solutions to 'trick' algae into a high light acclimation state in dense cultures without detrimentally tampering with their genetic makeup.

Future works built on the results of this study include: 1) the generation of combinations of specific LHC knockout mutants, by mating mutants available from the Stanford collection, to examine the effects on acclimation and fluctuating light, 2) the use of transcriptomics to map molecular pathways and genes that lead to low and high light acclimation; and 3) experimental work to investigate the effects of adding a signalling agent known to initiate down-regulation of light harvesting antenna on acclimation and productivity.

It is also recommended for studies to investigate the regulation of Rubisco activity, particularly in the context of fluctuating light and for algae, which at present, seems to be a critical gap in knowledge (Gontero and Salvucci, 2014).

### 6.2 Modelling photosynthesis under highly dynamic light conditions

Whilst sophisticated models of steady state photosynthesis have been instrumental in progressing our understanding of key processes, incorporating highly dynamic responses to changing light conditions

has remained a key challenge to advance these models for both microalgal biotechnological applications and terrestrial crops.

This thesis highlighted that good productivity models require a balance between what Flynn (2005) described as 'unwanted detail *versus* unjustified simplification.' Simple models, whilst desired for their ease of application, are perhaps only applicable to the narrow set of conditions from which the parameters are established. The model presented in Chapter 5, although not intended to incorporate a complete representation of all photosynthetic processes, aimed to combine vital processes with a simple 3-state PSU model to better describe algal growth under dynamic light conditions more typical of 'real-world' systems. For instance, a key finding was that the light history of the cell, not just the instantaneous light encountered, was critical in examining the extent of photoinhibition, since it is the net result of dynamic damage and repair processes that operate at different timescales.

### 6.2.1 Opportunities and future directions

The final dynamic model presented provides a good basis for future refinement. It is recognised that greater analyses are required to properly parameterise the model and validate it against a broader range of boundary conditions (i.e. different culture depths, two-sided FPRs and for other algal species). The necessary equipment to perform these extended studies are available at the SBRC.

Future directions of this project include an experimental study that will use the high-throughput TECAN screening system (as described in Chapter 4) to vary key elements of the light regime including: duty cycle, light fraction and maximum irradiance. Changes in growth, chlorophyll fluorescence of PSII and pigments will be monitored to obtain a more comprehensive data set of these variables that will then be used for parameter fitting and to refine the model structure if necessary. Further validation experiments will be conducted using the ePBR matrix in conjunction with the Ralph group at UTS, and may include cultivation of algal species more appropriate for biotechnology applications, as well as longer incubation periods, variations of pathlength, and a proper analysis of fluid dynamics.

To enhance its value as a tool for process optimisation in outdoor production systems, productivity models should ideally incorporate variables other than light. A key limitation of this study was its failure to account for temperature effects, which has a coupled relationship with light and influences photosynthesis and respiration rates (Béchet et al., 2015). Furthermore, temperature varies dramatically during the day (Wolf J., 2016), and the heating/cooling requirements to keep temperature constant will impede both economic and energy returns. In addition to temperature, nutrient consumption is another important factor for predictive modelling to ensure nutrient concentrations

that are neither limiting or greatly in excess. Future investigations are planned to integrate the effects of temperature and nutrient consumption to the final light-limited model. To date, an elementary nutrient model has been developed based on the well-established Droop model (Droop, 1974, Droop, 1975). In addition, a model predicting changes in temperature of the liquid culture has been developed as described by Béchet et al. (2010). Planned experiments will be undertaken to assess the changes in key model parameters in response to temperature variations, in a similar manner to that proposed by Béchet et al. (2015).

Finally, model simulations revealed that a broad range of productivities could be attained under different design and operational scenarios. Predictions showed that optimally spaced arrays of FPRs could achieve 10–11 fold and 2–3 fold increases in volumetric and areal productivities than open ponds, respectively. Of course, maximising biomass yields is only one element to enhancing the economic viability, net energy returns and sustainability (i.e. greenhouse gas emissions) which are the true measures of assessing the potential of this technology. Therefore, productivity models must form part of a larger tool set that includes techno-economic and life-cycle analyses in order to truly guide the 'best' design and operation of systems and of large-scale facilities. These modelling efforts are vital to reduce the cost and time associated with expensive pilot or demonstration scale trials. Future works are therefore planned to integrate the final productivity model with techno-economic and life cycle models into one program, the *Algal Process Simulator* (APS), which is currently under development within this research group.

## 6.3 Conclusion

According to Wagner et al. (2016), global population and economic growth is forecast to require 50% more fuel, 70% more food and 50% more fresh water by 2050 to sustain the needs of humans. In parallel, $CO_2$ emissions reductions of 50% are required by 2020 to keep global mean temperature increases to within 1.5$^{o}$C, as aspired by the international agreement of The United Nations Conference on Climate Change (Paris 2015). Although challenging, photosynthetic algal fuel systems could theoretically supply today's global energy demand at PCEs already achieved (~2%) using ~2% of the Earth's surface (cf. non-arable land is ~25%) and saline or wastewater, thereby reducing pressure on food production and freshwater (Ringsmuth, 2016). Critical breakthroughs are still required, however, to increase the financial viability, net energy returns and GHG emissions of this technology. This study has elucidated possibilities to improve light-to-biomass conversion efficiencies in outdoor production systems without additional expenses and energy inputs, and developed a novel model representing algal dynamics under real world systems that will aid future TCA and LCA studies.

# 7 References


Acién Fernández, F. G., García Camacho, F., & Chisti, Y. (1999). Photobioreactors: light regime, mass transfer, and scaleup. *Progress in Industrial Microbiology, 35*, 231-247.

Adir, N., Shochat, S., & Ohad, I. (1990). Light-dependent D1 protein synthesis and translocation is regulated by reaction center II. Reaction center II serves as an acceptor for the D1 precursor. *Journal of Biological Chemistry, 265*(21), 12563-12568.

Adir, N., Zer, H., Shochat, S., & Ohad, I. (2003). Photoinhibition–a historical perspective. *Photosynthesis research, 76* (1-3), 343-370.

Aiba, S. (1982). Growth kinetics of photosynthetic microorganisms. *Advances in Biochemical Engineering 23*, 85–156.

Allorent, G., Tokutsu, R., Roach, T., Peers, G., Cardol, P., Girard-Bascou, J., . . . Finazzi, G. (2013). A dual strategy to cope with high light in *Chlamydomonas reinhardtii*. *Plant Cell, 25*(2), 545-557.

Alric, J., Lavergne, J., & Rappaport, F. (2010). Redox and ATP control of photosynthetic cyclic electron flow in *Chlamydomonas reinhardtii* (I) aerobic conditions.. *Biochimica et Biophysica Acta, 1797*(1), 44-51.

Apel, K., & Hirt, H. (2004). Reactive oxygen species: metabolism, oxidative stress, and signal transduction. *Annual Review Plant Biology, 55*, 373-399.

Asada, K. (1999). The water-water cycle in chloroplasts: Scavenging of Active Oxygens and Dissipation of Excess Photons. *Annual Review of Plant Physiology and Plant Molecular Biology, 50*(1), 601-639.

Austin, J. R., & Staehelin, L. A. (2011). Three-dimensional architecture of grana and stroma thylakoids of higher plants as determined by electron tomography. *Plant physiology, 155*(4), 1601-1611.

Baker, N. R. (2008). Chlorophyll fluorescence: a probe of photosynthesis in vivo. *Anuual Review of Plant Biology, 59*, 89-113.

Ballottari, M., Dall'Osto, L., Morosinotto, T., & Bassi, R. (2007). Contrasting behavior of higher plant photosystem I and II antenna systems during acclimation. *Journal of Biological Chemistry, 282*(12), 8947-8958.

Barbosa, M. (2003). Optimisation of cultivation parameters in photobioreactors for microalgae cultivation using the A-stat technique. *Biomolecular Engineering, 20*(4-6), 115-123.

Barbosa, M. (2014). *Algaeparc: scale-up challenges in microalgae mass production.* Paper presented at the 5th Congress of the International Society for Applied Phycology, Sydney.

Barbosa, M.J., Janssen, M., Ham, N., Tramper, J., & Wijffels, R.H. (2003). Microalgae cultivation in air-lift reactors: modeling biomass yield and growth rate as a function of mixing frequency. *Biotechnology and Bioengineering, 82*(2), 170-179.

Baroli, I., Do, A. D., Yamane, T., & Niyogi, K. K. (2003). Zeaxanthin Accumulation in the Absence of a Functional Xanthophyll Cycle Protects *Chlamydomonas reinhardtii* from Photooxidative Stress. *The Plant Cell, 15*(4), 992-1008.

Béchet, Q., Shilton, A., Fringer, O. B., Munoz, R., & Guieysse, B. (2010). Mechanistic Modeling of Broth Temperature in Outdoor Photobioreactors. *Environmental Science & Technology, 44*(6), 2197-2203.

Béchet, Q., Shilton, A., & Guieysse, B. (2013). Modeling the effects of light and temperature on algae growth: State of the art and critical assessment for productivity prediction during outdoor cultivation. *Biotechnologyogy Advances, 31*(8), 1648-1663.

Béchet, Q., Chambonnière, P., Shilton, A., Guizard, G., & Guieysse, B. (2015). Algal productivity modeling: A step toward accurate assessments of full-scale algal cultivation. *Biotechnologyogy and bioengineering, 112*(5), 987-996.

Beckmann, J., Lehr, F., Finazzi, G., Hankamer, B., Posten, C., Wobbe, L., & Kruse, O. (2009). Improvement of light to biomass conversion by de-regulation of light-harvesting protein translation in *Chlamydomonas reinhardtii*. *Journal of Biotechnology, 142*(1), 70-77.

Beer, S., & Björk, M. (2000). Measuring rates of photosynthesis of two tropical seagrasses by pulse amplitude modulated (PAM) fluorometry. *Aquatic Botany, 66*(1), 69-76.

Berberoglu, H., Pilon, L., & Melis, A. (2008). Radiation characteristics of *Chlamydomonas reinhardtii* CC125 and its truncated chlorophyll antenna transformants tla1, tlaX and tla1-CW+. *International Journal of Hydrogen Energy, 33*(22), 6467-6483.

Berberoglu, H., Yin, J., & Pilon, L. (2007). Light transfer in bubble sparged photobioreactors for H2 production and CO2 mitigation. *International Journal of Hydrogen Energy, 32*(13), 2273-2285.

Bernardi, A., Perin, G., Sforza, E., Galvanin, F., Morosinotto, T., & Bezzo, F. (2014). An identifiable state model to describe light intensity influence on microalgae growth. *Industrial & engineering chemistry research, 53*(16), 6738-6749.

Bernasconi, A. (2014). Global Ingredient Market for EPA and DHA Up 10 Percent in Value. *Omega 3 Supply Side Insights*.

Bidigare, R. R., Ondrusek, M. E., Morrow, J. H., & Kiefer, D. A. (1990). *In-vivo absorption properties of algal pigments.* Paper presented at the Orlando'90, 16-20 April.

Bohren, C. F., & Huffman, D. R. (2008). *Absorption and scattering of light by small particles*. John Wiley & Sons.

Bonente, G., Ballottari, M., Truong, T. B., Morosinotto, T., Ahn, T. K., Fleming, G. R., . . . Bassi, R. (2011). Analysis of LhcSR3, a protein essential for feedback de-excitation in the green alga *Chlamydomonas reinhardtii*. *PLoS Biology, 9*(1), e1000577.

Bonente, G., Pippa, S., Castellano, S., Bassi, R., & Ballottari, M. (2012). Acclimation of *Chlamydomonas reinhardtii* to different growth irradiances. *The Journal of Biological Chemistry, 287*, 5833-5847.

Borisova-Mubarakshina, M. M., Ivanov, B. N., Vetoshkina, D. V., Lubimov, V. Y., Fedorchuk, T. P., Naydov, I. A., . . . Cazzaniga, S. (2015). Long-term acclimatory response to excess excitation energy: evidence for a role of hydrogen peroxide in the regulation of photosystem II antenna size. *Journal of experimental botany*, erv410.

Borkenstein, C. G., Knoblechner, J., Fruhwirth, H., & Schagerl, M. (2011). Cultivation of Chlorella emersonii with flue gas derived from a cement plant. *Journal of Applied Phycology, 23*(1), 131-135.

Borowitzka, M. (1997). Microalgae for aquaculture: Opportunities and constraints. *Journal of Applied Phycology, 9*(5), 393-401.

Borowitzka, M.A. (1999). Commercial production of microalgae: ponds, tanks, tubes and fermenters. *Journal of Biotechnologyogy, 70*(1-3), 313-321.

Breyton, C., Nandha, B., Johnson, G. N., Joliot, P., & Finazzi, G. (2006). Redox modulation of cyclic electron flow around photosystem I in C3 plants. *Biochemistry, 45*(45), 13465-13475.

Buchanan, B. B., & Balmer, Y. (2005). Redox regulation: a broadening horizon. *Annual Review Plant Biology, 56*, 187-220.

Canadell, J. G., Le Quéré, C., Raupach, M. R., Field, C. B., Buitenhuis, E. T., Ciais, P., . . . Marland, G. (2007). Contributions to accelerating atmospheric CO2 growth from economic activity, carbon intensity, and efficiency of natural sinks. *Proceedings of the National Academy of Sciences, 104*(47), 18866-18870.

Cardol, P., Alric, J., Girard-Bascou, J., Franck, F., Wollman, F.-A., & Finazzi, G. (2009). Impaired respiration discloses the physiological significance of state transitions in *Chlamydomonas*. *Proceedings of the National Academy of Sciences, 106*(37), 15979-15984.

Cardol, P., Forti, G., & Finazzi, G. (2011). Regulation of electron transport in microalgae. *Biochimica et Biophysica Acta (BBA) - Bioenergetics, 1807*(8), 912-918.

Cardozo, K. H., Guaratini, T., Barros, M. P., Falcao, V. R., Tonon, A. P., Lopes, N. P., . . . Pinto, E. (2007). Metabolites from algae with economical impact. *Comparitive Biochemistry and Physiolology Part C Toxicology and Pharmacology, 146*(1-2), 60-78.

Carvalho, A.P., Meireles, L.A., & Malcata, F.X. (2006). Microalgal Reactors: A Review of Enclosed System Designs and Performances. *Biotechnology Progress, 22*(6), 1490-1506.

Carvalho, A.P., Pontes, I., Gaspar, H., & Malcata, F.X. (2006). Metabolic relationships between macro- and micronutrients, and the eicosapentaenoic acid and docosahexaenoic acid contents of *Pavlova lutheri*. *Enzyme and Microbial Technology, 38*(3-4), 358-366.

Chandrasekhar, S. (1960). Radiative heat transfer. *Dover Publications, New York, 11*, 11-12.

Chow, Y., & Thung, L. (2015). Quantifying the competitive advantage of light green algal strains in batch culture. *Journal of Applied Phycology*, *27*(5), 1805-1812.

Clowez, S., Godaux, D., Cardol, P., Wollman, F.A., & Rappaport, F. (2015). The Involvement of Hydrogen-producing and ATP-dependent NADPH-consuming Pathways in Setting the Redox Poise in the Chloroplast of *Chlamydomonas reinhardtii* in Anoxia. *Journal of Biological Chemistry, 290*(13), 8666-8676.

Collares-Pereira, M., & Rabl, A. (1979). The average distribution of solar radiation-correlations between diffuse and hemispherical and between daily and hourly insolation values. *Solar energy, 22*(2), 155-164.

Cornet, J. F., Dussap, C. G., & Dubertret, G. (1992). A structured model for simulation of cultures of the cyanobacterium Spirulina platensis in photobioreactors: I. Coupling between light transfer and growth kinetics. *Biotechnology Bioeng, 40*(7), 817-825.

Craggs, R. J. (2005). Advanced integrated wastewater ponds. *In: Shilton A (ed) Pond treatment technology. IWA scientific and technical report series.* (pp. 282-310). London: IWA.

Dall'Osto, L., Cazzaniga, S., Havaux, M., & Bassi, R. (2010). Enhanced photoprotection by protein-bound *vs* free xanthophyll pools: a comparative analysis of chlorophyll *b* and xanthophyll biosynthesis mutants. *Molecular Plant, 3*, 576-593.

Dang, K.V., Plet, J., Tolleter, D., Jokel, M., Cuine, S., Carrier, P., . . . Peltier, G. (2014). Combined increases in mitochondrial cooperation and oxygen photoreduction compensate for deficiency in cyclic electron flow in *Chlamydomonas reinhardtii*. *Plant Cell, 26*(7), 3036-3050.

Dangoor, I., Peled-Zehavi, H., Wittenberg, G., & Danon, A. (2012). A chloroplast light-regulated oxidative sensor for moderate light intensity in Arabidopsis. *The Plant Cell, 24*(5), 1894-1906.

de Mooij, T., Janssen, M., Cerezo-Chinarro, O., Mussgnug, J., Kruse, O., Ballottari, M., . . . Wijffels, R. (2014). Antenna size reduction as a strategy to increase biomass productivity: a great potential not yet realized. *Journal of Applied Phycology*, 1-15.

de Oliveira Dal'Molin, C. G., Quek, L.-E., Palfreyman, R. W., & Nielsen, L. K. (2011). AlgaGEM–a genome-scale metabolic reconstruction of algae based on the *Chlamydomonas reinhardtii* genome. *BMC genomics, 12*(4), S5.

Dekker, J. P., & Boekema, E. J. (2005). Supramolecular organization of thylakoid membrane proteins in green plants. *Biochimica et Biophysica Acta, 1706*(1-2), 12-39.

Denman, K. L., & Marra, J. (1986). Modelling the time dependent photoadaptation of phytoplankton to fluctuating light. *Elsevier oceanography series, 42*, 341-359.

Depège, N., Bellafiore, S., & Rochaix, J.D. (2003). Role of chloroplast protein kinase Stt7 in LHCII phosphorylation and state transition in *Chlamydomonas*. *Science, 299*(5612), 1572-1575.

Dillschneider, R., & Posten, C. (2013). Closed Bioreactors as Tools for Microalgae Production Advanced Biofuels and Bioproducts. In J. W. Lee (Ed.), (pp. 629-649): Springer New York.

Draaisma, R. B., Wijffels, R. H., Ellen Slegers, P., Brentner, L. B., Roy, A., & Barbosa, M. J. (2012). Food commodities from microalgae. *Current Opinion in Biotechnology*.

Droop, M. (1974). The nutrient status of algal cells in continuous culture. *Journal of the Marine Biological Association of the United Kingdom, 54*(04), 825-855.

Droop, M. (1975). The nutrient status of algal cells in batch culture. *Journal of the Marine Biological Association of the United Kingdom, 55*(03), 541-555.

Drop, B., Webber-Birungi, M., Fusetti, F., Kouřil, R., Redding, K. E., Boekema, E. J., & Croce, R. (2011). Photosystem I of *Chlamydomonas reinhardtii* contains nine light-harvesting complexes (Lhca) located on one side of the core. *Journal of Biological Chemistry, 286*(52), 44878-44887.

Dubinsky, Z., & Stambler, N. (2009). Photoacclimation Processes in Phytoplankton: Mechanisms, Consequences, and Applications *Aquatic Microbial Ecology, 56*(2-3), 163-176.

Duffie, J. A., & Beckman, W. A. (1980). *Solar Engineering of Thermal Processes*. John Wiley & Sons, New York.

Durnford, D., & Falkowski, P. (1997). Chloroplast redox regulation of nuclear gene transcription during photoacclimation. *Photosynthesis Research, 53*(2-3), 229-241.

Ebenhöh, O., Houwaart, T., Lokstein, H., Schlede, S., & Tirok, K. (2011). A minimal mathematical model of nonphotochemical quenching of chlorophyll fluorescence. *Biosystems, 103*(2), 196-204.

Eilers, P.H.C., & Peeters, J.C.H. (1988). A model for the relationship between light intensity and the rate of photosynthesis in phytoplankton. *Ecological Modelling, 42*(3–4), 199-215.

Elrad, D., Niyogi, K. K., & Grossman, A. R. (2002). A major light-harvesting polypeptide of photosystem II functions in thermal dissipation. *The Plant Cell, 14*(8), 1801-1816.

Endo, T., & Asada, K. (2008). Photosystem I and photoprotection: cyclic electron flow and water-water cycle. *Photoprotection, Photoinhibition, Gene Regulation, and Environment* (pp. 205-221): Springer.

Engel, B.D., Schaffer, M., Cuellar, L.K., Villa, E., Plitzko, J.M., & Baumeister, W. (2015). Native architecture of the *Chlamydomonas* chloroplast revealed by in situ cryo-electron tomography. *ELife, 4*, e04889.

Escoubas, J.M., Lomas, M., LaRoche, J., & Falkowski, P.G. (1995). Light intensity regulation of cab gene transcription is signaled by the redox state of the plastoquinone pool. *Proceedings of the National Academy of Sciences, 92*(22), 10237-10241.

Falk, S., & Samuelsson, G. (1992). Recovery of photosynthesis and phtosystem II fluorescence in *Chlamydomonas reinhardtii* after exposure to three levels of high light. *Physiologia Plantarum, 85*(1), 61-68.

Falkowski, P., & Wirick, C. (1981). A simulation model of the effects of vertical mixing on primary productivity. *Marine Biology, 65*(1), 69-75.

Falkowski, P. G., & LaRoche, J. (1991). Acclimation to spectral irradiance in algae. *Journal of Phycology, 27*(1), 8-14.

Farquhar, G., & Von Caemmerer, S. (1982). Modelling of photosynthetic response to environmental conditions. *Physiological plant ecology II* (pp. 549-587): Springer.

Fell, D., Poolman, M., & Gevorgyan, A. (2010). Building and analysing genome-scale metabolic models. *Biochemical Society Transactions, 38*(5), 1197.

Ferrante, P., Ballottari, M., Bonente, G., Giuliano, G., & Bassi, R. (2012). LHCBM1 and LHCBM2/7 polypeptides, components of major LHCII complex, have distinct functional roles in photosynthetic antenna system of *Chlamydomonas reinhardtii*. *Journal of Biological Chemistry, 287*(20), 16276-16288.

Fietz, S., & Nicklisch, A. (2002). Acclimation of the diatom Stephanodiscus neoastraea and the cyanobacterium *Planktothrix agardhii* to simulated natural light fluctuations. *Photosynthesis Research, 72*(1), 95-106.

Finazzi, G., & Minagawa, J. (2014). High Light Acclimation in Green Microalgae. *Non-Photochemical Quenching and Energy Dissipation in Plants, Algae and Cyanobacteria* (pp. 445-469). Springer.

Flameling, I. A., & Kromkamp, J. (1997). Photoacclimation of *Scenedesmus protuberans* (Chlorophyceae) to fluctuating irradiances simulating vertical mixing. *Journal of plankton research, 19*(8), 1011-1024.

Fleischmann, M. M., Ravanel, S., Delosme, R., Olive, J., Zito, F., Wollman, F.-A., & Rochaix, J.-D. (1999). Isolation and Characterization of Photoautotrophic Mutants of *Chlamydomonas reinhardtii* Deficient in State Transition. *Journal of Biological Chemistry, 274*(43), 30987-30994.

Flynn, K. J. (2005). Castles built on sand: dysfunctionality in plankton models and the inadequacy of dialogue between biologists and modellers. *Journal of Plankton Research, 27*(12), 1205-1210.

Food and Agriculture Organization of the Unitied Nations (FaAOotUN). (2009). How to Feed the World in 2050.

Formighieri, C., Franck, F., & Bassi, R. (2012). Regulation of the pigment optical density of an algal cell: filling the gap between photosynthetic productivity in the laboratory and in mass culture. *Journal of Biotechnology, 162*, 115-123.

Fouchard, S., Hemschemeier, A., Caruana, A., Pruvost, J., Legrand, J., Happe, T., . . . Cournac, L. (2005). Autotrophic and mixotrophic hydrogen photoproduction in sulfur-deprived *Chlamydomonas* cells. *Applied and environmental microbiology, 71*(10), 6199-6205.

Franck, F., & Houyoux, P.A. (2008). The Mehler reaction in *Chlamydomonas* during photosynthetic induction and steady-state photosynthesis in wild-type and in a mitochondrial mutant. *Photosynthesis. Energy from the Sun* (pp. 581-584). Springer.

García-Camacho, F., Sánchez-Mirón, A., Molina-Grima, E., Camacho-Rubio, F., & Merchuck, J. C. (2012). A mechanistic model of photosynthesis in microalgae including photoacclimation dynamics. *Journal of Theoretical Biology, 304*(0), 1-15.

Geider, R.J., MacIntyre, H.L., & Kana, T.M. (1996). A Dynamic Model of Photoadaptation in Phytoplankton. *Limnology and Oceanography, 41*(1), 1-15.

Givan, A. L., & Levine, R. (1967). The photosynthetic electron transport chain of *Chlamydomonas reinhardtii*. VII. Photosynthetic phosphorylation by a mutant strain of *Chlamydomonas reinhardtii* deficient in active P700. *Plant physiology, 42*(9), 1264-1268.

Gontero, B., & Salvucci, M. E. (2014). Regulation of photosynthetic carbon metabolism in aquatic and terrestrial organisms by Rubisco activase, redox-modulation and CP12. *Aquatic Botany, 118*, 14-23.

Gordon, J., & Polle, J. W. (2007). Ultrahigh bioproductivity from algae. *Applied Microbiology and Biotechnologyogy, 76*(5), 969-975.

Grobbelaar, J. (1994). Turbulence in mass algal cultures and the role of light/dark fluctuations. *Journal of Applied Phycology, 6*(3), 331-335.

Grobbelaar, J., Nedbal, L., & Tichý, V. (1996). Influence of high frequency light/dark fluctuations on photosynthetic characteristics of microalgae photoacclimated to different light intensities and implications for mass algal cultivation. *Journal of Applied Phycology, 8*(4-5), 335-343.

Grobbelaar, J.U. (2010). Microalgal biomass production: challenges and realities. [Review]. *Photosynthesis Research, 106*(1-2), 135-144.

Grobbelaar, J.U., Nedbal, L., Tichy, L., & Setlik, I. (1995). Variation in Some Photosynthetic Characteristics of Microalgae Cultured in Outdoor Thin-Layered Sloping Reactors. *Journal of Applied Phycology, 7*(2), 175-184.

Gross, L., Kirschbaum, M., & Pearcy, R. (1991). A dynamic model of photosynthesis in varying light taking account of stomatal conductance, C3-cycle intermediates, photorespiration and Rubisco activation. *Plant, Cell & Environment, 14*(9), 881-893.

Grossman, A.R., Lohr, M., & Im, C.S. (2004). *Chlamydomonas reinhardtii* in the landscape of pigments. *Annual Review of Genetics, 38*, 119-173.

Han, B.P. (2002). A Mechanistic Model of Algal Photoinhibition Induced by Photodamage to Photosystem-II. *Journal of Theoretical Biology, 214*(4), 519-527.

Harris, E. H. (2001). *Chlamydomonas* as a model organism. *Annual review of plant biology, 52*(1), 363-406.

Havaux, M., & Davaud, A. (1994). Photoinhibition of photosynthesis in chilled potato leaves is not correlated with a loss of Photosystem-II activity : Preferential inactivation of Photosystem I. *Photosynthesis Research, 40*(1), 75-92.

Havaux, M., & García-Plazaola, J. I. (2014). Beyond Non-Photochemical Fluorescence Quenching: The Overlapping Antioxidant Functions of Zeaxanthin and Tocopherols *Non-Photochemical Quenching and Energy Dissipation in Plants, Algae and Cyanobacteria* (pp. 583-603): Springer.

Havelková-Doušová, H., Prášil, O., & Behrenfeld, M. (2004). Photoacclimation of *Dunaliella tertiolecta* (Chlorophyceae) under fluctuating irradiance. *Photosynthetica, 42*(2), 273-281.

Hemaiswarya, S., Raja, R., Ravi Kumar, R., Ganesan, V., & Anbazhagan, C. (2011). Microalgae: a sustainable feed source for aquaculture. *World Journal of Microbiology and Biotechnologyogy, 27*(8), 1737-1746.

Hoefnagel, M. H., Atkin, O. K., & Wiskich, J. T. (1998). Interdependence between chloroplasts and mitochondria in the light and the dark. *Biochimica et Biophysica Acta (BBA)-Bioenergetics, 1366*(3), 235-255.

Hudek, K., Davis, L. C., Ibbini, J., & Erickson, L. (2014). Commercial Products from Algae. In R. Bajpai, A. Prokop & M. Zappi (Eds.), *Algal Biorefineries* (pp. 275-295): Springer Netherlands.

Huesemann, M., Hausmann, T., Bartha, R., Aksoy, M., Weissman, J., & Benemann, J. (2009). Biomass productivities in wild type and pigment mutant of *Cyclotella* sp. (Diatom). *Applied Biochemistry and Biotechnology, 157*, 507-526.

Hunn, B., & Calafell, D. (1977). Determination of average ground reflectivity for solar collectors. *Solar Energy, 19*(1), 87-89.

Ibelings, B.K., B.M.A.; Mur, L.R. (1994). Acclimation of photosystem II in a cyanobacterium and a eukaryotic green alga to high and fluctuating photosynthetic photon flux densities, simulating light regimes induced by mixing in lakes. *New Phytologist, 128*(3), 407-424.

Iigusa, H., Yoshida, Y., & Hasunuma, K. (2005). Oxygen and hydrogen peroxide enhance light-induced carotenoid synthesis in *Neurospora crassa*. *FEBS letters, 579*(18), 4012-4016.

Intergovernmental Panel on Climate Change (IPCC). (2014). The Fifth Assessment Report.

International Energy Agency (IEA). (2010). IEA World Energy Outlook 2010.

International Energy Agency (IEA), (2015). Key Renewables Trends. Excerpt from: Renewables Information.

Jacobshagen, S., & Johnson, C. H. (1994). Circadian rhythms of gene expression in *Chlamydomonas reinhardtii*: circadian cycling of mRNA abundances of cab II, and possibly of beta-tubulin and cytochrome c. *EurJournalCell Biology, 64*(1), 142-152.

Jahns, P., Latowski, D., & Strzalka, K. (2009). Mechanism and regulation of the violaxanthin cycle: the role of antenna proteins and membrane lipids. *Biochimica et Biophysica Acta (BBA)-Bioenergetics, 1787*(1), 3-14.

Jakob, T., Wagner, H., Stehfest, K., & Wilhelm, C. (2007). A complete energy balance from photons to new biomass reveals a light-and nutrient-dependent variability in the metabolic costs of carbon assimilation. *Journal of experimental botany, 58*(8), 2101-2112.

Jakob, G., Wolf, J., Bui, T. V., Posten, C., Kruse, O., Stephens, E., . . . Hankamer, B. (2013). Surveying a diverse pool of microalgae as a bioresource for future biotechnological applications. *Journal of Phylogenetics and Evolutionary Biology, 4*(153).

Janssen, M., Janssen, M., de Winter, M., Tramper, J., Mur, L.R., Snel, J., & Wijffels, R.H. (2000). Efficiency of light utilization of *Chlamydomonas reinhardtii* under medium-duration light/dark cycles. *Journal of Biotechnologyogy, 78*(2), 123-137.

Janssen, M., Kuijpers, T.C., Veldhoen, B., Ternbach, M.B., Tramper, J., Mur, L.R., & Wijffels, R. H. (1999). Specific growth rate of *Chlamydomonas reinhardtii* and Chlorella sorokiniana under medium duration light/dark cycles: 13–87 s. *Journal of Biotechnologyogy, 70*(1–3), 323-333.

Janssen, M., Slenders, P., Tramper, J., Mur, L.R., & Wijffels, R. (2001). Photosynthetic efficiency of Dunaliella tertiolecta under short light/dark cycles. *Enzyme and Microbial Technology, 29*(4–5), 298-305.

Johnson, X., Steinbeck, J., Dent, R. M., Takahashi, H., Richaud, P., Ozawa, S., . . . Alric, J. (2014). PGR5-mediated cyclic electron flow under ATP-or redox-limited conditions: a study of ΔATPase pgr5 and ΔrbcL pgr5 mutants in *Chlamydomonas reinhardtii*. *Plant Physiology*, *165*(1), 438-452.

Jokel, M., Kosourov, S., Battchikova, N., Tsygankov, A.A., Aro, E.M., & Allahverdiyeva, Y. (2015). *Chlamydomonas* flavodiiron proteins facilitate acclimation to anoxia during sulfur deprivation. *Plant and Cell Physiology, 56*(8), 1598-1607.

Kelley, C. P., Mohtadi, S., Cane, M. A., Seager, R., & Kushnir, Y. (2015). Climate change in the Fertile Crescent and implications of the recent Syrian drought. *Proceedings of the National Academy of Sciences, 112*(11), 3241-3246.

Kliphuis, A.M.J., Martens, D.E., Janssen, M., & Wijffels, R. H. (2011). Effect of $O_2$:$CO_2$ Ratio on the Primary Metabolism of *Chlamydomonas reinhardtii*. *Biotechnology amd Bioengineering, 108*(10), 2390-2402.

Kok, B. (1956). Photosynthesis in flashing light. *Biochimica et Biophysica Acta, 21*, 245–258.

Kok, B. (1956). On the inhibition of photosynthesis by intense light. *Biochimica et Biophysica Acta, 21*(2), 234-244.

Kono, M., Noguchi, K., & Terashima, I. (2014). Roles of the cyclic electron flow around PSI (CEF-PSI) and $O_2$-dependent alternative pathways in regulation of the photosynthetic electron flow in short-term fluctuating light in *Arabidopsis thaliana*. *Plant and Cell Physiology, 55*(5), 990-1004.

Külheim, C., Ågren, J., & Jansson, S. (2002). Rapid regulation of light harvesting and plant fitness in the field. *Science, 297*(5578), 91-93.

Kumar, A., Kumar, S., & Kumar, S. (2005). Biodegradation kinetics of phenol and catechol using Pseudomonas putida MTCC 1194. *Biochemical Engineering Journal, 22*(2), 151-159.

Lardon, L., Helias, A., Sialve, B., Steyer, J.P., & Bernard, O. (2009). Life-cycle assessment of biodiesel production from microalgae. *Environmental science & technology, 43*(17), 6475-6481.

Lavorel, J., & Levine, R. (1968). Fluorescence properties of wild-type *Chlamydomonas reinhardtii* and three mutant strains having impaired photosynthesis. *Plant physiology, 43*(7), 1049-1055.

Lee, E., Pruvost, J., He, X., Munipalli, R., & Pilon, L. (2013). Design Tool and Guidelines for Outdoor Photobioreactors. *Chemical Engineering Science, 106*, 18-29.

Lemaire, C., Wollman, F.-A., & Bennoun, P. (1988). Restoration of phototrophic growth in a mutant of *Chlamydomonas reinhardtii* in which the chloroplast atpB gene of the ATP synthase has a deletion: an example of mitochondria-dependent photosynthesis. *Proceedings of the National Academy of Sciences, 85*(5), 1344-1348.

Liguori, N., Roy, L. M., Opacic, M., Durand, G. g., & Croce, R. (2013). Regulation of light harvesting in the green alga *Chlamydomonas reinhardtii*: the C-terminus of LHCSR is the knob of a dimmer switch. *Journal of the American Chemical Society, 135*(49), 18339-18342.

Lim, H.-C., Kim, H., Jang, K., Kim, J.-Y., Baek, J.-H., Yang, S.-J., . . . Park, J.-R. (2015). Design and fabrication of light-guiding plate for a photobioreactor that utilizes sunlight. *Optical Review, 22*(5), 779-785.

Litchman, E. (2000). Growth rates of phytoplankton under fluctuating light. *Freshwater Biology, 44*(2), 223-235.

Lucker, B.F., Hall, C.C., Zegarac, R., & Kramer, D.M. (2014). The environmental photobioreactor (ePBR): An algal culturing platform for simulating dynamic natural environments. *Algal Research, 6*, 242-249.

Macedo, I. C., Seabra, J. E. A., & Silva, J. E. A. R. (2008). Green house gases emissions in the production and use of ethanol from sugarcane in Brazil: The 2005/2006 averages and a prediction for 2020. *Biomass and Bioenergy, 32*(7), 582-595.

März, U. (2011). The Global Market for Carotenoids.

Mätzler, C. (2002). MATLAB Functions for Mie Scattering and Absorption. Research Report No. 2002-08 June 2002 Institut für Angewandte Physik Mikrowellenabteilung.

Matuszyńska, A., & Ebenhoeh, O. (2015). A reductionist approach to model photosynthetic self-regulation in eukaryotes in response to light. *Biochemical Society Transactions, 43*(6), 1133-1139.

McMichael, P. (2009). A food regime analysis of the 'world food crisis'. *Agriculture and Human Values, 26*(4), 281-295.

Meinshausen, M., Meinshausen, N., Hare, W., Raper, S.C.B., Frieler, K., Knutti, R., . . . Allen, M. R. (2009). Greenhouse-gas emission targets for limiting global warming to 2$^{o}$C. *Nature, 458*(7242), 1158-1162.

Melis, A. (1999). *Dunaliella salina* (Chlorophyta) with small chlorophyll antenna sizes exhibit higher photosynthetic productivities and photon use efficiences than normally pigmented cells. *Journal of Applied Phycology. 10*(6) 515-525.

Melis, A. (2009). Solar energy conversion efficiencies in photosynthesis: Minimizing the chlorophyll antennae to maximize efficiency. *Plant Science, 177*(4), 272-280.

Meyer, C. H., & Sekundo, W. (2005). Nutritional supplementation to prevent cataract formation. *Developments in Ophthalmology, 38*, 103-119.

Michelet, L., Zaffagnini, M., Morisse, S., Sparla, F., Pérez-Pérez, M. E., Francia, F., . . . Lemaire, S. D. (2013). Redox regulation of the Calvin-Benson cycle: something old, something new. [Review]. *Frontiers in Plant Science, 4*.

Mitra, M., Kirst, H., Dewez, D., & Melis, A. (2012). Modulation of the light-harvesting chlorophyll antenna size in *Chlamydomonas reinhardtii* by TLA1 gene over-expression and RNA interference. *Philo Trans Royal Soc B-Biol Sci, 367*, 3430-3443.

Mitra, M., & Melis, A. (2008). Optical properties of microalgae for enhanced biofuels production. *Opt. Express, 16*(26), 21807-21820.

Molina Grima, E., Fernández, F. G. A., García Camacho, F., & Chisti, Y. (1999). Photobioreactors: light regime, mass transfer, and scaleup. *Journal of Biotechnology, 70*(1–3), 231-247.

Morel, A., & Bricaud, A. (1981). Theoretical results concerning light absorption in a discrete medium, and application to specific absorption of phytoplankton. *Deep Sea Research Part A. Oceanographic Research Papers, 28*(11), 1375-1393.

Morel, A., & Smith, R. C. (1974). *Relation between total quanta and total energy for aquatic photosynthesis*: American Society of Limnology and Oceanography.

Morosinotto, T., & Bassi, R. (2014). Molecular mechanisms for activation of non-photochemical fluorescence quenching: from unicellular algae to mosses and higher plants *Non-Photochemical Quenching and Energy Dissipation in Plants, Algae and Cyanobacteria* (pp. 315-331): Springer.

Muller-Feuga, A. (2000). The role of microalgae in aquaculture: situation and trends. *Journal of Applied Phycology, 12*(3-5), 527-534.

Munekage, Y., Hojo, M., Meurer, J., Endo, T., Tasaka, M., & Shikanai, T. (2002). PGR5 is involved in cyclic electron flow around photosystem I and is essential for photoprotection in Arabidopsis. *Cell, 110*(3), 361-371.

Murphy, T.E., & Berberoğlu, H. (2011). Effect of algae pigmentation on photobioreactor productivity and scale-up: A light transfer perspective. *Journal of Quantitative Spectroscopy and Radiative Transfer, 112*(18), 2826-2834.

Mussgnug, J.H., Thomas-Hall, S., Rupprecht, J., Foo, A., Klassen, V., McDowall, A., . . . Hankamer, B. (2007). Engineering photosynthetic light capture: impacts on improved solar energy to biomass conversion. *Plant Biotechnologyogy Journal, 5*(6), 802-814.

Neale, P., & Marra, J. (1985). Short-term variation of Pmax under natural irradiance conditions – A model and its implications. *Marine Ecology Progress Series, 26*(1-2), 113-124.

Neale, P.J., & Melis, A. (1990). Activation of a reserve pool of photosystem II in *Chlamydomonas reinhardtii* counteracts photoinhibition. *Plant physiology, 92*(4), 1196-1204.

Newswire, P. (2015). from http://www.prnewswire.com/news-releases/global-astaxanthin-market---sources-technologies-and-applications-300066562.html.

Nikolaou, A., Bernardi, A., Bezzo, F., Morosinotto, T., & Chachuat, B. (2014). *A Dynamic Model of Photoproduction, Photoregulation and Photoinhibition in Microalgae using Chlorophyll Fluorescence.* Paper presented at the World Congress.

Nikolaou, A., Bernardi, A., Meneghesso, A., Bezzo, F., Morosinotto, T., & Chachuat, B. (2015). A model of chlorophyll fluorescence in microalgae integrating photoproduction, photoinhibition and photoregulation. *Journal of biotechnology, 194*, 91-99.

Niyogi, K. K., Bjorkman, O., & Grossman, A. R. (1997). *Chlamydomonas* xanthophyll cycle mutants identified by video imaging of chlorophyll fluorescence quenching. *The Plant Cell, 9*(8), 1369-1380.

Oey, M., Ross, I. L., Stephens, E., Steinbeck, J., Wolf, J., Radzun, K. A., . . . Hankamer, B. (2013). RNAi Knock-Down of LHCBM1, 2 and 3 Increases Photosynthetic $H_2$ Production Efficiency of the Green Alga *Chlamydomonas reinhardtii. PLoS ONE, 8*(4), e61375.

Office of the White House Secretary. (2014). FACT SHEET: U.S.-China Joint Announcement on Climate Change and Clean Energy Cooperation Retrieved 10 October 2015, 2015, from https://www.whitehouse.gov

Oja, V., & Laisk, A. (2000). Oxygen yield from single turnover flashes in leaves: non-photochemical excitation quenching and the number of active PSII. *Biochimica et Biophysica Acta (BBA) - Bioenergetics, 1460*(2–3), 291-301.

Oligae.com. Retrieved November, 2015, http://www.oilgae.com/non_fuel_products/chlorella.html

Ono, E., & Cuello, J. L. (2006). Feasibility Assessment of Microalgal Carbon Dioxide Sequestration Technology with Photobioreactor and Solar Collector. *Biosystems Engineering, 95*(4), 597-606.

Organisation for Economic Co-operation and Development (OECD). (2014). Environmental Outlook to 2050.

Park, J.B.K., Craggs, R.J., & Shilton, A.N. (2011). Wastewater treatment high rate algal ponds for biofuel production. *Bioresource Technology, 102*(1), 35-42.

Peltier, G., Tolleter, D., Billon, E., & Cournac, L. (2010). Auxiliary electron transport pathways in chloroplasts of microalgae. *Photosynthesis Research, 106*(1-2), 19-31.

Peers, G., Truong, T. B., Ostendorf, E., Busch, A., Elrad, D., Grossman, A. R., . . . Niyogi, K. K. (2009). An ancient light-harvesting protein is critical for the regulation of algal photosynthesis. *Nature, 462*(7272), 518-521.

Perez, R., Seals, R., Ineichen, P., Stewart, R., & Menicucci, D. (1987). A new simplified version of the perez diffuse irradiance model for tilted surfaces. *Solar Energy, 39*(3), 221-231.

Perrine, Z., Negi, S., & Sayre, R. T. (2012). Optimization of photosynthetic light energy utilization by microalgae. *Algal Research, 1*(2), 134-142.

Platt, T., Gallegos, C. L., & Harrison, W. G. (1980). *Photoinhibition of photosynthesis in natural assemblages of marine phytoplankton*.

Piccolo, A. (2012). Spirulina: A Livehood And A Business Venture.

Pilon, L., Berberoglu, H., & Kandilian, R. (2011). Radiation transfer in photobiological carbon dioxide fixation and fuel production by microalgae. *Journal of Quantitative Spectroscopy & Radiative Transfer, 112*(17), 2639-2660.

Polle, J., Kanakagiri, S., & Melis, A. (2003). *tla1*, a DNA insertional transformant of the green alga *Chlamydomonas reinhardtii* with a truncated light-harvesting chlorophyll antenna size. *Planta, 217*, 49-59.

Pongratz, J., Lobell, D. B., Cao, L., & Caldeira, K. (2012). Crop yields in a geoengineered climate. *Nature Climate Change, 2*(2), 101-105.

Pottier, L., Pruvost, J., Deremetz, J., Cornet, J. F., Legrand, J., & Dussap, C. G. (2005). A fully predictive model for one-dimensional light attenuation by *Chlamydomonas reinhardtii* in a torus photobioreactor. *Biotechnology Bioeng, 91*(5), 569-582.

Pruvost, J., Cornet, J. F., Goetz, V., & Legrand, J. (2011). Modeling Dynamic Functioning of Rectangular Photobioreactors in Solar Conditions. *Aiche Journal, 57*(7), 1947-1960.

Quaas, T., Berteotti, S., Ballottari, M., Flieger, K., Bassi, R., Wilhelm, C., & Goss, R. (2015). Non-photochemical quenching and xanthophyll cycle activities in six green algal species suggest mechanistic differences in the process of excess energy dissipation. *Journal of Plant Physiology, 172*, 92-103.

Rasala, B., & Mayfield, S. (2015). Photosynthetic biomanufacturing in green algae; production of recombinant proteins for industrial, nutritional, and medical uses. *Photosynthesis Research, 123*(3), 227-239.

Radzun, K. A., Wolf, J., Jakob, G., Zhang, E., Stephens, E., Ross, I., & Hankamer, B. (2015). Automated nutrient screening system enables high-throughput optimisation of microalgae production conditions. *Biotechnology Biofuels, 8*, 65.

Ralph, P. J., & Gademann, R. (2005). Rapid light curves: A powerful tool to assess photosynthetic activity. *Aquatic Botany, 82*(3), 222-237.

Retallack, G. J. (2002). Carbon dioxide and climate over the past 300 Myr. *Philosophical Transactions of the Royal Society of London A: Mathematical, Physical and Engineering Sciences, 360*(1793), 659-673.

Ringsmuth, A. K., Landsberg, M.J. and Hankamer, B. (2016). Can photosynthesis enable a global transition from fossil fuels to solar fuels, to mitigate climate change and fuel-supply limitations? *PLos One (In press)*.

Rochaix, J.D. (2002). *Chlamydomonas*, a model system for studying the assembly and dynamics of photosynthetic complexes. *FEBS letters, 529*(1), 34-38.

Rochaix, J.D. (2011). Reprint of: Regulation of photosynthetic electron transport. *Biochimica et Biophysica Acta (BBA)-Bioenergetics, 1807*(8), 878-886.

Rubio, F.C., Camacho, F.G., Sevilla, J.M.F., Chisti, Y., & Grima, E.M. (2003). A mechanistic model of photosynthesis in microalgae. *Biotechnology and Bioengineering, 81*(4), 459-473.

Sarvikas, P., Tyystjärvi, T., & Tyystjärvi, E. (2010). Kinetics of prolonged photoinhibition revisited: photoinhibited Photosystem II centres do not protect the active ones against loss of oxygen evolution. *Photosynthesis Research, 103*(1), 7-17.

Schenk, P. M., Thomas-Hall, S. R., Stephens, E., Marx, U. C., Mussgnug, J. H., Posten, C., . . . Hankamer, B. (2008). Second Generation Biofuels: High-Efficiency Microalgae for Biodiesel Production. *Bioenergy Research, 1*(1), 20-43.

Schmer, M. R., Vogel, K. P., Mitchell, R. B., & Perrin, R. K. (2008). Net energy of cellulosic ethanol from switchgrass. *Proceedings of the National Academy of Sciences, 105*(2), 464-469.

Schreiber, U. (2004). *Pulse-Amplitude-Modulation (PAM) Fluorometry and Saturation Pulse Method: An Overview*. The Netherlands.

Schürmann, P., & Buchanan, B. B. (2008). The ferredoxin/thioredoxin system of oxygenic photosynthesis. *Antioxidants & redox signaling, 10*(7), 1235-1274.

Sforza, E., Simionato, D., Giacometti, G. M., Bertucco, A., & Morosinotto, T. (2012). Adjusted Light and Dark Cycles Can Optimize Photosynthetic Efficiency in Algae Growing in Photobioreactors. *Plos One, 7*(6), e38975.

Shapira, M., Lers, A., Heifetz, P. B., Irihimovitz, V., Osmond, C. B., Gillham, N. W., & Boynton, J. E. (1997). Differential regulation of chloroplast gene expression in *Chlamydomonas reinhardtii* during photoacclimation: light stress transiently suppresses synthesis of the Rubisco LSU protein while enhancing synthesis of the PS II D1 protein. *Plant Molecular Biology, 33*(6), 1001-1011.

Shen, W., Wei, Y., Dauk, M., Tan, Y., Taylor, D. C., Selvaraj, G., & Zou, J. (2006). Involvement of a glycerol-3-phosphate dehydrogenase in modulating the NADH/NAD+ ratio provides evidence of a mitochondrial glycerol-3-phosphate shuttle in Arabidopsis. *The Plant Cell, 18*(2), 422-441.

Slegers, P.M., van Beveren, P.J.M., Wijffels, R.H., van Straten, G., & van Boxtel, A.J.B. (2013). Scenario analysis of large scale algae production in tubular photobioreactors. *Applied Energy, 105*(0), 395-406.

Slegers, P.M., Wijffels, R.H., van Straten, G., & van Boxtel, A.J.B. (2011). Design scenarios for flat panel photobioreactors. *Applied Energy, 88*(10), 3342-3353.

Smil, V. (2008). *Energy in Nature and Society: General Energetics of Complex Systems.* . Cambridge, MA,: The MIT Press.

Sonoike, K., & Terashima, I. (1994). Mechanism of photosystem-I photoinhibition in leaves of Cucumis sativus L. *Planta, 194*(2), 287-293.

Sowers, J., Vengosh, A., & Weinthal, E. (2011). Climate change, water resources, and the politics of adaptation in the Middle East and North Africa. *Climatic Change, 104*(3-4), 599-627.

Stephens, E., Ross, I.L., & Hankamer, B. (2013). Expanding the microalgal industry – continuing controversy or compelling case? *Current Opinion in Chemical Biology, 17*(3) 444-452.

Stephens, E., Ross, I.L., King, Z., Mussgnug, J. H., Kruse, O., Posten, C., . . . Hankamer, B. (2010). An economic and technical evaluation of microalgal biofuels. *Nature Biotechnology, 28*(2), 126-128.

Strand, D.D., Fisher, N., Davis, G.A., & Kramer, D.M. (2016). Redox regulation of the antimycin A sensitive pathway of cyclic electron flow around photosystem I in higher plant thylakoids. *Biochimica et Biophysica Acta (BBA)-Bioenergetics, 1857*(1), 1-6.

Strickland, J.D., & Parsons, T.R. (1972). A practical handbook of seawater analysis. Pigment analysis. Bulletin of Fisheries Research Board of Canada 167. Ottawa: Queen's Printer.

Sukenik, A., Bennett, J., & Falkowski, P. (1987). Light-saturated photosynthesis — Limitation by electron transport or carbon fixation? *Biochimica et Biophysica Acta (BBA) - Bioenergetics, 891*(3), 205-215.

Takache, H., Pruvost, J., & Marec, H. (2015). Investigation of light/dark cycles effects on the photosynthetic growth of *Chlamydomonas reinhardtii* in conditions representative of photobioreactor cultivation. *Algal Research, 8*(0), 192-204.

Takahashi, H., Clowez, S., Wollman, F.A., Vallon, O., & Rappaport, F. (2013). Cyclic electron flow is redox-controlled but independent of state transition. *Nature communications, 4*.

Tamburic, B., Guruprasad, S., Radford, D. T., Szabó, M., Lilley, R. M., Larkum, A. W. D., . . . Ralph, P. J. (2014). The Effect of Diel Temperature and Light Cycles on the Growth of *Nannochloropsis oculata* in a Photobioreactor Matrix. *PLoS ONE, 9*(1), e86047.

Terashima, M., Petroutsos, D., Hüdig, M., Tolstygina, I., Trompelt, K., Gäbelein, P., . . . Finazzi, G. (2012). Calcium-dependent regulation of cyclic photosynthetic electron transfer by a CAS, ANR1, and PGRL1 complex. *Proceedings of the National Academy of Sciences, 109*(43), 17717-17722.

Tikkanen, M., Grieco, M., Kangasjärvi, S., & Aro, E.-M. (2010). Thylakoid protein phosphorylation in higher plant chloroplasts optimizes electron transfer under fluctuating light. *Plant Physiology, 152*(2), 723-735.

Tikkanen, M., Grieco, M., Nurmi, M., Rantala, M., Suorsa, M., & Aro, E. M. (2012). Regulation of the photosynthetic apparatus under fluctuating growth light. *Philos Trans R Soc Lond B Biol Sci, 367*(1608), 3486-3493.

Tokutsu, R., Kato, N., Bui, K. H., Ishikawa, T., & Minagawa, J. (2012). Revisiting the supramolecular organization of photosystem II in *Chlamydomonas reinhardtii*. *Journal of Biological Chemistry, 287*(37), 31574-31581.

Tomaselli, L., Boldrini, G., & Margheri, M. (1997). Physiological behaviour of Arthrospira (Spirulina) maxima during acclimation to changes in irradiance. *Journal of applied phycology, 9*(1), 37-43.

Treves, H., Raanan, H., Finkel, O. M., Berkowicz, S. M., Keren, N., Shotland, Y., & Kaplan, A. (2013). A newly isolated *Chlorella* sp. from desert sand crusts exhibits a unique resistance to excess light intensity. *FEMS Microbiol Ecol, 86*(3), 373-380.

Ullah, K., Ahmad, M., Sofia, Sharma, V. K., Lu, P., Harvey, A., . . . Anyanwu, C. N. (2014). Algal biomass as a global source of transport fuels: Overview and development perspectives. *Progress in Natural Science: Materials International, 24*(4), 329-339.

United Nations (2013). World Population Prospects: The 2012 Revision.

United Nations Framework Convention on Climate Change (UNFCOCC). (2015). New Draft Paris Agreement of 12 December, "Adoption of the Paris Agreement" (FCCC/CP/2015/L.9 ed.).

United Nations High Commissioner for Regugees (UNHCR). (2015). Retrieved 10 October 2015, 2015, from http://www.unhcr.org

Ünlü, C., Drop, B., Croce, R., & van Amerongen, H. (2014). State transitions in *Chlamydomonas reinhardtii* strongly modulate the functional size of photosystem II but not of photosystem I. *Proceedings of the National Academy of Sciences, 111*(9), 3460-3465.

Vasconcelos Fernandes, T., Shrestha, R., Sui, Y., Papini, G., Zeeman, G., Vet, L.E.M., . . . Lamers, P. (2015). Closing Domestic Nutrient Cycles Using Microalgae. *Environmental Science & Technology*.

Versyck, K.J., Claes, J.E., & Van Impe, J.F. (1997). Practical identification of unstructured growth kinetics by application of optimal experimental design. *Biotechnology progress, 13*(5), 524-531.

Vincent, W.F., Bertrand, N., & Frenette, J.J. (1994). Photoadaptation to intermittent light across the St. Lawrence Estuary freshwater-saltwater transition zone. *Marine Ecology-Progress Series, 110*, 283-283.

Viskanta, R., & Menguc, M. (1989). Radiative transfer in dispersed media. *Applied Mechanics Reviews, 42*(9), 241-259.

Wagner, H., Jakob, T., & Wilhelm, C. (2006). Balancing the energy flow from captured light to biomass under fluctuating light conditions. *New Phytologist, 169*(1), 95-108.

Wagner, L., Ross, I., Foster, J., & Hankamer, B. (2016). Trading off global fuel supply, $CO_2$ emissions and sustainable development. *Plos One*, *In press*.

Weissman, J.C., & Goebel, R. (1987). Design and analysis of microalgal open pond systems for the purpose of producing fuels: a subcontract report: Solar Energy Research Inst., Golden, CO (USA).

Wigmosta, M.S., Coleman, A.M., Skaggs, R.J., Huesemann, M.H., & Lane, L.J. (2011). National microalgae biofuel production potential and resource demand. *Water Resources Research, 47*(3).

Wilhelm, C., & Selmar, D. (2011). Energy dissipation is an essential mechanism to sustain the viability of plants: The physiological limits of improved photosynthesis. *Journal of Plant Physiology, 168*(2), 79-87.

Wijffels, R.H., & Barbosa, M.J. (2010). An Outlook on Microalgal Biofuels. *Science, 329*(5993), 796-799.

Wolf, J., Ross, I.L., Radzun, K.A., Jakob, G., Stephens, E., & Hankamer, B. (2015). High-throughput screen for high performance microalgae strain selection and integrated media design. *Algal Research, 11*, 313-325.

Wolf J., Stephens, E., Steinbusch, S., Yarnold, J., Ross, I.L., Steinweg, C., Doebbe, A., Krolovitsch, C., Müller, S., Brillault, L., Jakob, G., Kruse, O., Posten, C., & Hankamer, B. (2016). Multifactorial comparison of photobioreactor geometries in parallel microalgae cultivations. *Algal Research, In press*.

Wu, X., & Merchuk, J.C. (2001). A model integrating fluid dynamics in photosynthesis and photoinhibition processes. *Chemical Engineering Science, 56*(11), 3527-3538.

Wu, X.X., & Merchuk, J.C. (2002). Simulation of algae growth in a bench-scale bubble column reactor. *Biotechnologyogy and Bioengineering, 80*(2), 156-168.

Xue, X., Gauthier, D. A., Turpin, D. H., & Weger, H. G. (1996). Interactions between Photosynthesis and Respiration in the Green Alga *Chlamydomonas reinhardtii* (Characterization of Light-Enhanced Dark Respiration). *Plant Physiology, 112*(3), 1005-1014.

Yarnold, J., Ross, I.L., & Hankamer, B. (2016). Photoacclimation and productivity of *Chlamydomonas reinhardtii* grown in fluctuating light regimes which simulate outdoor algal culture conditions. *Algal Research, 13*, 182-194.

Zhang, N., & Portis, A. R., Jr. (1999). Mechanism of light regulation of Rubisco: a specific role for the larger Rubisco activase isoform involving reductive activation by thioredoxin-f. *Proceedings of the National Academy of Sciences, 96*(16), 9438-9443.

Zonneveld, C. (1998). Light-limited microalgal growth: a comparison of modelling approaches. *Ecological Modelling, 113*(1-3), 41-54.

Zonneveld, C. (1998). Photoinhibition as Affected by Photoacclimation in Phytoplankton: a Model Approach. *Journal of Theoretical Biology, 193*(1), 115-123.

Zonneveld, C., vandenBerg, H.A., & Kooijman, S. (1997). Modeling carbon cell quota in light-limited phytoplankton. *Journal of Theoretical Biology, 188*(2), 215-226.

# 8 Appendices

## 8.1 Validation of incident light calculations

Model predicted incident half-hourly irradiance was validated from a series of outdoor light experiments. Briefly, the experiment consisted of taking light measurements on:

1) a horizontal surface (indicative of light received at the surface of an open pond);
2) two sides of a tilted surface, with the large illuminated panel face oriented in a north-south or east-west direction (indicative of unshaded individual FPRs); and
3) on two sides of panels placed in parallel to another panel (indicative of FPR arrays subject to shadow effects and reflection from adjacent panels at three spacing distance to panel reactor height ratios of 1/6 (spacing = 150 mm); 1/3 (spacing = 300mm) and 2/3 (spacing = 600 mm).

### 8.1.1 Methods

Measurements were taken using a cosine corrected sensor (Walz, Germany) every 30 minutes from 8am to 4pm representing the peak solar hours of a given day. The setup consisted of 900m high x 1,000m wide panels made of 9 mm thick blue board (painted black to simulate full absorption by algal culture) and with 3mm Perspex outer sheets to simulate reflective PBR surface material. Global (direct and diffuse) photosynthetic photon flux density, $I$ (PPFD, μmol.m$^{-2}$.s$^{-1}$) was measured in direct sunlight. Diffuse PPFD, $I_d$ was measured in the shade and direct PPFD, $I_b$ was deduced ($I_b = I - I_d$). One light measurement was taken on the horizontal surface in direct sunlight, one on a horizontal plane in the shade (to measure diffuse sunlight), three measurements were taken on the vertical outer panels (sun facing and shaded sides at 0mm, 450mm and 900mm; and seven points on either side of the parallel placed panels (at 150mm intervals). The height of the shadow between parallel panels was also measured at each time point. Black sheeting was used to avoid ground reflection. Ground reflected PFD, $I_r$ was calculated as the difference in measurements taken on a tilted surface on the SBRC's pilot plant pad (white concrete) and that taken on a surface covered with black sheeting.

### 8.1.2 Results

Measurements of half hourly irradiance on a horizontal surface, $I$, and unshaded tilted surface were in good agreement with model predictions. For arrayed panels, shading and specular reflection from adjacent panels effectively creates three illumination zones along the vertical axis: 1) an illuminated zone, $f_{illum}$, receiving global irradiance on one side and diffuse on the reverse side; 2) a reflected zone $f_{refl}$, where specular reflected irradiance coming from the front side of one reactor is received onto the

reverse side of the adjacent reactor, as well as diffuse radiation on both sides; and 3) a shaded zone, $f_{shade}$, where only diffuse radiation is received on both sides. The height of each zone varies with the time of day due to the angle of the sun, as well as the spacing distance between reactors. Model-predicted irradiance for each of the three zones is compared at both NS and EW orientations at panel spacing : reactor height ratios of 1/6, 1/3 and 2/3 (**Figure 8-1**). Some discrepancies between experimental and predicted data were found for the amount of specular reflected radiation for the measurements of EW, at a spacing to height ratio of 1/3 (**Figure 8-1C**) and NS, at a spacing : height ratio of 2/3 (**Figure 8-1F**), but overall these were small in the context of total radiation received by the system and may be artefacts of the system setup (i.e. slight warping of the Perspex sheets). Overall, the model satisfactorily predicted incident irradiance under clear sky conditions.

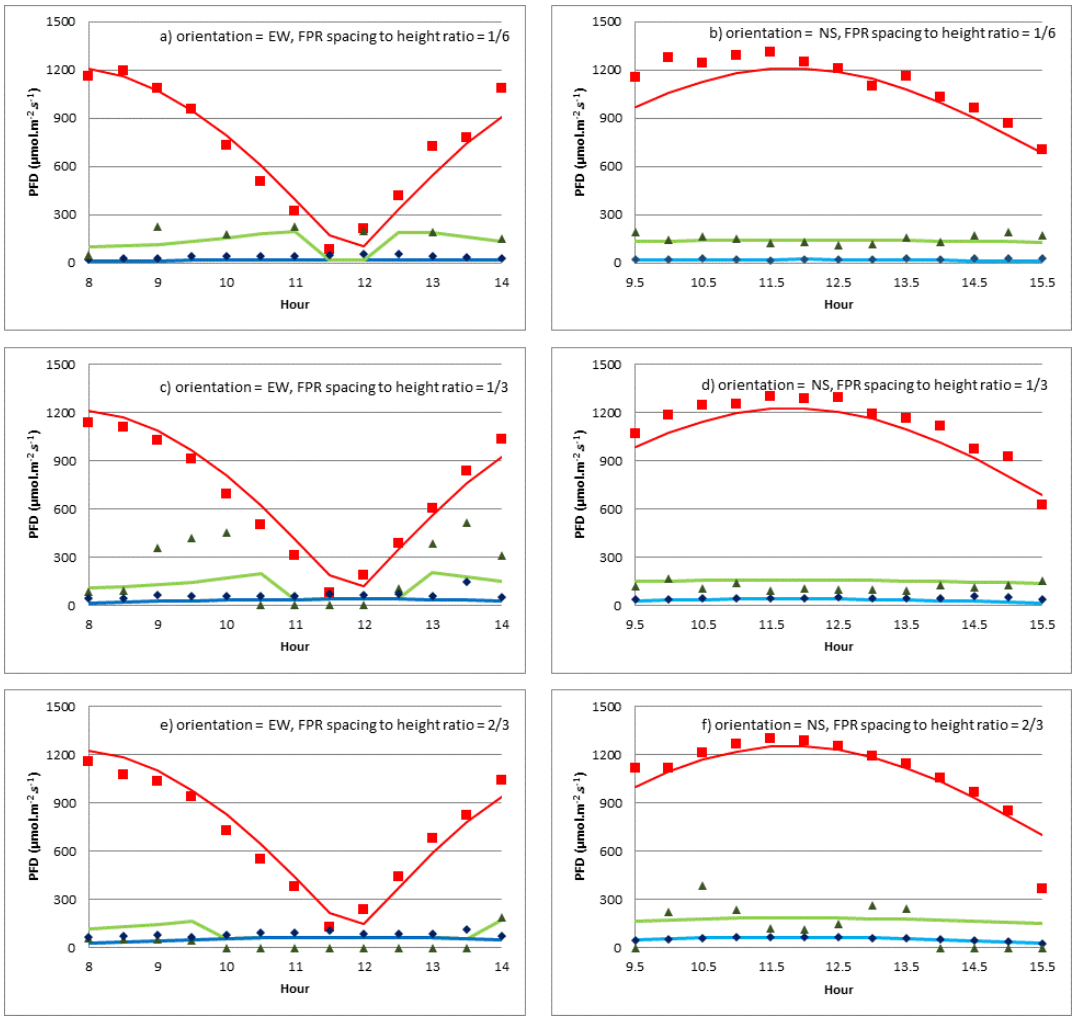


**Figure 8-1**. Incident irradiance, $I_0$ measurements taken 21-22 August 2013 on a 900 mm panel and model predictions along the vertical axis of parallel stacked flat panels at three spacing to panel height ratios of A,B 1/6: C, D 1/3; and E, F 2/3. Left and right panels show east-west and north-south orientations respectively. Red squares = measured $I_0$ in the illuminated (unshaded) portion of the reactor; purple triangles = $I_0$ in the shaded portion of the reactor and receiving specular reflection from adjacent panel; blue diamonds = $I_0$ in the shaded portion of the reactor. Red, green and blue lines are modelled predictions for each region respectively.

## 8.2 Spectral composition of light emitting diodes and sunlight

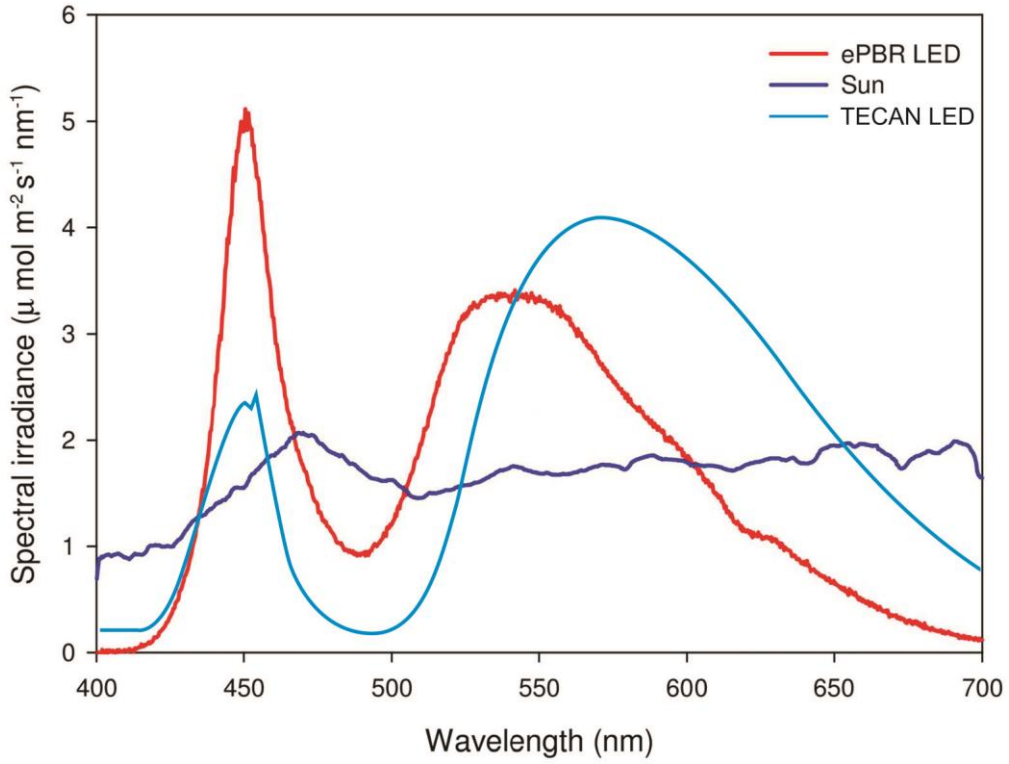


**Figure 8-2**. Approximation of the spectral irradiance over the PAR spectrum (400-700nm) showing the difference between sunlight (dark blue line), the cool white LEDs of the ePBR matrix (red line) and the warm white LEDs of the TECAN system. ePBR and Sun spectrum reproduced from Tamburic et al. (2014). TECAN spectrum reproduced from World of Thought Pty Ltd, Australia (www.worldofthought.com.au).

## 8.3 Immunoblot analysis of LHCSR3 and RbcL

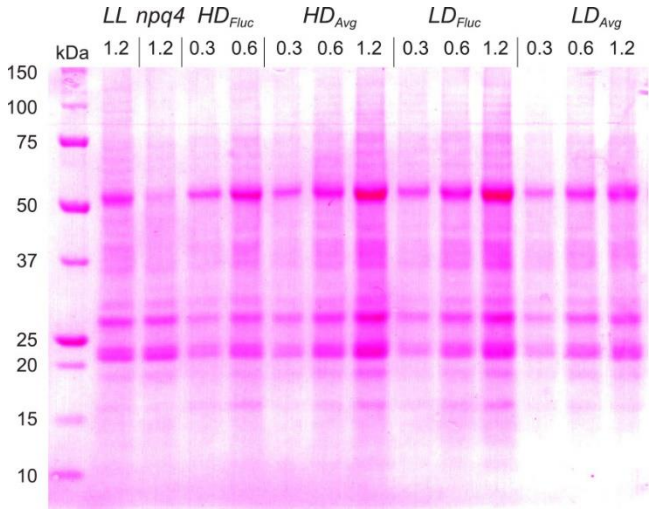


**Figure 8-3**. Ponceau Red S. stained membrane of immunoblot analysis of LHCSR3 and RbcL normalised to total chlorophyll content. Chlorophyll reported above lanes in micrograms. L1: ladder; L2: Wt *C. reinhardtii* (CC125) grown on TAP under low-light (neg control); L3: LHCSR3-less mutant *npq4* (negative control); Cell samples were harvested at ~1pm.

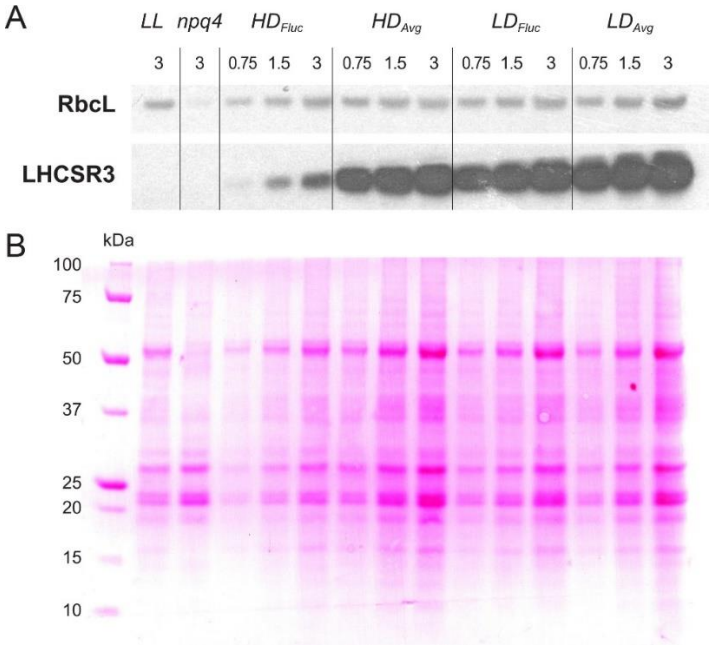


**Figure 8-4.** A) Western blot analysis of LHCSR3 and the large subunit of Rubisco (RbcL) normalised to total protein content. The amount of protein loaded into each lane is reported in micrograms. *LL = C. reinhardtii* cells cultivated in TAP under external low light levels (25 µmol.m$^{-2}$.s$^{-1}$) and *npq4* = the LHCSR3 deficient mutant. Both *LL* and *npq4* were used as negative controls. B) Ponceau Red S. stained membrane of immunoblot analysis of LHCSR3 and RbcL normalised to three different chlorophyll concentrations. L1: ladder, L2–15: correspond to the sample as indicated above in S2A. Note: insufficient sample of $HD_{Fluc}$ was available for three dilutions.